R-05-55

Neutron data for accelerator-driven transmutation technologies

Annual Report 2004/2005

J Blomgren, L Nilsson, P Mermod, N Olsson,
S Pomp, A Öhrn, M Österlund
Department of Neutron Research, Uppsala University

September 2005

Svensk Kärnbränslehantering AB
Swedish Nuclear Fuel
and Waste Management Co
Box 5864
SE-102 40 Stockholm Sweden
Tel 08-459 84 00
+46 8 459 84 00
Fax 08-661 57 19
+46 8 661 57 19

ISSN 1402-3091
SKB Rapport R-05-55

Neutron data for accelerator-driven transmutation technologies

Annual Report 2004/2005

J Blomgren, L Nilsson, P Mermod, N Olsson,
S Pomp, A Öhrn, M Österlund
Department of Neutron Research, Uppsala University

September 2005

This report concerns a study which was conducted for SKB. The conclusions and viewpoints presented in the report are those of the authors and do not necessarily coincide with those of the client.

A pdf version of this document can be downloaded from www.skb.se

Summary

The project NATT, Neutron data for Accelerator-driven Transmutation Technology, is performed within the nuclear reactions group of the Department of neutron research, Uppsala university. The activities of the group are directed towards experimental studies of nuclear reaction probabilities of importance for various applications, like transmutation of nuclear waste, biomedical effects and electronics reliability. The experimental work is primarily undertaken at the The Svedberg Laboratory (TSL) in Uppsala, where the group has previously developed two world-unique instruments, MEDLEY and SCANDAL.

Highlights from the past year:

- An article on three-body force effects has been on the top-ten downloading list of Physics Letters B, one of the very most prestigious journals in subatomic physics.
- Uppsala had the largest foreign delegation at the International Conference on Nuclear Data for Science and Technology in Santa Fé, New Mexico, USA, and presented the largest number of papers of all experimental groups.
- A neutron flux monitor for the new FOI neutron beam facility has been developed, commissioned and taken into regular operation.
- Within the project, one licentiate exam has been awarded.
- The new neutron beam facility at TSL has been taken into commercial operation and is now having the largest commercial turnover of all European facilities in the field.

Sammanfattning

Projektet NATT, Neutrondata för Acceleratordriven Transmutationsteknik, bedrivs inom kärnreaktionsgruppen vid institutionen för neutronforskning, Uppsala universitet. Gruppens verksamhet är inriktad mot experimentella studier av kärnfysikaliska reaktionssannolikheter för olika tillämpningsområden, som transmutation av kärnavfall, biomedicinska effekter och tillförlitlighet hos elektronik. Den experimentella verksamheten bedrivs huvudsakligen vid The Svedberglaboratoriet (TSL) i Uppsala, där gruppen tidigare utvecklat två världsunika instrument, MEDLEY och SCANDAL.

Höjdpunkter från det gångna verksamhetsåret:

- En artikel om trekropparkrafter har varit en av de tio mest nedladdade från den mycket prestigefylla tidsskriften Physics Letters B.
- Vid den internationella konferensen om kärndata för vetenskap och teknologi i Santa Fé, New Mexico, USA, utgjorde Uppsala den största utländska delegationen, och fick flest presentationer av alla experimentgrupper.
- En monitor för neutronflödesbestämningar har utvecklats och tagits i reguljärt bruk vid FOIs nya neutronfacilitet.
- Inom projektet har en doktorand disputerat för licentiatexamen.
- Den nya neutronfaciliteten som gruppen utvecklat vid The Svedberglaboratoriet har tagits i reguljär kommersiell drift och har nu Europas största omsättning inom området.

Contents

X P Mermod, J Blomgren, B Bergenwall, A Hildebrand, C Johansson, J Klug, L Nilsson, N Olsson, M Österlund, S Pomp, U Tippawan, O Jonsson, A V Prokofiev, P-U Renberg, P Nadel-Turonski, Y Maeda, H Sakai, A Tamii. Investigation of three-body force effects in neutron-deuteron scattering at 95 MeV. Proceedings of International Conference on Nuclear Data for Science and Technology, Santa Fé, New Mexico, USA, September 26–October 1, 2004. AIP Conference Proceedings 769 (2005) 688. 93

XI J Blomgren. Neutrons for science and industry – Uppsala neutron beam activities. Proceedings of International Conference on Nuclear Data for Science and Technology, Santa Fé, New Mexico, USA, September 26–October 1, 2004. AIP Conference Proceedings 769 (2005) 730 (invited). 97

XII S Pomp, A V Prokofiev, J Blomgren, C Ekström, O Jonsson, D Reistad, V Ziemann, N Haag, A Hildebrand, L Nilsson, B Bergenwall, C Johansson, P Mermod, N Olsson, M Österlund, U Tippawan. The new Uppsala neutron beam facility. Proceedings of International Conference on Nuclear Data for Science and Technology, Santa Fé, New Mexico, USA, September 26–October 1, 2004. AIP Conference Proceedings 769 (2005) 780. 103

XIII A Prokofiev, S Pomp, U Tippawan, B Bergenwall, S Dangtip, L Einarsson, Yu Gavrikov, N Haag, A Hildebrand, C Johansson, A Kotov, P Mermod, L Vaishnene, M Österlund, J Blomgren. A new facility for high-energy neutron-induced fission studies. Proceedings of International Conference on Nuclear Data for Science and Technology, Santa Fé, New Mexico, USA, September 26–October 1, 2004. AIP Conference Proceedings 769 (2005) 800. 107

XIV C Johansson, J Blomgren, A Ataç, B Bergenwall, A Hildebrand, J Klug, P Mermod, L Nilsson, S Pomp, U Tippawan, M Österlund, O Jonsson, A V Prokofiev, P-U Renberg, P Nadel-Turonski, N Olsson, S Dangtip. Forward-angle *np* scattering at 96 MeV and normalization of neutron-induced nuclear reactions. Proceedings of International Conference on Nuclear Data for Science and Technology, Santa Fé, New Mexico, USA, September 26–October 1, 2004. AIP Conference Proceedings 769 (2005) 804. 111

XV A Hildebrand, J Blomgren, B Bergenwall, C Johansson, J Klug, P Mermod, L Nilsson, S Pomp, U Tippawan, N Olsson, O Jonsson, A V Prokofiev, P Nadel-Turonski, M Österlund, V Blideanu, J F Lecolley, F R Lecolley, N Marie-Noury, F Haddad. Elastic neutron scattering at 96 MeV. Proceedings of International Conference on Nuclear Data for Science and Technology, Santa Fé, New Mexico, USA, September 26–October 1, 2004. AIP Conference Proceedings 769 (2005) 853. 115

XVI G A Tutin, I V Ryzhov, V P Eismont, A N Mitrukhin, V S Oplavin, S M Soloviev, J Blomgren, H Condé, N Olsson, P-U Renberg. Measurement of neutron-induced fission cross sections of ^{205}Tl, ^{204,206,207,208}Pb, ^{nat}Pb and ^{209}Bi using quasi-monoenergetic neutrons of 35 MeV to 174 MeV. Proceedings of International Conference on Nuclear Data for Science and Technology, Santa Fé, New Mexico, USA, September 26–October 1, 2004. AIP Conference Proceedings 769 (2005) 937. 119

1 Background

1.1 The NATT project

The present project, Neutron data for Accelerator-driven Transmutation Technology (NATT), supported as a research task agreement by Statens Kärnkraftinspektion (SKI), Svensk Kärnbränslehantering AB (SKB), Ringhalsverket AB and Totalförsvarets forskningsinstitut (FOI), started 2002-07-01. The primary objective from the supporting organizations is to promote research and research education of relevance for development of the national competence within nuclear energy.

The aim of the project is in short to:

- promote development of the competence within nuclear physics and nuclear technology by supporting licenciate and PhD students,
- advance the international research front regarding fundamental nuclear data within the presently highlighted research area accelerator-driven transmutation,
- strengthen the Swedish influence within the mentioned research area by expanding the international contact network,
- provide a platform for Swedish participation in relevant EU projects,
- monitor the international development for the supporting organizations,
- constitute a basis for Swedish participation in the nuclear data activities at IAEA and OECD/NEA.

The project is operated by the Department of Neutron Research (INF) at Uppsala University, and is utilizing the unique neutron beam facility at the The Svedberg Laboratory (TSL) at Uppsala University.

In this document, we give a status report after the third year (2004-07-01–2005-06-30) of the project.

2 Introduction

Transmutation techniques in accelerator-driven systems (ADS) involve high-energy neutrons, created in the proton-induced spallation of a heavy target nucleus. The existing nuclear data libraries developed for reactors of today go up to about 20 MeV, which covers all available energies for that application; but with a spallator coupled to a core, neutrons with energies up to 1–2 GeV will be present. Although a large majority of the neutrons will be below 20 MeV, the relatively small fraction at higher energies still has to be characterized. Above about 200 MeV, direct reaction models work reasonably well, while at lower energies nuclear distortion plays a non-trivial role. This makes the 20–200 MeV region most important for new experimental cross section data /Blomgren, 2002, 2004/.

Ten years ago, very little high-quality neutron-induced data existed in this energy domain. Only the total cross section /Finlay et al. 1993/ and the *np* scattering cross section had been investigated extensively. Besides this, there were data on neutron elastic scattering from UC Davis at 65 MeV on a few nuclei /Hjort et al. 1994/. Programmes to measure neutron elastic scattering had been proposed or begun at Los Alamos /Rapaport and Osborne/ and IUCF /Finlay et al. 1992/, with the former resulting in a thesis on data on a few nuclei.

The situation was similar for (n,xp) reactions, where programmes have been run at UC Davis /Ford et al. 1989/, Los Alamos /Rapaport and Sugarbaker, 1994/, TRIUMF /Alford and Spicer, 1998/ and TSL Uppsala /Olsson, 1995; Blomgren, 1997/, but with limited coverage in secondary particle energy and angle. Better coverage had been obtained by the Louvain-la-Neuve group up to 70 MeV /Slypen et al. 1994/.

Thus, there was an urgent need for neutron-induced cross section data in the region around 100 MeV, which is an area where very few facilities in the world can give contributions. By international collaboration within an EU supported Concerted Action, which has been followed by the full scale projects HINDAS and EUROTRANS, the level of ambition for the present project has been increased, and the potential of the unique neutron beam facility at The Svedberg Laboratory in Uppsala has been well exploited.

During the last few years, the situation has improved dramatically, especially due to the HINDAS activities. At present, the nuclear data situation for ADS applications is relatively satisfactory up to 100 MeV. At 100 MeV, the hitherto most common energy at TSL, there are elastic neutron scattering data, neutron-induced light ion production data, neutron-induced activation, and fission cross sections available, in all cases on a series of nuclei. Some results have been published already, and there is a wealth of data under analysis and documentation. The present report will present some glimpses of this ongoing work.

Looking into the future, it can be envisioned that the coming 5–10 years will be devoted to similar activities at higher energies, i.e. up to 180 MeV, which is the highest neutron energy available at TSL. This has been made possible by the development of a new neutron beam facility, which is described below.

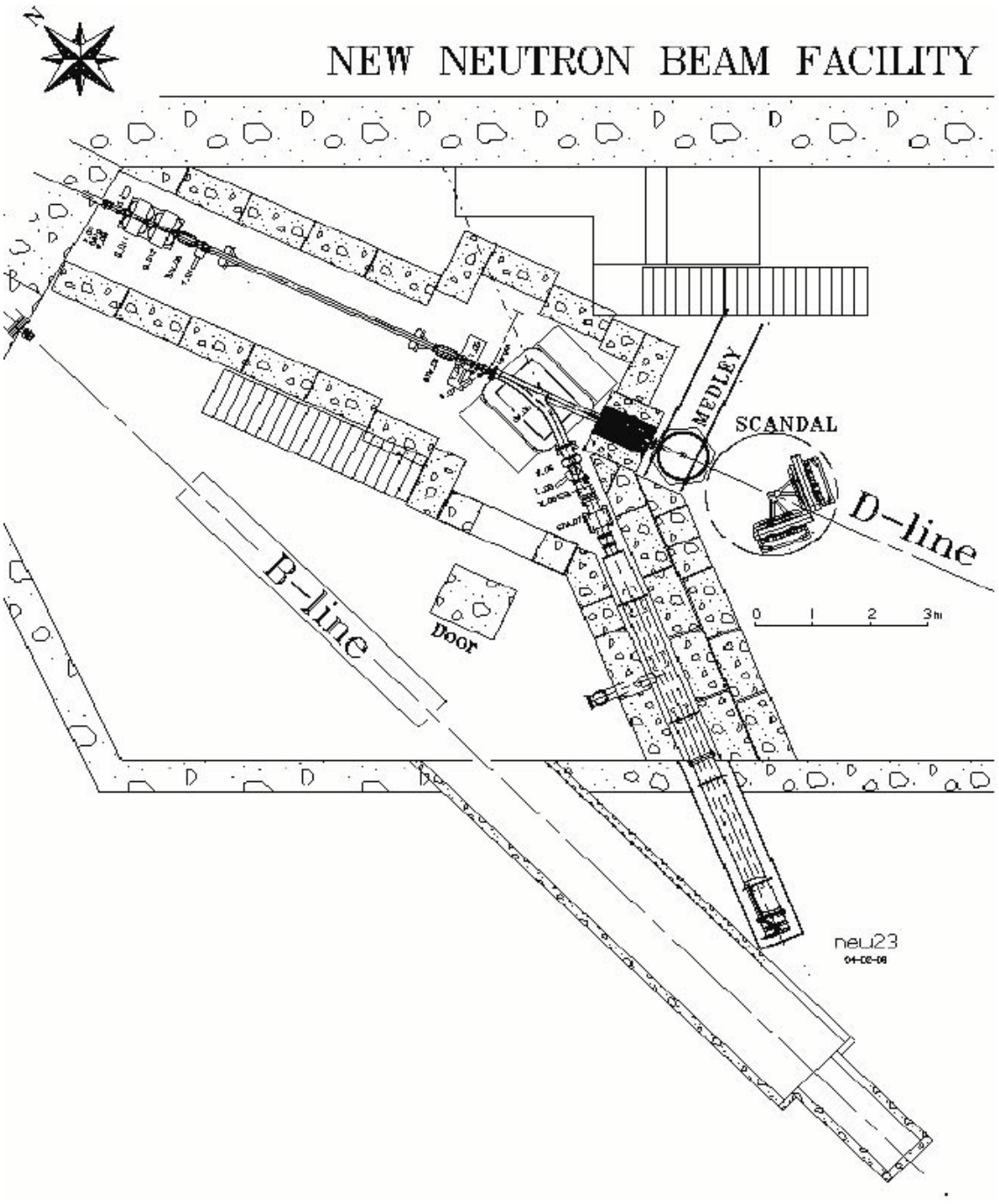

Figure 2-1. *The TSL neutron beam facility.*

3 Experimental setup and techniques

3.1 The TSL neutron beam facility

At TSL, quasi-monoenergetic neutrons are produced by the reaction ^{7}Li(p,n)^{7}Be in a ^{7}Li target bombarded by 50–180 MeV protons from the cyclotron, as is illustrated in Figure 2-1. (Appendix XII). After the target, the proton beam is bent by a dipole magnet into a concrete tunnel, where it is stopped in a well-shielded Faraday cup, used to measure the proton beam current. A narrow neutron beam is formed in the forward direction by a collimator with a total thickness of about one metre.

The energy spectrum of the neutron beam consists of a high-energy peak, having approximately the same energy as the incident proton beam, and a low-energy tail. About half of all neutrons appear in the high-energy peak, while the rest are roughly equally distributed in energy, from the maximum energy and down to zero. The thermal contribution is small. The low-energy tail of the neutron beam can be reduced using time-of-flight (TOF) techniques over the distance between the neutron source and the reaction target.

The relative neutron beam intensity is monitored by integrating the charge of the primary proton beam, as well as by using thin film breakdown counters, placed in the neutron beam, measuring the number of neutron-induced fissions in ^{238}U.

Two multi-purpose experimental setups are semi-permanently installed at the neutron beam line, namely MEDLEY and SCANDAL. These were described in detail in the annual report 1999/2000 of the previous KAT project, and only a brief presentation is given here.

3.2 The MEDLEY setup

The MEDLEY detector array /Dangtip et al. 2000/, shown in Figure 3-1, is designed for measurements of neutron-induced light-ion production cross sections of relevance for applications within ADS and fast-neutron cancer therapy and related dosimetry. It consists of eight particle telescopes, installed at emission angles of 20–160 degrees with 20 degrees separation, in a 1 m diameter scattering chamber, positioned directly after the last neutron collimator. All the telescopes are fixed on a turnable plate at the bottom of the chamber, which can be rotated without breaking the vacuum.

Each telescope is a ΔE-ΔE-E detector combination, where the ΔE detectors are silicon surface barrier detectors with thicknesses of 50 or 60 μm and 400 or 500 μm, respectively, while the E detector is a 50 mm long inorganic CsI(Tl) crystal. ΔE-ΔE or ΔE-E techniques are used to identify light charged particles (p, d, t, 3He, α). The chosen design gives a sufficient dynamic range to distinguish all charged particles from a few MeV up to more than 100 MeV.

The solid angle of the telescopes is defined by active collimators, designed as thin hollow plastic scintillator detectors, mounted on small photomultiplier tubes. A signal from such a detector is used to veto the corresponding event, thereby ensuring that only particles that pass inside the collimator are registered.

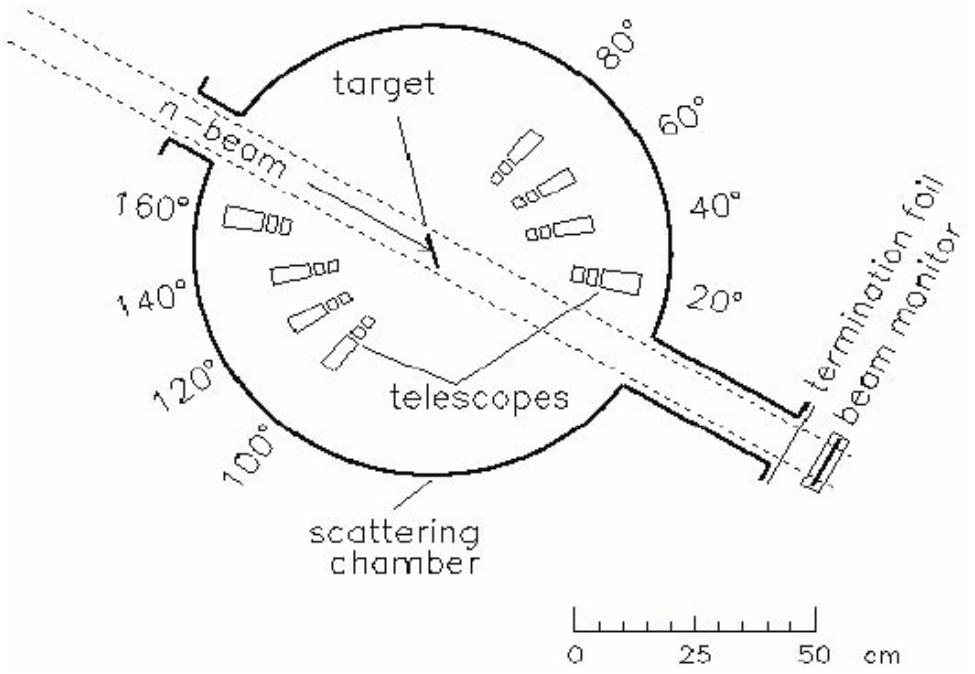

Figure 3-1. *The MEDLEY setup.*

3.3 The SCANDAL setup

The SCANDAL setup /Klug et al. 2002/ is primarily intended for studies of elastic neutron scattering, i.e. (n,n) reactions. Neutron detection is accomplished via conversion to protons by the H(n,p) reaction. In addition, (n,xp) reactions in nuclei can be studied by direct detection of protons. This feature is also used for calibration, and the setup has therefore been designed for a quick and simple change from one mode to the other.

The device is illustrated in Figure 3-2. It consists of two identical systems, in most cases located on each side of the neutron beam. The design allows the neutron beam to pass through the drift chambers of the right-side setup, making low-background measurements close to zero degrees feasible.

In neutron detection mode, each arm consists of a 2 mm thick veto scintillator for fast charged-particle rejection, a neutron-to-proton converter which is a 10 mm thick plastic scintillator, a 2 mm thick plastic scintillator for triggering, two drift chambers for proton tracking, a 2 mm thick ΔE plastic scintillator, which is also part of the trigger, and an array of 12 large CsI detectors for energy determination. The trigger is provided by a coincidence of the two trigger scintillators, vetoed by the front scintillator. The compact geometry allows a large solid angle for protons emitted from the converter. Recoil protons are selected using the ΔE and E information from the plastic scintillators and the CsI detectors, respectively. The energy resolution is about 3.7 MeV (FWHM), which is sufficient to resolve elastic and inelastic scattering in several nuclei. The angular resolution is calculated to be about 1.4 degrees (rms) when using a cylindrical scattering sample of 5 cm diameter.

When SCANDAL is used for (n,xp) studies, the veto and converter scintillators are removed. A multitarget arrangement can be used to increase the target content without impairing the energy resolution, which is typically 3.0 MeV (FWHM). This multitarget box allows up to seven targets to be mounted simultaneously, interspaced with multi-wire proportional counters (MWPC). In this way it is possible to determine in which target

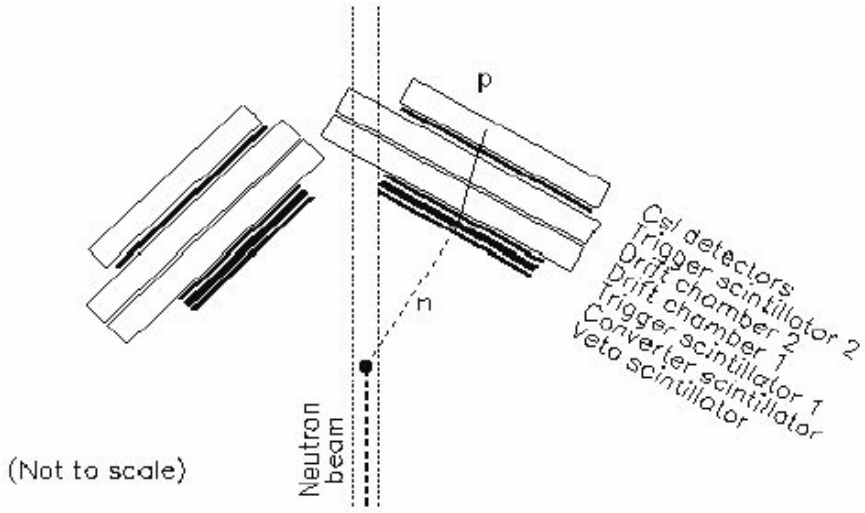

Figure 3-2. *The SCANDAL setup.*

layer the reaction took place, and corrections for energy loss in the subsequent targets can be applied. In addition, different target materials can be studied simultaneously, thus facilitating absolute cross section normalization by filling a few of the multitarget slots with CH2 targets. The first two slots are normally kept empty, and used to identify charged particles contaminating the neutron beam.

3.4 New neutron beam facility at TSL

The rapidly increasing number of neutron beam users has motivated a new facility to be built. Practical work begun in spring 2002, which included re-building of beam line magnets, removal of obsolete heavy equipment and procurement of concrete for the new shielding walls. Major installations were undertaken in autumn 2003, during which the experimental program was resting. First beam was delivered early January 2004. During the first half of spring 2004, a series of commissioning runs were undertaken to characterize the beam, i.e. to measure beam energy spectra, intensity profiles, etc. First beam to commercial customers was delivered in May 2004, and the first physics experiment were carried out in August 2004.

During 2004–05, the new neutron beam facility has gone into regular operation. The largest use is commercial, i.e. tests of the sensitivity of electronics concerning the neutron component of cosmic radiation. This is a rapidly growing reliability concern of the electronics industry, and it is commonly believed that this effect could terminate the further development of silicon-based circuit technology /Slayman, 2004; Tang/. This new facility has rapidly become the largest installation in Europe for this purpose, and the commercial potential is large. In combination with proton therapy of cancer, neutron irradiations of electronics provide adequate funding for the operation of TSL.

3.5 Future activities

The new neutron beam facility provides a significantly higher intensity than the previous installation. This allows nuclear data experiments of high quality to be extended from the previous practical limit of 100 MeV up to the maximum energy of the facility, i.e. 180 MeV. This requires, however, a matching upgrade of the experimental devices. Both multipurpose experimental setups (MEDLEY and SCANDAL) are in principle possible to upgrade, i.e. the techniques as such can be expected to work also at higher energies. The cost, however, is very different. The MEDLEY setup is already under upgrade, since the cost is fairly limited, while upgrading of SCANDAL is pending due to financial limitations.

A new nuclear data project, similar to the present NATT project, but concentrating on light-ion production and fission studies at higher energies, is under consideration.

4 Results

4.1 Elastic scattering

A number of experimental observations seem to indicate that three-body forces exist in nuclei. Recent calculations /Witala et al. 1998/ have indicated that measurements of the differential cross section for elastic neutron-deuteron (*nd*) scattering in the 60–200 MeV range should be useful in searches for three-nucleon (*3N*) force effects. The *nd* elastic scattering differential cross section has been measured using both MEDLEY and SCANDAL at 95 MeV incident neutron energy. The results are presented in Figure 4-1 as the ratio between proton and deuteron production. It is evident that models based on inclusion of *3N* forces describe *nd* data in the angular region of the cross-section minimum very well, while models without 3N forces cannot account for the data. The MEDLEY data have previously been analyzed and published, and during the last year, additional data obtained with SCANDAL have been analyzed. The results corroborate the MEDLEY results, and a paper has recently been accepted for publication. A large publication, describing the experiments and analysis in detail is underway.

Results on elastic scattering from carbon and lead have been published before. New experiments on carbon, nitrogen, oxygen, silicon, calcium, iron and yttrium are under analysis.

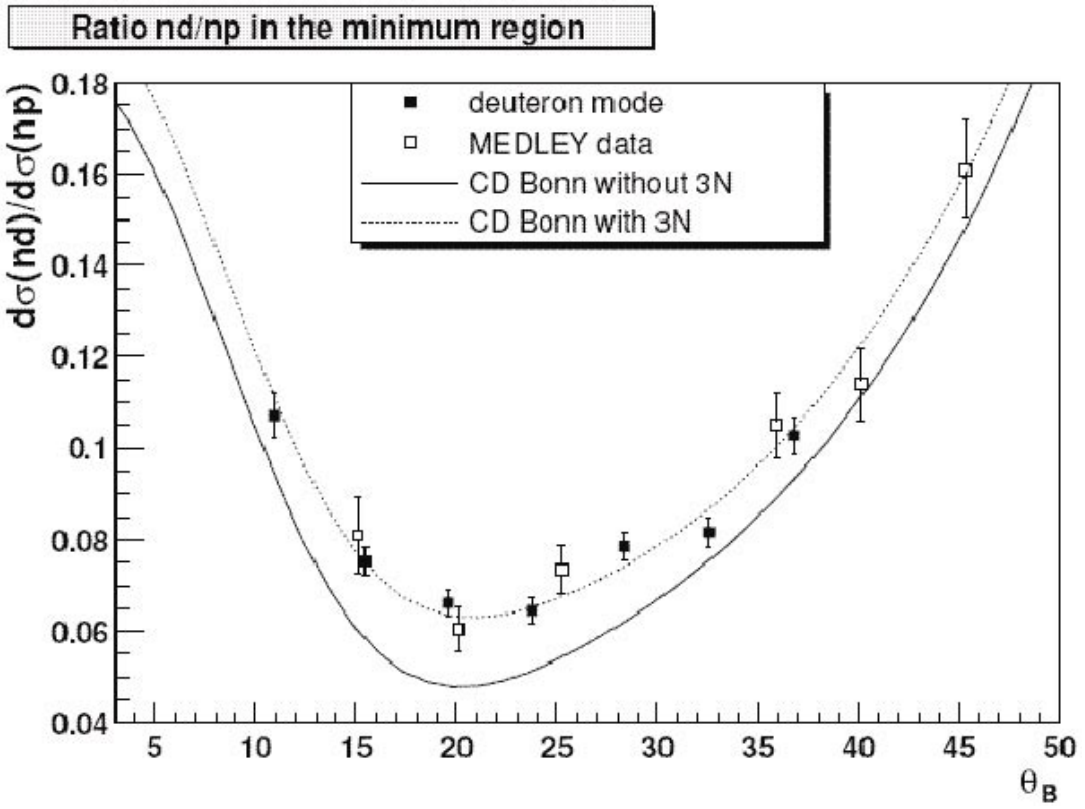

Figure 4-1. *The ratio of the neutron-deuteron and neutron-proton scattering cross sections at 95 MeV. The solid line is a theory prediction based on two-body forces only, while the dotted line includes three-body forces. Open symbols refer to previously published data with the MEDLEY setup, while filled symbols are the newly analyzed SCANDAL results.*

4.2 (n,xlcp) reactions

In parallel with the other experiments mentioned above and below, data have been taken with the MEDLEY setup on light-ion production reactions. During the last years, results on silicon, iron, lead and uranium have been published. A publication on oxygen is in a final stage, and data on carbon, calcium, silver and molybdenum remain to be analyzed.

4.3 (n,xn') reactions

We have a collaboration project with a group from Caen, France, on (n,xn') reactions. For these studies, a modified SCANDAL converter (CLODIA) has been designed and built in Caen. A large experiment on lead and iron targets was conducted in August 2004. This experiment is our deliverable in the EU 6th FWP EUROTRANS.

4.4 Tagged neutron-proton scattering

Neutron-proton scattering is the reference cross section for fast-neutron reactions, i.e. it is the standard which all other cross sections are measured relative to. Besides our activities at TSL, we have been involved in a similar experiment at Indiana University Cyclotron Facility (IUCF), Bloomington, Indiana, USA. The results have recently been published in Physical Review Letters (Appendix III).

4.5 Fission

We are working on the development of a setup for fission studies, based on MEDLEY in a revised geometric configuration. The setup has been tested and found to meet the specifications, and first experiments are in progress. One interesting feature of the new setup is that it allows a precise determination of the absolute cross section by measuring *np* scattering simultaneously. This is important, since only one previous experiment on high-energy fission has been performed with a reasonably good control of the absolute scale. Preliminary results have been presented at international conferences (Appendix XIII).

In addition, we have a long-term collaboration with a fission experiment group at Khlopin Radium Institute (KRI) in St. Petersburg, Russia (Appendices I, IV, VI, VII, VIII, IX and XVI).

4.6 Neutron beam monitoring

A facility for neutrons in the 1–20 MeV range has recently been installed at the Swedish Defense Research Agency (FOI), Stockholm. A monitor for flux measurements has been developed within a joint INF-PTB-FOI collaboration /Hildebrand, 2005/. The monitor has been built and tested at the Physikalisch-Techniche Bundesanstalt (PTB), Braunschweig, Germany. Angelica Hildebrand has spent a three-month research internship there for the development. The monitor has now been installed at FOI, it works according to the specifications and is used in regular operation.

5 International activities

5.1 Collaborations

During 2005, the 6th EU framework program EUROTRANS started. Our group and our long-term collaborators from LPC Caen, France, have merged our activities in EUROTRANS, and we have a joint deliverable concerning (n,xn') reactions (see above).

The enlargement of the European union has motivated a process of merging nuclear data activities in the EU and the candidate countries. Jan Blomgren has participated in this process, exemplified by a contribution to a recent enlargement workshop (Appendix XXI).

5.2 Meetings and conferences

During the last year, the largest conference in the field, Nuclear data for Science and Technology, was held in Santa Fé, New Mexico, USA. Our group was very well represented (Appendices V–XVIII), i.e. 14 accepted contributions which was the largest number by any experimental group. Moreover, in total only three PhD students gave oral presentations, all of them being from Uppsala, whereof two active in the NATT project.

Nils Olsson is Swedish representative in the OECD/NEA Nuclear Science Committee (NSC) and its Executive Group.

6 Administrative matters

6.1 Staff and students

During the project year, Jan Blomgren has been project leader, active on a 25–50% basis within the project. His other major activities are teaching and duties as director of studies, both at INF and the Swedish Nuclear Technology Center (SKC). Assistant professor (forskarassistent) Stephan Pomp has worked essentially full time within the project with research and student supervision. Associate professor (universitetslektor) Michael Österlund is involved in part-time research within the group. Leif Nilsson, retired professor, has been employed on about 10% time for student supervision. Nils Olsson was adjunct professor (20%) until 2004-12-31.

Two PhD students are directly connected to and financed by the present project, Angelica Hildebrand (from June 2005 named Angelica Öhrn due to marriage) and Philippe Mermod, which both are connected to the research school AIM (Advanced Instrumentation and Measurements).

6.2 Reference group

The reference group consists of Per-Eric Ahlström (SKB), Benny Sundström (SKI), Katarina Wilhelmsen (FOI) and Fredrik Winge (BKAB). A reference group meeting was held in Uppsala 2005-05-18. Scientific and administrative reports on the progress of the project were given at the meeting.

In addition to this meeting, the progress of the work has continuously been communicated to the reference group members by short, written, quarterly reports.

References

Alford W P, Spicer B M, 1998. Nucleon charge-exchange reactions at intermediate energy, Advances in Nuclear Physics 24, 1.

Blomgren J, 1997. The (n,p) reaction – Not So Boring After All? Proceedings from International Symposium on New Facet of Spin Giant Resonances in Nuclei, Tokyo, 1997, p 70. (Invited talk)

Blomgren J, 2002. Experimental activities at high energies, Proceedings from an international symposium on Accelerator Driven Systems for Energy production and Waste Incineration: Physics, Design and Related Nuclear Data, Trieste, 2002, p 327. (Invited talk)

Blomgren J, 2004. Nuclear data for accelerator-driven systems – Experiments above 20 MeV, Proceedings from EU enlargement workshop on Neutron Measurements and Evaluations for Applications, Bucharest, Romania, October 20–23, 2004 (invited).

Dangtip S, Atac A, Bergenwall B, Blomgren J, Elmgren K, Johansson C, Klug J, Olsson N, Alm Carlsson G, Söderberg J, Jonsson O, Nilsson L, Renberg P-U, Nadel-Turonski P, Le Brun C, Lecolley F-R, Lecolley J-F, Varignon C, Eudes Ph, Haddad F, Kerveno M, Kirchner T, Lebrun C, 2000. A facility for measurements of nuclear cross sections for fast neutron cancer therapy, Nucl. Instr. Meth. A452, 484.

Finlay R, Abfalterer W P, Fink G, Montei E, Adami T, Lisowski P W, Morgan G L, Haight R C, 1993. Neutron total cross sections at intermediate energies, Phys. Rev. C 47, 237.

Finlay R et al. 1992. Proposal to the NSF for support of CHICANE/Spectrometer System for the IUCF Cooler Ring.

Ford T D, Brady F P, Castaneda C M, Drummond J R, McEachern B, Romero J L, Sorenson D S, 1989. A large dynamic range detector for measurement of neutron-induced charged particle spectra down to zero degrees, Nucl. Instr. Meth. A274, 253.

Hildebrand A, Park H, Khurana S, Nolte R, Schmidt D, 2005. Experimental determination of the response matrix of a BC501 scintillation detector using a wide neutron spectrum: a status report, PTB report 6.42-05-1.

Hjort E L, Brady F P, Romero J L, Drummond J R, Sorenson D S, Osborne J H, McEachern B, 1994. Measurements and analysis of neutron elastic scattering at 65 MeV, Phys. Rev. C 50, 275.

Klug J, Blomgren J, Atac A, Bergenwall B, Dangtip S, Elmgren K, Johansson C, Olsson N, Rahm J, Jonsson O, Nilsson L, Renberg P-U, Nadel-Turonski P, Ringbom A, Oberstedt A, Tovesson F, Le Brun C, Lecolley J-F, Lecolley F-R, Louvel M, Marie N, Schweitzer C, Varignon C, Eudes Ph, Haddad F, Kerveno M, Kirchner T, Lebrun C, Stuttgé L, Slypen I, Prokofiev A, Smirnov A, Michel R, Neumann S, Herpers U, 2002. SCANDAL – A facility for elastic neutron scattering studies in the 50–130 MeV range, Nucl. Instr. Meth. A489, 282.

Olsson N, 1995. Studies of spin-isospin excitations at TSL in Uppsala, Nucl. Phys. News 5, no 2, 28.

Rapaport J, Sugarbaker E, 1994. Isovector excitations in nuclei, Ann. Rev. Nucl. Part. Sci. 44, 109.

Rapaport J, private communication, **Osborne J**, thesis, unpublished.

Slayman C, 2004. Terrestial neutron single-event effects in workstations and servers, Proceedings of the 6th International Workshop on Radiation Effects on Semiconductor Devices for Space Applications, Tsukuba, Japan, October 6–8, 2004, p 17.

Slypen I, Corcalciuc V, Ninane A, Meulders J P, 1994. Charged particles produced in fast neutron induced reactions 12C in the 45–80 MeV energy range, Nucl. Instr. Meth. A337, 431.

Tang H H K, private communication.

Witala H, Glöckle W, Hüber D, Golak J, Kamada H, 1998. Cross section minima in elastic Nd scattering: Possible evidence for three-nucleon force effects, Phys. Rev. Lett. 81, 1183.

Appendix I

PHYSICAL REVIEW C **70**, 054603 (2004)

Measurements of neutron-induced fission cross sections for ^{209}Bi, ^{nat}Pb, ^{208}Pb, ^{197}Au, ^{nat}W, and ^{181}Ta in the intermediate energy region

A. N. Smirnov,* V. P. Eismont, and N. P. Filatov
V. G. Khlopin Radium Institute, 2oi Murinskiy Prospect 28, Saint-Petersburg 194021, Russia

J. Blomgren† and H. Condé
Department of Neutron Research, Ångström Laboratory, Uppsala University, Box 525, S-751 20 Uppsala, Sweden

A. V. Prokofiev‡
The Svedberg Laboratory, Uppsala University, Box 533, S-751 21 Uppsala, Sweden
and V. G. Khlopin Radium Institute, 2oi Murinskiy Prospect 28, Saint-Petersburg 194021, Russia

P.-U. Renberg
The Svedberg Laboratory, Uppsala University, Box 533, S-751 21 Uppsala, Sweden

N. Olsson
Department of Neutron Research, Ångström Laboratory, Uppsala University, Box 525, S-751 20 Uppsala, Sweden
and Swedish Defense Research Agency (FOI), S-172 90 Stockholm, Sweden
(Received 8 July 2004; published 4 November 2004)

Neutron-induced fission cross-section ratios ^{nat}Pb/^{209}Bi, ^{208}Pb/^{209}Bi, ^{197}Au/^{209}Bi, ^{nat}W/^{209}Bi, ^{181}Ta/^{209}Bi, and ^{209}Bi/^{238}U have been measured in the 30–180 MeV energy range using the neutron beam facility at The Svedberg Laboratory in Uppsala. The ^{7}Li(p,n) reaction was employed as a neutron source. The fission fragments were detected by thin-film breakdown counters. Cross sections at specific energies were determined using unfolding techniques with respect to the excitation function and the neutron spectra, the latter obtained from recent measurements and an evaluation. The absolute fission cross sections were obtained using the standard ^{238}U(n,f) cross section. The ^{nat}W(n,f) and ^{181}Ta(n,f) cross sections have been measured for the first time. The results for ^{209}Bi(n,f), ^{nat}Pb(n,f), ^{208}Pb(n,f), and ^{197}Au(n,f) cross sections have been compared with available literature data. A universal easy-to-use parametrization has been suggested for all measured cross sections. The common features of subactinide neutron-induced fission cross sections are found to be similar to those of the proton-induced fission data.

DOI: 10.1103/PhysRevC.70.054603 PACS number(s): 25.85.Ec, 25.40.−h, 28.20.−v, 27.80.+w, 27.70.+q

I. INTRODUCTION

Concepts of accelerator-driven systems (ADS) for incineration of long-lived radioactive waste and energy production (see, e.g., [1]) suggest irradiation of a massive target made of heavy elements by a high-intensity charged particle beam. As a result of nuclear interactions in the target, caused by the primary beam and secondary particles, an intense spallation neutron source is created with an energy distribution extending up to the incident particle energy. This source is intended to feed a subcritical reactor that surrounds the neutron production target and contains the nuclides to be transmuted.

One of the prerequisites for computational modeling of ADS is the availability of evaluated nuclear data for the most important reactions involved. This motivates the choice of nuclides and reactions included in the high priority request list of intermediate-energy nuclear data, which is formulated and periodically updated by Koning *et al.* [2]

The recent high priority list includes requests for nucleon-induced fission cross-section data for a few nuclides considered as prospective spallation target materials. The fission channel contributes to the radioactivity produced in the spallation target, as well as to the chemical and radiological toxicity of the reaction products. For example, fission products in a lead target irradiated by 1.6-GeV protons will contribute 10–15 % to the overall residual activity after one year of cooling [3]. On the other hand, the predictive power of available nuclear reaction models and codes (e.g., LAHET [4], CEM95 [5]) with respect to the description of the fission process is not sufficiently good at present (see, e.g., the studies of Prael [4], Prokofiev *et al.* [5], Duijvestijn *et al.* [6], and a recent comparison of codes for activation yield calculation [7]). For example, the ^{nat}W(p,f) cross section predicted by the LAHET code was found to be about 20 times lower than the experimental result of Ref. [6]. Further progress in nuclear reaction modeling, especially with respect to fission, may therefore lead to significant improvements in ADS performance calculations.

Data on intermediate energy fission cross sections are important also for nuclear theory, e.g., in connection with stud-

*Electronic address: Smirnov@atom.nw.ru
†Electronic address: jan.blomgren@tsl.uu.se
‡Electronic address: Alexander.Prokofiev@tsl.uu.se

 ©2004 The American Physical Society

ies of the dynamic effects of the nuclear fission process, which reflect the connection between collective and single-particle degrees of freedom in nuclei (see, e.g., [8]).

Proton-induced fission cross sections have been studied extensively (see, e.g., a recent review [9] and references therein). On the other hand, neutron-induced fission experiments above 20 MeV are sparse, mainly because of the lack of suitable neutron sources. In addition, a truly monoenergetic neutron source is not available in this energy domain. Neutron data measurement and processing techniques are therefore unavoidably more complicated than in the case of charged particle beams.

The (n,f) cross-section database is especially poor for subactinide nuclei. The early experiments of Kelly and Wiegand [10], Goldanskiy *et al.* [11], Reut *et al.* [12], and Dzhelepov *et al.* [13] are rather of a qualitative character. The studies of Vorotnikov and Larionov [14] and Vorotnikov [15] are of a high methodological quality, but cover only a narrow energy region near the fission barrier, where the cross sections are extremely small, and therefore only upper limits for cross sections could be obtained in many cases.

During the last decades, a new generation of intermediate energy neutron sources has become available. At a few of them, (n,f) cross-section measurements, in particular, for subactinide nuclei have been included in the experimental programs.

The measurements at the LANSCE neutron facility at Los Alamos National Laboratory were performed by Vonach *et al.* [16] and Staples *et al.* [17,18] in the early 1990s using a parallel-plate ionization chamber. None of these studies has resulted in a final publication. A similar technique was employed in the work of Shcherbakov *et al.* [19] performed at the neutron facility GNEIS at Petersburg Nuclear Physics Institute in Gatchina, and in the work of Nolte *et al.* [20] performed at neutron facilities in Louvain-la-Neuve and Cape Town. A complication in interpreting data of this type is the need to separate subactinide fission events from background of nonfission products, which contribute significantly to the pulse height spectra.

The (n,f) cross-section measurements at the neutron facility in The Svedberg Laboratory (TSL) in Uppsala are part of an experimental program performed in the framework of collaboration between V.G. Khlopin Radium Institute, St. Petersburg, and Uppsala University. Measurements for subactinide nuclei have been performed using two different techniques for fission fragment detection, thin-film breakdown counters (TFBC) [21–26], and a Frisch-gridded ionization chamber [24,27–29].

This paper presents final (n,f) cross-section data for ^{209}Bi, ^{nat}Pb, ^{208}Pb, ^{197}Au, ^{nat}W, and ^{181}Ta, obtained with the TFBC technique. The measurements for natural lead, tungsten, and tantalum are important because these elements are either considered as candidates to the neutron production target material in concepts of future ADS or are already used in existing spallation neutron sources. The doubly magic nucleus ^{208}Pb is included because of its importance for improvements in the theoretical modeling of the fission process. In addition, the ^{197}Au(n,f) cross section was studied in view of its recent application in neutron monitoring [30].

Earlier analyses and preliminary experimental data have been published elsewhere [21–26]. In the present study, the results of further measurements have been added, and the data from our earlier studies have been reanalyzed using new neutron spectrum data [31] and new calculations of energy-dependent detection efficiency corrections [32,33].

II. EXPERIMENTAL APPARATUS AND PROCEDURE

The measurements were performed at the TSL neutron beam facility in Uppsala, using the Gustaf Werner cyclotron to produce neutrons through the ^{7}Li(p,n) reaction. The neutron beam facility and the positioning of the experimental chambers in the beam are described in Sec. II A.

Because of the low beam intensity, inherent for secondary beams, the irradiation position for the most measurements of the present experiment was chosen to be at a short distance from the neutron production target. The incident neutron spectrum is not monoenergetic, but consists of a high-energy peak accompanied by a low-energy tail, which also contributes to the fission reaction rate. To determine the (n,f) cross section at the energy of the peak, one needs to know the fraction of fission events due to that peak. This fraction can be determined using the time-of-flight (TOF) technique. However, in most cases it was not possible to implement the TOF techniques because of the short flight path in combination with the limited time resolution, dominated by duration of the proton beam pulse. Therefore, the fraction of peak fission events was obtained in an iterative unfolding procedure, taking into account relative fission reaction rates at as many incident neutron energies as possible, together with corresponding information on the neutron spectra. The determination of the latter is discussed in Sec. II B.

A severe γ-radiation background was present at the irradiation position chosen for most of the studied reactions. This hampered the use of traditional fission fragment detection techniques and justified the choice of TFBCs, which are sensitive only to particles with specific ionization losses exceeding the detection threshold. The TFBCs and the experimental chambers are described in Sec. II C.

The preparation and characterization of the samples are discussed in Sec. II D. Finally, an outline of the electronics and the data acquisition system is given in Sec. II E.

Most of the studied cross sections were measured relative to the ^{209}Bi(n,f) one. The latter has already been studied in earlier experiments (see, e.g., [21,22]) and has been adopted by IAEA/NDS as a secondary neutron standard [34]. However, further measurements of the ^{209}Bi(n,f) cross section and a new analysis of the earlier results have led to some changes that are discussed in Sec. IV B.

A. Neutron beam facility

An overview of the neutron beam facility is presented in Fig. 1. A comprehensive description of the facility can be found in [35,36], and therefore only the features essential for the present experiment are discussed below.

The proton beam from the Gustaf Werner cyclotron impinged on a 4–15-mm-thick target of lithium, enriched to

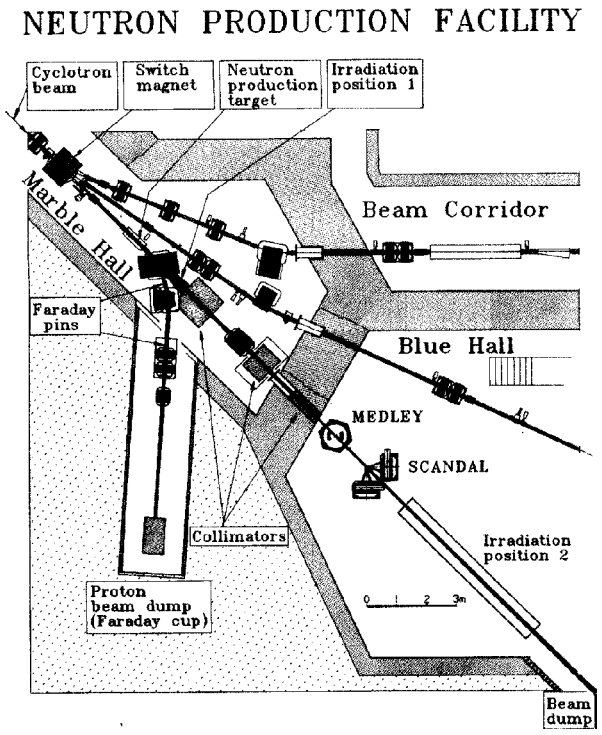

FIG. 1. An overview of the neutron beam facility.

99.98% in ^{7}Li. Downstream of the target, the proton beam was deflected by two magnets into an 8-m-long tunnel, where it was focused onto a water-cooled graphite beam dump. The neutrons produced within a 60-msr cone around 0° passed through a collimating system before reaching the experimental hall at a distance of about 8 m from the production target. The respective area is marked as Irradiation position 2 in Fig. 1. This position was employed in our earlier studies [21,22] and kept in the present work for the ^{209}Bi/^{238}U ratio measurements above 50 MeV, due to a rather large magnitude of the studied cross sections. On the contrary, it was found impractical to measure cross sections of nuclei lighter than Bi and the ^{209}Bi(n,f) cross section below 50 MeV in Irradiation position 2 because of insufficient neutron flux density and small cross-section values. Therefore, in these cases the experimental setup had to be positioned closer to the production target. On the other hand, the neutron field in the irradiation position has to be clean from contamination by primary or scattered protons. In addition, locations close to the 0° direction are preferable, because the production of high-energy neutrons is strongly forward-peaked. The given conditions were satisfied by placing the experimental setup between the proton bending magnet and the first neutron collimator, at a distance of about 2 m from the production target (Irradiation position 1, see Fig. 1). To facilitate simultaneous experiments at the neutron beam line, the setup was placed outside the vacuum tube at an angle of about 4° to the beam axis.

Thus, the TFBC-based chambers with samples of ^{238}U, ^{209}Bi, ^{nat}Pb, ^{208}Pb, ^{197}Au, ^{nat}W and ^{181}Ta were installed in Irradiation position 1, and the chambers with ^{238}U and ^{209}Bi were installed in Irradiation position 2. In addition to count-rate determination, the chamber with ^{238}U was employed as a neutron spectrum sensor (see Sec. II B).

Table I shows thicknesses of the ^{7}Li targets and various energy parameters of the primary proton and secondary neutron beams employed in the different irradiations. In most of the runs, the energy of the protons irradiating the lithium target was measured by time-of-flight techniques with an uncertainty as given in Table I. From this information, the peak neutron energy was calculated using the reaction Q value and the energy loss in the lithium target, estimated using the SRIM code [37].

The proton beam current at the production target was typically 4–6 μA in the 30–100 MeV energy range and 0.3–0.6 μA at the higher energies. The resulting flux density of high-energy peak neutrons at Irradiation position 1 amounted to (3×10^{4})–(3×10^{5}) s^{-1} cm^{-2}, which is a factor of 30–40 more than in Irradiation position 2. This gain was acquired at the price of a limited access to the setup in the course of the experiment and harder requirements on the stability of the detectors with respect to radiation.

The Irradiation position 1 was situated close to the facility for neutron activation studies [36,38]. In Ref. [38], the relative proton (and/or H^0 atom) contamination in the neutron field was estimated to be as much as 4×10^{-3}. However, in that case most of the protons were produced inside the activation target stack itself. Since the thickness of the stack was much larger than the total amount of material between the neutron production target and any sample in the present experiment, the estimate given above can be considered as an upper limit for the proton or H^0 atom contamination of the neutron beam that encounters the fission samples.

B. Neutron spectrum

As was mentioned, an unfolding procedure is needed to obtain fission cross sections from the measured reaction

TABLE I. Thicknesses of the ^{7}Li targets and energy parameters of the primary proton and secondary neutron beams.

E_p primary (MeV)	^{7}Li target thickness (mm)	E_p average in the target (MeV)	E_{npeak} average (MeV)
37.96±0.07	4	36.4	34.5
49.2±0.1	4	48.2	46.3
69.1±0.2	4	68.4	66.6
76.4±0.2	4	75.8	73.9
92.1±0.3	4	91.4	89.6
96.8±0.3	4	96.3	94.5[a]
	8	95.6	93.8[a]
114.2±2.0	8	113.1	111.3
136.7±1.0	15	134.7	132.9
148.4±0.6	15	146.4	144.6
177.3±1.0	15	175.2	173.3

[a]The peak neutron energy averaged over the two production modes is 94.1 MeV.

rates. Information on the neutron spectrum at the irradiation position for the various incident neutron energies is therefore required.

A complete set of characterization measurements is not available for the TSL neutron beam. Moreover, the intense background radiation around the production target would hamper the use of most instruments for neutron beam characterization. The present study therefore relies on the following assumptions about the neutron spectrum:

(i) The neutron spectrum at the Irradiation position 1 is a sum of two components. One of them originates directly from the ^{7}Li target. The other is a background arising from interactions of primary protons with the beam transport system, the beam dump, the walls, and other material in the surroundings, with subsequent propagation and slowing-down of secondary neutrons.

(ii) The background component dominates in the low-energy end of the spectrum and vanishes at neutron energies of about 10 MeV [38]. This component could hamper cross-section measurements for reactions with a threshold at lower energy, e.g., ^{238}U(n,f) or ^{235}U(n,f). For subactinide nuclei, with the fission reaction threshold of about 20 MeV or more, the influence of the low-energy background is negligible.

(iii) The energy and angular distribution of neutrons in the first component is defined only by the double-differential cross section (DDX) of the ^{7}Li(p,n) reaction. The basis of this assumption is that no significant amounts of material were present between the neutron production target and the fission samples.

Support for the last assumption is given by the fact that the neutron spectra measured at TSL agree with data from other sources. Figure 2 shows neutron spectra obtained in the course of earlier *n-p* scattering studies at TSL [35,39] at 0° for the peak neutron energies 98, 133, and 160 MeV (shown by filled circles). For comparison, neutron spectra from other facilities are shown as open symbols. The shown spectra were obtained by Byrd and Sailor [40] (triangles) and by Stamer *et al.* [41] (diamonds) at the Indiana University Cyclotron Facility, and by Nakao *et al.* [42] at the RIKEN facility (squares) at peak neutron energies close to the ones in the TSL data. For readability of Fig. 2, the spectra from Refs. [40–42] are shifted by a few MeV in order to match the position of the high-energy peaks. The solid curves represent the neutron spectrum calculations discussed further in the text.

As seen in Fig. 2, the neutron spectrum consists of a high-energy peak and a low-energy tail. The high-energy peak corresponds to the ^{7}Li(p,n) reactions that leave the ^{7}Be nucleus in the ground state or in the first excited state at 0.43 MeV. The low-energy tail is related to excitation of higher states in ^{7}Be and to break-up reactions.

The neutron spectrum calculations were performed in two different ways depending on the peak neutron energy. For peak energies below 45 MeV, interpolated and smoothed experimental data of Byrd and Sailor [40], Baba *et al.* [43], and Schuhmacher *et al.* [44] were used. In cases when the measured spectra do not cover a sufficiently wide range of secondary neutron energies, we used a constant extrapolation to lower energies, which was found to be a reasonable approximation, according to Nolte *et al.* [45]. Above 45 MeV, the

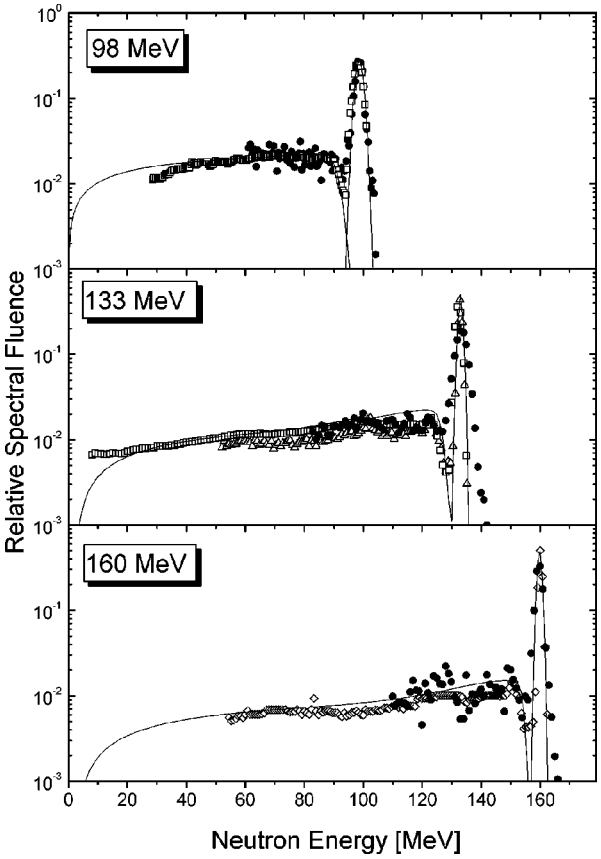

FIG. 2. Neutron spectra from the ^{7}Li(p,n) reaction at 0° for the peak energy of 98, 133, and 160 MeV. The filled circles represent measurements at the TSL neutron facility [35,39] in Irradiation position 2. The open symbols represent data from other facilities: the Indiana University Cyclotron Facility [40,41] (shown as triangles and diamonds, respectively) and the RIKEN facility [42] (shown as squares). The lines represent the neutron spectrum calculations discussed in the text. All spectra are normalized so that the area under the high-energy peak is unity.

calculations employed semiempirical systematics developed in [31], which is based on a phase-space distribution [46] corresponding to the three-body breakup process ^{7}Li$(p,n^{3}$He$)^{4}$He for description of the continuum part of neutron spectra and an empirical correction factor taking into account experimentally observed peculiarities of the high-energy part of the continuum spectra.

As has been mentioned, the experimental setup in Irradiation position 1 was placed at an angle of 4° with respect to the primary proton beam direction. As soon as the production of high-energy neutrons is strongly forward-peaked, the difference between the neutron spectra at 0° and 4° has to be taken into account.

A correction taking into account the decrease in high-energy peak neutron production at 4° relative to 0° was obtained by least-squares fitting to experimentally measured angular distributions from the literature [47–51], with subsequent fitting with respect to incident proton energy. The correction increases from 4% at 38 MeV to 24% at 177 MeV.

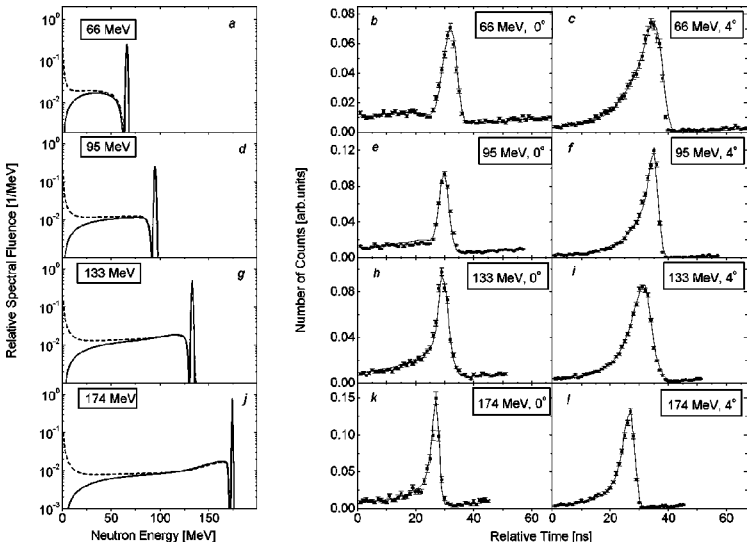

FIG. 3. Calculations of neutron spectra (left panel) for the incident proton energies of 69.1 (a), 96.8 (d), 136.7 (g), and 177.3 MeV (j) used in the present experiment for 0° (solid lines) and 4° (dashed lines). The middle panel (b, e, h, k) represents experimental (symbols) and calculated (lines) distributions of ^{238}U fission events induced by neutrons at a flight path of about 10 m at 0° (in Irradiation position 2). The right panel column (c, f, i, l) represents experimental (symbols) and calculated (lines) distributions of ^{238}U fission events induced by neutrons at a flight path of about 2 m at 4° (in Irradiation position 1).

For continuum neutron production, similar corrections were calculated, which depend on the incident proton energy and the secondary neutron energy. The calculations employed angular distribution data for continuum neutrons from the ^{7}Li(p,n) reaction included in the LA150 library [52]. The latter were obtained with the GNASH code [53], which, in turn, employs the Kalbach representation of the angular distribution [54]. At the 150–175 MeV region, where the LA150 data are not available, an extrapolation was made on the basis of the correction obtained at lower energies.

Validation of the calculations was carried out by means of folding of the calculated spectra with the standard ^{238}U neutron fission cross section [34], followed by conversion to the TOF scale and folding with a function that takes into account the time resolution of the measurement system. Modeled in this way, time distributions of ^{238}U neutron-induced fission events were compared with experimental data obtained both at 0° at Irradiation position 2 and at 4° at Irradiation position 1 simultaneously in the same neutron beam.

In Fig. 3, we show the calculated relative neutron spectral fluence at 0° and 4° for several incident proton energies used in the present experiment, and corresponding calculated and experimental time distributions of fission events in ^{238}U. The spectra at 4° are the sum of the two components mentioned above. The background component is described by a $1/E_n$ distribution. The relative intensity of the background component was fitted to reproduce the experimental distributions of the ^{238}U(n,f) events obtained at Irradiation position 1.

As seen in Fig. 3, the experimental time distributions of the ^{238}U(n,f) events can be successfully reproduced by the model. This ensures adequacy of the chosen representation of the neutron spectra.

C. Fission fragment detectors and experimental chambers

The fission fragments were detected by thin-film breakdown counters (TFBC). A detailed description of the TFBC technique can be found in [55] and references therein; only a brief description is given here. The operation principle of the TFBC is based on the phenomenon of electric breakdown in a MOS structure caused by an ion passing through a thin silicone dioxide layer. The breakdowns are nonshorting, since they lead to vaporization of a small part of the electrode area and leave no conducting path between the electrodes. The features of the TFBCs are threshold behavior, i.e., the insensitivity to light charged particles, neutrons and γ-radiation, real-time operation and good timing properties, easy operation (no high voltage required, no gases, large output signals, which makes preamplifiers unnecessary), compact design, and long-term stability under heavy radiation conditions. The last feature was of primary importance for the present experiment, because of the severe γ-radiation background in the Irradiation position 1.

The choice of detection system design is governed first by the low beam intensity, which necessitates the use of sandwich geometry, i.e., the detector has to be situated as close as possible to the fission sample. The sample-detector sandwich and its mechanical housing constitute an experimental chamber, which is placed in the neutron beam. The amount of material in a chamber along the beam direction is dominated by the thickness of the TFBC (0.3 mm Si). Consequently, the probability of interaction of an incident neutron with the chamber is small, and it is possible to stack several chambers after each other in the neutron beam without any significant influence on the beam characteristics. In this way, relative fission cross sections can be measured using detectors sandwiched with samples of different nuclides and being irradiated by the same neutron beam.

The detection system design is further governed by a trade-off between count rate and time resolution. The latter can be as good as several hundreds of picoseconds for a single TFBC of 1 cm^2 sensitive area. However, to get sufficient statistics, a larger area is required. This can only be achieved at the price of a worsening of the time resolution, because of the unavoidable spread in propagation time of signals originating from different parts of the sensitive area. To achieve both good timing and sufficient count rate, mosaic TFBC arrangements were employed.

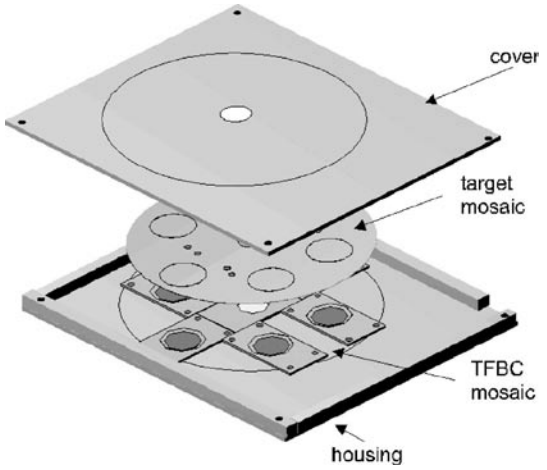

FIG. 4. The design of an experimental chamber.

The design of a single experimental chamber is shown in Fig. 4. The chamber consists of a mosaic arrangement of detectors, a similar arrangement of samples, and a thin mechanical housing. Each chamber contains six TFBCs with a diameter of about 1 cm, placed symmetrically in the plane perpendicular to the neutron beam direction. Six samples of the same nuclide were placed face-to-face to the detectors so that the sensitive area of each detector received fission fragments emitted by the corresponding sample in the forward hemisphere. The distance between the sample and the detector sensitive area (not more than 0.5 mm) could be passed by fission fragments in air without any significant energy loss. Therefore, evacuation of the chamber was not necessary. Upstream and downstream of the sample-detector sandwiches, the incident neutron beam passed through the entrance and exit windows, respectively, which were made of 0.2-mm-thick aluminum foils.

The entire experimental setup consisted of six to nine chambers described above, depending on the specific irradiation. The chambers were stacked along the neutron beam direction, so that each set of sample-detector sandwiches was exposed to virtually the same neutron fluence. Each chamber was equipped either with samples of one of the studied nuclides (^{209}Bi, ^{nat}Pb, ^{208}Pb, ^{197}Au, ^{nat}W, and ^{181}Ta) or with the monitor samples (^{238}U or ^{209}Bi).

All detectors have common bias voltage and a common signal output. Typically, the mosaic arrangement provides an output pulse height of about 1–2 V and a time resolution of about 2 ns (full width at half maximum).

D. Fission samples

The samples were prepared by deposition on circular 0.1-mm-thick aluminum backings of 1 cm^2 area. In all cases, the area of the sample exceeded the sensitive area of the respective TFBC. Therefore, the latter defined the effective area of the sandwich.

The employed deposition techniques, the chemical composition, and the thickness of the samples are listed in Table II. The samples of ^{208}Pb and ^{238}U had an isotopic purity of 98.7% and 99.999%, correspondingly, while the other samples contained either monoisotopic elements (^{209}Bi, ^{197}Au, ^{181}Ta) or natural isotopic compositions (^{nat}Pb, ^{nat}W).

TABLE II. Characteristics of the fission samples.

Target	Chemical composition	Deposition technique	Average sample thickness (mg/cm^2)
^{238}U	$^{238}U_3O_8$	multiple smearing	0.1–1.1
^{209}Bi	^{209}Bi	vacuum evaporation	1.1–3.1
^{nat}Pb	^{nat}Pb	vacuum evaporation	1.1–2.4
^{208}Pb	^{208}Pb	vacuum evaporation	1.3–2.4
^{197}Au	^{197}Au	vacuum evaporation	2.8
^{nat}W	$^{nat}WO_3$	vacuum evaporation	2
^{181}Ta	^{181}Ta	magnetron evaporation	0.5–1.2

The thickness of the samples was determined by Rutherford backscattering spectroscopy (in the case of the subactinide targets), by direct α-spectroscopy (in the case of ^{238}U), and/or by direct weighing of the sample backing before and after deposition of the material.

Since the expected fission cross sections of the studied subactinide nuclei were a few orders of magnitude smaller than those of actinide nuclei, the actinide contamination of the samples was checked using the following techniques:

(i) Direct α-spectroscopy measurements using semiconductor detectors.

(ii) α-activity measurements using low-background nuclear track detectors [56].

(iii) Irradiation by a 21-MeV neutron beam. Because of the very low fission cross sections of the studied nuclei at this energy, virtually all detected fission events could be attributed to actinide contaminants.

In addition, an upper limit of the contamination could be deduced from the TOF spectra of fission events accumulated during the irradiations. The results obtained with the listed techniques were mutually compatible. The obtained upper limit for the relative abundance of actinide nuclei in the subactinide samples amounted to 10^{-5}–10^{-6} depending on the studied nuclide.

E. Electronics and data acquisition system

A schematic view of the electronics and the data acquisition system is shown in Fig. 5. Since the signals from the TFBCs are large (see Sec. II C), they could be fed into a fast multichannel leading-edge discriminator without any preceding amplification. The discrimination level could always be set so that virtually all detector pulses were accepted. The logical signals from the discriminator were summed and fed into the start input of a TDC. A pulse, phase-locked to the cyclotron RF, served as the stop signal for the TDC. In addition, the discriminated signal from each fission chamber was recorded by a scaler, and this information was used in the analysis to separate the TOF spectra of fission events from the different chambers. The TOF spectra and the count-

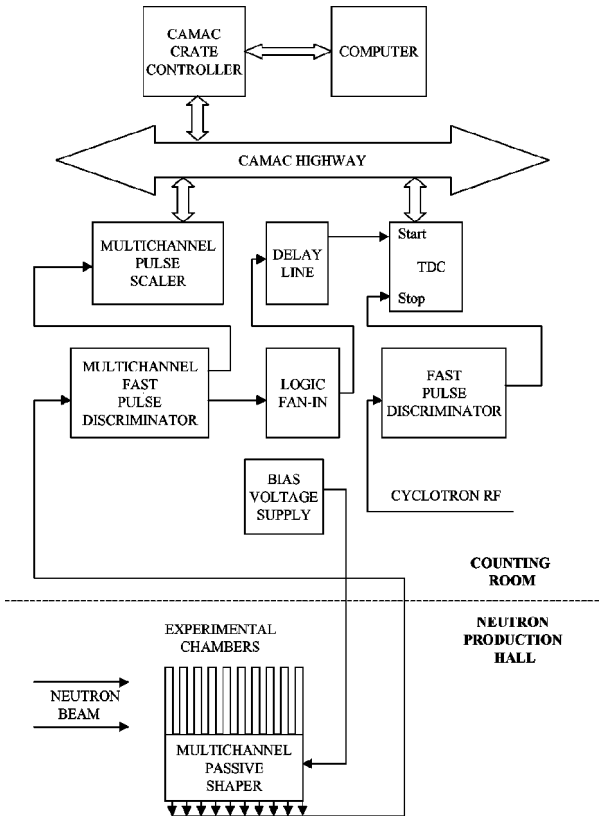

FIG. 5. A schematic view of the electronics and the data acquisition system.

rate data were stored in a computer on an event-by-event basis and could be inspected on-line.

As discussed above, in most cases it was not possible to fully separate the high-energy peak fissions from those of the low-energy tail using TOF techniques. Nevertheless, TOF techniques were useful for rejection of intrinsic detector background events, as well as of those from spontaneous fission of contaminating nuclides. In addition, inspection of the low-energy part in the TOF spectra allowed us to check that no significant actinide contamination was present in the subactinide fission samples.

III. DATA ANALYSIS

A. Fission cross-section ratio

The number of detected fission events per unit incident energy, induced by neutrons with an arbitrary spectrum, is

$$n_f(E) = \rho S_{sample} \varphi_n(E) \sigma_f(E) \varepsilon(E), \tag{1}$$

where E is the incident neutron energy, ρ is the number of nuclei in the sample per unit area, S_{sample} is the sample area (1 cm^2 in our case), $\varphi_n(E)$ is the spectral density of the neutron fluence, $\sigma_f(E)$ is the fission cross section, and $\varepsilon(E)$ is the detection efficiency, defined as the ratio of the number of detected fragments to the number of fissions in the sample.

The efficiency, as defined above, accounts for the anisotropy of the fragment angular distribution in the laboratory frame, as well as for loss of fragments due to a possible mismatch between the area of the sample and the sensitive area of the TFBC, S_{TFBC}. Since each TFBC was exposed to a calibration sample of 1 cm^2 area containing ^{252}Cf, the difference between S_{sample} and individual S_{TFBC} was automatically taken into account, and the detection efficiency for fragments of neutron-induced fission can be expressed as

$$\varepsilon(E) = k_\varepsilon(E) \varepsilon^{\mathrm{Cf}}, \tag{2}$$

$$\varepsilon^{\mathrm{Cf}} = n_{sf}/a_{sf}, \tag{3}$$

where n_{sf} is the count rate of fragments from spontaneous fission, a_{sf} is the spontaneous fission activity of the ^{252}Cf sample, and

$$k_\varepsilon^X(E) = \frac{\varepsilon_{ac}^X(E)}{\varepsilon_{ac}^{\mathrm{Cf}}}, \tag{4}$$

where $\varepsilon_{ac}^{\mathrm{Cf}}$ and ε_{ac}^X are the calculated absolute detection efficiencies of the TFBC and a sample of unit area for the fragments of ^{252}Cf spontaneous fission and induced fission of nuclide X, respectively.

Combining Eqs. (1) and (2) gives

$$n_f(E) = \langle \rho \varepsilon^{\mathrm{Cf}} \rangle k_\varepsilon^X(E) \varphi_n(E) \sigma_f(E), \tag{5}$$

where $\langle \rho \varepsilon^{\mathrm{Cf}} \rangle$ is the product of the values ρ and $\varepsilon^{\mathrm{Cf}}$ averaged over all sandwiches for the corresponding fission chamber. Integration over the entire incident neutron spectrum gives the total number of detected fissions,

$$N_f = \langle \rho \varepsilon^{\mathrm{Cf}} \rangle \int_0^{E_{\max}} k_\varepsilon^X(E) \varphi_n(E) \sigma_f(E) dE. \tag{6}$$

The number of fissions induced by the high-energy peak neutrons in the quasimonoenergetic spectrum can be obtained by integration over the peak only. Since the relative efficiency and the fission cross section vary slowly with energy, they can be replaced by the values corresponding to the peak energy E_0, i.e., $k_{\varepsilon 0} = k_\varepsilon^X(E_0)$ and $\sigma_{f0} = \sigma_f(E_0)$. Thus,

$$N_{fpeak} = \langle \rho \varepsilon^{\mathrm{Cf}} \rangle k_{\varepsilon 0} \sigma_{f0} \Phi_{n0}, \tag{7}$$

where Φ_{n0} is the fluence of the high-energy peak neutrons. The fraction of detected fissions due to the peak, $k_{peak} = N_{fpeak}/N_f$, can be deduced from Eqs. (6) and (7),

$$k_{peak} = \frac{\sigma_{f0} k_{\varepsilon 0} \Phi_{n0}}{\int_0^{E_{\max}} k_\varepsilon(E) \varphi_n(E) \sigma_f(E) dE}. \tag{8}$$

Combining Eqs. (6) and (8) gives the peak fission cross section

$$\sigma_{f0} = \frac{N_f k_{peak}}{\langle \rho \varepsilon^{\mathrm{Cf}} \rangle k_{\varepsilon 0} \Phi_{n0}}. \tag{9}$$

Finally, the fission cross-section ratio measured with a pair of sandwich arrangements X and Y, stacked one after the other in the neutron beam, is

$$\frac{\sigma_{f0(X)}}{\sigma_{f0(Y)}} = \frac{N_{f(X)}\langle\rho\varepsilon^{\mathrm{Cf}}\rangle_{(Y)}k_{peak(X)}\varepsilon^{X}_{ac}(E_0)R^2_{(X)}}{N_{f(Y)}\langle\rho\varepsilon^{\mathrm{Cf}}\rangle_{(X)}k_{peak(Y)}\varepsilon^{Y}_{ac}(E_0)R^2_{(Y)}}, \qquad (10)$$

where R is the distance between the production target and the chamber. The quantities $\langle\rho\varepsilon^{\mathrm{Cf}}\rangle$, R, and N_f were obtained in direct measurements for the respective chambers. The latter quantity was corrected for intrinsic detector background on the basis of the obtained TOF spectra of fission events. The determination of the remaining parameters in Eq. (10), $\varepsilon^{X}_{ac}(E)$ and k_{peak}, is discussed in Secs. III B and III C, respectively.

B. Determination of the detection efficiency

The detection efficiency of a TFBC in sandwich geometry cannot be directly measured for a particle source with unknown intensity and arbitrary angular-energy distribution, since the counting characteristics (efficiency versus bias voltage) does not have a plateau corresponding to detection of all fragments that reach the sensitive area. Instead, a model calculation has to be employed, and the parameters of the model have to be determined in dedicated measurements for each specific detector (or for a group of detectors with similar properties), operated at a given bias voltage.

A model and a computer code for calculation of the TFBC detection efficiency have been described in our earlier report [32]. A thorough description is going to be published elsewhere [33]. A brief outlook of the model and the code is given below.

The model and the code are based on semiempirical dependences of the detection threshold voltage on specific energy losses of fission fragments in SiO_2 and on the incident angle of fission fragments to the sensitive surface of the detector [57]. The code makes use of Monte Carlo techniques to model the process of detection for fission fragments from either spontaneous or nucleon-induced fission. The model takes into account angular anisotropy of fission and transferred longitudinal momentum that define angular distributions of fission fragments. A change in fission fragment kinetic energy due to the transferred momentum is taken into account, as well as the energy losses of fission fragments in the sample material and their dependence on the fragment angular distribution.

The input data of the code include the following.

(i) Charge, mass, and kinetic energy distributions of fission fragments, taking into account the emission of prefission neutrons. In the case of the ^{238}U(n,f) reaction, experimental data of Zoller [58] were employed. At present, data of this type for neutron-induced fission of subactinide nuclei remain unmeasured. Therefore, we used symmetric Gaussian-shaped charge and mass distributions that are typical for similar fissioning systems formed in reactions of charged particles with subactinide nuclei [59,60].

(ii) The total kinetic energy of fission fragments from the systematics of Viola *et al.* [61].

(iii) Energy-range data [62] for fission fragments in sample materials and SiO_2.

(iv) Energy-dependent data on fission anisotropy and longitudinal linear momentum transferred to fissioning nuclei, from systematics developed in [26].

The code was verified using experimental results for TFBC detection efficiency for spontaneous fission of ^{252}Cf as well as for proton- and neutron-induced fission of different nuclides [32,33]. The estimated error of the calculated efficiency is not more than 5% for the whole range of the projectile energies.

The calculated absolute efficiency is plotted in Fig. 6 versus incident neutron energy for the samples of $^{238}U_3O_8$, ^{209}Bi, ^{nat}Pb, ^{208}Pb, ^{197}Au, $^{nat}WO_3$, and ^{181}Ta samples employed in the present study. The values given in the graphs represent the sample thickness, averaged over the corresponding mosaic arrangement. As can be seen, the efficiency for a given sample material and neutron energy decreases with the sample thickness, which reflects the increase in the fraction of fragments escaping detection due to the energy loss in the sample. The results for different sample materials show a decrease in efficiency from the heaviest considered nuclides, ^{238}U and ^{209}Bi, to the lightest, ^{181}Ta, which is mainly governed by a decrease in the average fragment kinetic energy. A special case is the samples of tungsten trioxide. The presence of oxygen atoms in the sample material increases its stopping power and, therefore, diminishes the detection efficiency. This effect is not so pronounced for

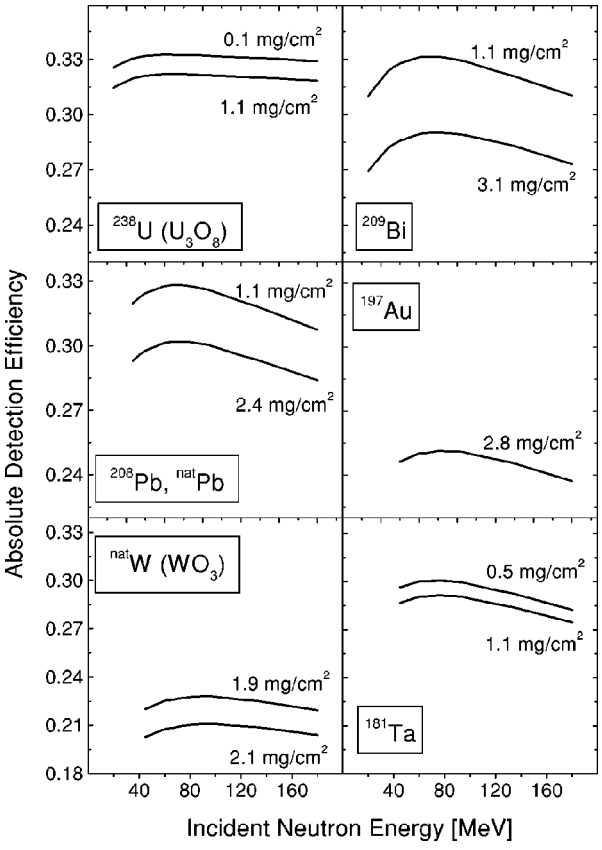

FIG. 6. The calculated fission fragment detection efficiency for the TFBC and a sample of the unit area, versus incident neutron energy.

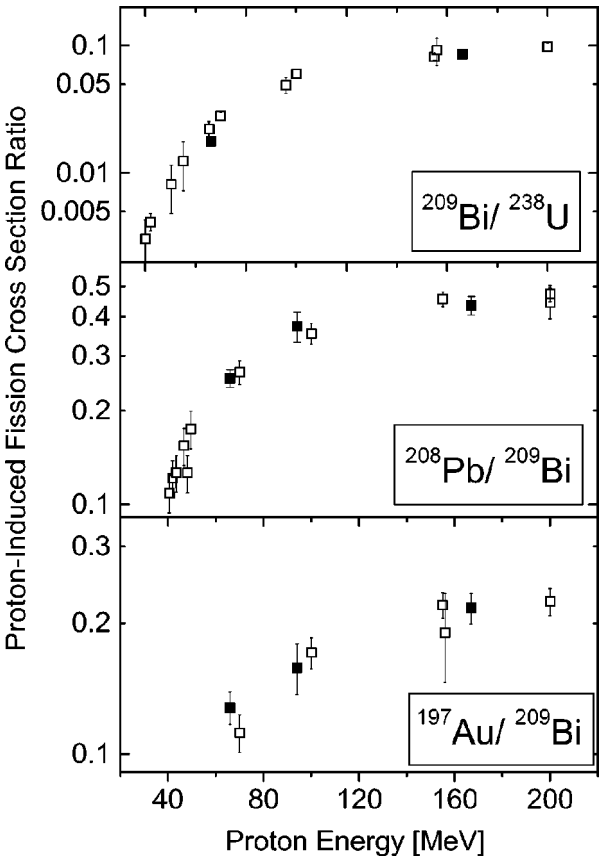

FIG. 7. Energy dependences of the ^{209}Bi/^{238}U, ^{208}Pb/^{209}Bi, and ^{197}Au/^{209}Bi proton-induced fission cross-section ratios. The filled symbols represent the results of the present work. The open symbols represent results extracted from a compilation of literature experimental data [9].

the $^{238}U_3O_8$ samples because of their relatively small thickness.

The same model and code were employed in processing of experimental data on proton-induced fission cross sections [32], obtained at the broad proton beam facility at TSL [63] with the same detector arrangement as in the present study. The relative (p,f) cross-section results are presented in Fig. 7 together with data of other authors from a review [9]. As seen in Fig. 7, the data of our work [32] agree with the literature data within the uncertainty limits. This provides an additional check of the developed model and code for detection efficiency calculations.

C. Determination of the fraction of peak fission events

To determine the fraction of peak fission events, k_{peak}, defined in Eq. (8), two different methods were employed.

(i) For the ^{238}U(n,f) reaction, we used TOF techniques supplemented by model calculations (see Sec. III C 1).

(ii) For the other studied reactions, an iterative unfolding procedure was used (see Sec. III C 2).

Uncertainties in determination of the factor k_{peak} are discussed in Sec. III C 3.

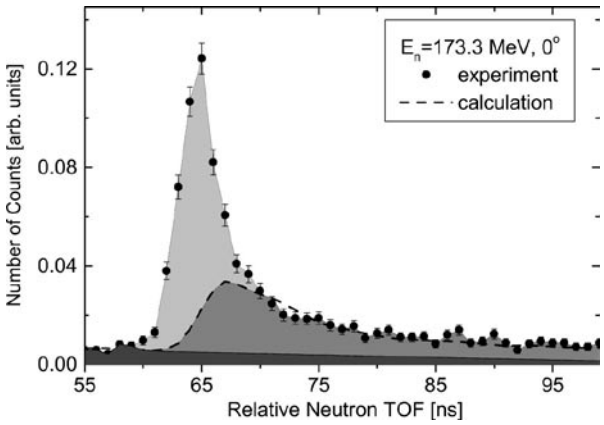

FIG. 8. The TOF spectrum of ^{238}U neutron-induced fission events induced by neutrons from the 7Li(p,n) reaction with the peak neutron energy of 173.3 MeV and its decomposition. The symbols represent experimental data of the present work. The dashed curve represents calculated TOF distribution of fission events induced by the continuum part of the neutron spectrum. The light-gray area represents fission events induced by high energy peak neutrons. The events in the dark-gray area originate from high energy continuum neutrons with energy above about 60 MeV. The black area corresponds to fission events induced by "wrap-around" neutrons with energy lower than 60 MeV, which are produced by previous proton beam micropulses.

1. Determination of the factor k_{peak} using TOF techniques

Distributions of ^{238}U fission events on the relative neutron TOF were measured using an experimental chamber placed at a flight path of about 10 m at 0°. An exemplary distribution, shown in Fig. 8, was obtained in irradiation by neutrons with the peak energy of 173.3 MeV. The light-gray area in the spectrum corresponds to fission events induced by the high-energy peak neutrons. Thus, the sought factor is a ratio between the light-gray area and the total area under the spectrum.

Fission events in the dark-gray area in Fig. 8 originate from high-energy continuum neutrons with energy above about 60 MeV. The black area corresponds to fission events induced by "wrap-around" neutrons with energy lower than 60 MeV, which are produced by previous proton beam micropulses. In order to estimate and subtract the last two components, the studied TOF distribution was modeled. Input data for the model calculations included the standard ^{238}U(n,f) cross section [34] and the incident neutron spectra. The latter were either calculated according to the systematics [31] or interpolated or extrapolated from the experimentally measured spectra [35,39–44]. The resulting values of the factor k_{peak} are given in Table III.

Similar TOF spectra were obtained for ^{209}Bi fission events at the same flight path of about 10 m. However, the statistics was not sufficient for the spectrum decomposition procedure. The decomposition was not possible either for the nuclides lighter than Bi, because those measurements were performed only at a short flight path. Therefore, for all subactinide nuclei, we had to skip the TOF information and to employ an

TABLE III. Correction factor k_{peak} for the ^{238}U(n,f) and ^{209}Bi(n,f) reactions for neutron spectra at 0°.

E_{npeak} (MeV)	$k_{peak}(^{238}\mathrm{U})$	$k_{peak}(^{209}\mathrm{Bi})$
34.5	0.55±0.02	0.98±0.02
34.5	0.43±0.02[a]	0.97±0.02[a]
34.5	0.35±0.02[b]	0.96±0.02[b]
46.3	0.44±0.01	0.95±0.03
66.6	0.37±0.01	0.82±0.01
73.9	0.36±0.01	0.81±0.01
89.6	0.37±0.01	0.73±0.02
94.1	0.37±0.01	0.71±0.02
111.3	0.37±0.01	0.67±0.02
132.9	0.39±0.01	0.64±0.01
144.6	0.35±0.01	0.61±0.01
173.3	0.42±0.01	0.63±0.01

[a]Correction factor at the position of the facility for activation studies [36,38] at about 1°.
[b]Correction factor at the irradiation position 1 at about 4°.

iterative unfolding procedure discussed in the subsequent subsection.

2. Determination of the factor k_{peak} using the iterative unfolding procedure

The unfolding procedure in the present work is similar to the one that was implemented in an analysis of neutron-induced single-event upsets performed by Johansson *et al.* [64]. However, the present study makes use of a more advanced description of the incident neutron spectrum (see Sec. II B). The procedure is described below for the ^{209}Bi(n,f) reaction.

To get a first estimate of the factor k_{peak}, we constructed a trial input cross section $\sigma_f(^{209}\mathrm{Bi}) = \sigma_f(^{238}\mathrm{U}) N_f(^{209}\mathrm{Bi})/N_f(^{238}\mathrm{U})$, where $\sigma_f(^{238}\mathrm{U})$ is the standard ^{238}U(n,f) cross section [34], and N_f denotes the fission count rate for a given nuclide, integrated over the whole corresponding TOF spectrum. The trial cross section, fitted by a smooth curve, together with the experimental [35,39–44] or calculated [31] neutron spectra at 0° and the relative detection efficiency, were used to calculate the factor k_{peak} for each beam energy employed in the study. Then, the ^{209}Bi/^{238}U fission cross-section ratios were calculated according to Eq. (10), using the factors $k_{peak}(^{209}\mathrm{Bi})$ obtained as described above and the factors $k_{peak}(^{238}\mathrm{U})$ obtained with TOF techniques as described in Sec. III C 1. Finally, multiplication of the obtained ^{209}Bi/^{238}U ratios and the standard ^{238}U(n,f) cross section [34], with subsequent smoothing of the energy dependence, resulted in the new trial ^{209}Bi(n,f) cross section. The procedure was repeated until convergence was reached. Usually, two iterations were sufficient. The correction in the last iteration did not exceed 0.5%. The resulting values of $k_{peak}(^{209}\mathrm{Bi})$ are presented in Table III.

A similar procedure was employed for the studied reactions with the nuclei lighter than Bi. In this case, only the calculated neutron spectra at 4° were used. The factor k_{peak} for the monitor ^{209}Bi(n,f) reaction was calculated using the parametrization of the experimental cross section obtained in the present work (see Sec. IV D). In all cases, the result was found to be independent of the initially assumed cross section.

3. Uncertainties in the factor k_{peak}

The uncertainties in the factor k_{peak} amounted to 2–3 % depending on the neutron energy and the studied reaction. In the case of the ^{238}U(n,f) reaction, the uncertainties reflect statistical errors in the TOF spectra, as well as uncertainties in the input data of the model calculations and ambiguities in the spectrum decomposition procedure. For the other reactions, the uncertainties reflect the ones in the neutron spectrum data, which served as input in the unfolding procedure.

The studied excitation functions of the subactinide fission reactions have rather similar shapes, and therefore it is possible to further suppress the contribution that comes from the determination of the factor to the total uncertainty in the relative cross-section measurement. For this purpose, we studied sensitivity of the ratio $k_{peak}(X)/k_{peak}(^{209}\mathrm{Bi})$ (where X denotes the studied target nuclide) to the neutron spectrum data used as input in the unfolding procedure. Using different experimental [42,43] and calculated [31] neutron spectra, we estimated that the variation in the ratio $k_{peak}(X)/k_{peak}(^{209}\mathrm{Bi})$ did not exceed 1% for any studied nuclide.

IV. EXPERIMENTAL RESULTS

A. The ^{209}Bi(n,f) cross section

The ^{209}Bi/^{238}U ratios measured in the present work were converted into absolute values using the standard ^{238}U(n,f) cross section taken from the work of Carlson *et al.* [34]. The ^{209}Bi(n,f) cross sections obtained in our earlier studies [21,22] have been revised using the new approach to the fission fragment detection efficiency and the factor k_{peak}, and have been taken into account in processing of the results of the present work. The results are presented in Table IV.

TABLE IV. Neutron-induced fission cross section of ^{209}Bi.

E_{npeak} (MeV)	^{209}Bi$(n,f)/^{238}$U(n,f) cross-section ratio	^{209}Bi(n,f) cross section (mb)
34.5	$(1.90\pm0.20)\times10^{-4}$	0.311±0.034
46.3	$(1.05\pm0.10)\times10^{-3}$	1.71±0.17
66.6	0.0054±0.0005	8.42±0.81
73.9	0.0082±0.0007	12.6±1.2
89.6	0.0133±0.0012	19.2±1.9
94.1	0.0157±0.0014	22.4±2.2
111.3	0.0247±0.0027	33.5±3.9
132.9	0.0307±0.0027	40.5±4.1
144.6	0.0335±0.0031	44.2±4.7
160.0	0.0415±0.0038	54.6±5.7
173.3	0.0417±0.0040	54.9±5.9

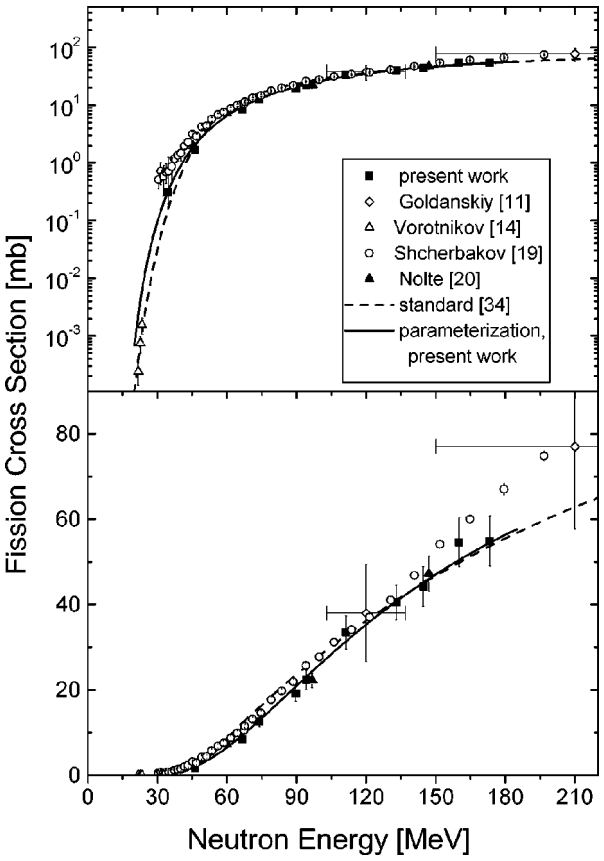

FIG. 9. Absolute neutron-induced fission cross sections of ^{209}Bi. The scale of the vertical axis is logarithmic and linear in the upper and lower panels, respectively, in order to show the behavior of the cross section in the different energy regions.

The uncertainties in the absolute fission cross sections given in Table IV include the uncertainty in the standard ^{238}U(n,f) cross section [34], which amounts to 2–5 % depending on the neutron energy. The uncertainties in the relative measurements are discussed in Sec. IV B for all studied reactions together.

Our data on the ^{209}Bi(n,f) cross sections are shown in Fig. 9 together with earlier data of Vorotnikov *et al.* [14], as well as with recent data of Nolte *et al.* [20] and Shcherbakov *et al.* [19]. In order to avoid complicating the figure, we do not show data of Staples *et al.* [17,18], because they are very close to the results of Shcherbakov *et al.* [19].

As seen in Fig. 9, our data agree within the uncertainties with the data of Shcherbakov *et al.* [19] in the neutron energy range above about 95 MeV. However, there is a systematic deviation at lower energies. The latter data systematically exceed our data in the energy range from 30 to about 95 MeV. The deviation is most clearly seen in the energy region below about 50 MeV. This could possibly be explained by a well-known problem of nonfission background in ionization chambers discussed frequently in the literature (see, e.g., [29]). The data of Nolte *et al.* [20] are in good agreement with our data in the entire neutron-energy range of their measurements.

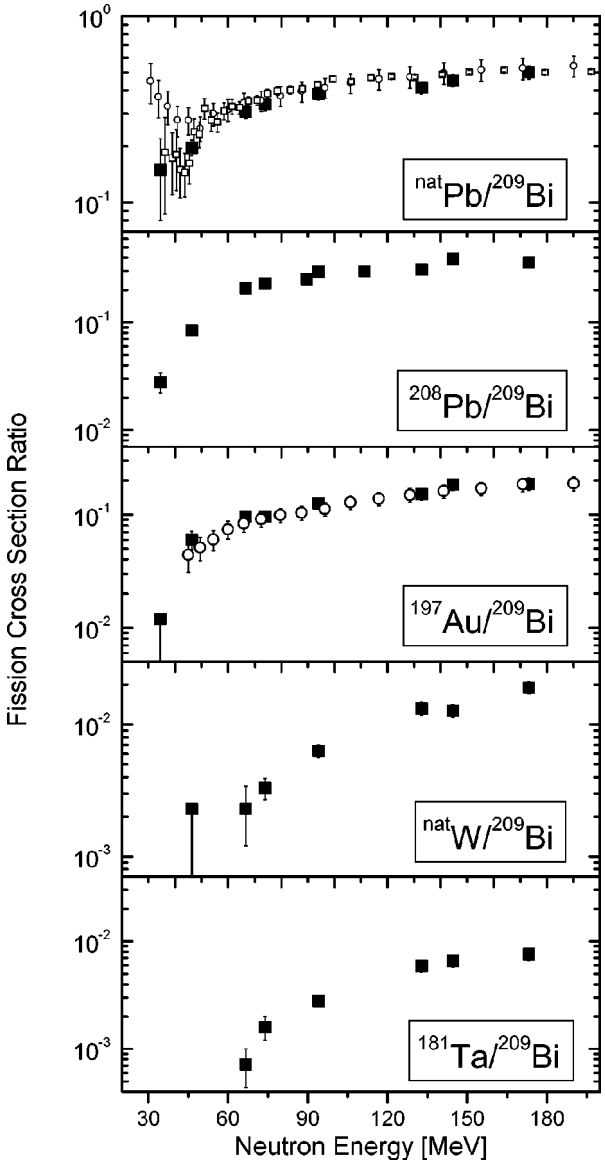

FIG. 10. Neutron-induced fission cross-section ratios ^{nat}Pb/^{209}Bi, ^{208}Pb/^{209}Bi, ^{197}Au/^{209}Bi, ^{nat}W/^{209}Bi, and ^{181}Ta/^{209}Bi versus incident energy. The results of the present study are shown as filled squares. The open squares and circles show data deduced from the results of Shcherbakov *et al.* [19] and Staples *et al.* [17,18], respectively.

The ^{209}Bi(n,f) cross section has been adopted as standard in 1996 [34], and the corresponding parametrization is shown in Fig. 9 as a dashed line. However, in the recommendations of the IAEA [34], it was noted that the available experimental database was not sufficient, and new experimental results were needed in order to make a more accurate parametrization. Such new parametrization is suggested in the present work (see Sec. IV D) and shown in Fig. 9 as a solid line. A comparison of the recent parametrization with the standard one [34] shows considerable differences. The standard fit lies about 40% lower than the new one in the

TABLE V. Relative neutron-induced fission cross sections for the nuclei lighter than Bi.

E_{npeak} (MeV)	Fission cross-section ratios $^{nat}Pb/^{209}Bi$	$^{208}Pb/^{209}Bi$	$^{197}Au/^{209}Bi$	$^{nat}W/^{209}Bi$	$^{181}Ta/^{209}Bi$
34.5	0.15±0.07	0.028±0.006	<0.012		
46.3	0.197±0.019	0.084±0.007	0.060±0.011	<0.0023	
66.6	0.306±0.023	0.208±0.016	0.096±0.011	0.0023±0.0011	(7.2±2.8)10⁻4
73.9	0.336±0.026	0.230±0.018	0.096±0.010	0.0033±0.0006	0.0016±0.0004
89.6		0.252±0.020			
94.1	0.383±0.028	0.297±0.023	0.126±0.013	0.0063±0.0007	0.0028±0.0003
111.3		0.301±0.026			
132.9	0.414±0.031	0.310±0.024	0.151±0.017	0.0132±0.0015	0.0059±0.0007
144.6	0.452±0.034	0.39±0.03	0.184±0.021	0.0127±0.0014	0.0066±0.0008
173.3	0.50±0.04	0.36±0.03	0.187±0.023	0.019±0.002	0.0076±0.0009

20–45 MeV energy range, and about 20% higher between 50 and 90 MeV. For energies above 90 MeV, the standard fit lies not more than 10% higher than the new one. The mentioned differences, however, are within the declared uncertainties for the standard parametrization [34].

B. Relative cross sections for the nuclei lighter than Bi

The fission cross-section ratios obtained in this work for the nuclei lighter than Bi are given in Table V and are shown in Fig. 10 together with data deduced from the previously reported results of Staples *et al.* [17,18] for $^{209}Bi/^{235}U$, $^{nat}Pb/^{235}U$, and $^{197}Au/^{235}U$ fission cross-section ratios and Shcherbakov *et al.* [19] for $^{209}Bi/^{235}U$ and $^{nat}Pb/^{235}U$.

The following uncertainties for the relative fission cross sections were considered.

(i) Sample thickness determination (2–7 % depending on specific sample arrangement).

(ii) Counting statistics in the ^{252}Cf calibration (1–2 % depending on specific detector arrangement).

(iii) Calculation of relative detection efficiency (5%).

(iv) Variations of neutron beam intensity, sample thickness, and detection efficiency from one sandwich to another in a mosaic arrangement ($\leqslant$0.3% in most cases, 0.6% in the worst case).

(v) In-beam counting statistics and subtraction of background (0.5–50 % depending on neutron energy and specific detector-sample arrangement).

(vi) Determination of the fraction of peak fission events k_{peak} ($\leqslant$4% for the $^{209}Bi/^{238}U$ ratio and $\leqslant$1% for the other ratios, see Sec. III C 3).

The total uncertainties of the obtained cross-section ratios given in Tables IV and V amount typically to 10–15 %, depending on the studied reaction and neutron energy. At the lowest energy points, the total uncertainties are dominated by statistical errors and amount to 20–50 % depending on the studied reaction.

A number of other possible error sources were considered. The direct measurements of the irradiation geometry gave uncertainty contributions of not more than 0.1%. The influence on the results caused by proton (and/or H^0 atom) contamination in the neutron field was estimated using the (p,f)

TABLE VI. Absolute neutron-induced fission cross sections.

E_{npeak} (MeV)	Fission cross section ^{nat}Pb (mb)	^{208}Pb (mb)	^{197}Au (mb)	^{nat}W (mb)	^{181}Ta (mb)
34.5	0.047±0.021	0.0087±0.0021	<0.0038		
46.3	0.336±0.044	0.143±0.018	0.103±0.019	<0.004	
66.6	2.58±0.30	1.75±0.21	0.81±0.12	0.020±0.010	0.0061±0.0024
73.9	4.24±0.47	2.90±0.33	1.20±0.17	0.041±0.008	0.020±0.005
89.6		4.8±0.5			
94.1	8.6±1.0	6.6±0.8	2.81±0.39	0.141±0.020	0.063±0.009
111.3		10.1±1.3			
132.9	16.8±1.7	12.6±1.3	6.1±0.9	0.53±0.08	0.24±0.04
144.6	20.0±2.3	17.3±2.0	8.1±1.2	0.56±0.08	0.29±0.05
173.3	27.5±3.7	19.9±2.7	10.3±1.6	1.04±0.15	0.42±0.07

systematics [9] and was found to be negligible. The attenuation of the neutron beam along the stack of the experimental chambers in Irradiation position 1 was measured directly with a pair of chambers with ^{209}Bi samples placed upstream and downstream of the other chambers in the stack, and no significant effect was found. No correction was necessary for neutron-induced and spontaneous fission of contaminating heavier nuclides in the subactinide samples. The calibrations with a ^{252}Cf sample were performed before and after each experimental period, in order to reveal possible changes in the detector efficiency and sensitive area. In addition, possible drifts of the detector parameters during the beam exposure were checked by monitoring the respective count-rate ratios. In all cases, no effect was found outside the statistical uncertainties.

In many cases, the presented data were determined with samples of different thicknesses and obtained during different experimental periods. In all cases, the results agreed within the uncertainties, and therefore the respective weighted average values were adopted as final.

The presented upper limits of the cross sections were obtained using the prescriptions of Schmidt *et al.* [65] for analysis of data with small counting statistics.

C. Absolute cross sections for the nuclei lighter than Bi

The relative fission cross sections for the nuclei lighter than Bi were converted into absolute ones using the revised set of the experimental ^{209}Bi(n,f) cross-section data given in Table IV. The resulted absolute cross sections are given in Table VI and shown in Fig. 11 together with our earlier data for ^{208}Pb [21,22], as well as with earlier data of Reut *et al.* for ^{197}Au and $^{\text{nat}}$Pb [12], Dzhelepov *et al.* for $^{\text{nat}}$W [13], Vorotnikov *et al.* [14], Shcherbakov *et al.* [19], and Nolte *et al.* [20] for $^{\text{nat}}$Pb, Vorotnikov [15], and Staples *et al.* [17,18] for ^{197}Au. The given uncertainties of our results include those of the new data set for the ^{209}Bi(n,f) cross section (see Table IV). The absolute data of Staples *et al.* shown in Fig. 11 were deduced by multiplying the ^{197}Au/^{235}U ratios [17,18] with the standard ^{235}U(n,f) cross section [34].

D. Cross-section parametrizations

Parametrizations of the absolute (n,f) cross sections of subactinide nuclei suggested in the present work are based on our data presented in Tables IV and VI, together with the data of Nolte *et al.* [20] for ^{209}Bi and $^{\text{nat}}$Pb. The following universal parametrization of the cross section σ_f versus neutron energy E_n is suggested:

$$\sigma_f(E_n) = P_1 \exp[-(P_2/E_n)^{P_3}], \tag{11}$$

where P_1, P_2, and P_3 are fitting parameters that depend on the target nuclide. The values of the parameters, obtained by the least-squares method, are given in Table VII. The parametrizations are shown as solid lines in Figs. 9 and 11.

V. DISCUSSION

The first published measurement results are presented for the $^{\text{nat}}$Pb, ^{197}Au, $^{\text{nat}}$W, and ^{181}Ta(n,f) cross sections. The

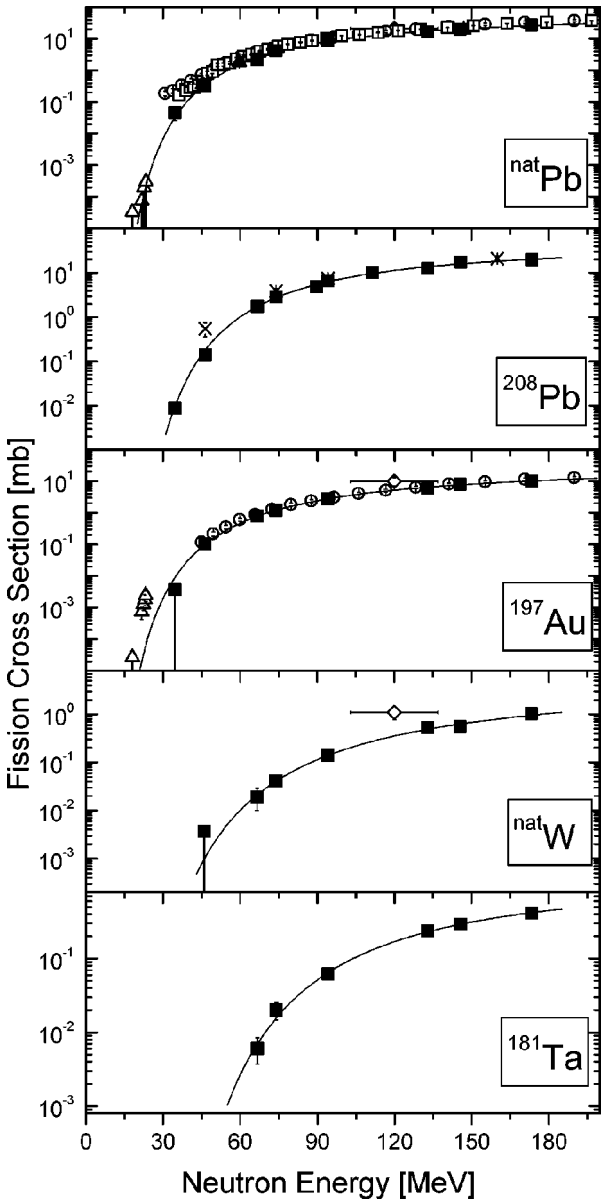

FIG. 11. Absolute neutron-induced fission cross sections of $^{\text{nat}}$Pb, ^{208}Pb, ^{197}Au, $^{\text{nat}}$W, and ^{181}Ta. The results of the present study are shown as filled squares. Crosses represent our earlier data for ^{208}Pb [21,22]. Filled triangles represent recent data of Nolte *et al.* for $^{\text{nat}}$Pb [20]. Open squares, circles, and triangles represent data of Shcherbakov *et al.* [19], Staples *et al.* [17,18], and Vorotnikov *et al.* [14,15], respectively. Results of Reut *et al.* [12] and Dzhelepov *et al.* [13] are shown as diamonds, with horizontal error bars that represent the energy spread of the neutron beam. The lines represent parametrizations of the present work (see the text).

^{208}Pb(n,f) reaction has been studied by our group earlier [21,22], and those results, shown as crosses in Fig. 11, are in reasonable agreement with the present ones. The only exclusion is the datum at 45 MeV, which is believed to be erroneous in our early study, due to a poor signal-to-background ratio in that particular measurement. The present results are

TABLE VII. Parameters of the (n,f) cross-section parametrizations in Eq. (11).

Target nuclide	P_1 (mb)	P_2 (MeV)	P_3	χ^2/ν	Energy region of applicability (MeV)
^{209}Bi	109.2	131.5	1.32	1.33	30–180
^{nat}Pb	70.4	171.9	1.27	0.53	30–180
^{208}Pb	45.4	150.3	1.47	0.64	30–180
^{197}Au	35.0	207.2	1.18	0.09	45–180
^{nat}W	6.1	292.5	1.17	0.47	60–180
^{181}Ta	1.29	186.0	1.61	0.32	60–180

obtained with better counting statistics and more sophisticated data processing techniques.

Earlier measurements for ^{197}Au and ^{nat}Pb in the energy region 18–23 MeV were performed by Vorotnikov [15] and Vorotnikov and Larionov [14], respectively, using a *d*-*T* neutron source and solid-state nuclear track detectors. Their results for ^{nat}Pb are compatible with the present data, while the results for ^{197}Au seem to be too high.

A measurement for ^{nat}Pb and ^{197}Au was performed by Staples *et al.* [17,18] using a parallel-plate ionization chamber irradiated by neutrons from the LANSCE facility with a "white" spectrum. Only preliminary data are available. The data for ^{197}Au are in reasonable agreement with the present ones, while the data for ^{nat}Pb lie systematically higher. In the energy range below about 50 MeV, the data of Staples *et al.* for ^{nat}Pb are distinctly larger. The disagreement increases with decreasing incident energy and amounts to about one order of magnitude at 35 MeV. Furthermore, the ^{nat}Pb/^{209}Bi ratios deduced from the data of Staples *et al.* (see Fig. 10) show an unexpected energy dependence. As the neutron energy decreases to below 50 MeV, the smooth decrease of the ratio turns into a sharp rise, which is difficult to understand, having in mind that the fission barrier for lead isotopes is higher than that for bismuth [66]. This leads to the suggestion that some background contribution may not have been fully taken into account in the LANSCE measurements. A similar feature is seen in the dataset of Shcherbakov *et al.* for ^{nat}Pb [19] obtained at the "white" neutron source at the GNEIS facility in Gatchina. Their data are similar to the data of Staples *et al.* at neutron energies above about 45 MeV, although at lower energies they are somewhat closer to our results. The disagreement with our data amounts to a factor of about 3 at about 35 MeV.

Early measurements by Reut *et al.* [12] for ^{nat}Pb and ^{197}Au and by Dzhelepov *et al.* [13] for ^{nat}W were made using neutrons from the Cu(d,n) reaction with a broad spectrum, as indicated by the horizontal error bars in Fig. 11. The results agree qualitatively with the more recent and precise data.

The data presented in Fig. 11 allow some conclusions on common features of subactinide neutron fission cross sections. The cross section increases with neutron energy and with the atomic number of the target nucleus. The slope of the cross section versus energy is steepest in the near-barrier region (20–25 MeV), and becomes flatter with increasing energy. The slope at a specific incident energy is steeper for lighter nuclei. The properties summarized above (see also [24]) are similar to those of the (p,f) data (see, e.g., [9]).

VI. CONCLUSIONS

Experimental (n,f) cross sections for subactinide nuclei in the intermediate energy region have been measured. Most of the data are obtained for the first time. Progress in data processing has been achieved due to good control of the incident neutron spectrum and the detection efficiency corrections. In most cases, the results are compatible with scarcely available earlier data, but a large discrepancy is observed with respect to the recent data of Staples *et al.* [17,18] and Shcherbakov *et al.* [19] for the ^{209}Bi(n,f) and ^{nat}Pb(n,f) cross sections at energies below 50 MeV.

ACKNOWLEDGMENTS

The authors are thankful to the staff of The Svedberg Laboratory where the experimental part of the study was performed. The samples were partly provided and/or characterized by Dr. S.M. Soloviev, Dr. Yu.G. Pokrovskiy, and Dr. A.V. Gromov at V.G. Khlopin Radium Institute. The present work was supported in part by ISTC.

[1] H. Nifenecker, S. David, J. M. Loiseaux, and O. Meplan, Nucl. Instrum. Methods Phys. Res. A **463**, 428 (2001).
[2] A. J. Koning, J.-P. Delaroche, and O. Bersillon, Nucl. Instrum. Methods Phys. Res. A **414**, 49 (1998).
[3] Yu. N. Shubin, A. V. Ignatyuk, A. Yu. Konobeev, V. P. Lunev, and E. V. Kulikov, in *Proceedings of the 2nd Conference on ADTT, Kalmar, Sweden, 1996*, edited by H. Condé (Uppsala University, 1997), Vol. 2, p. 953.
[4] R. E. Prael, Trans. Am. Nucl. Soc. **73**, 349 (1995).
[5] A. V. Prokofiev, S. G. Mashnik, and A. J. Sierk, Nucl. Sci. Eng. **131**, 78 (1999).
[6] M. C. Duijvestijn, A. J. Koning, J. P. M. Beijers, A. Ferrari, M. Gastal, J. van Klinken, and R. W. Ostendorf, Phys. Rev. C **59**, 776 (1999).
[7] R. Michel and P. Nagel, NEA Report NSC/DOC(97)-1, January, 1997.
[8] W. U. Schröder and J. R. Huizenga, Nucl. Phys. **A502**, 473 (1989).
[9] A. V. Prokofiev, Nucl. Instrum. Methods Phys. Res. A **463**, 557 (2001).
[10] E. L. Kelly and C. Wiegand, Phys. Rev. **73**, 1135 (1948).
[11] V. I. Goldanskiy, V. S. Penkina, and E. Z. Tarumov, Sov. Phys. JETP **29**, 778 (1955) (in Russian).
[12] A. A. Reut, G. I. Selivanov, and V. V. Yuriev, Institute of

Nuclear Problems report, Moscow, 1950 (in Russian).
[13] V. P. Dzhelepov, B. M. Golovin, and Yu. M. Kazarinov, Institute of Nuclear Problems report, Moscow, 1950 (in Russian).
[14] P. E. Vorotnikov and L. S. Larionov, Sov. J. Nucl. Phys. **40**, 552 (1984).
[15] P. E. Vorotnikov, Sov. J. Nucl. Phys. **47**, 1147 (1988).
[16] H. Vonach, A. Pavlik, R. Nelson, and S. Wender (unpublished); R. E. Prael, Report LA-UR-94-1817, Los Alamos National Laboratory, 1994 (unpublished); H. Vonach (private communication).
[17] P. Staples, P. W. Lisowski, and N. W. Hill, presented in APS/AAPT Conference, Washington, D.C., 1995; Bull. Am. Phys. Soc. **40**, 962 (1995).
[18] P. Staples (private communication) (1996) with an update of the data from Ref. [17].
[19] O. Shcherbakov, A. Donets, A. Evdokimov, A. Fomichev, T. Fukahori, A. Hasegawa, A. Laptev, V. Maslov, G. Petrov, S. Soloviev, Y. Tuboltsev, and A. Vorobyev, J. Nucl. Sci. Technol. **2**, 230 (2002).
[20] R. Nolte, M. S. Allie, P. J. Binns, F. D. Brooks, A. Buffler, V. Dangendorf, K. Langen, J.-P. Meulders, W. D. Newhauser, F. Ross, and H. Schuhmacher, J. Nucl. Sci. Technol. **2**, 311 (2002).
[21] V. P. Eismont, A. V. Prokofiev, A. N. Smirnov, K. Elmgren, J. Blomgren, H. Condé, J. Nilsson, N. Olsson, T. Rönnqvist, and E. Tranéus, Phys. Rev. C **53**, 2911 (1996).
[22] V. P. Eismont, A. V. Prokofiev, A. N. Smirnov, J. Blomgren, H. Condé, K. Elmgren, J. Nilsson, N. Olsson, and E. Ramström, in *Proceedings of the 2nd International Conference on Accelerator Driven Transmutation Technologies and Applications, Kalmar, Sweden, 1996*, edited by H. Condé (Uppsala University, 1997), Vol. 2, p. 606.
[23] V. P. Eismont, A. V. Prokofiev, A. N. Smirnov, S. M. Soloviev, H. Condé, K. Elmgren, and N. Olsson, Proceedings of the 3rd International Conference on Accelerator Driven Transmutation Technologies and Applications, Praha (Pruhonice), Czech Republic, 1999 (available as CD-ROM, paper Mo-O-C8).
[24] V. P. Eismont (Project Manager), Measurements of Neutron-Induced Fission Cross Sections in Energy Region $15 < En < 160$ MeV for Basic and Applied Researches, Final Project Technical Report of ISTC 540-97, V.G.Khlopin Radium Institute, St.-Petersburg, 1999.
[25] V. P. Eismont, I. V. Ryzhov, A. N. Smirnov, G. A. Tutin, H. Condé, N. Olsson, and A. V. Prokofiev, Proceedings of the 6th OECD/NEA Information Exchange Meeting on Actinide and Fission Product Partitioning and Transmutation, Madrid, 2000 (available as CD-ROM, paper 36).
[26] A. Prokofiev, Ph.D. thesis, Uppsala University (2001).
[27] V. P. Eismont, A. V. Kireev, I. V. Ryzhov, G. A. Tutin, H. Condé, K. Elmgren, and S. Hultqvist, in *Proceedings of the 2nd International Conference on Accelerator Driven Transmutation Technologies and Applications, Kalmar, Sweden, 1996*, edited by H. Condé (Uppsala University, 1997), Vol. 2, p. 618.
[28] V. P. Eismont, A. V. Kireev, I. V. Ryzhov, S. M. Soloviev, G. A. Tutin, H. Condé, K. Elmgren, N. Olsson, and P.-U. Renberg, Proceedings of the 3rd International Conference on Accelerator Driven Transmutation Technologies and Applications, Praha, Czech Republic, 1999 (available as CD-ROM, paper Mo-O-C7).
[29] I. V. Ryzhov, G. A. Tutin, V. P. Eismont, A. G. Mitryukhin, V. S. Oplavin, S. M. Soloviev, H. Condé, N. Olsson, and P.-U. Renberg, J. Nucl. Sci. Technol. **2**, 1410 (2002).
[30] R. K. Jain, A. V. Prokofiev, A. N. Smirnov, and L. Tommasino, Radiat. Meas. **34**, 129 (2001).
[31] A. V. Prokofiev, S. G. Mashnik, M. B. Chadwick, N. Olsson, and L. S. Waters, J. Nucl. Sci. Technol. **2**, 112 (2002).
[32] V. P. Eismont (Project Manager), Measurements and Comparison of Proton- and Neutron-Induced Fission Cross Sections of Lead and Neighboring Nuclei in the 20-200 MeV Energy Region, Final Project Technical Report of ISTC 1309-99, V.G. Khlopin Radium Institute, St.-Petersburg, 2002.
[33] V. P. Eismont, A G. Mitryukhin, V. S. Oplavin, I. V. Ryzhov, A. N. Smirnov, S. M. Solovjev, G. A. Tutin, H. Conde, N. Olsson, O. Jonson, and P.-U. Renberg, TSL Progress Report 2000–2001, edited by A. Ingemarsson (Uppsala University, 2002), p. 42; A. N. Smirnov, N. P. Filatov, A. V. Prokofiev, and P.-U. Renberg (unpublished).
[34] A. D. Carlson, S. Chiba, F.-J. Hambsch, N. Olsson, and A. N. Smirnov, IAEA Report INDC(NDS)-368, Vienna, 1997; Proceedings of the International Conference on Nuclear Data for Science and Technology, Trieste, Italy, 1997, Part II, p. 1223.
[35] H. Condé, S. Hultqvist, N. Olsson, T. Rönnqvist, R. Zorro, J. Blomgren, G. Tibell, A. Hakånsson, O. Jonsson, A. Lindholm, L. Nilsson, P.-U. Renberg, A. Brockstedt, P. Ekström, M. Österlund, F. P. Brady, and Z. Szeflinski, Nucl. Instrum. Methods Phys. Res. A **292**, 121 (1990).
[36] J. Klug, J. Blomgren, A. Atac, B. Bergenwall, S. Dangtip, K. Elmgren, C. Johansson, N. Olsson, A. V. Prokofiev, J. Rahm, O. Jonsson, L. Nilsson, P.-U. Renberg, P. Nadel-Turonski, A. Ringbom, A. Oberstedt, F. Tovesson, C. Le Brun, J. F. Lecolley, F. R. Lecolley, M. Louvel, N. Marie, C. Schweitzer, C. Varignon, Ph. Eudes, F. Haddad, M. Kerveno, T. Kirchner, C. Lebrun, L. Stuttge, I. Slypen, A. N. Smirnov, R. Michel, S. Neumann, and U. Herpers, Nucl. Instrum. Methods Phys. Res. A **489**, 282 (2002).
[37] J. F. Ziegler, J. P. Biersack, and U. Littmark, *The Stopping and Range of Ions in Solids* (Pergamon Press, New York, 1985).
[38] S. Neumann, Ph.D. thesis, University of Hannover (1999); R. Michel, W. Glasser, S. Neumann, A. N. Smirnov, A. V. Prokofiev, P. Malmborg, and O. Jonsson, The Svedberg Laboratory Progress Report 1998-1999, Uppsala, 2000, p. 20 (unpublished).
[39] T. Rönnqvist (private communication).
[40] R. C. Byrd and W. C. Sailor, Nucl. Instrum. Methods Phys. Res. A **274**, 494 (1989).
[41] S. Stamer, W. Scobel, and R. C. Byrd, Proceedings of a Specialists' Meeting on Neutron Cross-Section Standards for the Energy Region above 20 MeV, Uppsala, Sweden, 1991, NEANDC-305/U, p. 154.
[42] N. Nakao, Y. Uwamino, T. Nakamura, T. Shibata, N. Nakanishi, M. Takada, E. Kim, and T. Kurosawa, Nucl. Instrum. Methods Phys. Res. A **420**, 218 (1999).
[43] M. Baba, Y. Nauchi, T. Iwasaki, T. Kiyosumi, M. Yoshioka, S. Matsuyama, N. Hirakawa, T. Nakamura, Su. Tanaka, S. Meigo, H. Nakashima, Sh. Tanaka, and N. Nakao, Nucl. Instrum. Methods Phys. Res. A **428**, 454 (1999).
[44] H. Schuhmacher, H. J. Brede, V. Dangendorf, M. Kuhfuss, J. P. Meulders, W. D. Newhauser, and R. Nolte, Nucl. Instrum. Methods Phys. Res. A **421**, 284 (1999).
[45] R. Nolte, M. S. Allie, P. J. Binns, F. Brooks, A. Buffler, V.

Dangendorf, J. P. Meulders, F. Roos, H. Schuhmacher, and B. Wiegel, Nucl. Instrum. Methods Phys. Res. A **476**, 369 (2002).
[46] G. G. Ohlsen, Nucl. Instrum. Methods **37**, 240 (1965).
[47] S. D. Schery, L. E. Young, R. R. Doering, S. M. Austin, and R. K. Bhowmik, Nucl. Instrum. Methods **147**, 399 (1977).
[48] H. Orihara, S. Nishihara, K. Furukawa, M. Kabasawa, T. Kawamura, Y. Takahashi, T. Nakagawa, and K. Maeda, Nucl. Instrum. Methods Phys. Res. A **257**, 189 (1987).
[49] C. J. Batty, B. E. Bonner, E. Friedman, C. Tschalar, L. E. Williams, A. S. Clough, and J. B. Hunt, Nucl. Phys. **A120**, 297 (1968).
[50] J. W. Watson, B. D. Anderson, A. R. Baldwin, C. Lebo, B. Flanders, W. Pairsuwan, R. Madey, and C. C. Foster, Nucl. Instrum. Methods Phys. Res. **215**, 413 (1983).
[51] X. Yang, L. Wang, J. Rapaport, C. D. Goodman, C. C. Foster, Y. Wang, E. Sugarbaker, D. Marchlenski, S. de Lucia, B. Luther, L. Rybarcyk, T. N. Taddeucci, and B. K. Park, Phys. Rev. C **52**, 2535 (1995).
[52] S. G. Mashnik, M. B. Chadwick, P. G. Young, R. E. MacFarlane, and L. S. Waters, LANL Report LA-UR-00-1067, Los Alamos (2000) (unpublished); presented at 2000 ANS/ENS International Meeting, Nuclear Applications of Accelerator Technology (AccApp00), November 12-16, Washington, D.C.; http://xxx.lanl.gov/e-print/nucl-th/0011066.
[53] M. B. Chadwick, P. G. Young, S. Chiba, S. C. Frankle, G. M. Hale, H. G. Hughes, A. J. Koning, R. C. Little, R. E. MacFarlane, R. E. Prael, and L. S. Waters, Nucl. Sci. Eng. **131**, 293 (1999).
[54] C. Kalbach, Phys. Rev. C **37**, 2350 (1988).
[55] V. P. Eismont, A. V. Prokofiev, and A. N. Smirnov, Radiat. Meas. **25**, 151 (1995).
[56] V. A. Nikolaev, Radiat. Meas. **25**, 337 (1995).
[57] V. P. Eismont and A. N. Smirnov, Prib. Tekh. Eksp. **6**, 5 (1983) (in Russian).
[58] C. M. Zoller, Ph.D. thesis, University of Darmstadt (1995) (in German).
[59] Yu. P. Gangrskiy, B. Dalhsuren, and B. N. Markov, *Nuclear Fission Fragments* (Energoatomizdat, Moscow, 1986) (in Russian).
[60] M. C. Duijvestijn, A. J. Koning, and F.-J. Hambsch, Phys. Rev. C **64**, 014607 (2001).
[61] V. E. Viola, K. Kwiatkowski, and M. Walker, Phys. Rev. C **31**, 1550 (1985).
[62] L. C. Northcliffe and R. F. Schilling, At. Data Nucl. Data Tables **A7**, 233 (1970).
[63] O. Jonsson, P.-U. Renberg, A. Prokofiev, and A. Smirnov, TSL Progress Report 1998-1999, edited by A. Ingemarsson, Uppsala University (2000), p. 43 (unpublished).
[64] K. Johansson, P. Dyreklev, B. Granbom, N. Olsson, J. Blomgren, and P.-U. Renberg, IEEE Trans. Nucl. Sci. **45**, 2519 (1998).
[65] K.-H. Schmidt, C.-C. Sahm, K. Pielenz, and H.-G. Clerc, Z. Phys. A **316**, 29 (1984).
[66] A. V. Ignatyuk, G. N. Smirenkin, M. G. Itkis, S. I. Mulgin, and V. N. Okolovich, Sov. J. Part. Nucl. **16**, 307 (1985).

Appendix II

A NEW NEUTRON FACILITY FOR SINGLE-EVENT EFFECT TESTING

A. V. Prokofiev, L.-O. Andersson, T. Bergmark, O. Byström, H. Calén, L. Einarsson, C. Ekström, J. Fransson, K. Gajewski, N. Haag, T. Hartman, E. Hellbeck, T. Johansen, O. Jonsson, B. Lundström, L. Pettersson, D. Reistad, P.-U. Renberg, D. Wessman, V. Ziemann, J. Blomgren[1)], S. Pomp[1)], M. Österlund[1)], U. Tippawan[1,2)]

The Svedberg Laboratory, Uppsala University, Box 533, S-751 21 Uppsala, Sweden

1) Department of Neutron Research, Uppsala University, Box 525, S-751 20 Uppsala, Sweden

2) Fast Neutron Research Facility, Chiang Mai University, P.O. Box 217, Chiang Mai 50202, Thailand

Abstract

A new facility producing intense mono-energetic neutron beams has been developed at The Svedberg Laboratory (TSL), Uppsala, Sweden. The facility utilizes the existing cyclotron and a flexible lithium target in a rebuilt beam line. The new facility can operate at unsurpassed mono-energetic neutron intensities and provides flexibility of the neutron beam properties, like energy and geometrical shape.

1. Introduction

Careful testing of neutron-induced single-event effects (SEE) in semiconductor materials [1] using the natural flux of cosmic neutrons is very time-consuming. To speed up the measurements, one needs to use neutron beams produced with particle accelerators.

The procedures for the accelerated testing of memory devices are summarized in the recent JEDEC Test Specification [2]. According to the standard, one of the ways to perform the accelerated testing is to irradiate a device under study by monoenergetic neutrons with nominal energies of 20, 50, 100, and 150 MeV. Such an approach is a viable alternative to the testing with a "white" neutron spectrum, if the intensity of monoenergetic neutrons is enough to cause reasonably high SEE rates.

To satisfy these needs, an upgrade of the old neutron facility [3, 4] at The Svedberg Laboratory (TSL) has been undertaken with a primary goal to increase the neutron beam intensity and, thereby, to make the facility competitive for SEE testing and for studies of SEE mechanisms. In addition, the new facility offers an unsurpassed flexibility of the neutron beam properties, like energy and geometrical shape.

2. Technical Specification

An overview of the neutron beam facility is presented in Fig. 1. The facility makes use of the proton beam from the Gustaf Werner cyclotron with the energy variable in the 20-180 MeV range. The proton beam is incident on a target of lithium, enriched to 99.99% in ^{7}Li. The available targets are 2, 4, 8, 16, and 24 mm thick. The targets are rectangular in shape, 20x32 mm, and are mounted in a remotely controlled water-cooled copper rig. An additional target position contains a fluorescent screen viewed by a TV camera, which is used for beam alignment and focusing. Downstream the target, the proton beam is deflected by a magnet into a 10-m long dumping line, where it is guided onto a heavily shielded water-cooled graphite beam dump.

The neutron beam is formed geometrically by a cylindrically shaped iron collimator block, 50 cm in diameter and 100 cm long, with a cylindrical or conical hole of variable diameter. The collimator is surrounded by concrete to form the end wall of the production line towards the experimental area. Thereby, efficient shielding from the production target region is achieved. A modular construction of the collimator allows the user to adjust the diameter of the neutron beam to the needs of a specific experiment. At present, the available collimator openings are 2, 3, 5.5, 10, 15, 20, and 30 cm. Other collimator diameters in the 0-30 cm range, as well as other shapes than circular can be provided upon request. Even beam diameters of up to 1 m are obtainable at a larger distance from the production target. The increased diameter of the beam may be used for testing a larger number of devices simultaneously, or a larger device like a whole electronic card.

After passing the collimator, neutrons reach the experimental area at a distance of about 3 m from the production target. Reduction of this distance to the minimum has led to an increase of the neutron flux by about one order of magnitude in comparison with the old TSL neutron facility [3, 4].

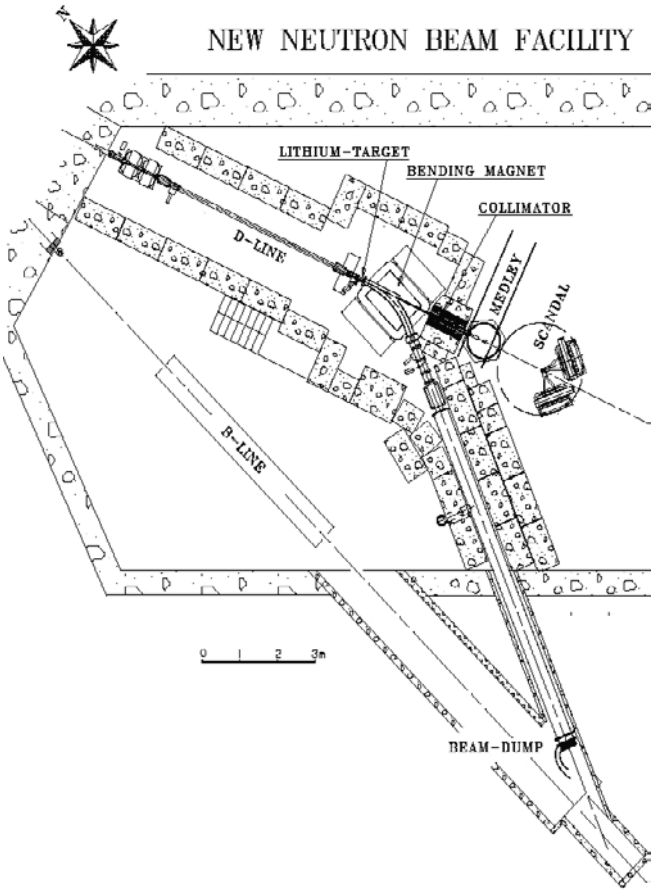

Figure 1. An overview of the neutron beam facility.

3. Commissioning, tests and characterization of the facility

The first neutron beam at the new facility was delivered in January 2004. An extensive characterization of the facility has been performed, including measurements of neutron flux, spectra, and profile. Below, first results are reported. They were acquired with a proton beam of about 100 MeV energy and about 5 μA intensity, incident on an 8-mm thick lithium target.

3.1 Dumping efficiency

The dumping efficiency, i.e., the share of primary protons that reach the beam dump after passing the lithium target, was typically 90-95%. Taking into account the uncertainty in the measurement of about 10% and loss of protons due to nuclear reactions in the target (up to 2% depending on proton energy and target thickness), one can conclude that few protons are lost on their way from the target to the dump.

3.2 Neutron flux

The typical neutron flux during the test runs amounted to about $5*10^5$ $cm^{-2}s^{-1}$ at the entrance to the experimental area. This value is about one order of magnitude larger than at the old neutron facility at TSL [3, 4] with the same target thickness, proton energy and current.

3.3 Neutron spectrum

First results for the neutron spectrum at the experimental area are shown in Fig. 2. The spectrum is mainly defined by the double-differential cross-section of the ^{7}Li(p,n) reaction at forward angles. The reaction energy spectrum is dominated by a peak situated a few MeV below the energy of the primary protons. The high-energy peak in the neutron spectrum comprises about half of the total number of neutrons. The measured spectra (shown by symbols connected by a solid line) are compared with predictions of the systematics for the ^{7}Li(p,n) reaction developed by Prokofiev et al. [5] (shown by a dashed line in panels *b, c, d*). For the lowest of the studied incident energies (24.7 MeV), the systematics [5] is not applicable. Instead, an evaluation of Mashnik et al. [6] was employed for the description of the neutron spectrum. The differential cross-section for high-energy peak neutron production at 0° was obtained my multiplication of the total cross-section of the ^{7}Li(p,n)^{7}Be reaction [6] to the "index of forwardness" from the systematics of Uwamino et al. [7]. The narrow peaks in the upper continuum region correspond to excitation of higher states in residual ^{7}Be nuclei. This process was included in the model calculation of Mashnik et al. [6]. However, the energy resolution in the experiment does not allow us to observe these peaks.

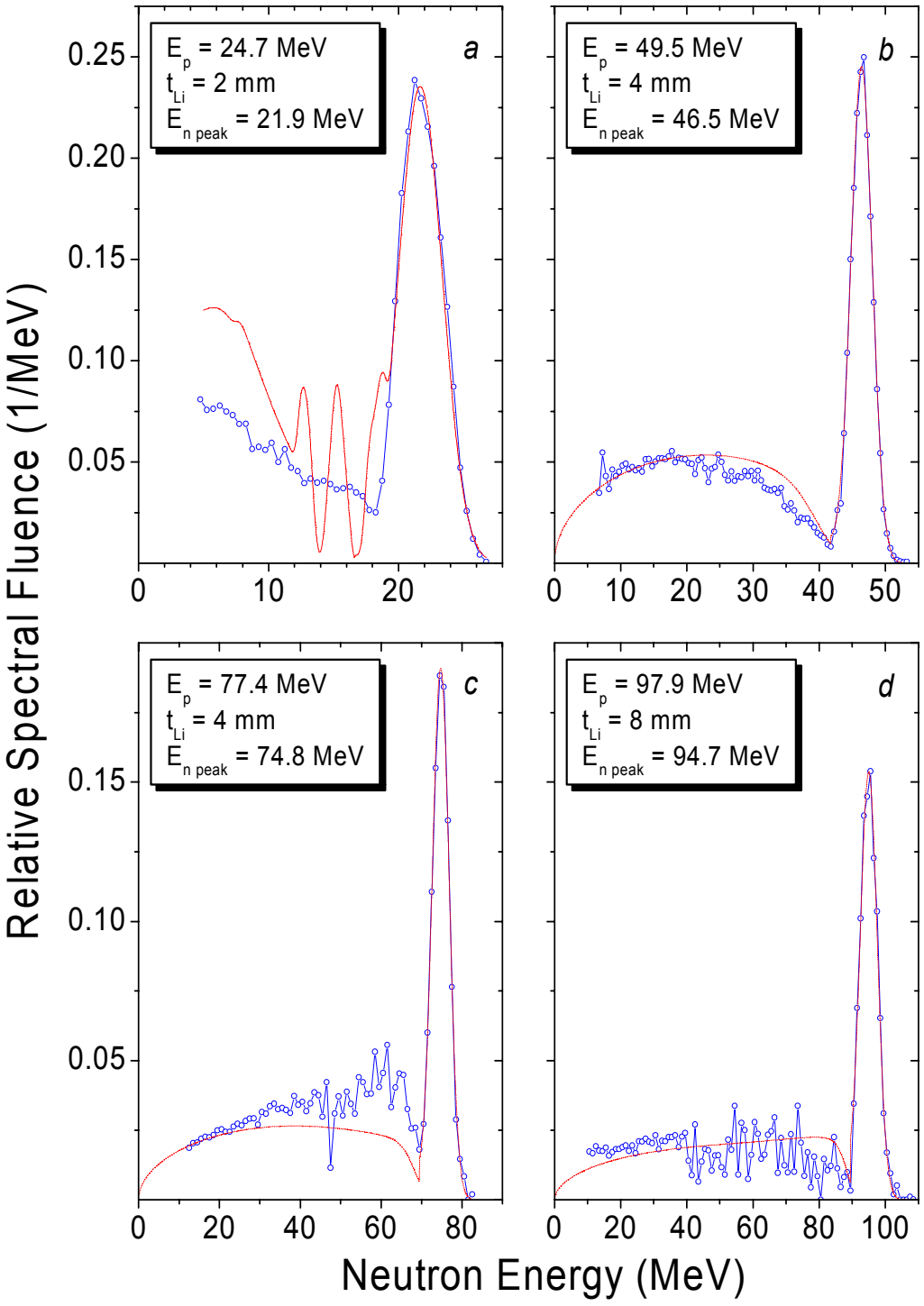

Figure 2. The neutron spectra at 0º for different incident proton energies and ^{7}Li target thicknesses. Symbols connected by a solid line represent experimental data obtained in the present work. A dashed line in panels *b, c, d* represents the predictions of the systematics developed by Prokofiev et al [5]. A dash-dotted line in panel *a* represents the LA150 evaluation [6] combined with systematics of Uwamino et al [7]. In all cases, the width of the predicted high-energy peak component is adjusted to the experimental data. Both experimental and calculated data are normalized so that the area under the high-energy peak is unity.

The overall agreement between the presented experimental data and the calculations [5, 6] is not worse than to a factor of 2.

3.4 Contamination of the neutron beam

Measured contamination of the neutron beam at the experimental area due to interactions of the primary protons with beam transport elements (mainly the target frame) did not exceed 0.2%. Such interactions can only lead to a weak surplus of neutrons at the experimental area, because any charged particles produced near the lithium target and upstream are bent away by the deflection magnet.

The contamination of protons (above 15 MeV) in the neutron beam amounts to about 10^{-5}, which can hardly be a problem for any application.

3.5 Residual radioactivity

No significant excess of radioactivity over natural background has been detected in the experimental area. This, together with the fully functional laboratory radiation protection system, ensures safety for beam users and personnel.

3.6 Availability for users

The facility is now available for regular operation. First beams for commercial electronics testing, as well as applied nuclear physics research, have already been delivered.

4. Summary and outlook

A new neutron facility, optimized for SEE testing, has been constructed and put into operation at TSL, Uppsala, Sweden. The facility is capable to deliver neutrons in the 20-175 MeV range. This makes TSL the only laboratory in the world offering full monoenergetic neutron testing according to the JEDEC Test Specification [2]. In addition, TSL offers testing with protons in the 20-180 MeV energy range, and with a wide range of heavy ions. Thus, TSL has the unique feature to provide neutron, proton, and heavy ion testing at the same laboratory.

Further information on the neutron facility and characterization measurements is presented elsewhere [8].

References

[1] H. H. K. Tang, *IBM J. Res. Develop*., vol. 40, pp. 91-108 (1996).

[2] JEDEC Standard. Measurements and Reporting of Alpha Particles and Terrestrial Comic Ray-Induced Soft Errors in Semiconductor Devices. JESD89, August 2001.

[3] H. Condé, S. Hultqvist, N. Olsson, T. Rönnqvist, R. Zorro, J. Blomgren, G. Tibell, A. Håkansson, O. Jonsson, A. Lindholm, L. Nilsson, P.-U. Renberg, A. Brockstedt, P. Ekström, M. Österlund, F. P. Brady, and Z. Szeflinski. *Nucl. Instr. Meth. A*, vol. 292, pp. 121-128 (1990).

[4] J. Klug, J. Blomgren, A. Ataç, B. Bergenwall, S. Dangtip, K. Elmgren, C. Johansson, N. Olsson, S. Pomp, A.V. Prokofiev, J. Rahm, U. Tippawan, O. Jonsson, L. Nilsson, P.-U. Renberg, P. Nadel-Turonski, A. Ringbom, A. Oberstedt, F. Tovesson, V. Blideanu, C. Le Brun, J.F. Lecolley, F.R. Lecolley, M. Louvel, N. Marie, C. Schweitzer, C. Varignon, Ph. Eudes, F. Haddad, M. Kerveno, T. Kirchner, C. Lebrun, L. Stuttgé, I. Slypen, A.N. Smirnov, R. Michel, S. Neumann, and U. Herpers, *Nucl. Instr. Meth. A*, vol. 489, pp. 282-303 (2002).

[5] A.V. Prokofiev, M.B. Chadwick, S.G. Mashnik, N. Olsson, and L.S. Waters, *J. Nucl. Sci. Techn.*, Suppl. 2, pp. 112-115 (2002).

[6] S.G. Mashnik, M.B. Chadwick, P.G. Young, R.E. MacFarlane, and L.S. Waters, LANL Report LA-UR-00-1067 (2000).

[7] Y. Uwamino et al., Nucl. Instr. Meth. A, vol. 389, pp. 463-473 (1997).

[8] S. Pomp et al., Int. Conf. on Nuclear Data for Science and Technology, Santa Fé, NM, September 26 – October 1, 2004 (accepted).

Appendix III

Measurement of the Absolute np Scattering Differential Cross Section at 194 MeV

M. Sarsour,[1] T. Peterson,[1,*] M. Planinic,[1,†] S. E. Vigdor,[1] C. Allgower,[1] B. Bergenwall,[2] J. Blomgren,[2] T. Hossbach,[1] W. W. Jacobs,[1] C. Johansson,[2] J. Klug,[2] A. V. Klyachko,[1] P. Nadel-Turonski,[2] L. Nilsson,[2] N. Olsson,[2] S. Pomp,[2] J. Rapaport,[3] T. Rinckel,[1] E. J. Stephenson,[1] U. Tippawan,[2,4] S. W. Wissink,[1] and Y. Zhou[1]

[1]*Indiana University Cyclotron Facility and Department of Physics, Bloomington, Indiana 47408, USA*
[2]*Uppsala University, Uppsala, Sweden*
[3]*Ohio University, Athens, Ohio, USA*
[4]*Chiang Mai University, Chiang Mai, Thailand*

(Received 11 December 2004; published 3 March 2005)

We describe a double-scattering experiment with a novel tagged neutron beam to measure differential cross sections for np backscattering to better than $\pm 2\%$ absolute precision. The measurement focuses on angles and energies where the cross section magnitude and angle dependence constrain the charged pion-nucleon coupling constant, but existing data show serious discrepancies among themselves and with energy-dependent partial-wave analyses. The present results are in good accord with the partial-wave analyses, but deviate systematically from other recent measurements.

DOI: 10.1103/PhysRevLett.94.082303 PACS numbers: 25.40.Dn, 13.75.Gx, 25.10.+s, 28.20.Cz

The neutron-proton elastic scattering database at intermediate energies is plagued by experimental inconsistencies and cross section normalization difficulties [1–3]. These problems have led the most sophisticated partial-wave analyses (PWAs) of the data [4–6] to ignore the majority (including the most recent) of measured cross sections, while the literature is filled with heated debates over experimental and theoretical methods [7,8], including proposed radical "doctoring" (angle-dependent renormalization) to "salvage" allegedly flawed data [9]. Meanwhile, an empirical evaluation of a fundamental parameter of meson-exchange theories of the nuclear force—the charged πNN coupling constant f_c^2—hangs in the balance [8]. We report here the results of a new experiment, carried out utilizing quite different techniques from earlier measurements in an attempt to resolve the most worrisome experimental discrepancies.

The present experiment involves a kinematically complete double-scattering measurement to produce and utilize a "tagged" intermediate-energy neutron beam [10], thus greatly reducing the usual systematic uncertainties associated with the determination of neutron flux. Products from the second scattering were detected over the full angle range of interest simultaneously in a large-acceptance detector array, to eliminate the need for cross normalization of different regions of the angular distribution. The use of carefully matched solid CH_2 and C targets permitted frequent measurement and accurate subtraction of quasi-free scattering background, thereby minimizing reliance on kinematic cuts to isolate the free np scattering sample. These methods, combined with multiple internal cross-checks built into the data analysis procedures, have allowed us to achieve systematic error levels in the absolute cross section below 2%. In addition to addressing the previous discrepancies, the results provide a useful absolute cross section calibration for intermediate-energy neutron-induced reactions.

The experiment was carried out during the final year of operation of the Indiana University Cyclotron Facility's Cooler ring [11], with apparatus illustrated in Fig. 1 and described in detail in [10]. Neutrons of 185–197 MeV were produced via the charge-exchange reaction $p + d \rightarrow n + 2p$, initiated by a stored, electron-cooled 203 MeV proton beam, with typical circulating current of 1–2 mA, in a windowless deuterium gas jet target (GJT) of thickness ≈ 2–4×10^{15} atoms/cm^2. The ultrathin target permitted detection of the two low-energy recoil protons in an array ("tagger" in Fig. 1) of four 6.4×6.4 cm^2 double-sided silicon strip detectors (DSSD's) with 480 μm readout pitch in two orthogonal directions, each followed by a silicon pad ("backing") detector (BD) of the same area. Only recoil protons ($\lesssim 11$ MeV) that stopped in either the DSSD's or BD's were considered in the data analysis. Measurements of energy, arrival time, and two-dimensional position for both recoil protons in the tagger, when combined with precise knowledge of cooled p beam direction and energy, allowed four-momentum determination for each produced neutron on an event-by-event basis.

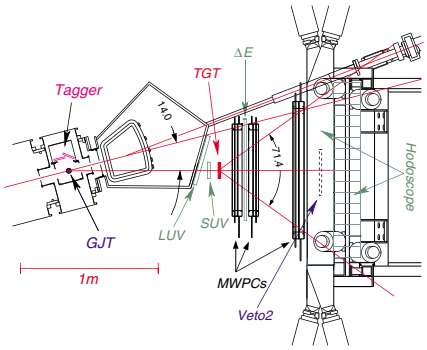

FIG. 1 (color online). Top view of the np scattering experiment setup.

 © 2005 The American Physical Society

The (uncollimated) tagged neutrons were distributed over a significant range in energy and angle, but these parameters were measured for each produced neutron with resolutions $\sigma_E \approx 60$ keV and $\sigma_{\text{angle}} \approx 2$ mrad.

The forward setup included a solid secondary scattering target of CH_2 or graphite positioned 1.1 m downstream of the GJT, centered on a neutron production laboratory angle of 14.0°. Both solid targets had transverse dimensions 20×20 cm^2 and thickness of 0.99×10^{23} carbon atoms/cm^2. The typical rate of tagged neutrons with energy above 185 MeV intercepting the secondary target was 200 s^{-1}. A large and a small upstream veto scintillator (LUV and SUV, respectively, in Fig. 1) vetoed tagged neutrons that interacted before the secondary target. Following the target was a forward array of plastic scintillators for triggering and energy information and a set of three (three-plane) multiwire proportional chambers (MWPC's) to track forward protons. The forward detector acceptance was nearly 100% for np scattering events with $\theta_{\text{c.m.}} \geq 130°$, falling to 50% by $\theta_{\text{c.m.}} = 90°$. The MWPC between the secondary target and ΔE scintillator allowed discrimination against np events initiated in that scintillator. The rear hodoscope comprised 20 plastic scintillator bars of sufficient thickness (20 cm) to stop 200 MeV protons and give 15–20% detection efficiency for 100–200 MeV neutrons.

Specially designed DSSD front-end electronics [10] permitted a tagger-based event trigger on neutron candidates (consistent with two distinct tagger hits and no accompanying signals from LUV or SUV), whether or not the neutrons interacted in the forward target and/or detectors. Tagged neutron events were recorded in three mutually exclusive event streams [10], coupling the tagger trigger with (1) no rear hodoscope coincidence (providing a prescaled sample for neutron flux monitoring); or (2) a coincidence with both the ΔE scintillator and rear hodoscope (for np scattering candidates); or (3) a coincidence with the rear hodoscope but not ΔE (for evaluating the neutron detection efficiency of the hodoscope). Comparative analyses of the three separate event streams, with respective yields N_1, N_2, and N_3, facilitated cross-checks to calibrate the system [10] and to study potential systematic errors.

Neutron beam properties were defined by identical cuts for all three event streams, so that associated systematic uncertainties would cancel in the yield ratios from which the absolute np scattering cross section is extracted. Among the common cuts are ones on DSSD vs BD energy deposition in the tagger [10], used to select two tagged neutron classes for analysis: (a) "2-stop" events, where both recoil protons stopped inside the DSSD's (either the same or different quadrants of the tagger); (b) "1-punch" events, where one of two recoil protons incident on different quadrants punched through into the corresponding BD and stopped there. These classes differ significantly in neutron energy (E_n) and position profiles [10], allowing an important crosscheck on the accuracy of the tagging technique by comparing np cross sections extracted independently from each class. Other common cuts defined a fiducial area for neutrons impinging on the secondary target and eliminated common-mode BD noise (via pulse-height correlations among quadrants) that sometimes led to misidentification of event class.

Additional misidentification discovered during data analysis was attributed to an electronics malfunction in the gating or clearing circuit for one analog-to-digital converter module, that removed all valid BD energy signals for some fraction of events. The corrupted events were misidentified as 2-stop events, with systematically incorrect predictions of tagged neutron trajectory (since some recoil proton energy was missed), and hence of np scattering angle for event stream 2. A subsample of these corrupted events could be isolated by means of their valid BD timing signals, and their properties were accurately reproduced by appropriately scaling the surviving sample of all events with valid BD energies and times, after setting these energies to zero in software. Thus, the surviving punch-through events permitted a reliably unbiased subtraction of the corrupted 2-stop events, independently for each event stream. The subtraction confirmed that the same fraction (typically 23%) of punch-through events was lost from each event stream, with no net effect on the extracted 1-punch cross sections.

Kinematic cuts applied exclusively to event stream 2 to define np free-scattering events from the secondary target were used sparingly. We relied instead on accurate background subtraction facilitated by frequent interchange of the carefully matched CH_2 and C targets. The CH_2 and C runs were normalized via the pd elastic scattering yield from the GJT measured in a fourth event stream for the two targets. The pd events were identified by their clear kinematic locus in the energy of recoil deuterons detected in the tagger *vs* the position of coincident forward protons in the front MWPC. The subtraction removed not only quasifree scattering off carbon nuclei in the target, but also background from other sources, such as tagged n scattering from the aluminum support platform on which the secondary target sat, or protons produced in the GJT that passed above the top of the LUV and SUV scintillators, mocking up np backscattering events.

The success of the background subtraction is illustrated in Fig. 2, where 2(a) and 2(b) show the vertical position

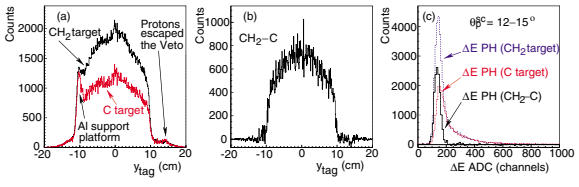

FIG. 2 (color online). Distributions of np scattering candidate events in y_{tag} (a), (b) and ΔE (c) for CH_2 and C targets and their difference.

($y_{\rm tag}$) of neutrons on the secondary target, as reconstructed from the tagger, for CH_2 and normalized C targets, and for their difference. Figure 2(c) shows the ΔE pulse-height spectrum within a given scattering angle (θ_p^{sc}) bin for both targets and for their difference. Prominent background features associated both with the secondary target (e.g., the long quasifree scattering tail in ΔE) and with other sources [e.g., the peak in frame (a) from the Al support platform] are simultaneously accurately removed by the subtraction. The subtraction reveals in frame (b) a $y_{\rm tag}$ distribution reflecting the tagged n (2-stop + 1-punch) beam profile, convoluted with the np scattering cross section, forward detector acceptance and sharp CH_2 target edges (the sharpness illustrating the good spatial resolution of the tagging).

Background-subtracted spectra such as that in Fig. 2(c) were used to evaluate efficiencies for the few loose cuts imposed on event stream 2 to improve the free-scattering signal-to-background ratio, including ones on ΔE *vs* θ_p^{sc} and on MWPC proton track quality. Cuts on the hodoscope pulse height were avoided, to remove reliance on detailed understanding of the nuclear reaction tail for protons stopping in this thick scintillator.

The forward detector acceptance was determined as a function of θ_p^{sc} from simulations matched to *measured* distributions of np free-scattering events in proton azimuthal angle ϕ_p. In the simulations, the longitudinal coordinate of the n production vertex within the GJT and its transverse coordinates on the secondary target were generated randomly for each event, but within distributions determined from the experiment. These coordinates determined the incident n angle. Generated outgoing p trajectories were accepted if they produced signals above the hodoscope threshold (required in the trigger) and in all three MWPCs (required in the data analysis). Forward

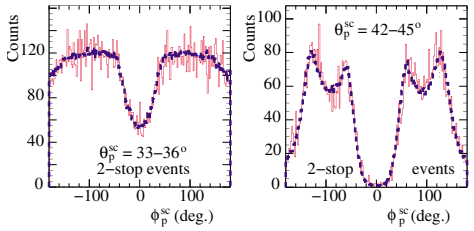

FIG. 3 (color online). The distribution of free (CH_2-C) np scattering events with respect to proton azimuthal angle ϕ, for two laboratory scattering angle bins. The solid (dashed) histograms are measured (simulated and normalized to fit the measurements).

detector location parameters were tuned to reproduce the measured ϕ_p distributions for all θ_p^{sc} bins and for 1-punch and 2-stop samples simultaneously. Typical fits in Fig. 3 reveal a structure of purely geometric origin, from rectangular detector edges projected on θ and ϕ. For $\theta_p^{sc} \leq 24\,^\circ$ the measured and simulated ϕ distributions are uniform, since the scattered protons are completely contained within the forward array.

Absolute differential cross sections were obtained from the yields in event streams 1, 2, and 3 defined above:

$$\left(\frac{d\sigma}{d\Omega}\right)_{\rm lab} = \frac{N_2(\theta_p^{sc}) \prod c_i}{(N_1 + N_2 + N_3) t_H |d\cos(\theta_p^{sc})| a_\phi(\theta_p^{sc})}, \quad (1)$$

where N_j represents the number of events (corrected for prescaling where appropriate) surviving all relevant cuts and background subtractions for event stream j; the c_i are small corrections, summarized in Table I, for inefficiencies, tagged neutron losses or backgrounds, and software cut and dead time differences among event streams; $t_H = (1.988 \pm 0.008) \times 10^{23}$ H atoms/cm^2 for the CH_2

TABLE I. Correction factors (c_i) and systematic uncertainties in correction factors for the np cross sections.

Source	Correction factor	Uncertainty
Accidental tagger coincidences	1.0003	$< \pm 0.001$
Non-D_2 tagger background	1.0067 (2-stop); 1.0044 (1-punch)	± 0.002
n position uncertainty on CH_2	1.0000	± 0.001
n attenuation before CH_2	1.005	± 0.0025
C background subtraction	1.0000	± 0.004
Reaction tail losses	1.004	± 0.002
Neutron polarization effects	Angle dependent: >0.9988 (1-punch); <1.0014 (2-stop)	± 0.001
Software cut losses	1.010	± 0.005
Sequential reactions and $x_{\rm tag}(n)$ errors	1.063	± 0.010
CH_2 target thickness	1.0000	± 0.004
np scattering acceptance	1.0000	$\leq \pm 0.001$ ($>120\,^\circ$) $\rightarrow \pm 0.017$ ($90\,^\circ$)
MWPC inefficiency	1.017	± 0.002
Trigger inefficiency	$1.002 + 0.008 \times \cos^2(\theta_p^{\rm LAB})$	$\pm[0.001 + 0.004 \times \cos^2(\theta_p^{\rm LAB})]$
Dead time differences	0.991	± 0.005
Scattering angle errors	1.000	angle dependent, $\leq \pm 0.004$
Corruption subtraction	1.000	$< \pm 0.001$
Net	≈ 1.10	$\approx \pm 0.015$

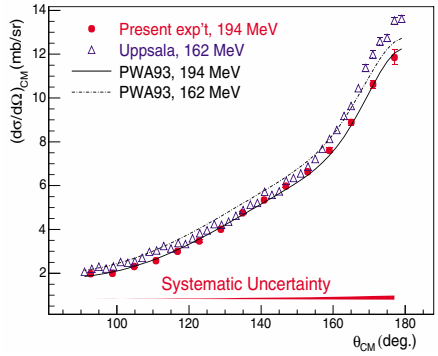

FIG. 4 (color online). Absolute differential cross section from the present experiment, compared with data from Ref. [3] and with PWA calculations at two relevant energies. The error bars and shaded band for the present results represent, respectively, statistical (including background subtraction) and systematic (including overall normalization) uncertainties.

target; and a_ϕ is the azimuthal acceptance determined from simulations for the given angle bin. The data were analyzed in 1 MeV wide E_n slices from 185 to 197 MeV. An effective cross section at $\langle E_n \rangle = 194.0 \pm 0.15$ MeV was extracted by applying small (always $<1\%$) corrections to the results for each E_n slice, based on the energy dependence calculated with the Nijmegen PWA [4].

Cross sections extracted independently for the 1-punch and 2-stop samples agree within statistical uncertainties (χ^2/point ≈ 1.0) in both magnitude and angular shape. This comparison supports the reliability of the experiment and analysis, as these events come from complementary regions of the tagged beam spatial and energy profiles [10]. Cross sections extracted for different time periods within the production runs, and with different sets of cuts, are also consistent within the uncertainties. The results, averaged over the 2-stop and 1-punch samples, are compared in Fig. 4 with previous experimental results at 162 MeV [3] and with the Nijmegen partial-wave analysis (PWA93) at the two relevant energies [12].

By using a tagged beam, we have sacrificed statistical precision for better control of systematic errors, in order to assess which previous experiments may have suffered from unrecognized systematic problems. Each systematic uncertainty summarized in Table I has been evaluated in a separate analysis, sometimes involving auxiliary measurements. The errors are, except where noted otherwise in the Table, angle-independent normalization uncertainties. The largest correction to the data and attendant uncertainty arise from cuts to remove stream 2 (but not 1 or 3) events where the np scattering vertex transverse coordinates predicted from n tagging vs p ray tracing disagree by more than 3 times the resolution σ. The removed events (6.3% of the total sample) are affected by several factors—e.g., sequential reactions in the secondary target and upstream material, or errors associated with recoil protons stopping in dead layers within the tagger—that lead to ambiguities in neutron energy and scattering angle. Combining all effects in Table I and summing uncertainties in quadrature, the net correction ($\prod c_i$) applied to raw cross sections is $\approx 1.10 \pm 0.015$, with an angle dependence of the systematic uncertainty indicated by the shaded band in Fig. 4.

The present results are in quite good absolute agreement with the Nijmegen PWA93 calculations, over the full angular range covered. The small deviations seen might be removed by minor tuning of phase shifts. In contrast, the present results deviate systematically, especially in the steepness of the back-angle cross section rise, from earlier measurements [2,3] that the Nijmegen group had rejected in their analyses by applying controversial criteria. These deviations are larger than the differences expected from the neutron energy changes among the various experiments. As the back-angle rise is particularly influential in pole extrapolations used [8,13] to extract the pion-nucleon-nucleon coupling constant, the present data strongly favor the value ($f_c^2 = 0.0748 \pm 0.0003$) given by the Nijmegen [6] and other [5] partial-wave analyses.

We thank the operations staff of the Indiana University Cyclotron Facility for providing the superior quality cooled beams, and Hal Spinka and Catherine Lechanoine-Leluc for the loan of detector hardware critical for successful execution of this experiment. We acknowledge the support of the U.S. National Science Foundation under grant no. NSF-PHY-9602872 and no. NSF-PHY-0100348.

*Present address: Department of Radiology and Radiological Sciences, Vanderbilt University, Nashville, TN, USA
†Present address: Department of Physics, University of Zagreb, Zagreb, Croatia

[1] B. E. Bonner *et al.*, Phys. Rev. Lett. **41**, 1200 (1978).
[2] J. Franz *et al.*, Phys. Scr. **T87**, 14 (2000).
[3] J. Rahm *et al.*, Phys. Rev. C **57**, 1077 (1998).
[4] V. Stoks *et al.*, Phys. Rev. C **48**, 792 (1993).
[5] D. V. Bugg and R. Machleidt, Phys. Rev. C **52**, 1203 (1995).
[6] M. C. M. Rentmeester, R. G. E. Timmermans and J. J. de Swart, Phys. Rev. C**64**, 034004 (2001).
[7] M. C. M. Rentmeester *et al.*, Phys. Rev. Lett. **81**, 5253 (1998); T. E. O. Ericson *et al.*, *ibid.* **81**, 5254 (1998).
[8] *Proceedings of Workshop on Critical Issues in the Determination of the Pion-Nucleon Coupling Constant*, edited by J. Blomgren [Phys. Scr. T87 (2000)].
[9] J. J. de Swart and R. G. E. Timmermans, Phys. Rev. C **66**, 064002 (2002).
[10] T. Peterson *et al.*, Nucl. Instrum. Methods Phys. Res., Sect. A **527**, 432 (2004).
[11] R. E. Pollock, Annu. Rev. Nucl. Part. Sci. **41**, 357 (1991).
[12] http://nn-online.org/NN/
[13] T. E. O. Ericson *et al.*, Phys. Rev. Lett. **75**, 1046 (1995).

Available online at www.sciencedirect.com
SCIENCE DIRECT®
ELSEVIER
Nuclear Physics A 760 (2005) 19–39
NUCLEAR PHYSICS A

Influence of multichance fission on fragment angular anisotropy in the ^{232}Th(n, f) and ^{238}U(n, f) reactions at intermediate energies

I.V. Ryzhov [a], M.S. Onegin [b], G.A. Tutin [a], J. Blomgren [c], N. Olsson [c,e], A.V. Prokofiev [a,d,*], P.-U. Renberg [d]

[a] *V.G. Khlopin Radium Institute, 2nd Murinski Prospect 28, 194021 Saint-Petersburg, Russia*
[b] *Petersburg Nuclear Physics Institute of Russian Academy of Science, 188350 Gatchina, Leningrad district, Russia*
[c] *Department of Neutron Research, Uppsala University, Box 525, S-75120 Uppsala, Sweden*
[d] *The Svedberg Laboratory, Uppsala University, Box 533, S-75121 Uppsala, Sweden*
[e] *Swedish Defence Research Agency (FOI), S-172 90 Stockholm, Sweden*

Received 21 February 2005; received in revised form 7 April 2005; accepted 1 June 2005

Available online 24 June 2005

Abstract

Fission fragment angular distributions have been measured for the ^{232}Th(n, f) and ^{238}U(n, f) reactions in the neutron energy range 20–100 MeV. The fragment angular anisotropy for ^{232}Th was found to be systematically larger than that for ^{238}U. The obtained results have been analyzed in the framework of the statistical saddle-point model combined with pre-equilibrium and Hauser–Feshbach calculations of partial fission cross sections. The calculations have revealed that fission following multiple neutron emission takes place in both reactions, resulting in a considerable contribution of high chances to the total fission fragment angular anisotropy. This gives grounds to expect that the observed difference is mainly due to nuclei fissioning at the end of the neutron evaporation chain.
© 2005 Elsevier B.V. All rights reserved.

* Corresponding author.
E-mail address: alexander.prokofiev@tsl.uu.se (A.V. Prokofiev).

0375-9474/$ – see front matter © 2005 Elsevier B.V. All rights reserved.
doi:10.1016/j.nuclphysa.2005.06.003

PACS: 24.75.+i; 25.85.Ec; 27.90.+b

Keywords: NUCLEAR REACTIONS ^{232}Th, ^{238}U(n, f), $E = 10$–100 MeV; measured fission fragments angular distributions, anisotropy. ^{232}Th, ^{238}U(n, f), E; 80 MeV; ^{232}Th, ^{238}U$(n, 2n)$, $(n, 3n)$, (n, xnf), E; 20 MeV; calculed σ, fission fragments angular anisotropy. Multichance fission, saddle-point statistical model analysis.

1. Introduction

Multichance fission (i.e., fission preceded by neutron evaporation) is possible if the excitation energy of the compound nucleus (CN) exceeds the sum of the fission barrier and the neutron binding energy. In this case, any fission observable, including fission fragment angular distribution (FFAD), is a superposition of contributions from various fission chances. From theoretical arguments (see, e.g., Ref. [1]), it follows that rather "cold" nuclei undergoing fission at the late stages of the statistical decay can play an important role in the formation of the resulting FFAD. The strongest effect can be expected for nuclei in the vicinity of thorium, for which the multichance fission is not as strongly suppressed as for subactinides or heavier actinides.

Studies of FFAD for such nuclei have some important aspects. The first one is related to the chance structure of the fission cross section, which is crucial for an adequate description of fission observables. At present there is no consensus on this subject even in case of well-explored reactions. For instance, the decomposition of the fission cross section into chance components recently made by Kawano et al. [2] for the ^{238}U(n, f) reaction (at neutron energies $E_n \leqslant 20$ MeV) differs dramatically from the one given in the Evaluated Nuclear Data File (ENDF/B-VI) [3], especially at high chances. If it is granted that FFAD is sensitive to the chance structure, the inclusion of angular anisotropy into the statistical-model analysis may impose additional constraints on the model parameters. Notice that the existing theory of intermediate-energy neutron-induced fission runs into problems with consistent description of integral and differential fission observables. For example, Duijvestijn et al. [4] had to use different values of the saddle-point to ground state level density ratio, a_f/a_n, in order to reproduce fission cross sections and fragment mass distributions for the ^{238}U(n, f) reaction.

Another direction of fission studies concerns properties of strongly deformed neutron-deficient nuclei, which could reveal themselves in characteristics of FFAD for fission following multiple neutron emission. Recent experiments on electromagnetic-induced fission of various nuclides between actinium and uranium at excitation energies peaked around 11 MeV [5] showed that a transition from asymmetric to mixed (triple-humped) fission takes place at less neutron-deficient isotopes for thorium than for uranium. Since the formation of mass and angular distributions is closely related to features of the potential-energy landscape behind the second minimum, it would be of interest to understand to which extent the topography of this landscape could affect the FFAD in multichance fission.

Considering different aspects of FFAD studies at intermediate energies, one should bear in mind that at $E_n \gtrsim 15$ MeV fission is preceded not only by compound processes, but also by pre-equilibrium ones, including multiple pre-equilibrium emission (MPE). In terms of fragment angular anisotropy, pre-equilibrium emission may result in two opposite effects.

First, in contrast to statistical evaporation, emission of fast pre-equilibrium particles can involve a significant decrease and deorientation of angular momentum of a fissioning nucleus and, as a result, a decrease in the total anisotropy. On the other hand, the pre-equilibrium emission is an effective de-excitation channel. The decrease in average excitation energy of fissioning nuclei leads to an increase in anisotropy. The competing influence of these two factors on fragment angular anisotropy has never been studied in detail.

The present work is the first systematic study of fission fragment angular anisotropy for the ^{232}Th(n, f) and ^{238}U(n, f) reactions in the 20–100 MeV energy region. The experimental arrangement and the data analysis are briefly described in Section 2. Section 3 contains the framework of the standard saddle-point statistical model (SSPSM) [6] applied to (n, f) reactions at intermediate energies. The details of the calculation procedure are described in Section 4. The calculation results are presented and discussed in Section 5.

2. Experiment, data analysis and results

The experimental part of this work has been described in detail recently [7], and therefore only a brief survey is given below. The measurements were performed at the neutron beam facility of The Svedberg Laboratory (TSL) [8] (see Fig. 1). Quasi-monoenergetic neutrons with peak energies of 21, 35, 46, 66, 75 and 95 MeV were produced via the ^{7}Li$(p, n)^{7}$Be reaction in targets of 99.98% isotopically pure ^{7}Li. After passage through the target, the proton beam was bent into a well-shielded beam dump. Neutrons were guided to the experimental area through a system of three collimators. The vacuum system was terminated after the first collimator with a 1-mm-thick aluminum plate. Charged particles produced in the plate were deflected by a clearing dipole magnet.

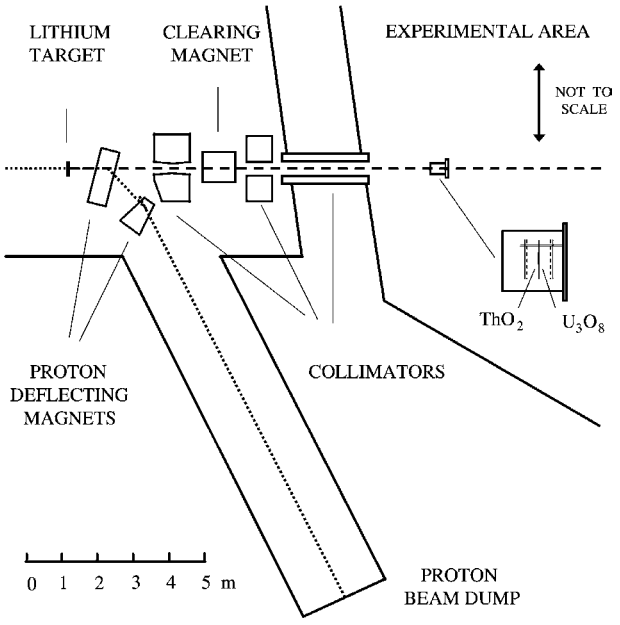

Fig. 1. Overview of the TSL neutron beam facility.

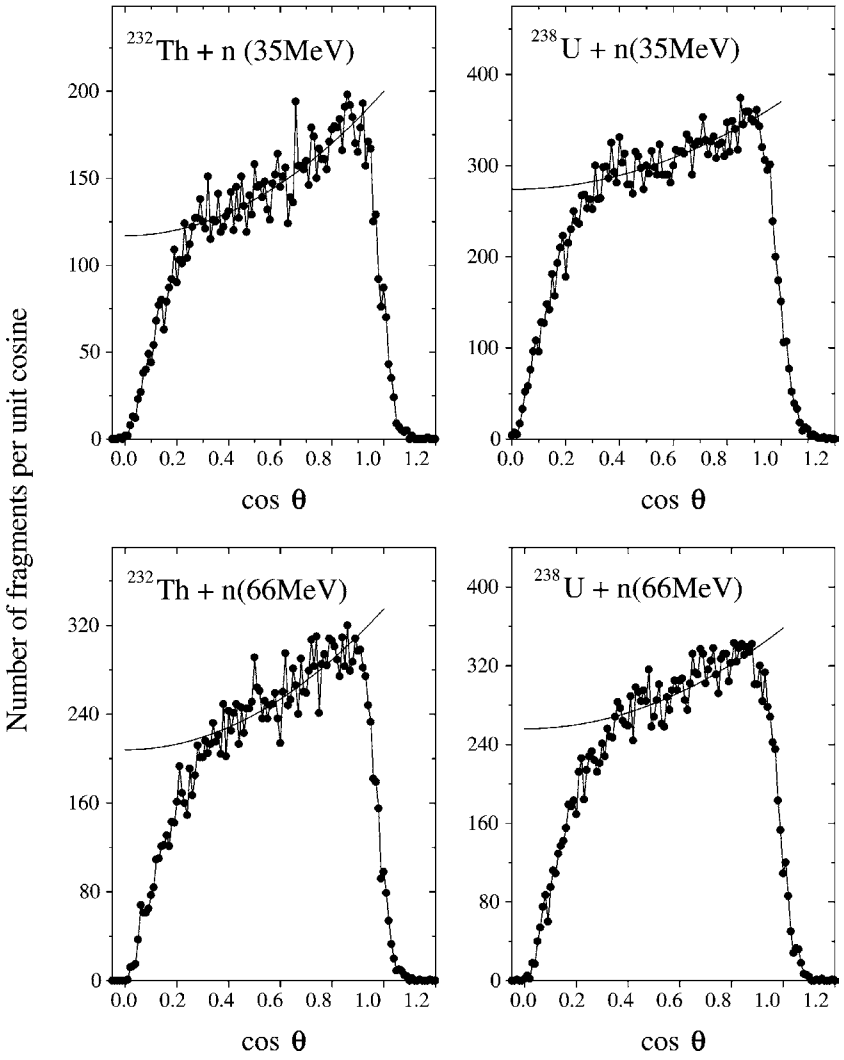

Fig. 2. Angular distributions of forward emitted fragments for the ^{232}Th(n, f) and ^{238}U(n, f) reactions at the neutron energies 35 and 66 MeV. The distributions are fitted with a function $W(\theta) \sim 1 + B\cos^2\theta$ in the cosine range 0.3–0.9 (solid lines).

Fission fragments were detected with a twin Frisch-gridded ionization chamber Ref. [7]. The fission targets, $^{232}ThO_2$ and $^{nat}U_3O_8$, were deposited back-to-back on a common cathode within a circle of 78 mm in diameter. The target thicknesses were 0.49 mg/cm^2 and 0.42 mg/cm^2 for the thorium and uranium samples, respectively. The detector was positioned at a distance of about 10 m from the lithium target, where the intensity of high-energy peak neutrons was about 10^6 s^{-1} over the fission target area. The detector could simultaneously measure energy of a fission fragment and its emission angle with respect to the neutron beam axis. To take into account the linear momentum transfer, the measurements were performed with two opposite orientations of the chamber axis relative to the neutron beam direction. Examples of FFAD in the forward hemisphere are given in Fig. 2. The distortions visible at the ends of the distributions are caused by fragment losses in the deposit and by finite angular resolution of the detector. The data were fitted in the undis-

Table 1
Anisotropy factors (in c.m.s.) obtained for the ^{232}Th(n, f) and ^{238}U(n, f) reactions

E_n [MeV]	B ($n + ^{232}$Th)	B ($n + ^{238}$U)
21	0.57 ± 0.16	0.56 ± 0.13
35	0.53 ± 0.07	0.30 ± 0.06
46	0.63 ± 0.08	0.41 ± 0.06
66	0.53 ± 0.09	0.29 ± 0.06
75	–	0.21 ± 0.07[a]
95	0.35 ± 0.09	0.22 ± 0.06

[a] The datum is from our earlier work [9].

torted region ($0.3 < \cos\theta < 0.9$) with a function $W(\theta) \sim 1 + B\cos^2\theta$. The anisotropy factor $B = W(0°)/W(90°) - 1$ in the center of mass system was deduced as the average of the ones obtained for the two orientations of the chamber.

The high frequency of proton beam pulses (13–25 MHz) resulted in a frame-overlapping structure of the time-of-flight (TOF) spectra. This complicates separation of "peak" fission events from the low-energy background. In order to correct the measured angular anisotropy for admixture of fission events induced by "non-peak" neutrons, Monte Carlo simulations of TOF spectra and FFAD have been performed for each experimental run (see Ref. [7] for more details). The final anisotropy factors are presented in Table 1 together with uncertainties, which largely stem from the fitting procedure. It can be seen that the fission fragment angular anisotropy for the ^{232}Th(n, f) reaction is larger than the one for the ^{238}U(n, f) reaction in the whole studied energy region.

3. Theoretical framework

The SSPSM is based on the following postulates: (1) the fission fragments separate along the nuclear symmetry axis, and (2) the component of the total angular momentum along the nuclear symmetry axis (the parameter K) is a good quantum number beyond the saddle point of the fission process. Under these assumptions, the FFAD is uniquely defined by the rotational wave function $\mathrm{d}^J_{M,K}(\theta)$ [1]:

$$W^J_{M,K}(\theta) = \frac{2J+1}{2}\left|\mathrm{d}^J_{M,K}(\theta)\right|^2, \tag{1}$$

where J is the total angular momentum, M is its projection on a space-fixed Z axis, and θ is the angle between the nuclear symmetry axis and the space-fixed axis, which is usually taken as the beam direction. As long as the transition nucleus is "cold" enough, the fission process occurs through one or only a few transition states (channels) with specific quantum numbers. As the excitation energy increases, a continuum set of transition states comes into play. Statistical consideration in conjunction with a Fermi gas model predicts the distribution of the parameter K to be Gaussian. The square of its standard deviation K_0^2 is related to the temperature above the fission barrier T and to the effective moment of inertia at the saddle point J_{eff} as follows:

$$K_0^2 = \frac{J_{\mathrm{eff}}T}{\hbar^2}. \tag{2}$$

The J_{eff} is defined as $J_{\text{eff}} = J_\perp J_\parallel/(J_\perp - J_\parallel)$, where $J_\perp$ and $J_\parallel$ are the moments of inertia about axes perpendicular and parallel to the symmetry axis, respectively. The effective moment of inertia is a function of the atomic number of the fissioning nucleus Z, its mass number A, and the excitation energy at the saddle point U. The latter is given by

$$U = E - B_f = a_f T^2, \tag{3}$$

where E is the excitation energy at the equilibrium deformation, B_f is the fission barrier height, and a_f is the level density parameter at the saddle point. In the statistical domain, Eq. (1) takes the following form:

$$W^J_{M,U}(\theta, Z, A) \propto \frac{2J+1}{2} \sum_{K=-J}^{K=J} \left|\mathrm{d}^J_{M,K}(\theta)\right|^2 \exp\left(-K^2/2K_0^2(U, Z, A)\right). \tag{4}$$

Since a large number of nuclides with different A, Z, J, M, and E can undergo fission at intermediate energies, the resulting FFAD reads as

$$W(\theta) \propto \frac{1}{\sigma_f^{\text{tot}}} \sum_{A,Z,J,M} \int W^J_{M,U}(\theta, Z, A)\sigma_f(A, Z, J, M, E)\,\mathrm{d}E, \tag{5}$$

where the total fission cross section σ_f^{tot} is the sum of partial fission cross sections $\sigma_f(A, Z, J, M, E)$ (per unit energy) taken over all the nuclei and nuclear states contributing to fission:

$$\sigma_f^{\text{tot}} = \sum_{A,Z,J,M} \int \sigma_f(A, Z, J, M, E)\,\mathrm{d}E. \tag{6}$$

Thus, the calculation of partial fission cross sections $\sigma_f(A, Z, J, M, E)$ is the main problem to be solved if one wants to calculate the fission fragment angular distributions at fairly high excitation energies. Along with $\sigma_f(A, Z, J, M, E)$, it is important to know the energy dependence of $W^J_{M,U}(\theta, Z, A)$. Actually, this problem is reduced (as seen from Eq. (4)) to the variation of K_0^2 (or J_{eff}) with U. The calculation procedure for $\sigma_f(A, Z, J, M, E)$ and $K_0^2(U)$ is discussed in more detail in the subsequent section.

4. Calculation procedure

4.1. Partial fission cross sections

The partial fission cross section depends on the reaction paths leading to the formation of the nuclide with A, Z, J, M and E as well as on the fission probability for this system. The basic relation is given by the statistical model of nuclear reactions:

$$\sigma_f(A, Z, J, M, U) = \sum_\pi P(\alpha)\frac{\Gamma_f(\alpha)}{\Gamma_{\text{tot}}(\alpha)}, \tag{7}$$

where α denotes a state of nucleus with A, Z, J, M, E and parity π, $P(\alpha)$ is the population of α-state (in terms of cross section per unit energy), $\Gamma_f(\alpha)$ and $\Gamma_{\text{tot}}(\alpha)$ are the fission

and total decay widths, respectively. Since neutron emission and fission are the only important statistical decay channels, the relation $\Gamma_{\rm tot}(\alpha) \approx \Gamma_n(\alpha) + \Gamma_f(\alpha)$, where $\Gamma_n(\alpha)$ is the neutron decay width, holds with good accuracy.

4.1.1. Calculation of $P(\alpha)$

The population of the compound nucleus state α_c is given by

$$P(\alpha_c) = \sigma_{\rm abs}(\alpha_c) f_{\rm pre}(\alpha_c) \delta\big(E_c - \epsilon - B_c^n\big). \tag{8}$$

Here ϵ and B_c^n are incident and binding neutron energies, $\sigma_{\rm abs}(\alpha_c)$ is the partial neutron absorption cross section, and $f_{\rm pre}(\alpha_c)$ is the fractional reduction of $\sigma_{\rm abs}(\alpha_c)$ due to pre-equilibrium reactions. The partial neutron absorption cross section for a spinless target can be expressed in terms of optical model transmission coefficients $T_l(\epsilon)$ as follows:

$$\sigma_{\rm abs}(\alpha_c) = \frac{1}{2}\frac{\pi}{k^2}\frac{(2J_c+1)}{(2s_n+1)} \sum_{l=|J_c-\frac{1}{2}|}^{J_c+\frac{1}{2}} \eta(l,\pi_c) T_l(\epsilon), \tag{9}$$

where k and s_n are the wave vector and spin of a neutron, while the function $\eta(l,\pi_c) = \delta_{(-1)^l,\pi_c}$ ensures parity conservation. The factor $\frac{1}{2}$ in Eq. (9) accounts for populating of α_c with a particular M_c ($\pm\frac{1}{2}$). The transmission coefficients $T_l(\epsilon)$ averaged over entrance channel spin have been obtained using the non-relativistic SCAT2 code by Bersillon [10] with the optical potential proposed by Young [11].

The factor $f_{\rm pre}(\alpha_c)$ in Eq. (8) can be defined as

$$f_{\rm pre}(\alpha_c) = 1 - \frac{1}{\sigma_{\rm abs}(\alpha_c)} \sum_i \sigma_{\rm pre}^i(\alpha_c), \tag{10}$$

where the sum runs over all the pre-equilibrium reactions going through the intermediate state α_c. In our calculations, only neutron and proton pre-equilibrium emission has been considered.

The states of the residual nucleus with $A_c - 1$ and Z_c (specified below by α_1) are populated through emission of either statistical or non-equilibrium neutrons from the compound nucleus:

$$P(\alpha_1) = \rho(\alpha_1) \sum_{J_c,\pi_c} \int_{E_1+B_c^n}^{E_c} P(\alpha_c) \frac{\Gamma_n(\alpha_c \to \alpha_1)}{\Gamma_{\rm tot}(\alpha_c)} {\rm d}E_c + \frac{{\rm d}\sigma_{n,n'}(\alpha_1)}{{\rm d}E_1}, \tag{11}$$

where $\Gamma_n(\alpha_c \to \alpha_1)$ is the neutron decay width of the compound nucleus state α_c into the state of the residual nucleus α_1 with the continuum level density $\rho(\alpha_1)$, and $\Gamma_{\rm tot}(\alpha_c)$ is the total decay width of α_c-state. The latter term in Eq. (11) is the cross section for formation of α_1-state by pre-equilibrium (n,n') reactions. The summation includes all α_c-states related to the α_1-state via spin and parity conservation laws.

In addition, the contribution of $(n,2n)$, (n,p), and (n,np) reactions to the level population of the residual nuclides was taken into account. By analogy with Eq. (11) one can write

$$P(\alpha_2) = \rho(\alpha_2) \sum_{J_1,\pi_1} \int_{E_2+B_1^n}^{E_c-B_1^n} P(\alpha_1) \frac{\Gamma_n(\alpha_1 \to \alpha_2)}{\Gamma_{\rm tot}(\alpha_1)} \mathrm{d}E_1 + \frac{\mathrm{d}\sigma_{n,2n}(\alpha_2)}{\mathrm{d}E_2}, \tag{12}$$

$$P(\alpha_3) = \frac{\mathrm{d}\sigma_{n,p}(\alpha_3)}{\mathrm{d}E_3}, \tag{13}$$

$$P(\alpha_4) = \rho(\alpha_4) \sum_{J_3,\pi_3} \int_{E_4+B_3^n}^{E_c-B_c^p} P(\alpha_3) \frac{\Gamma_n(\alpha_3 \to \alpha_4)}{\Gamma_{\rm tot}(\alpha_3)} \mathrm{d}E_3 + \frac{\mathrm{d}\sigma_{n,np}(\alpha_4)}{\mathrm{d}E_4}. \tag{14}$$

Here α_2, α_3 and α_4 denote the states of nuclides with nucleon composition (A_c-2, Z_c), (A_c-1, Z_c-1) and (A_c-2, Z_c-1), respectively. Hereinafter, the notation $B_i^{n(p)}$ is used for the neutron (proton) binding energy relevant to α_i-state.

The corresponding precompound cross sections were obtained with the geometry dependent hybrid model (GDH) [12] modified to account for the MPE processes and J^π-conservation as proposed in Refs. [13] and [14,15], respectively. The population of α-states different in nucleon compositions from those listed above has been calculated within the statistical Hauser–Feshbach theory implemented in the computer code STAPRE [16,17].

4.1.2. Statistical decay widths

For an equilibrated system, the neutron decay width is given by the statistical decay theory as

$$\Gamma_n(\alpha) = \frac{1}{2\pi\rho_{\rm eq}(\alpha)} \sum_{J'=0}^{\infty} \sum_{\pi'} \sum_{j=J'-J}^{J'+J} \int_0^{E-B_n} \rho_n(\alpha') T_n^{l,j}(E - B_n - E')\, \mathrm{d}E', \tag{15}$$

where B_n is the neutron binding energy for a fissioning nucleus in the α-state (A, Z, J, M, E, π), $\rho_n(\alpha')$ and $\rho_{\rm eq}(\alpha)$ are the level densities of the residual and fissioning nuclei at the equilibrium deformation, respectively, and $T_n^{l,j}(\epsilon)$ stands for the transmission coefficient for a neutron having channel energy $\epsilon = E - B_n - E'$ and orbital angular momentum l. The latter is coupled with the neutron spin to form the channel angular momentum j.

The fission decay width reads:

$$\Gamma_f(\alpha) = \frac{1}{2\pi\rho_{\rm eq}(\alpha)} \frac{N_A N_B}{N_A + N_B}, \tag{16}$$

where N_A and N_B are the numbers of available levels at the first (inner) and the second (outer) barrier, respectively:

$$N = \int_0^{\infty} \rho_f(\alpha) \big(1 + \exp\big[2\pi(U + B_f - E)/\hbar\omega\big]\big)^{-1} \mathrm{d}U. \tag{17}$$

Here B_f and $\hbar\omega$ are the height and curvature of fission barrier for nucleus in α-state, U is the excitation energy above the barrier, and $\rho_f(\alpha)$ is the level density of the fissioning nucleus at the saddle configuration. The parity selection rules are implicit in Eqs. (15) and (17).

The level densities at the equilibrium deformation were calculated with the back-shifted Fermi gas model by Dilg et al. [18] with the model parameters from Ref. [19]. Calculations of fission level densities were performed using the phenomenological level density model by Ignatyuk et al. [20] with shell corrections from Ref. [21]. The fission barrier heights and curvatures were also taken from Ref. [21]. The ratio a_f/a_n was 1 for all nuclides except ^{239}U and ^{238}U, for which values 1.06 and 1.01 were used, respectively.

4.2. Calculation of K_0^2

For nuclides contributing to fission, the energy dependence of K_0^2 has been calculated with the following function:

$$K_0^2 = \begin{cases} 2.5, & U \leqslant 1 \text{ MeV}, \\ k_1 + k_2 U, & 1 \text{ MeV} < U \leqslant U_{\text{cr}}, \\ k_3 + k_4 U, & U_{\text{cr}} < U \leqslant U_{\text{sym}}, \\ J_{\text{eff}}^{\text{LDM}} \sqrt{U/a_f}/\hbar^2, & U > U_{\text{sym}}, \end{cases} \tag{18}$$

where U_{cr} is the critical energy for the phase transition between the superconductive (superfluid) state and the Fermi gas, and U_{sym} is the transition energy from asymmetric to symmetric fission. The meaning of the factors $k_1, \ldots, k_4$ is explained in the subsequent text.

The SSPSM is expected to fail at excitation energies only slightly larger than the fission barrier, because in this case the fission process goes through only a few transition state levels. We have assumed that K_0^2 is never less than a fixed value over the excitation energy interval from 0 to 1 MeV, otherwise (when $K_0^2 \to 0$) the SSPSM predicts the anisotropy to go to infinity. This value was set as 2.5 to fit the anisotropy "jumps" at the thresholds of (n, nf) and $(n, 2nf)$ reactions.

At excitation energies larger than U_{sym}, the symmetric fission becomes dominant. This may be interpreted as a wash-out of the nuclear shell structure. In this case, the effective moment of inertia is a characteristic of liquid drop deformation, and K_0^2 shows a square-root dependence upon U, as predicted by the Fermi gas model (see Eq. (2)). The transition energy from asymmetric to symmetric fission was set (for all nuclides) at $U_{\text{sym}} = 30$ MeV according to conclusion made by authors of Ref. [22], where the neutron-induced fission of ^{235}U has been studied for incident neutron energies from 1 to 250 MeV. The liquid drop values of the effective moment of inertia $J_{\text{eff}}^{\text{LDM}}$ were calculated with the rotating-liquid-drop model (RLDM) by Sierk [23] implemented in the MOMFIT code [24].

The critical energy was found from the relation $U_{\text{cr}} \simeq 0.481 a_f \Delta_f$ [1], where $2\Delta_f$ is the pairing gap at the saddle point. For all nuclides we have used the value $\Delta_f = 1.7$ MeV obtained for ^{236}U [25]. This gives the critical energy at the saddle point about 9.5 MeV with $a_f = A/9$. The same value of the critical energy was obtained by Smirenkin et al. [26] for ^{240}Pu. The parameter J_{eff} differs from the liquid drop value $J_{\text{eff}}^{\text{LDM}}$ in the energy interval between a few MeV and U_{cr}, because of nuclear pairing interactions and shell structure effects [27]. Bearing this in mind and assuming a linear increase of K_0^2 with the excitation energy, the coefficients k_1 and k_2 were derived from the following boundary conditions:

$$2.5 + \delta = k_1 + k_2, \qquad K_0^2(U_{\text{cr}}) = k_1 + k_2 U_{\text{cr}}. \tag{19}$$

Here δ stands for the step height of K_0^2 at $U = 1$ MeV. The value of δ was chosen to fit the anisotropy data below the threshold of the (n, nf) reaction, whereas $K_0^2(U_{\rm cr})$ was obtained according to Eq. (2) as

$$K_0^2(U_{\rm cr}) = \frac{J_{\rm eff}^{\rm ETFSI}}{\hbar^2}\sqrt{\frac{U_{\rm cr}}{a_f}}, \tag{20}$$

where the effective moment of inertia at the saddle point $J_{\rm eff}^{\rm ETFSI}$ was calculated with the shape parameters $\{c, \alpha, h\}$ [28] obtained in Ref. [29] with the use of the extended Thomas–Fermi plus Strutinsky integral (ETFSI) method. The $J_{\rm eff}^{\rm ETFSI}$ value appears to be smaller than the liquid-drop one, but approaches it at the excitation energy $U_{\rm sym}$. For the sake of simplicity, we assumed a linear increase of K_0^2 with the excitation energy in the interval $(U_{\rm cr}, U_{\rm sym})$, so that the coefficients k_3 and k_4 can be readily derived from the boundary conditions.

5. Calculation results and discussion

5.1. Cross sections of neutron-induced reactions

In order to impose constraints on the model parameters, we have performed a consistent analysis of experimental and evaluated data on neutron-induced reactions for ^{232}Th and ^{238}U. In particular, the calculated cross sections of (n, f), $(n, 2n)$, $(n, 3n)$ and (n, px) reactions have been compared with available data. The data on (n, f), $(n, 2n)$ and $(n, 3n)$ reactions at incident neutron energies below 20 MeV were taken from the ENDF/B-VI library [3]. The experimental ^{232}Th (n, f) cross section above 20 MeV was taken from Ref. [30]. For ^{238}U, both the evaluated (n, f) cross section [31] and the experimental total cross section for (n, px) reaction [32] have been considered above 20 MeV.

In Fig. 3, the GDH predictions for the total cross section of the ^{238}U(n, px) reaction are compared with the experimental data. It is seen that the GDH model enables description of the proton emission probability at the pre-equilibrium stage. Notice that emission of other light charged particles (lcp) has been ignored in the present calculations. As follows from Ref. [32], the relative contribution of (n, dx), (n, tx) and $(n, \alpha x)$ reactions to the total $(n, lcpx)$ cross section of ^{238}U is as low as about 30% at the incident neutron energies up to 63 MeV at least.

As seen from Fig. 4, the theoretical calculations fit well the experimental and evaluated total fission cross sections for both ^{232}Th and ^{238}U. On the other hand, the calculations slightly overestimate the $(n, 2n)$ reaction cross sections in both cases. The similar overestimation has been observed in Refs. [33,34], where a comprehensive analysis of neutron-induced reaction cross sections of ^{238}U was performed. It is conceivable that these discrepancies are caused by a common reason. A better fit can be achieved by adjusting the optical potential or pre-equilibrium model parameters (see, e.g., Ref. [35]).

In addition, our results on the chance decomposition of the total (n, f) cross section of ^{238}U have been compared with the ones from the ENDF/B-VI library [3] and with the calculations by Kawano et al. [2]. Cross sections of (n, xnf) reactions for ^{232}Th and ^{238}U

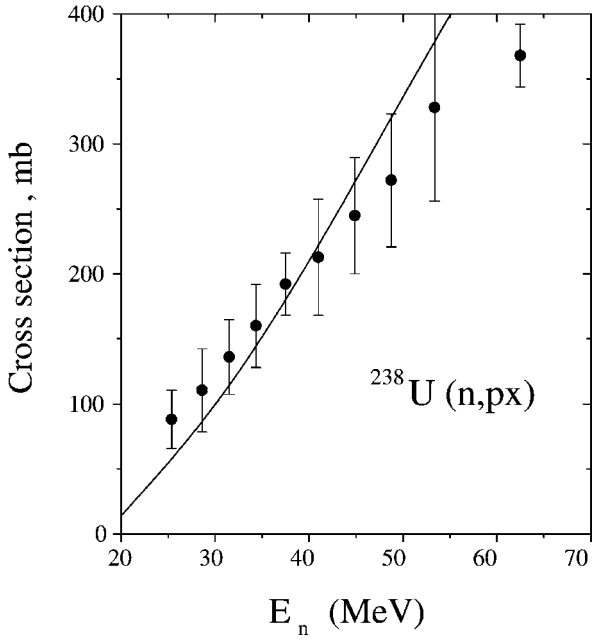

Fig. 3. Experimental total cross sections of the (n, px) reaction on ^{238}U [32] (filled circles) versus incident neutron energy compared to the present GDH calculations (solid line).

are given in Fig. 5 in the neutron energy range from the fission threshold up to 20 MeV. It is seen that the present calculations are in good agreement with the ENDF/B-VI data for ^{238}U, but differ dramatically from semi-empirical data presented in Ref. [2]. Note that similar calculations recently performed by Maslov et al. [36] at incident neutron energies below 20 MeV tend to support our results.

The above-mentioned difference in the (n, xnf) cross sections is hidden if one compares the total fission cross sections obtained by summing over all fission chances. This is not the case, however, for the total angular anisotropy, which appears to be quite sensitive to the chance structure of the total fission cross section. This is discussed in more detail in the subsequent subsection.

5.2. Angular anisotropy

The energy dependence of the fission fragment angular anisotropy for the ^{232}Th(n, f) and ^{238}U(n, f) reactions has been calculated with the set of the model parameters constrained by the cross section calculations described in the preceding subsection. The results of the anisotropy calculations are given in Fig. 6 in comparison with existing experimental data taken from the library of experimental nuclear reaction data (EXFOR) [37]. As one can see, the theoretical calculations predict that the periodic structure of anisotropy related to the onsets of (n, nxf) reactions is not extended beyond the threshold of $(n, 4nf)$ reaction at incident neutron energy $E_n \simeq 30$ MeV. Above this energy, a smooth decrease of the fragment anisotropy is predicted. From Fig. 6 it is also seen that the calculations reproduce well the data for ^{238}U, but underestimate the ones for ^{232}Th above 30 MeV. To elucidate

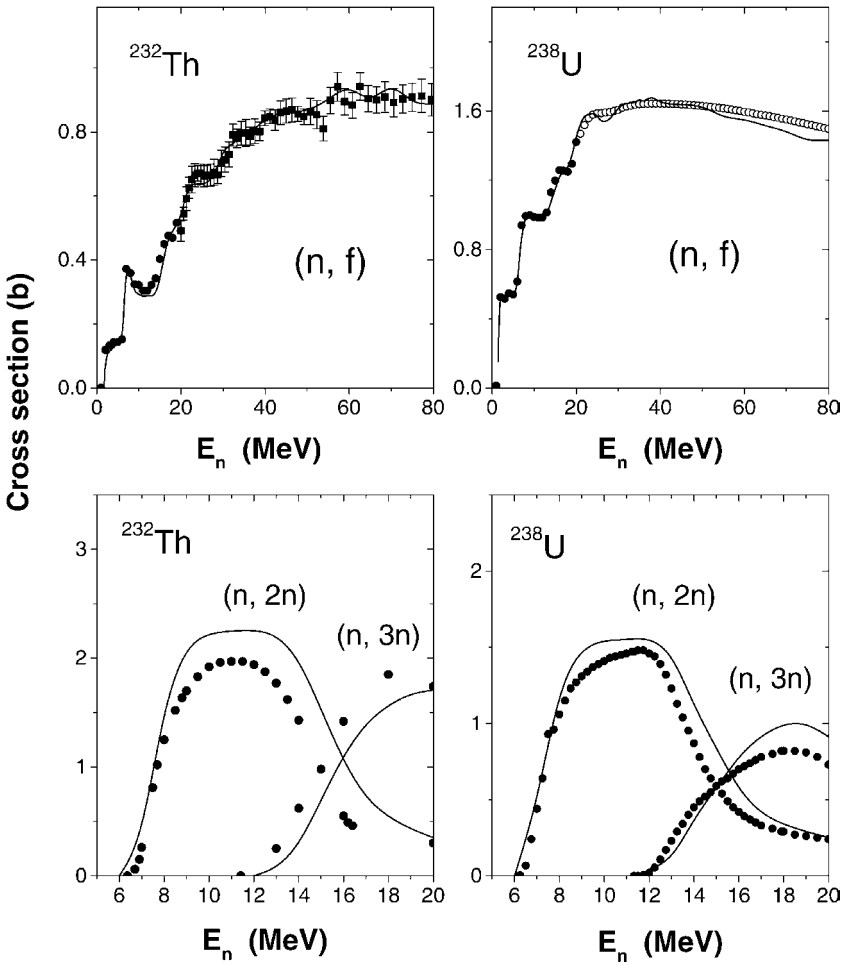

Fig. 4. Calculated (n, f), $(n, 2n)$ and $(n, 3n)$ cross sections (solid lines) in comparison with evaluated and experimental data for ^{232}Th (left panel) and ^{238}U (right panel). Filled and open circles show the evaluated data from ENDF/B-VI [3] and Ref. [31], respectively. Experimental data on (n, f) cross sections for thorium above 20 MeV [30] are shown as filled squares.

the cause of this disagreement, we have analyzed the role of the pre-equilibrium emission as well as of the emission of statistical neutrons in the formation of FFAD.

5.2.1. Influence of pre-equilibrium emission on fragment anisotropy

A qualitative analysis starts from Eq. (4), which describes the FFAD for a specific α-state. This expression, complemented by Eq. (18) for K_0^2, has been used to estimate the sensitivity of anisotropy to the variation of nuclear characteristics that undergo changes with neutron emission. As an example, Fig. 7 shows one-argument variations of anisotropy with J, M, and U relative to the initial value corresponding to fission of the compound nucleus formed in reaction $^{238}\mathrm{U} + n$ (40 MeV) at the maximum angular momentum.

The role of particles emitted at the pre-equilibrium stage is difficult to estimate, because the pre-equilibrium emission can be responsible for significant changes of J, M, and U. In addition, the contribution of non-statistical processes to the total reaction cross section

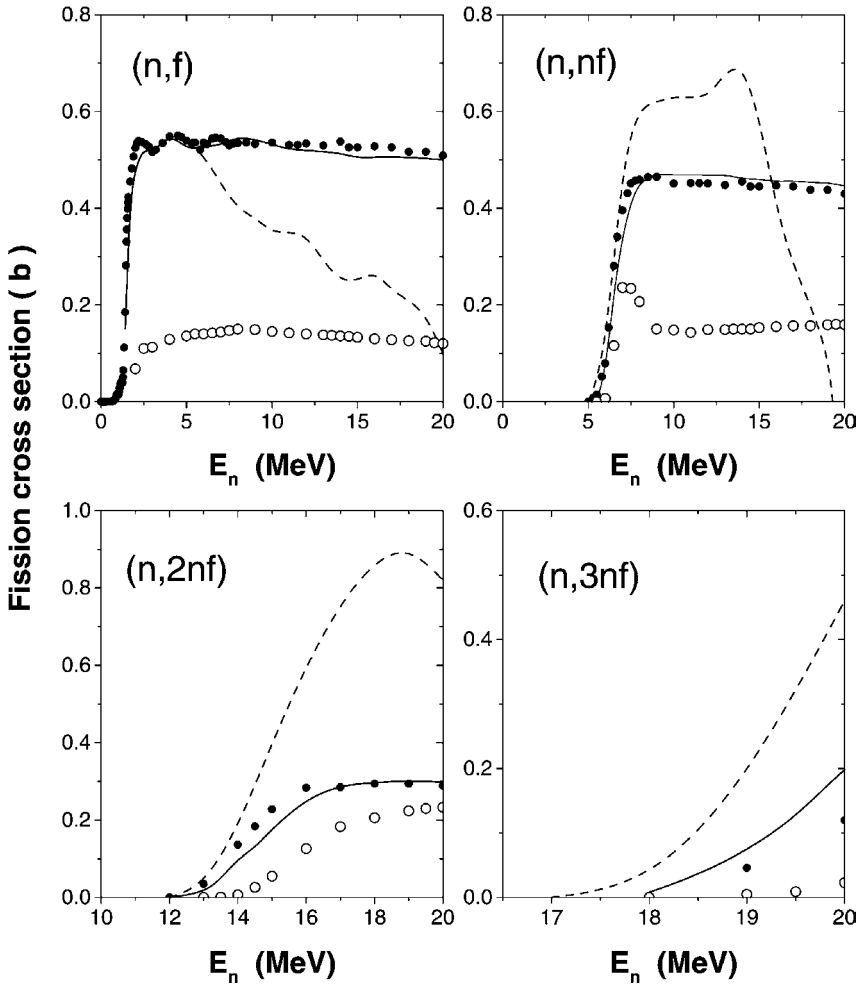

Fig. 5. Calculated (n, xnf) reaction cross sections for ^{232}Th and ^{238}U (solid lines) in comparison with calculations by Kawano et al. [2] (dashed lines) and the ENDF/B-VI evaluations. Full and open circles correspond to uranium and thorium evaluated data, respectively.

depends strongly on the incident neutron energy. Fig. 8 shows the calculated neutron absorption cross section σ_{abs} of ^{238}U as a function of E_n in comparison with the total cross section of the key pre-equilibrium reactions σ_{pre} (i.e., those resulting in population of the α_{1-4}-states). The above cross sections are related as follows:

$$\sigma_{\text{abs}} = \sigma_R(\text{CN}) + \sigma_{\text{pre}},$$

$$\sigma_{\text{pre}} = \sigma_{\text{pre}}(n, n') + \sigma_{\text{pre}}(n, np) + \sigma_{\text{pre}}(n, 2n) + \sigma_{\text{pre}}(n, p),$$

where $\sigma_R(\text{CN})$ is the cross section of the pure compound processes going without pre-equilibrium emission. From Fig. 8 one can see that σ_{pre} increases rapidly with increasing E_n, whereas the $\sigma_R(\text{CN})$ goes down. The main contribution to σ_{pre} comes from the (n, n') reaction leading to the population of α_1-states (see Eq. (11)). In order to estimate the effect

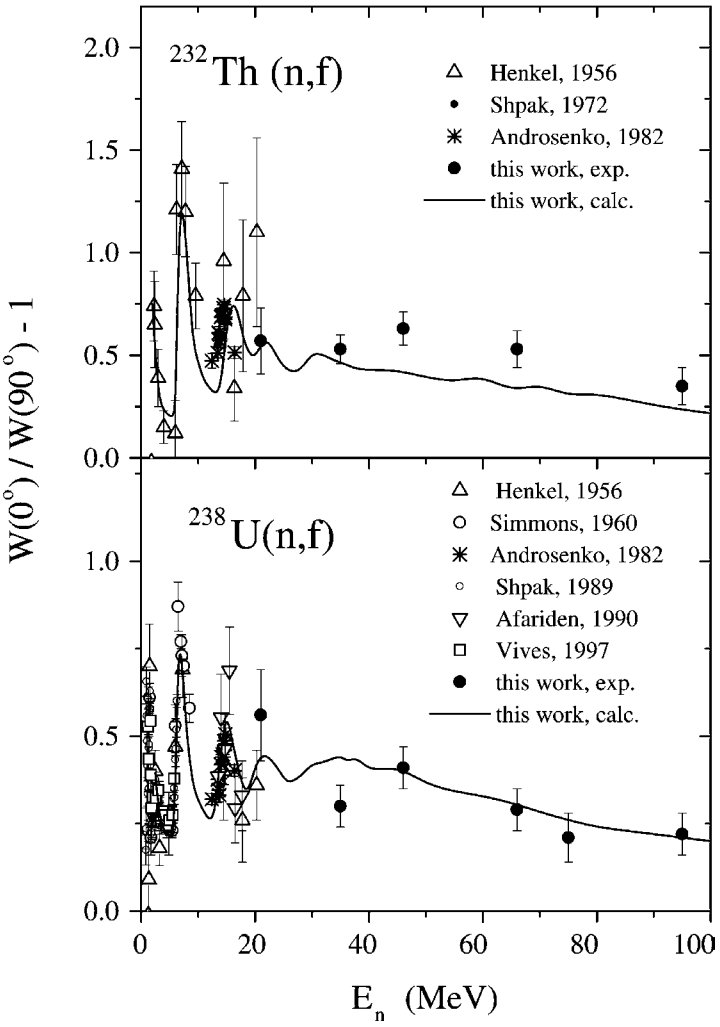

Fig. 6. Calculated fission fragment angular anisotropy for the ^{232}Th(n, f) and ^{238}U(n, f) reactions as a function of incident neutron energy (solid lines) in comparison with existing experimental data taken from the EXFOR database [37].

of this reaction on fragment anisotropy, we have turned to a simplified expression for the anisotropy factor

$$\frac{W(0^\circ)}{W(90^\circ)} - 1 = \frac{\langle J^2 \rangle}{4K_0^2}, \tag{21}$$

which is often used for analysis of FFAD in heavy-ion induced fission [38]. Here $\langle J^2 \rangle$ is the mean square spin of fissioning nucleus. If only statistical neutrons are emitted from the compound nucleus ($\sigma_{\rm pre} = 0$), it is straightforward to calculate the anisotropy as a function of E_n, taking the liquid drop values of K_0^2 at $U = E_n - B_f - 2\,T_{\rm CN}$ and approximating $\langle J^2 \rangle$ for α_1-states by the expression $\langle J^2 \rangle \simeq 2.5\,E_n$ commonly applied to the compound nucleus [6]. Anisotropy calculated for the ^{238}U(n, nf) reaction without taking into account pre-equilibrium reactions is shown in Fig. 9 by the dashed line. For comparison, a more

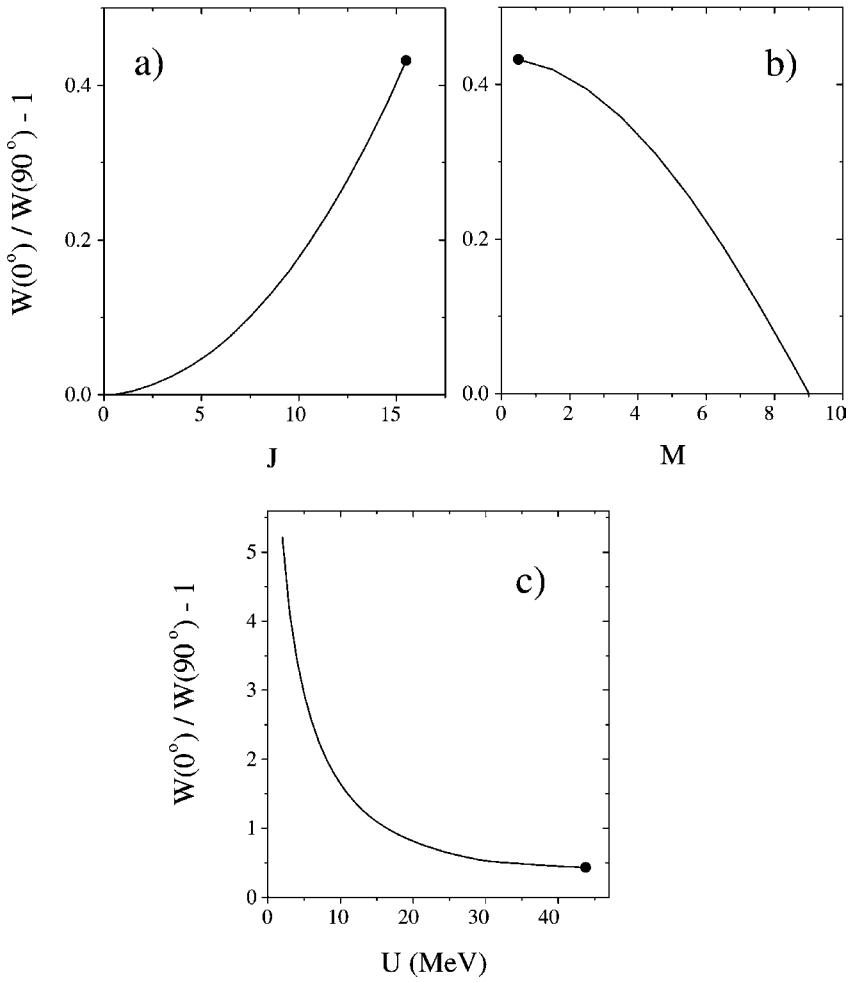

Fig. 7. One-argument variations of anisotropy with J(a), M(b), and U(c), calculated with Eqs. (4) and (18). The initial anisotropy value marked with the filled circle is the characteristic of the compound nucleus fission taking place in reaction $^{238}\mathrm{U}+n$ (46 MeV) at the maximum angular momentum.

realistic anisotropy estimation is presented in this figure by the solid line. The latter calculation was also done with Eq. (21), but in this case, an allowance for the $^{238}\mathrm{U}(n,n'f)$ reaction has been included into analysis by averaging of J^2 and U over all α_1- states according to Eq. (11). One can see that, in the absence of pre-equilibrium emission, the anisotropy of fissions taking place from the α_1-states tends to increase with E_n, but this increase is reduced to zero by the (n,n') reaction starting from E_n of about 20 MeV. Eq. (21) ignores the deorientation of angular momentum of fissioning nuclei due to neutron emission. Meanwhile, emission of fast pre-equilibrium neutrons can lead to the population of nuclear states with $M \gg M_c$, and, as a result, to an additional decrease of the anisotropy (see Fig. 7b). This effect is clearly seen in Fig. 10 where the full-scale anisotropy calculations (the same as in Fig. 6) are given in comparison with the ones, in which the projection of angular momentum is "frozen" at $M_c = 1/2$.

From the aforesaid it is believed that emission of non-statistical neutrons can have a profound impact on the fission fragment anisotropy in $(n,\ f)$ reactions at intermediate ener-

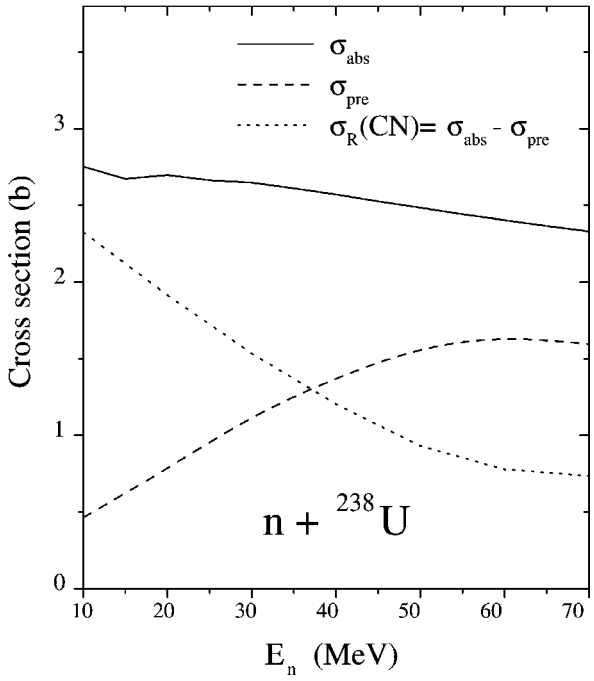

Fig. 8. The neutron absorption cross section of ^{238}U (solid line), the sum of the pre-equilibrium cross sections (dashed line) and the cross section of pure compound reactions (dotted line) calculated versus E_n.

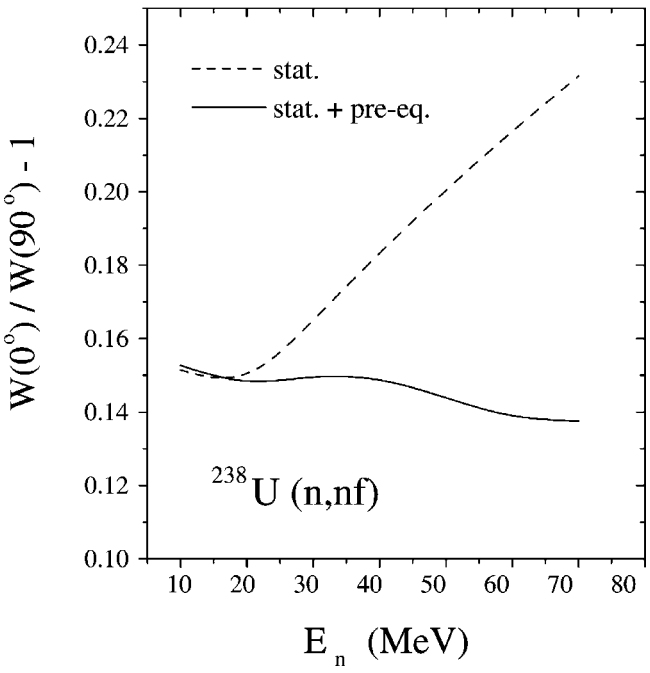

Fig. 9. The effect of pre-equilibrium neutron emission on fragment angular anisotropy in the ^{238}U(n, nf) reaction. The solid and dashed lines represent the simplified anisotropy calculations (see Eq. (21)) with and without considering the (n, n') reaction, respectively.

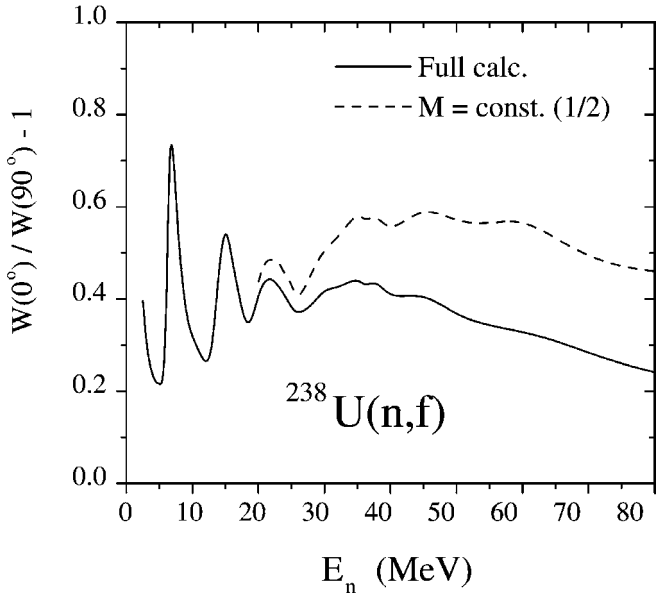

Fig. 10. The effect of deorientation of angular momentum on fragment angular anisotropy in the ^{238}U(n, f) reaction. The solid line is the same as in Fig. 6. The dashed line presents the similar calculations, but without variation of the parameter M.

gies. However, the optical + GDH model predicts the same contributions of non-compound processes to the total reaction cross section for ^{232}Th and ^{238}U. Thus, it is hard to expect that the difference in anisotropy observed for the ^{232}Th(n, f) and ^{238}U(n, f) reactions (see Table 1) is caused by the pre-equilibrium stage of the reaction.

5.2.2. Influence of multichance fission on fragment anisotropy

The average angular momentum carried away by a neutron evaporated at the statistical decay stage is about $0.5\hbar$ that results in only a slight variation of original J and M values along the decay chain. At the same time, the successive neutron evaporation is associated with “cooling" of the nucleus at a rate of about 7–8 MeV per evaporated neutron. As a consequence, there is an enhancement of anisotropy values for fissions taking place after emission of statistical neutrons (see Fig. 7c). Within the framework of the calculation procedure described in Section 4, we have traced the change of fragment anisotropy with the number of neutrons emitted before fission. Fig. 11 shows the average cumulative anisotropy versus the number of pre-fission neutrons in the ^{232}Th(n, f) and ^{238}U(n, f) reactions at $E_n = 46$ MeV. The proton emission is negligible at this incident neutron energy, so the anisotropy in either reaction is essentially determined by the isotope chain of the original compound nucleus. It is seen from Fig. 11 that the cumulative anisotropy increases progressively with the number of neutrons emitted, and, as a result, fission of the neutron-deficient isotopes has a decisive influence on the resulting anisotropy. At the same time, the distinction in the cumulative anisotropy of thorium and uranium is predicted over all fissioning isotopes starting from the compound nuclei. Such a shift of the cumulative anisotropy can be attributed to 10–15% difference in values of K_0^2 for thorium and uranium isotopes that follows from both RLDM and ETFSI estimations of J_{eff}. However, this effect

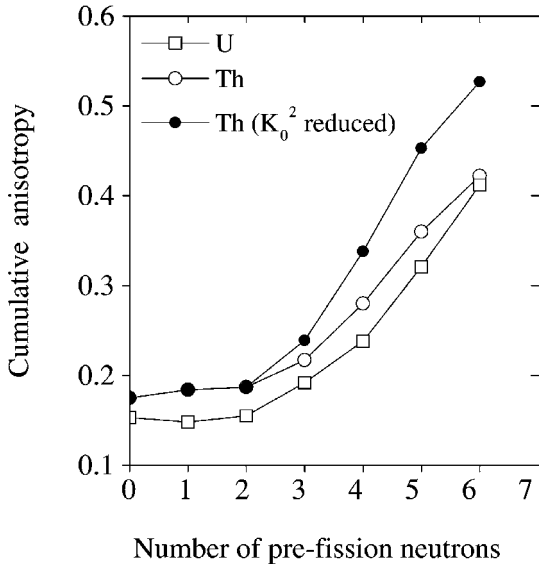

Fig. 11. Average cumulative anisotropy calculated versus the number of pre-fission neutrons in the ^{232}Th (n, f) (open circles) and ^{238}U (n, f) (open squares) reactions at $E_n = 46$ MeV. The full circles represent anisotropy of thorium calculated with reduced values of K_0^2 (see the text).

is too small to explain the difference in anisotropy of thorium and uranium observed in the experiment (see Table 1).

Bearing in mind the large contribution of the later-chance fissions to the resulting anisotropy, one can gain a better description of the thorium data at $E_n \geqslant 30$ MeV by varying the function $K_0^2(U)$ for neutron-deficient isotopes. The full circles in Fig. 11 represent the cumulative anisotropy for thorium calculated with values of K_0^2 reduced from those used to this point. The change of K_0^2 was implemented for all nuclides with $A \leqslant 230$ through a reduction of $K_0^2(U_{\rm cr})$ in Eq. (20) by 30%. The effect of such a variation of K_0^2 on the resulting anisotropy of thorium is shown in Fig. 12 for E_n above the threshold of the ^{232}Th$(n, 4nf)$ reaction.

A similar effect can be attained by modifying the chance structure of the total fission cross section of thorium. In particular, one can increase the relative number of the later-chance fissions (e.g., through a reduction of the ratio a_f/a_n) that will involve an enhancement of the resulting anisotropy. It is seen from Fig. 12 that changing the ratio a_f/a_n from 1 to 0.98 (without variation of K_0^2) enables an adequate description of the thorium data. However, the reduction of the ratio of a_f/a_n renders the calculation procedure inconsistent, since it leads to an underestimation of the total fission cross section of thorium.

The variation of K_0^2 discussed above for neutron-deficient isotopes of thorium has no influence on the fission cross section, but the issue of its validity remains open. An argument in favour of differences in values of K_0^2 between neutron-deficient isotopes of thorium and uranium may be adduced starting from the following experimentally established facts. The first one is the difference in threshold energies for symmetric and asymmetric fission of light actinides. For nuclei in the Th–U region, it was found that the barrier leading to the mass-symmetric valley is 2–3 MeV higher than the barrier leading to the mass-asymmetric valley [39,40]. In addition, there is an observation that the probability of symmetric fis-

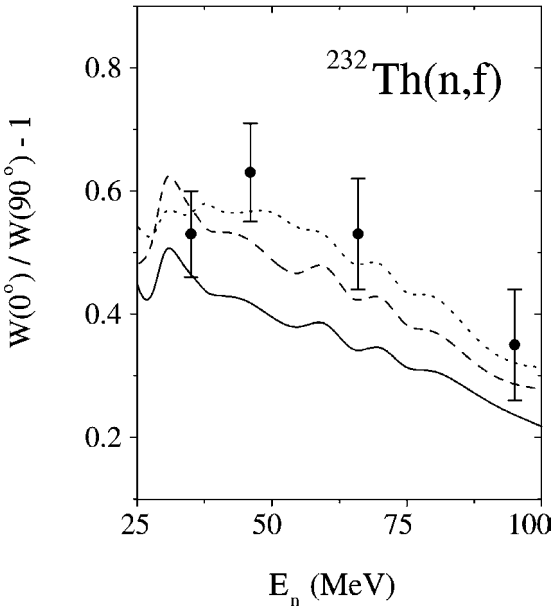

Fig. 12. The effect of reduction of K_0^2 (dashed line) and of the ratio a_f/a_n (dotted line) on fragment anisotropy of thorium. The solid line is the same as in Fig. 6.

sion of thorium isotopes at low excitation energies is significantly larger than that for uranium ones [5] that appear after emission of the same number of neutrons from the respective compound nucleus. Both these observations are consistent with recent calculations of potential-energy surfaces of fissioning nuclei by Möller et al. [41]. The calculations performed for radium and light actinides revealed that the fission paths beyond the second minimum split into symmetric and asymmetric valleys with different outer saddle point energies. The two valleys are separated from each other by a ridge which is different in height for thorium and uranium isotopes. The ridge for thorium is high enough to keep the symmetric and asymmetric valleys well separated until scission, whereas the lower separating ridge for uranium allows the symmetric path to revert back to the asymmetry valley. If this is the case, one can expect that the average saddle point temperature (and hence K_0^2) of the neutron-deficient isotopes of thorium is lower than for uranium ones.

6. Conclusions

A difference in fission fragment angular anisotropy has been observed for the neutron-induced fission of ^{232}Th and ^{238}U in the incident energy range 20–100 MeV. Analysis of the obtained data was performed starting from the SSPSM combined with pre-equilibrium and Hauser–Feshbach calculations of partial fission cross sections. The calculations fit well to the uranium anisotropy data, while the thorium ones appear to be underestimated.

According to the calculations, emission of both pre-equilibrium and statistical neutrons plays an important role in the formation of FFAD. At the pre-equilibrium stage, the (J, M)-variation caused by emission of non-statistical neutrons has a stronger influence on fragment anisotropy than the corresponding de-excitation of fissioning nuclei. As a result,

a smooth decrease of anisotropy takes place with incident neutron energy above 30 MeV. At the same time, our calculations give no grounds to expect that the difference in fragment anisotropy observed for the ^{232}Th(n, f) and ^{238}U(n, f) reactions is determined by the pre-equilibrium processes.

At the stage of the statistical decay, the neutron evaporation competes successfully with the fission process. As a consequence, multichance fission takes place in both reactions under study with a considerable contribution of high chances to the resulting angular anisotropy. Note that an important role of multi-chance fission in formation of other fission observable, fragment mass distribution, has been recently assumed by Maslov [42] to reproduce the measured branching ratio of symmetric and asymmetric fission events for the ^{238}U(n, f) reaction at neutron energies up to 200 MeV.

The anisotropy appears to be sensitive to the variation of the chance structure of the total fission cross section as well as to variation of the function $K_0^2(U)$ for nuclei fissioning at the later chances. A reduction of either the ratio a_f/a_n or $K_0^2(U_{\rm cr})$ enables an adequate fit of the thorium data. However, further investigations are needed to justify one or the other option.

Acknowledgements

The authors acknowledge the staff of The Svedberg Laboratory for providing excellent neutron beams. Two of the authors (I.V.R. and G.A.T.) wish to thank the Department of Neutron Research of the University of Uppsala, and especially H. Condé, for the hospitality and support they have received during this work. We are also indebted to A.J. Sierk for supplying us with the code MOMFIT. This work was supported in part by International Science and Technology Center (project # 540).

References

[1] R. Vandenbosch, J.R. Huizenga, Nuclear Fission, Academic Press, New York, 1973.
[2] T. Kawano, T. Ohsawa, M. Baba, T. Nakagawa, Phys. Rev. C 63 (2001) 034601.
[3] ENDF/B-VI library, National Nuclear Data Center, Brookhaven National Laboratory, http://www.nndc.bnl.gov/endf.
[4] M.C. Duijvestijn, A.J. Koning, F.-J. Hambsch, Phys. Rev. C 64 (2001) 014607.
[5] K.-H. Schmidt, S. Steinhäuser, C. Böckstiegel, A. Grewe, A. Heinz, A.R. Junghans, J. Benlliure, H.-G. Clerc, M. de Jong, J. Müller, M. Pfützner, B. Voss, Nucl. Phys. A 665 (2000) 221.
[6] I. Halpern, V.M. Strutinski, in: Proceedings of the International Conference on Peaceful Uses of Atomic Energy, Geneva 1955, vol. 2, United Nations, New York, 1956, p. 398.
[7] G.A. Tutin, I.V. Ryzhov, V.P. Eismont, A.V. Kireev, H. Condé, K. Elmgren, N. Olsson, P.-U. Renberg, Nucl. Instrum. Methods A 457 (2001) 646.
[8] H. Condé, S. Hultqvist, N. Olsson, T. Rönnqvist, R. Zorro, J. Blomgren, G. Tibell, A. Häkansson, O. Jonsson, A. Lindholm, L. Nilsson, P.-U. Renberg, A. Brockstedt, P. Ekström, M. Österlund, F.P. Brady, Z. Szeflinski, Nucl. Instrum. Methods A 292 (1990) 121.
[9] V.P. Eismont, A.V. Kireev, I.V. Ryzhov, G.A. Tutin, J. Blomgren, H. Condé, J. Rahm, and E. Ramström, in: Proceedings of the International Conference on Nuclear Data for Science and Technology Bologna, IPS, 1997, p. 658, Part II.
[10] O. Bersillon, Report CEA-N-2227, Bruyères-le-Châtel, 1981.

[11] P.G. Young, Handbook for Calculations of Nuclear Reaction Data, IAEA-TECDOC-1034, 1998, p. 131.
[12] M. Blann, Report COO-3494-10, Rochester University, 1978.
[13] M. Blann, H.K. Vonach, Phys. Rev. C 28 (1983) 1475.
[14] M. Ivascu, M. Avrigeanu, V. Avrigeanu, Z. Phys. A 329 (1988) 177.
[15] M. Avrigeanu, M. Ivascu, V. Avrigeanu, Report NP-63, 1987.
[16] M. Uhl, Acta Phys. Austriaca 31 (1970) 245.
[17] M. Uhl, B. Strohmaier, Report IRK-76/01, IRK Vienna, 1976.
[18] W. Dilg, W. Schantl, H. Vonach, M. Uhl, Nucl. Phys. A 217 (1973) 269.
[19] Huang Zhongfu, He Ping, Su Zongdi, Zhou Chunmei, Chin. J. Nucl. Phys. 13 (1991) 147, RIPL homepage, http://iaeand.iaea.or.at/ripl/densities.htm, file beijing_bs.dat.
[20] A.V. Ignatyuk, G.N. Smirenkin, A.S. Tishin, Sov. J. Nucl. Phys. 21 (1975) 255.
[21] RIPL homepage, http://iaeand.iaea.or.at/ripl/densities.htm, file .dat.
[22] W. Younes, J.A. Becker, L.A. Bernstein, P.E. Garrett, C.A. McGrath, D.P. McNabb, R.O. Nelson, G.D. Johns, W.S. Wilburn, D.M. Drake, Phys. Rev. C 64 (2001) 054613.
[23] A.J. Sierk, Phys. Rev. C 33 (1986) 2039.
[24] A.J. Sierk, private communication.
[25] H.C. Britt, J.R. Huizenga, Phys. Rev. C 9 (1974) 435.
[26] G.N. Smirenkin, V.G. Nesterov, A.S. Tishin, Report IPPI-67, 1966 (in Russian).
[27] M. Brack, J. Damgaard, A.S. Jensen, H.C. Pauli, V.M. Strutinsky, C.Y. Wong, Rev. Mod. Phys. 44 (1972) 320.
[28] R.W. Hasse, W.D. Myers, Geometrical Relationships of Macroscopic Nuclear Physics, Springer-Verlag, Berlin, 1988.
[29] A. Mamdouh, J.M. Pearson, M. Rayet, F. Tondeur, Nucl. Phys. A 644 (1998) 389.
[30] P.W. Lisowski, J.L. Ullmann, S.J. Balestrini, A.D. Carlson, O.A. Wasson, and N.W. Hill, in: Proceedings of the International Conference on Nuclear Data for Science and Technology, Mito, 1988, p. 97.
[31] A.D. Carlson, S. Chiba, F.-J. Hambsch, N. Olsson, and A.N. Smirnov, in: Proceedings of the International Conference on Nuclear Data for Science and Technology, Bologna, IPS, 1997, p. 1223, Part II.
[32] E. Raeymackers, S. Benck, I. Slypen, J.P. Meulders, N. Nica, V. Corcalciuc, A.J. Koning, in: Proceedings of the International Workshop on P&T and ADS developments, Mol, Belgium, 2003, http://www.sckcen.be/sckcen_en/activities/conf/conferences/20031006.
[33] J.P. Lestone, A. Gavron, Phys. Rev. C 49 (1994) 372.
[34] V.A. Konshin, JAERI-Research 95-036.
[35] A.V. Ignatyuk, V.M. Maslov, A.B. Paschenko, Sov. J. Nucl. Phys. 47 (1988) 224.
[36] V.M. Maslov, Yu.V. Porodzinskij, M. Baba, A. Hasegawa, N.V. Kornilov, A.B. Kagalenko, N.A. Tetereva, Phys. Rev. C 69 (2004) 034607.
[37] EXFOR library, National Nuclear Data Center, Brookhaven National Laboratory, http://www.nndc.bnl.gov/nndc/exfor.html, 2001.
[38] S. Kailas, Phys. Rep. 284 (1997) 381.
[39] T. Ohtsuki, H. Nakahara, Y. Nagame, Phys. Rev. C 48 (1993) 1667.
[40] S. Oberstedt, F.-J. Hambsch, F. Vivès, Nucl. Phys. A 644 (1998) 289.
[41] P. Möller, D.G. Madland, A.J. Sierk, A. Iwamoto, Nature 409 (2001) 785.
[42] V.M. Maslov, Eur. Phys. J. A 21 (2004) 281.

Neutron and Light Charged Particle Production in Neutron or Proton-induced Reaction on Iron, Lead and Uranium at Intermediate Energy (20 to 200 MeV) – The HINDAS Collaboration

F.-R. Lecolley[1], G. Ban[1], V. Blideanu[1], J. Blomgren[3], P. Eudes[2], Y. Foucher[2], A. Guertin[2], F. Hadad[2], A. Hildebrand[3], J.-F. Lecolley[1], T. Lefort[1], N. Marie[1], P. Mermod[3], N. Olsson[3], M. Osterlund[3], S. Pomp[3], A.V. Prokofiev[4], and C. Lebrun[5]

1 – LPC Caen, CNRS/IN2P3 – 6, Bld du Maréchal Juin, 14050 Caen Cedex (France)
2 – SUBATECH Nantes, CNRS/IN2P3 – 44070 Nantes Cedex 03 (France)
3 – Department of Neutron Research, Uppsala University – Box 525, 75120 Uppsala (Sweden)
4 – The Svedberg Laboratory, Uppsala University – Box 533, 75121 Uppsala (Sweden)
5 – LPSC Grenoble, CNRS/IN2P3 – 53, av des Martyrs, 38026 Grenoble (France)

Abstract. The process of particle emission in the pre-equilibrium stage has a very important contribution in this energy region and several approaches have been proposed to explain it. Their prediction power must be tested using comparison with the data for a variety of configurations. Calculations have been done using the exciton model and two main approaches proposed to improve its predictive power for complex particle emission. Data reported in this work allow the extension to higher energies of databases that are now limited to energies around 60 MeV. Together with other experimental results available in the literature they allow a more global view on the capabilities of each approach.

INTRODUCTION

An accelerator-driven system (ADS) consists of the coupling of a high-energy intense proton beam (~1 GeV) with a spallation target and a subcritical core. The proton beam that is incident on the ADS target will create a large amount of spallation products, mainly neutrons, protons and light charged particles with energies covering the full range up to the GeV region.

Although a large majority of the neutrons will be below 20 MeV, the relatively small fraction at higher energies still has to be characterized. Above 200 MeV, the already measured data have given enough constraints and the cross sections are predicted rather accurately by Intra Nuclear Cascade (INC) model [1,2]. For energy lower than 20 MeV, nuclear data libraries are nearly complete and have been extensively used for nuclear plant design and control under the IAEA direction.

In between (20-200 MeV), the situation is clearly the most unsatisfactory on the experimental and theoretical point of view. Very little high-quality data exist in this energy domain in particular above 60 MeV. The introduction of the so-called pre-equilibrium process in order to explain the smooth dependence of particle emission probability with angle and energy was the first major step in the evolution of nuclear reaction models in this energy range. During the last 40 years several approaches giving a theoretical description of the pre-equilibrium process have been proposed. While most of them have shown from the beginning a good predictive power for energy distributions of nucleons in nucleon-nucleus reactions over a wide body of experimental results, for complex particles however great difficulties have been encountered when trying to reproduce experimental distributions, since the production rate for these particles was systematically underestimated.

CP769, *International Conference on Nuclear Data for Science and Technology,*
edited by R. C. Haight, M. B. Chadwick, T. Kawano, and P. Talou
© 2005 American Institute of Physics 0-7354-0254-X/05/$22.50

A good example in that sense is the Griffin (or exciton) model originally introduce in 1966 [3]. Along the way, much physics has been added and important modifications have been made to this model in order to get a reasonable theoretical description especially for complex particle emission. The introduction of cluster formation probability during the nucleon-nucleon interaction inside the nucleus in the pre-equilibrium phase proposed in 1973 [4] and the completely different approach formulated by Kalbach in 1977 [5] considering the contribution of direct pick-up and knock-out mechanism in the outgoing spectra of complex particle are the two most important approaches and were developed in order to get a satisfactory agreement with the experimental results [5,6].

Using a new set of data recorded in the framework of the HINDAS program [7], we have tested the exciton model that is implemented in the GNASH code [8] and its improved version following the two approaches described above. In section I typical experimental results obtained within HINDAS are presented. Comparisons with the several theoretical approaches all based on the exciton model are shown in section II. Competition between pre-equilibrium emission and equilibrium emission is studied in section III. The conclusions of this work are given in the last section.

I. EXPERIMENTAL RESULTS

In the framework of the HINDAS program using several facilities available along Europe, we have performed a "complete" set of experiments in order to measure Double Differential Cross-Sections (DDCS) for neutrons and/or light charged particles (up to A=4) emitted in neutron or proton-induced reaction on iron, lead and uranium at intermediate energy. Full lists of the available results are presented in Table 1 below. As an illustration, some results obtained 96 MeV neutrons on iron, lead and uranium are presented in Fig. 1. More details can be found in the following references [9,10].

TABLE 1. HINDAS contribution at intermediate energy.

Incident Particle	Incident Energy	Emitted Particle	Target	Facility
neutron, proton	63 MeV	N, p, d, t, ^{3}He, ^{4}He	Co, Pb, U	Cyclone – Belgium
neutron	96 MeV	p, d, t, ^{3}He, ^{4}He	Fe, Pb, U	TSL – Sweden
proton	135 MeV	p, d, t, ^{3}He, ^{4}He	Fe, Pb, U	AGOR – Nederland

For a detail comparison with theoretical models, energy distributions are needed. They are derived from DDCS using the Kalbach systematic [11]. Results for the 96 MeV neutron-induced reaction on iron, lead and uranium are presented in Fig. 2.

One can see that for the heaviest target the distributions are quite similar in shape, small differences can be found in amplitude with an increase emission probability over all emitted particles for the uranium target. The main difference is found at low energy (below 20 MeV) where an isotropic component is dominant for the iron target. These low-energy particles are emitted mainly following the evaporation process of excited nuclei; for the lead and the uranium targets, this emission is strongly inhibited by Coulombian effects.

Integral yield can be extracted from energy distributions for each type of particle. Cross-sections in mb are listed for 96 MeV neutron-induced reactions on iron, lead and uranium in Table 2. One of the main information that can be extracted from those values is the contribution of complex particles over light charged particles. This contribution correspond at least to 30% whatever the target is and underline the need for theoretical approaches to be able to reproduce this contribution.

TABLE 2. Integral yield (mb) for 96 MeV neutron-induced reactions.

Emitted Particle	Fe	Pb	U
proton	584±29	485±24	589±29
deuteron	131±06	137±07	170±08
triton	21±01	53±03	54±03
helium 3	10±01	---	---
helium 4	167±08	45±02	52±03

II. COMPARISON WITH THEORETICAL PREDICTIONS

The exciton model [3] is one of the most common models used in calculation of the pre-equilibrium emission in nucleon-induced reactions at intermediate energy. In this approach, it is assumed that the excitation process takes place by successive nucleon-nucleon interactions inside the nucleus. Each interaction produces another exciton leading the system to the final state of statistical equilibrium through more complex states. Occasionally a particle can receive enough energy to leave the system and then be emitted. The pre-equilibrium spectrum is the sum of contribution from each state, particles emitted in the earlier stages having more energy than those emitted in the later stages. Only energy distributions of emitted particle can be calculated in the framework of this model.

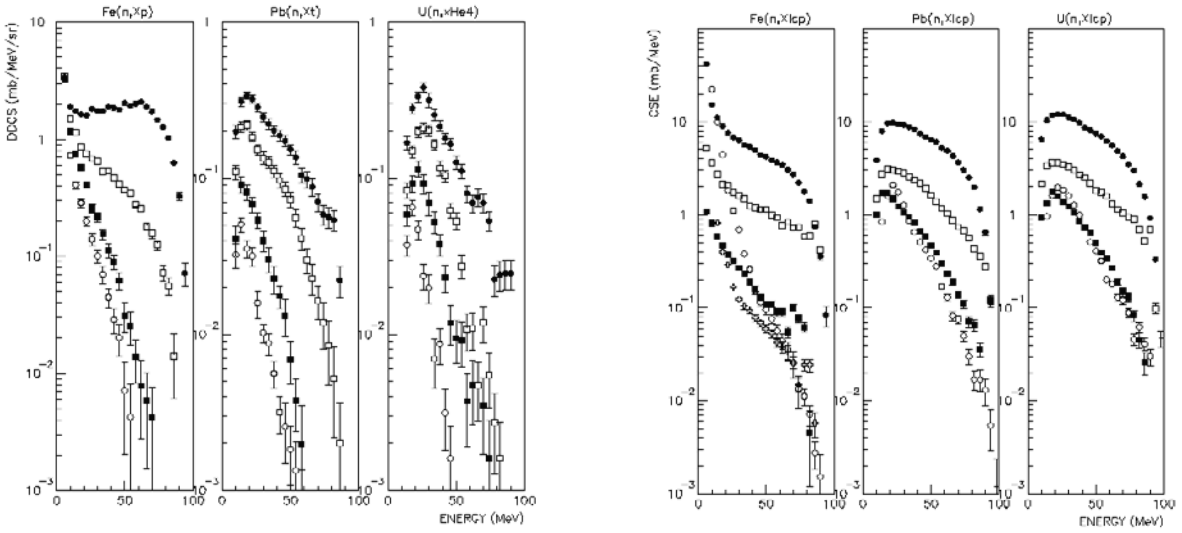

FIGURE 1. Left part: DDCS in 96 MeV neutron-induced proton emission on iron (left picture, triton emission on lead (central picture) and alpha particle emission on uranium (right picture) at 20° (black circle), 60° (open square), 100° (black square) and 140° (open circle). Right part: Energy Distribution for light charged particles emitted in 96 MeV neutron-induced reactions on iron (left picture), lead (central picture) and uranium (right picture); black circle are proton, open square deuteron, black square triton, open cross 3He and open circle alpha particles.

The GNASH code [8] used the exciton model to calculate the pre-equilibrium component while the equilibrium contribution is calculated using the Hauser-Feshbach formalism [12]. Cross-sections evaluated using GNASH are implemented in MCNPX, a largely used code in specific applications. The results obtained for neutron-induced reactions at 96 MeV on lead are compared to our data in Fig. 2.

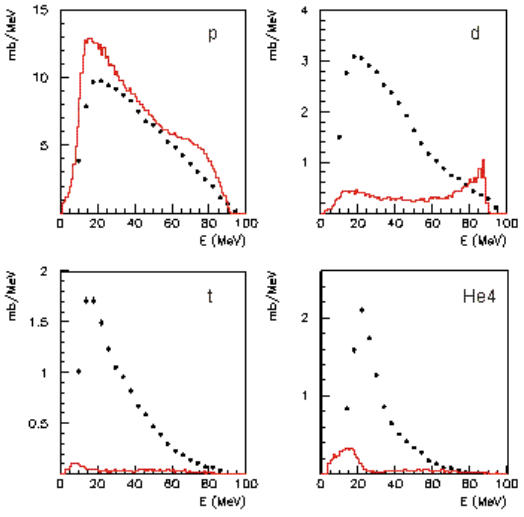

FIGURE 2. Energy distribution for proton, deuteron, triton and alpha particles emitted in 96 MeV neutron-induced reactions on lead. GNASH evaluation (curve), experimental results (dot).

While the proton emission is relatively well described, the production of complex particles is strongly underestimated in the GNASH calculations. This suggests the need of significant improvements in the exciton model in order to increase its prediction level in the case of cluster emission.

The first improvement was proposed by Ribansky and Oblozinsky [4] in 1973 by introducing in the particle production rate expression a multiplicative term containing the cluster formation probability. The physical background of this parameter has been given in [13] in the framework of the coalescence model. The cluster formation probability is a free parameter of the model and is calculated by adjusting energy differential distributions to experimental data. This approach is available to the community via the PREEQ program [14] and the latest version of the code GEANT, which is intensively used in simulations [15].

The first step in our analysis was the calculation of the free parameter using data recorded at 96 MeV neutron-induced reactions on iron and lead. The cluster formation probability has been determined by normalizing the calculated energy distributions for complex particles to the experimental data. The results are presented in Fig. 3 for the Fe(n,X) and Pb(n,X) reactions at 96 MeV incident energy. The shape of calculated distributions in the pre-equilibrium region is in good agreement with the experimental results. The amplitudes of the distributions in the case of protons are very well described by the model. However, no conclusion can be retained for the moment concerning the amplitude of calculated distributions for complex

amplitude of calculated distributions for complex particles since they were obtained by adjusting the cluster formation probability.

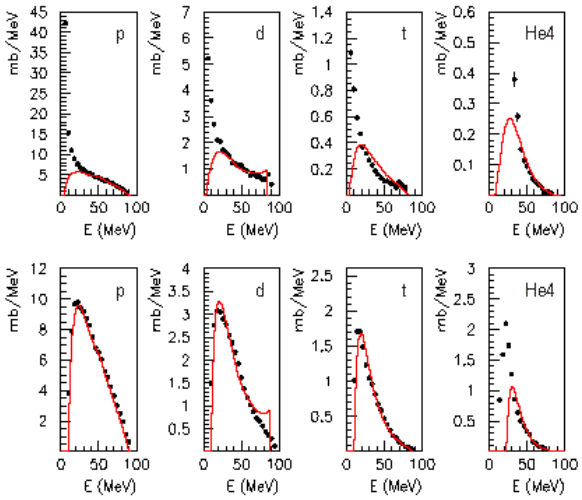

FIGURE 3. Energy distribution for light charged particles emitted in 96 MeV neutron-induced reactions on iron (top pictures) and lead (bottom pictures). PREEQ code (curve) and Experimental results (dot).

Therefore, the second step of our analysis was to check the stability of this free parameter while changing the incident energy and/or the projectile. Calculations have been redone for the reactions Bi(p,X) at 39 MeV and Pb(p,X) at 63 MeV incident energies using the same values for cluster formation probability. The calculations results are compared to data from [10] and [16] in Fig. 4. Again a good agreement is found between calculations and experimental results in the pre-equilibrium region (the contribution of direct reactions is not calculated by the model and is supposed to be dominant for high emission energies). The good reproduction of the amplitude of experimental distributions demonstrates a good predictive power of the model.

A completely different approach has been proposed in 1979 by C. Kalbach [5]. It is based on the fact that direct reactions are no taking into account in the exciton model. Therefore their contribution must be calculated and then added to the pre-equilibrium contribution calculated with the original exciton model. The code PRECO-2000 [17] calculates nucleon and complex particles pre-equilibrium spectra in nucleon-induced reactions using this approach and is open to the community via Data Bank Computer Program Services of NEA. The same approach has been recently implemented in the TALYS code [18], which is still under development and should be soon available to the community.

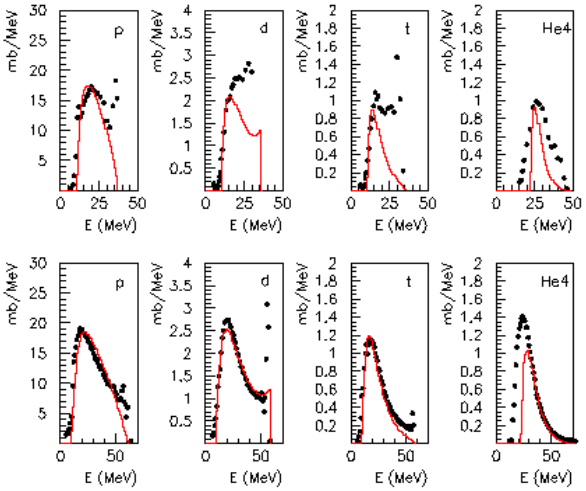

FIGURE 4. Energy distribution for light charged particles emitted in 39 MeV proton-induced reactions on bismuth (top pictures) and 63 MeV proton-induced reaction on lead (bottom pictures). PREEQ code (curve) and Experimental results (dot).

Calculations have been done with PRECO-2000 first for the reactions at 96 MeV neutrons. The results are presented in Fig. 5. The disagreement with the experimental distributions is rather strong for both reactions. In the case of the iron target non-equilibrium complex particle emission is overestimated while in the case of the lead target, its production is underestimated. Even if not so strong as in the case of complex particles, a disagreement is found however also for proton emission. Better agreement can be found when changing the incident energy and/or the projectile as it can be seen in Fig. 6. This shows that model predictions strongly depend on incident energy and the projectile type that is of course a shortcoming of the model. Same conclusions are obtained with the TALYS code.

III. COMPETITION BETWEEN PRE-EQUILIBRIUM EMISSION AND EQUILIBRIUM EMISSION

The calculations performed using the code PREEQ have shown that this approach allows a better description of particle emission in the pre-equilibrium stage. For this reason the results obtained using this model will be used in the further discussions.

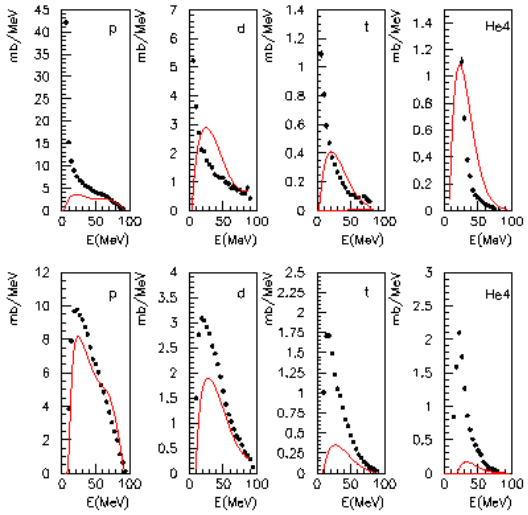

FIGURE 5. Energy distribution for light charged particles emitted in 96 MeV neutron-induced reactions on iron (top pictures) and lead (bottom pictures). PRECO-2000 code (curve) and Experimental results (dot).

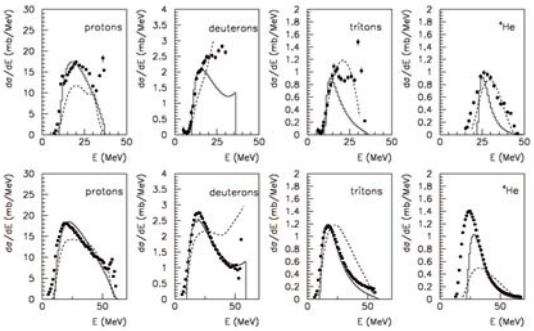

FIGURE 6. Energy distribution for light charged particles emitted in 39 MeV proton-induced reactions on bismuth (top pictures) and 63 MeV proton-induced reaction on lead (bottom pictures). PRECO code (dashed curve), PREEQ code (full curve) and Experimental results (dot).

The experimental results presented in Fig. 1 suggest that for heavier target nuclei almost all particles are emitted during the pre-equilibrium stage of the reaction while for light target nuclei the low energy component in the experimental distributions suggests that the particle emission at equilibrium is important in this case. This equilibrium contribution is calculated separately assuming that it results from two sources; the first one is the so-called "pure evaporation" and concerns the evaporation of the compound nucleus arrived at the statistical equilibrium; the second one is the evaporation of residual nuclei resulting after pre-equilibrium emission.

The fraction of pre-equilibrium emission considering n, p, d, t, He3 and alpha particles is determined using the pre-equilibrium spectra calculated with the PREEQ code. The result for Fe(n,X) reaction at 96 MeV is found to be 0.993 and is in agreement with other results obtained for the same reaction at lower incident energy. This means that the evaporation of the compound nucleus gives a very small component since its contributions is inferior to 1%. Again using PREEQ in order to determine the excitation energy of the residual nucleus resulting after pre-equilibrium emission and its formation probability, we were then able to calculate the evaporation spectra associated to the two sources using the Hauser-Feshbach formalism. The results obtained for the Fe(n,X) reaction at 96 MeV are given in Fig. 7 together with the pre-equilibrium component calculated in section II. The total particle emission spectrum given by the sum of the pre-equilibrium emission and equilibrium emission is also presented in the figure. The agreement found over the full energy range is relatively good except for alpha particles in the energy region around 20 MeV where the calculated distributions are below the experimental results. The same effect has been found for Pb(n,xHe4) reaction at 96 MeV, showing that pre-equilibrium contribution is underestimated in this energy region for all targets.

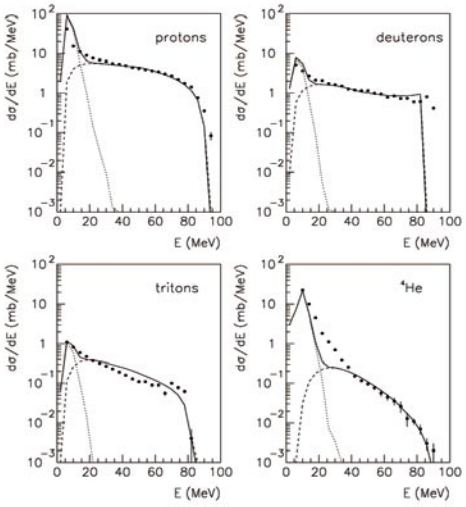

FIGURE 7. Energy distribution for light charged particles emitted in 96 MeV neutron-induced reactions on iron. Pre-equilibrium component (dashed line), Equilibrium component (dotted line), Total particle emission spectrum (full curve) and Experimental results (black dot). See text for more details.

Another way to study the competition between pre-equilibrium emission and equilibrium emission is to use the Kalbach parameterization [11] to calculate the fraction f_{PE} of the pre-equilibrium emission. In this parameterization, double differential distributions are derived from energy distributions. In Fig. 8 are presented the results obtained for proton emission in 96 MeV neutron-induced reactions on iron and lead for three energy domains selected from the emission spectra. A general agreement is found when

comparing calculation results with the experimental distributions. These calculations allow a better identification of different mechanisms that low energies, both evaporation and pre-equilibrium particles are emitted, their contribution depending on the target nucleus. The evaporation process is dominant for light targets (1- f_{PE} =0.88 and a quasi-isotropic distribution in the case of iron) while for the heavier target even low energy particles are emitted in the pre-equilibrium stage (f_{PE}=0.80 and a slightly forward peaked distribution). The emission of energetic particles occurs before equilibrium (f_{PE} =1). Similar agreement was also found for complex particle emission, showing that this parameterization is able to give a proper description of double differential distributions.

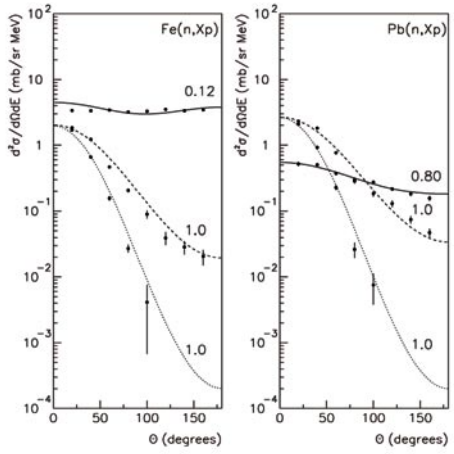

FIGURE 8. Angular distribution for proton emission in 96 MeV neutron-induced reactions on iron and lead and for three energy domain (8-12 MeV continuous line, 40-44 MeV dashed line, 68-72 MeV dotted line). Symbols are the experimental results obtained by our collaboration.

CONCLUSIONS

The extension to higher energies of the available results on nucleon-induced reactions in the 20-200 MeV range in the framework of the European Collaboration HINDAS together with the data already existing in the literature at lower energies allowed a detailed study of the predictive power of the exciton model and its improved version for the description of nucleons and complex particles emission. While all approaches are in a reasonable good agreement with experimental results for nucleon emission, only the PREEQ code was able to reproduce complex particle emission that represents at least 30% of the total cross-section for light charge particle emission. At intermediate energy and for all targets, the pre-equilibrium emission is the dominant process. Equilibrium emission comes mainly from the decay of residual nuclei obtained after pre-equilibrium emission. The Kalbach parameterization proposed by C. Kalbach for double differential distributions is still valid. This underlines the need for theoretical models to provide at least a good description of the energy-differential cross section.

ACKNOWLEDGMENTS

This work was supported by the European Community under contract No. FIKW-CT-2000-0031 and by the GDR GEDEPEON (research group CEA-CNRS-EDF-FRAMATOME).

REFERENCES

1. H.W. Bertini, *Phys. Rev.* **188**, (1969).
2. J. Cugnon et al, *Nucl. Phys. A* **620**, (1997).
3. J.J. Griffin, *Phys. Lett.* **17**, 478 (1966).
4. I. Ribansky and P. Oblozinsky, *Phys. Lett. B* **45**, 318 (1973).
5. C. Kalbach, *Z. Phys. A* **283**, 401 (1977).
6. J.R. Wu and C.C. Chang, *Phys. Rev. C* **17**, 1540 (1978).
7. HINDAS, *High and Intermediate energy Nuclear Data for Accelerator-driven Systems,* European Community, Contract No. FIKW-CT-2000-0031.
8. P.G. Young et al, *The GNASH Code*, LA-12343-MS, (1992).
9. V. Blideanu et al, *Phys. Rev. C* **70**, 014607 (2004).
10. A. Guertin, N. Marie et al, *Eur. Phys. J. A* **23**, 49 (2005).
11. C. Kalbach, *Phys. Rev. C* **37**, 2350 (1988).
12. W. Hauser and H. Feshbach, *Phys. Rev.* **87**, 366 (1952).
13. H. Machner, *Phys. Lett B* **86**, 129 (1979).
14. E. Betak, *Comp. Phys. Comm.* **9**, 92 (1975).
15. GEANT4 Physics Reference Manual, *http://wwwasd.web.cern.ch /wwwasd/geant4/geant4.html*
16. F.E. Bertrand and R.W. Peele, *Phys. Rev. C* **8**, 1045 (1973).
17. C. Kalbach-Walker, *Users Manual for PRECO-2000*, (2001).
18. A. Koning, unpublished.

Comparison of Measured and Calculated Mass Distributions of Fission Fragments in Proton-Induced Fission of ^{232}Th, ^{235}U, ^{238}U, and ^{237}Np at Intermediate Energies

Oleg I. Batenkov[1], Vilen P. Eismont[1], Mikhail J. Majorov[1], Andrey N. Smirnov[1], Kjell Aleklett[2], Walter Loveland[3], Jan Blomgren[4], Henri Condé[4], Marieke Duijvestijn[5], and Arjan Koning[5]

[1] *V.G. Khlopin Radium Institute, 2oi Murinskiy Prospect 28, Saint-Petersburg 194021, Russia*
[2] *Department of Radiation Sciences, Uppsala University, Box 535, S-751 21 Uppsala, Sweden*
[3] *Dept. of Chemistry, Oregon State University, Corvallis, OR 97331 USA*
[4] *Department of Neutron Research, Uppsala University, Box 525, S-751 20 Uppsala, Sweden*
[5] *Nuclear Research and Consultancy Group, Westerduinweg 3, NL - 1755 ZG Petten, Netherlands*

Abstract. The mass distributions of fragments produced by proton-induced fission of ^{232}Th, ^{235}U, ^{238}U, and ^{237}Np at proton energies of 50 and 96 MeV have been measured. The measurements were carried out at The Svedberg Laboratory, Uppsala, Sweden using a high-precision time-of-flight spectrometer for fission fragments and fission neutrons. The measured mass distributions are compared to ones calculated using the TALYS code. Using proton-induced reactions to simulate the outcome of more difficult measurements with neutron beams is discussed.

INTRODUCTION

The properties of the fission-fragment mass distributions and, in particular, the presence of symmetric and asymmetric mass splits of the fissioning nucleus, remains the one of the major questions in fission physics. Study of these properties over a wide excitation energy range may contribute to a better understanding of the fission process. Fission-fragment mass distributions are relatively well known only at low excitation energies (below 20 MeV). New technological developments, such as ADS, stimulate the study of fission-fragment mass distributions at higher energies. This paper presents measurements of the fission fragment mass distributions for the fission of ^{232}Th, ^{235}U, ^{238}U, and ^{237}Np induced by 50- and 96-MeV protons. Data for ^{235}U and ^{237}Np in this energy range were obtained for the first time.

EXPERIMENTAL

The measurements were carried out at the Gustaf Werner cyclotron of The Svedberg Lab, Uppsala University, within the framework of an international collaboration studying the fission process. The experiment was done with the use of a high-precision time-of-flight spectrometer for fragments and neutrons [1]. Experimental details and results of the neutron emission study (neutron multiplicity and energy distributions) are given in [2]. This paper presents experimental measurements of the properties of the fission fragments. The experimental setup involves a thin-walled stainless steel vacuum chamber with an array of fission fragment detectors inside. Fission fragment velocities were measured using a time-of-flight technique. The fission fragments passed through a pair of microchannel plate detectors (MCP) placed on either side of the target at 90^o with respect to the beam. Electrons, knocked out by fission fragments in passing through aluminum oxide foils (first foil: 60 μg/cm^2, 15 mm in diameter, located at distance of 10 mm from the target, second foil: 60 μg/cm^2, 30 mm

CP769, *International Conference on Nuclear Data for Science and Technology,*
edited by R. C. Haight, M. B. Chadwick, T. Kawano, and P. Talou
© 2005 American Institute of Physics 0-7354-0254-X/05/$22.50

in diameter, located at distance of 80 mm from the target), were focused on MCPs (start and stop detector). After passing through the time-of-flight arm, fission fragments could also strike silicon detectors (30 mm in diameter, 80 mm distance from the target), which were used to measure the fragment energies and to act as stop detectors for the time-of-flight measurement. The time resolution of the MCP detectors was 80 ps. This did not worsen the intrinsic fission-fragment mass resolution (due to the recoil of emitting neutrons) significantly. This resolution was found to be about 2 amu. As fission neutrons do not change the average velocity of fragments, fission-fragment masses defined according to this time-of flight technique are the primary, "pre-neutron emission" values.

The measured mass distributions (normalized to 200%) are shown in Fig. 1. The results for the fission of ^{232}Th at 50 MeV are compared to the results obtained in [4,5] for the same nucleus at E_p = 53 MeV by measuring energies of coincident pairs of fission fragments using surface barrier detectors. The results for ^{238}U at 50 MeV are compared to results [6] at the same energy, obtained by time-of-flight technique with two position sensitive avalanche counters, placed at 90^o to the beam and having angular acceptance of 56 degrees. The data for ^{232}Th at the higher excitation energy as well as the data for ^{235}U and ^{237}Np are new measurements. Our data agree with the previous measurements for the widths of the fission mass distributions. However, our data show more pronounced structure for near symmetric mass splits. At 96 MeV for ^{232}Th and ^{238}U, a symmetric fission peak in the mass distribution is especially pronounced, particularly for ^{232}Th. In comparing data from the various papers [4-6] at the same projectile energy one should take into account that the difference in mass distribution behavior may be due, in part, to an angular anisotropy of "cold" (asymmetric) and warmer (symmetric) fission. The higher symmetric fission yields for ^{232}Th may represent a nuclear structure effect in fission.

MASS DISTRIBUTION CALCULATIONS AND COMPARISON TO EXPERIMENTAL DATA.

Calculations of the fission mass distributions were carried out with the nuclear reaction code TALYS [10]. Fission cross sections were calculated assuming a Hill-Wheeler penetrability through a double-humped

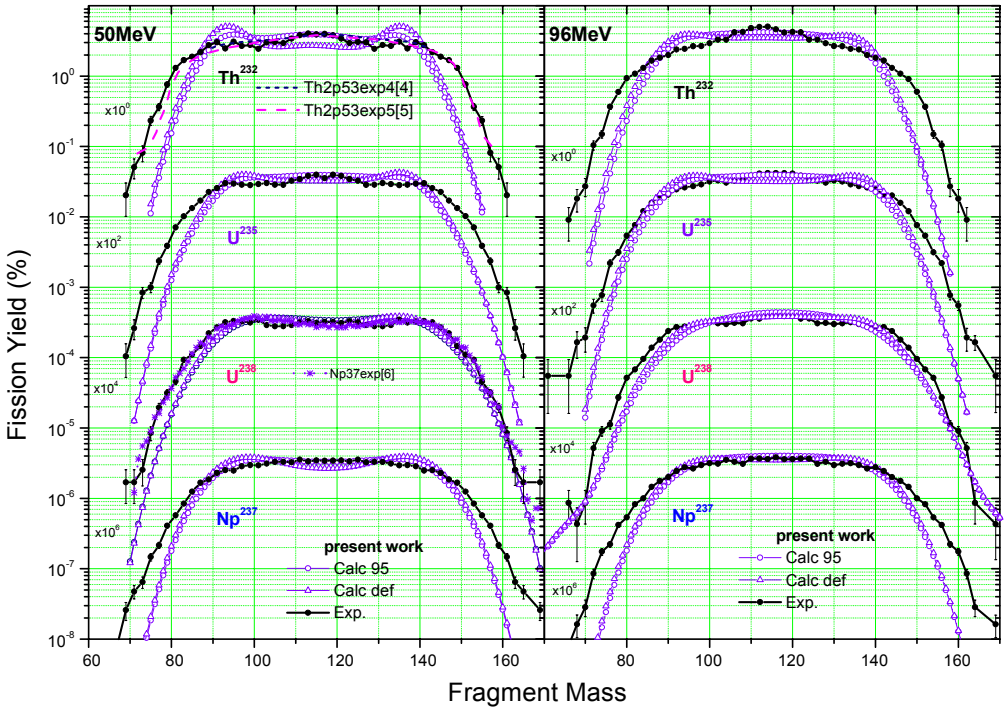

FIGURE 1. Mass yield curves for the proton-induced fission of ^{232}Th, ^{235}U, ^{238}U, ^{237}Np at Ep=50 MeV and 96 MeV.

fission barrier, including an explicit treatment of the collective effects on the level densities. The competition of all other reaction channels is taken into account over the whole evaporation chain. Subsequently, the fission-fragment mass yields are computed per fissioning system in two steps [3]: (i) the relative contributions of the different fission modes are evaluated using Hill-Wheeler penetrabilities with ground-state level densities and temperature-dependent barrier parameters, (ii) the mass yield curve corresponding to each fission mode is calculated in the framework of the multi-modal random-neck rupture model (MM-RNRM) by Brosa [7]. For each of the reactions studied in the present paper two results are presented: (a) Default TALYS calculations using the fission barriers for the fission modes SL, STI, and STII as they are predicted by the Brosa model (calc def) and (b) TALYS calculations with all SL-barriers reduced by 5% (calc 95).

As shown in Fig. 1, the calculations are sensitive to the height of the symmetric fission barrier. By means of a mass distribution decomposition into symmetric and asymmetric components, it was determined that the best fit to the experimental results was obtained with a 5% reduction of the SL barrier. A comparison of the calculated and measured results reveals a systematic underestimation of the mass distribution width. Furthermore, the calculation is not able to reproduce the distinct symmetric hump in the experimental mass yield curve of ^{232}Th and ^{235}U. Apparently, the MM-RNRM model overestimates the width of the SL mode and underestimates the width of the ST mode. In general, the fission-product mass yields are predicted within 30% for the mass range 90-140. The pre-fission (pre-equilibrium,ν_{pre}, and equilibrium, ν_{eq}) neutron multiplicities are a very important input for the theory, because they allow one to estimate the nuclear temperature at the scission point. Measured and calculated numbers of pre-fission neutrons are compiled in Table 1 for the reaction studied in this work. There is some disagreement between theory and experiment as to the relative numbers of pre-equilibrium and equilibrium neutrons. The total number of neutrons, however, agrees on average within the limits of the experimental uncertainties.

TABLE 1. Number of ν_{pre} and ν_{eq} neutrons emitted prior to fission.

Target	Ep=50 MeV				Ep=96 MeV			
	Exp.		Calc. [10]		Exp.		Calc. [10]	
	ν_{pre}	ν_{eq}	ν_{pre}	ν_{eq}	ν_{pre}	ν_{eq}	ν_{pre}	ν_{eq}
^{232}Th	0.5±0.3	2.4±0.3	0.3	3.2	1.1±0.3	3.4±0.3	0.4	5.0
^{238}U	0.5±0.3	2.6±0.3	0.2	1.3	1.1±0.3	2.9±0.3	0.3	3.0
^{235}U	0.5±0.3	1.5±0.3	0.3	1.6	1.1±0.3	2.7±0.3	0.4	3.7
^{237}Np	0.5±0.3	1.9±0.3	0.3	1.6	1.1±0.3	3.0±0.3	0.4	3.2

COMPARISON OF FISSION FRAGMENT MASS DISTRIBUTIONS IN PROTON AND NEUTRON INDUCED FISSION.

Fission fragment yields at intermediate neutron energies (above 20 MeV) are of interest in accelerator transmutation of waste. Theoretical studies of the mass distributions in proton- and neutron-induced fission at intermediate energies have been carried out [3]. If the same compound nucleus is produced in neutron and proton-induced reactions, then one expects the characteristics of fission will be identical. In reactions of neutrons and protons with heavy nuclei at energies less than 10-15 MeV, one expects a small contribution of direct reactions and most reactions will involve compound nucleus formation. In a recent paper [8], where variation of the ratio of yields of symmetric and asymmetric fission versus number of neutrons in the compound nucleus at the same excitation energy (14 MeV above fission threshold) was studied, no significant differences between neutron- and proton-induced reactions has been found. In all cases, the fraction of symmetric fission grows as the number of neutrons in the compound nucleus decreases. Generally speaking, at higher energies, as a result of the difference in direct processes for protons and neutrons, a difference in the properties of the fissioning nuclei (Z, N, E*) is possible, and hence, of integral yields observed in the experiment. Mass distributions obtained in this work and in [6] for the proton-induced fission of ^{238}U at proton energies 20-60 MeV were compared to results of [9] for neutron-induced fission of ^{238}U at neutron energies up to 200 MeV. In all cases the experimental mass distributions were represented by the sum of three Gaussians (two of them corresponding to asymmetric fission and one to symmetric fission). It was assumed that positions of maximum of the Gaussians were

defined by the mass of composite nucleus (corrected for pre–fission neutron emission), and that the widths and areas of the Gaussians corresponding to asymmetric component of fission, are equal. The symmetric fission yields so determined are presented in Fig. 2 as a function of the energy of the incident particles. It is seen that in each reaction the fraction of symmetric fission increases as the incident nucleon energy increases, but the rate of increase decreases with increasing energy. As in the above-considered case of the fission of compound nuclei the probability of symmetric fission increases as the number of neutrons decreases: from N=147 for ^{238}U+n to N=146 for ^{238}U+p and N=144, 143, 142 for ^{237}Np, ^{235}U and ^{232}Th+p, respectively. The observed trends are consistent with calculations [10].

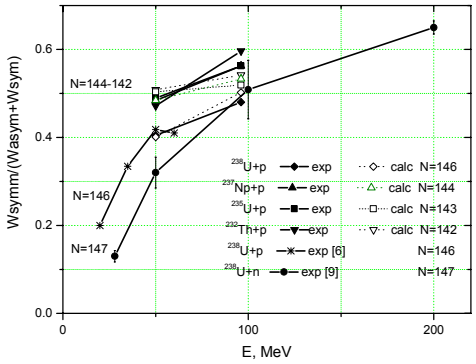

FIGURE 2. A comparison of the experimental and calculated [10] (calc 95) values of the percentage of symmetric fission for proton- and neutron-induced reactions.

The role of the nuclear structure of the composite nucleus in intermediate energy reactions, similar to the role of compound nucleus in low-energy reactions, was noted in [11]. In the latter work, the proton- and neutron-induced fission cross sections for composite nuclei with the same Z^2/A values were equal. This was explained by the similarity of the relevant nuclear characteristics (Z, N, E*) prior to fission. Thus, it seems that a determination of the dependence of fission mass distributions on the nuclear structure of the composite nuclei at various incident proton energies may replace measurements with neutrons. The latter are much more labour-intensive and uncertain since intermediate-energy neutron fluxes are 10^5-10^6 times lower than those of protons. Moreover the necessity for experimental setups with high detection efficiency (ionization chambers) do not allow direct determination of the masses because they do not measure velocities of fission fragments but their kinetic energies (which are distorted by neutrons emitted by the fragments). Low-intensity neutron beams do not allow experiments with coincidences with neutrons or charged particles following the fission process, and thus information about the energy of the fissioning system at different stages of the fission process is lost.

CONCLUSION

Fission-fragment mass distributions were analyzed for a number of newly studied nuclei in a wider energy range and in a coincidence with fission neutrons. One was able to study the "sensitivity" of calculations of mass distributions to the symmetric fission barrier height, to compare mass distributions for neutron- and proton-induced fission in the energy range up to 100 MeV, and to make conclusions about the possibility of using measurements with proton beams as surrogates for the more difficult measurements with neutron beams.

REFERENCES

1. O. Batenkov et al., *Nucl. Instrum. Methods Phys. Res.,* **A394**, 235, (1997)].
2. O. Batenkov et al., *Nucl. Phys. A* (submitted).
3. M. Duijvestijn et al., *Phys. Rev.* **C64**, 014607 (2001).
4. I.F. Croall et al., *Nucl. Phys.* **A125**, 402 (1969).
5. J.J. Hogan et al., *Phys. Rev*. **C20**, 1831 (1979).
6. V.A. Rubchenya et al., *Nucl. Instrum. Methods* **A463**, 653 (2001).
7. U. Brosa et al., *Phys. Rep.* **197**, 167 (1990).
8. T. Ohtsuki et al., *Phys Rev.* **C44**, 1405 (1991).
9. C.M. Zoller, Ph. D. thesis, TH Darmstadt, (1995).
10. A.J. Koning, S. Hilaire, M.C. Duijvestijn, in *International Conference on Nuclear Data for Science and Technology 2004*, AIP Conference Proceedings (Melville, New York, 2005).
11. A. Smirnov et al., in *International Conference on Nuclear Data for Science and Technology 2004*, AIP Conference Proceedings (Melville, New York, 2005).

On Nuclear Structure Effects in the Nucleon-Induced Fission Cross Sections of Nuclei near ^{208}Pb at Intermediate Energies

Vilen P. Eysmont[1], Nikolay P. Filatov[1], Andrey N. Smirnov[1], Gennady A. Tutin[1], Jan Blomgren[2], Henri Condé[2], Nils Olsson[2,3], Marieke Duijvestijn[4], and Arjan Koning[4]

[1]*V.G. Khlopin Radium Institute, 2oi Murinskiy Prospect 28, Saint-Petersburg 194021, Russia*
[2]*Department of Neutron Research, Uppsala University, Box 525, S-751 20 Uppsala, Sweden*
[3] *Swedish Defence Research Agency (FOI), S-172 90 Stockholm, Sweden*
[`4] *Nuclear Research and Consultancy Group, Westerduinweg 3, NL – 1755 ZG Petten, Netherlands*

Abstract. Recently measured energy dependences of fission cross sections of lead isotopes $^{204,206\text{-}208}$Pb at incident nucleon energies up to 180 MeV were analyzed. Regularities were established of the fission cross-section variation with the mass number of isotopes pointing to incomplete dumping of shell effects even at nucleon energies 150–180 MeV. The fission cross sections of lead isotopes, assumed as spherical nuclei, are compared with those of deformed nuclei. The experimental data are compared with calculations by the code TALYS.

INTRODUCTION

^{208}Pb is the only nucleus among the stable heavy nuclei that has closed proton and neutron shells (Z=82, A=126). The microscopic (shell) correction to its binding energy is about 14 MeV and approximately equal to the macroscopic contribution to the fission barrier. For better understanding of the behaviour of shell effects with increasing excitation energy, an interesting comparison is made of the variation of the fission cross section of this nuclide and its lighter isotopes having lower barriers. The fission barriers, B_f, fall with the decrease of atomic mass, A, due to the decrease of the shell corrections; thus ΔB_f for ^{208}Pb and ^{204}Pb is about 3 MeV. Such a comparison is carried out for the first time, and it has become possible due to the measurements of proton- and neutron-induced fission cross sections for separated lead isotopes (and neighbouring nuclei) in the intermediate energy region in the work [1].

The problem of the role of nuclear deformation (the sphericity of nuclei having closed shells) in the competition between fission and neutron emission - the possibility that the stabilizing influence of a high barrier is compensated by destabilizing effects due to the low collective enhancement of the level density of spherical nuclei - was recently raised in connection with the determination of the fission cross sections of Ra isotopes (near N=126) [2]. This issue is investigated by a comparison of the fission cross sections of lead isotopes with the ones of deformed nuclei.

The experimental data are compared with calculations performed by the code TALYS [3].

RELATIVE NEUTRON-INDUCED FISSION CROSS-SECTIONS OF LEAD ISOTOPES NEAR THE UPPER BOUNDARY OF THE ENERGY REGION

In Fig. 1, experimental data on neutron- and proton-induced fission cross sections relative to those of ^{209}Bi are presented for lead isotopes [1]. It is seen from the figure that in the high-energy region, the ratios for all isotopes reach a plateau for both neutrons (2a) and protons (2b). The values of the

CP769, *International Conference on Nuclear Data for Science and Technology,*
edited by R. C. Haight, M. B. Chadwick, T. Kawano, and P. Talou
© 2005 American Institute of Physics 0-7354-0254-X/05/$22.50

(n,f) cross-section ratio at the plateau are 0.35, 0.48, 0.6, and 1.0 for the isotopes ^{208}Pb, ^{207}Pb, ^{206}Pb, and ^{204}Pb, with corresponding errors of about 5%. The values of the (p,f) cross-section ratio at the plateau are 0.47, 0.52, 0.64, and 1.06 for the same isotopes with errors of about 10%. It is not hard to find from these data that at high energies, fission cross sections of the isotopes can be connected by the following relation:

$$\sigma_f(204+x) = \sigma_f(204)/q^x,$$

where the coefficient q is equal to 1.30±0.07 for neutrons and 1.25±0.13 for protons, and x is equal to 2, 3, and 4 for ^{206}Pb, ^{207}Pb, and ^{208}Pb, respectively.

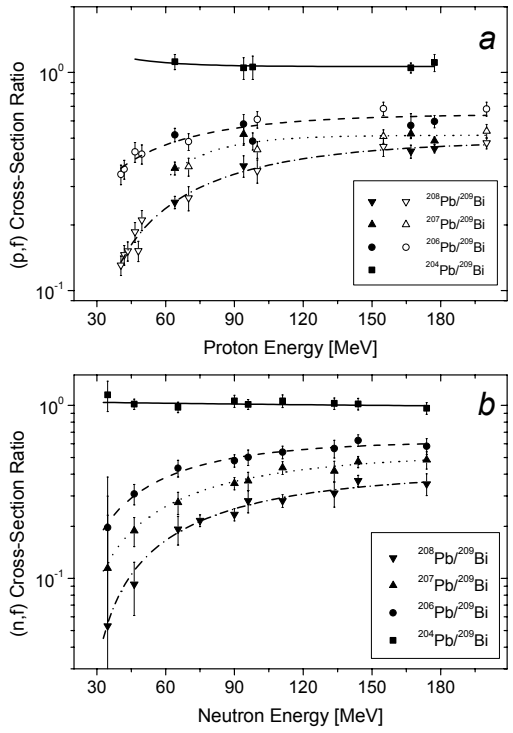

FIGURE 1. Experimental fission cross-section ratios of lead isotopes relative to the cross-section of ^{209}Bi for protons (a) and neutrons (b). Curves are the best fits.

In Fig. 2, results of calculations for the (p,f) and (n,f) cross-section ratios of the lead isotopes to ^{209}Bi are presented, obtained by the code TALYS. It is seen from the figure that in the high-energy region (above about 150 MeV), reasonable agreement is obtained between the calculation and the experimental data, represented by the best fits from Fig. 1. The values of the parameter q obtained from the calculated fission cross-section ratios are 1.23 for neutrons and 1.25 for protons.

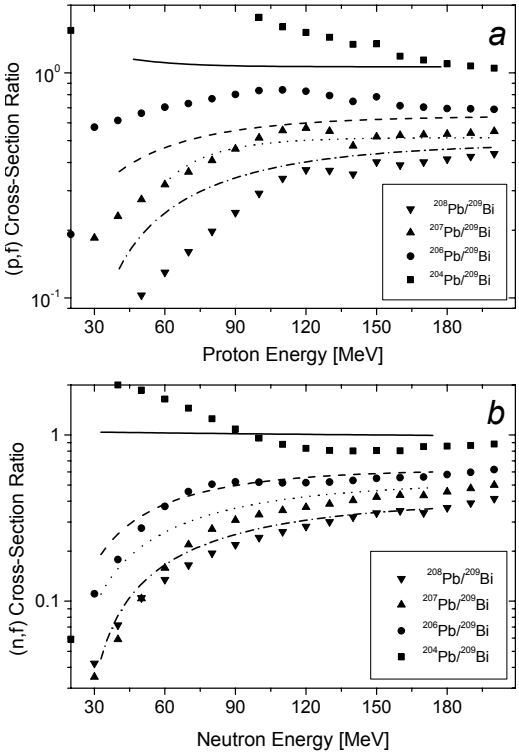

FIGURE 2. Fission cross-section ratios of lead isotopes relative to the cross section of ^{209}Bi for protons (a) and neutrons (b) calculated by the code TALYS. Curves are the best fits from Fig. 1.

Assuming that at excitation energies corresponding to this case,

$$\sigma_f \sim exp-[(B_f - B_n)/T],$$

where B_f is the fission barrier, B_n is the neutron binding energy, and T is the temperature of a nucleus, connected with the excitation energy, E^*, and a level density parameter, a, by the relation:

$$T = (E^*/a)^{1/2};$$

then, for any neighbouring isotopes with the mass numbers A and A-1

$$B_f(A) - B_f(A-1) + B_n(A-1) - B_n(A) = T \cdot \ln q \ .$$

Calculations show that at a nucleon energy of about 180 MeV, the average excitation energy is about 80 MeV, and the average mass is about 200 (moreover the charge shifts by unity). Thus, at a = A/10, temperature T = 2 MeV, and experimental values of q, the value of $B_f(A) - B_f(A-1) + B_n(A-1) - B_n(A)$ is equal to 0.52 MeV for neutrons and

0.44 MeV for protons. Since in this mass region $B_n(A\text{-}1) - B_n(A) \approx 0.14$ MeV (after averaging over odd-even effects), $B_f(A) - B_f(A\text{-}1)$ is equal to 0.38 for neutrons and 0.30 for protons. These values are smaller than the differences between the fission barriers of neighbouring nuclei, amounting to about 0.75 MeV, as was pointed out above. However, at present, in view of the uncertainty of the calculations, it is difficult to conclude to what degree the ratio of the barriers is connected with the change of the structure of the fissioning nuclei (the difference from magic or double magic target nuclei) or with the increase of the excitation energy. At the same time, the obtained value of $\Delta B_f/\Delta A$ seems to be larger than expected from the liquid drop model. Possibly, it gives evidence for a larger stability (i.e., for a lower value of the coefficient of the damping of shell effects) of nuclei having large microscopic corrections.

COMPARISON OF THE FISSION CROSS-SECTION OF THE LEAD ISOTOPES AND DEFORMED NUCLEI

To study incomplete damping of shell effects at energies higher than several tens of MeV, dependences of the (n,f) cross section for nuclei from ^{181}Ta to ^{238}U on the parameter Z^2/A for neutron energies >60 MeV have been plotted (there are no experimental data on the (n,f) cross sections for nuclei lighter than gold for lower energies). These dependences are shown in Fig. 3. It is seen that at a neutron energy of 60 MeV, the fission cross sections of the lead isotopes lie slightly lower than the common straight dependence, and the difference becomes stronger towards ^{208}Pb. With the increase of neutron energy, these irregularities become smaller.

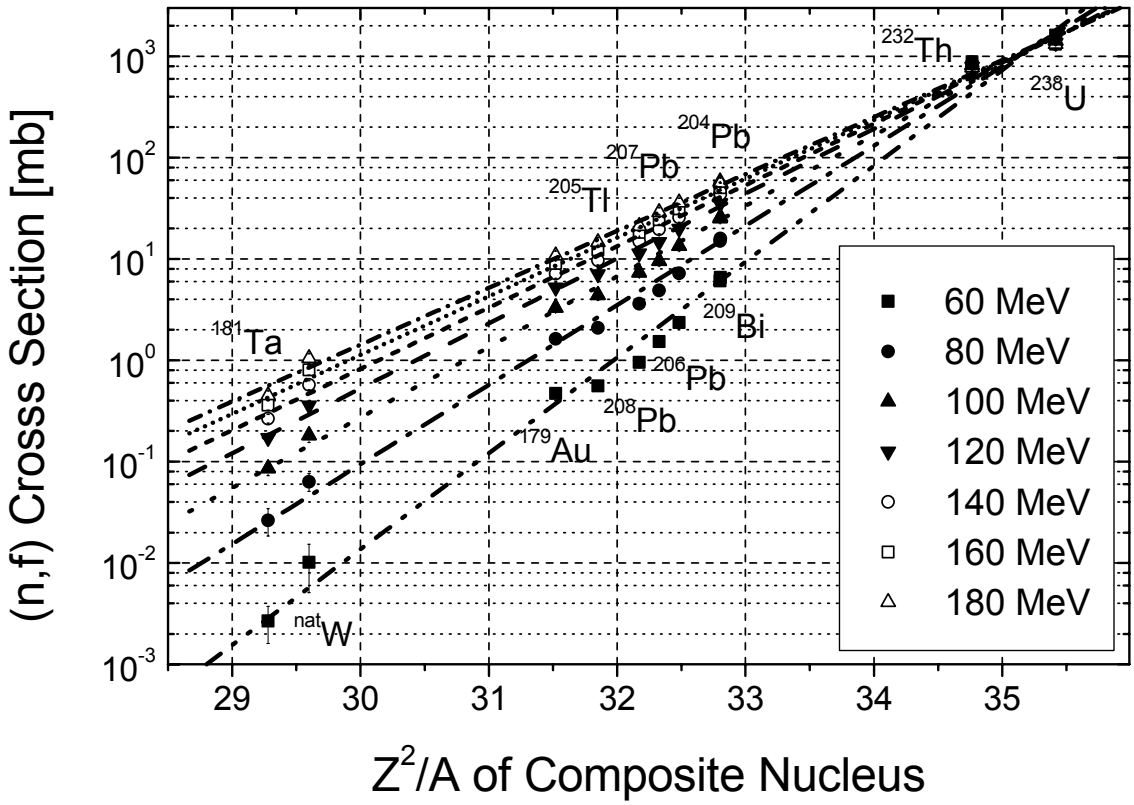

FIGURE 3. The (n,f) cross sections for a wide range of nuclei, from ^{181}Ta to ^{238}U, vs. the parameter Z^2/A of composite nuclei for different incident neutron energies.

However, in the comparison of fission cross sections of the lead isotopes, ^{209}Bi and ^{205}Tl with the cross sections of the other nuclei, i.e., ^{181}Ta and ^{nat}W (at the left of lead isotopes) and ^{232}Th and ^{238}U (at the right), one should keep in mind the difference in the shape of the basic states of the nuclei - the spherical shape of the lead isotopes and neighbouring nuclei, having closed or almost closed shells, and the

deformation of lighter and heavier nuclei, which influences the channel of neutron emission, which is competing with the fission channel. Recently this was shown in [2], where the cross sections of radium isotopes were measured. In this work no indications of the expected decrease of the cross sections near N=126 were found, though the excitation energy exceeded the barrier by a few MeV. It was concluded that a stabilizing influence, resulting from the higher fission barrier, seems to be compensated, or even over-compensated, by the destabilizing effect of the lower collective enhancement in the spherical ground-state shape.

CONCLUSION

From the comparison of the (n,f) and (p,f) cross sections of the lead isotopes with A = 208, 207, 206, and 204 at incident nucleon energies of about 150-180 MeV, a conclusion has been made about a possible incomplete damping of shell effects at average excitation energy of fissioning nuclei in the lead region at about 80 MeV, corresponding to the aforementioned energy of incident neutrons. In connection with this, it is noted that the absence of an expected large discrepancy between the behaviour of the cross sections of the lead isotopes and their neighbouring nuclei, in comparison with lighter and heavier nuclei, can be caused by the influence of the extent of shell filling on the shape of the nucleus in the ground state.

REFERENCES

1. V.P. Eismont (Project Manager), “Measurements and Comparison of Proton- and Neutron-Induced Fission Cross-sections of Lead and Neighboring Nuclei in the 20-200 MeV Energy Region.” Final Project Technical Report of ISTC 1309-99, V.G. Khlopin Radium Institute, St.-Petersburg, 2002.
2. A Heinz, K.-H. Schmidt, A.R. Junghans *et al*, Preprint GSI 2002-25 August,
3. A.J. Koning, S. Hilaire, M.C. Duijvestijn, in *International Conference on Nuclear Data for Science and Technology 2004*, AIP Conference Proceedings (Melville, New York, 2005).

Angular Anisotropy of Intermediate Energy Nucleon-Induced Fission of Pb Isotopes and Bi

Vilen P. Eysmont[1], Nikolay. P. Filatov[1], Andrey N. Smirnov[1], Jan Blomgren[2], Henri Condé[2], Nils Olsson[2,3], Marieke Duijvestijn[4], and Arjan Koning[4]

[1]*V.G. Khlopin Radium Institute, 2oi Murinskiy Prospect 28, Saint-Petersburg 194021, Russia*
[2]*Department of Neutron Research, Uppsala University, Box 525, S-751 20 Uppsala, Sweden*
[3] *Swedish Defence Research Agency (FOI), S-172 90 Stockholm, Sweden*
[4] *Nuclear Research and Consultancy Group, Westerduinweg 3, NL – 1755 ZG Petten, Netherlands*

Abstract. New results of measured anisotropy coefficients for proton-induced fission of ^{204,206,207,208}Pb and ^{209}Bi are presented at proton energies of 48, 98, and 177 MeV These results, together with earlier ones, are used for an estimation of the dependence of the anisotropy coefficients on proton energy in the framework of the standard statistical model, taking into account the characteristics of the intermediate compound nuclei formed in the process of the interaction of protons with lead and bismuth nuclei.

INTRODUCTION

Measurement of fission-fragment angular anisotropy is a way to determine the state of a fissioning nucleus at the saddle point. This is necessary for the understanding of the key characteristics and dynamics of the fission process. A semi-empirical description of experimental results on the anisotropy of fission induced by protons and neutrons in the energy range above 20 MeV has been presented recently [1], in the framework of the standard statistical (transition state) model [2,3]. Fission of heavy nuclei: ^{232}Th, ^{233}U, ^{235}U, and ^{238}U was considered. The correlation between experimental data on the angular anisotropy for (n,f) and (p,f) reactions has been analysed, and it has been concluded that the anisotropy for neutron-induced fission may be calculated using the anisotropy for proton-induced fission at the same energies for composite systems having the same fissility parameter, Z^2/A, taking into account the difference of the introduced momenta.

In the present work results of measurements of angular anisotropy in proton-induced fission of ^{204,206,207,208}Pb and ^{209}Bi are presented. Data for ^{204}Pb are obtained for the first time. The other results supplement essentially those of other work in this energy region. As in previous work, the dependence of the anisotropy on proton energy is estimated in the framework of the standard statistical model [2,3], taking into account the characteristics of the intermediate compound nuclei formed in the process of the interaction of protons with lead and bismuth nuclei. The latter are calculated using the TALYS code [4], for which a comparison with experimental values of anisotropy is a new form of testing and verification.

MEASUREMENTS AND EXPERIMENTAL RESULTS

Measurements of fission-fragment angular distributions for intermediate energy proton-induced fission of ^{204,206,207,208}Pb and ^{209}Bi were carried out at the proton beam of the The Svedberg Laboratory of the Uppsala University, Sweden, at the proton energies 49, 98, and 177 MeV. The experimental setup, measurement conditions, and the procedure of the processing of experimental results are described in detail in our report [5]. The anisotropy factor:

$$C = W'(0°)/W'(90°) - 1,$$

CP769, *International Conference on Nuclear Data for Science and Technology,*
edited by R. C. Haight, M. B. Chadwick, T. Kawano, and P. Talou
© 2005 American Institute of Physics 0-7354-0254-X/05/$22.50

where $W'(0°)$ and $W'(90°)$ are the probabilities of fragment emission at 0° and 90° with respect to the direction of the projectile beam, was obtained by means of fitting of the experimental angular distribution using well known expressions (see, e.g., [6]). The results for ^{209}Bi and ^{204,206,207,208}Pb are presented in Table 1 and shown in Fig. 1, together with earlier results of other authors [7]. As can be seen from the figure, the results of the present work are in good agreement with the earlier data within the stated errors.

TABLE 1. The anisotropy factor for proton-induced fission fragments.

E_p [MeV]	^{209}Bi	^{204}Pb	^{206}Pb	^{207}Pb	^{208}Pb
48±1	0.35±0.05	0.42±0.07	0.35±0.07	0.4±0.1	0.35±0.10
98±2	0.22±0.05	0.25±0.1	0.4±0.1	—	—
177.3±1.2	0.11±0.05	0.15±0.04	0.17±0.03	0.12±0.03	0.17±0.05

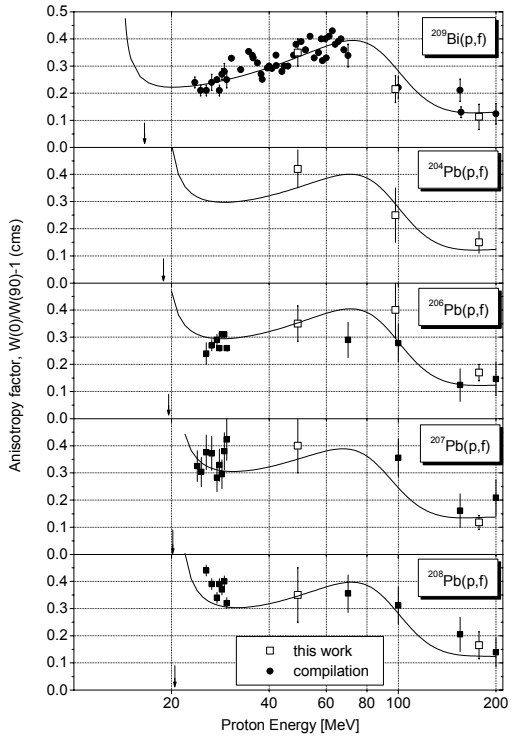

FIGURE 1. Energy dependence of the anisotropy factor for proton-induced fission.

SEMI-EMPIRICAL ANALYSIS OF ANGULAR ANISOTROPY

In the transition state model [2,3] the anisotropy factor C is merely connected with the mean square of the angular momentum of a nucleus at the saddle point $\langle I^2 \rangle$ and the dispersion of the momentum projection on the axis of the fissioning nucleus, K_o^2:

$$C = \left\langle I^2 \right\rangle / K_0^2 ,$$

where K_o^2 is determined by the effective moment of inertia, J_{eff}, and temperature, T, of a nucleus in this state,

$$K_0^2 = (1/\hbar^2) J_{eff} T .$$

To describe the dependence of the anisotropy factor on the projectile energy E, it is necessary to take into account the change with E of $\langle I^2 \rangle$ and K_o^2. For calculation of the maximum angular momentum introduced by protons, the following expression was used [8]:

$$I_m^2 = 2\left\langle I^2 \right\rangle = 4.17E - 30 .$$

A change of K_o^2 can be connected, in principle, to a change of both J_{eff} and T. However, in this work, the energy dependence of J_{eff} is not taken into account, because on one hand the minimum proton energy, for which experimental data exist, is about 25 MeV, and therefore the excitation energy at the saddle point is almost equal to a critical value, ~6 MeV, above which a transition begins from superfluid to the normal Fermi-gas state [9]. On the other hand, at higher energies, where shell effects could be revealed, the most striking feature of the experimental behaviour of J_{eff} is found to be a sudden change of its dependence on the parameter Z^2/A at Z^2/A=30 predicted by the liquid-drop model, which indicates a liquid-drop state of the nucleus at the saddle point [9]. Unfortunately, theoretical calculations of the influence of possible shell effects on the moment of inertia for nuclei in the lead region were not carried out. J_{eff} can also depend on the angular momentum, but the dependence is found to be strong only for $I_o \geq 20\ \hbar$. However, for such light particles such as protons and neutrons, the value of I does not exceed 20 $\hbar$ even at the maximum energy 200 MeV considered here. A small value of introduced angular momentum reduces, of course, the value of the anisotropy and makes a measurement of it difficult, but allows for avoiding the necessity of taking into

account the dependence on I of J_{eff} and other parameters of the model: the fission barrier B_f, and the level density parameter a_f. This is a stimulating factor for carrying out measurements of the angular anisotropy for light particles.

The temperature of a nucleus at the saddle point is calculated by the following relationship:

$$T = (E^* / a_f)^{1/2}$$
$$E^* = E + B_p - B_f - E_\nu - E_d ,$$

where E is the proton energy in the center of mass system, B_p is the proton binding energy, E_ν is the energy taken away by neutrons evaporated before the saddle point, and E_d is the energy taken away by the cascade and pre-equilibrium particles. Calculations show that even at E=200 MeV, the temperature $T \leq$ 2 MeV, and therefore the change of B_f with temperature was not taken into account. The dependence $B_f(I)$ was also not taken into account, because, like the dependence $J_{eff}(I)$, it is found to be weak at $I_o \geq 20$ ħ. [10]. The values of B_p and B_f used are from [9] and [11], respectively. For calculation of E_ν, it was supposed that one neutron is evaporated for every 6 MeV of excitation energy, which is close to the value from the statistical model. Cascade and pre-equilibrium particles arise in faster processes preceding fission in reactions with intermediate energy nucleons. As a result of these processes, a broad set of residual nuclei arises, which differ in nucleon composition, excitation energy, and magnitude and spatial orientation of the angular momentum. At sufficient excitation energy, such residual nuclei become "ancestors" for chains of emission (multi-chance) fission, i.e., for fissioning nuclei having new masses, excitation energies, and angular momenta. Each one of such nuclei introduces its own contribution to the anisotropy in accordance with $\langle I^2 \rangle$, and K_o^2. Therefore a quantitative analysis of the anisotropy requires a "differential" approach. Such an approach was applied in our previous work [12]. Here an "integral" description is given, where $\langle I^2 \rangle$ and K_o^2 are averaged over the states of the fissioning nuclei. The use of this approach is caused by the complexity of a quantitative consideration of the mentioned processes and is adequate for the tasks of the present work.

In accordance with this approach, we use the following relation to estimate the energy dependence of the anisotropy:

$$C = (a_f)^{1/2} \left\langle I^2 \right\rangle k / 4 J_{eff} (E + B_p - B_f - \Delta E) ,$$

where the coefficient k takes into account the angular momentum carried away and disoriented during the cascade and pre-equilibrium emission of the particles. The energy ΔE carried away by these particles was calculated using the code TALYS. In the absence at present of similar calculations for disoriented angular momenta, the coefficient $K(E)$ was fitted with the goal of getting a better description of the energy dependence of the anisotropy for the ^{209}Bi(p,f) reaction, for which a larger amount of experimental data exists. This parameter is equal to 1 below 20 MeV. Starting from this energy, i.e., the energy where direct processes arise, the coefficient falls, leading to a weak dependence of the anisotropy on E at $E \geq 150$ MeV. For all other nuclides, as well as for the (n,f) reactions, $K(E)$ was supposed to be the same (just as for the value of ΔE which, in accordance with calculations, is found to be almost the same for all nuclides). Of all the considered nuclides, only ^{209}Bi has a large spin, I_o=4/2 ħ. However, in this case the correction to the anisotropy,

$$[\left\langle I^2 \right\rangle - 2I_0(I_0 + 1)] / 18K_0^2 ,$$

is found to be small due to a large value of K_o^2 already at a nucleon energy of 25 MeV.

The dependence of the anisotropy factor calculated in this way is shown in Fig. 2. It is seen that the calculated curves satisfactorily describe the experimental results. The anisotropy drops as the proton energy exceeds the threshold value $(E_{th}=B_p-B_f)$, shown in the figure by arrows. Then, the anisotropy increases, reflecting the increase of introduced angular momentum, and then drops again as a result of the disorientation of the momentum by fast particles preceding fission (and some increase of the excitation energy of the intermediate compound nuclei). The main difference in the behaviour of the anisotropy for different nuclei takes place at low proton energies and is connected with the difference of the fission barriers (and, correspondingly, E_{th}). At higher energies individual differences disappear, as should be expected. The maximum of the anisotropy factor for all nuclides, with C~0.4, is found to be at an energy of about 70 MeV, while at an energy of about 150 MeV and higher, the anisotropy remains constant at a level of C=0.1-0.15.

In the same manner, the anisotropy for neutron-induced fission was calculated. Values of B_n and B_f for composite nuclides were taken from [11] and [9]. The introduced angular momentum was adopted to be $\langle I^2 \rangle = 2.5\ E$ [9], E_ν did not change, and E_d was

calculated using the code TALYS. Small corrections were introduced to the moment of inertia, J_{eff}, i.e., from 2% to 10%, on the already mentioned dependence J_{eff} (Z^2/A) [9]. The results are presented in Fig. 2.

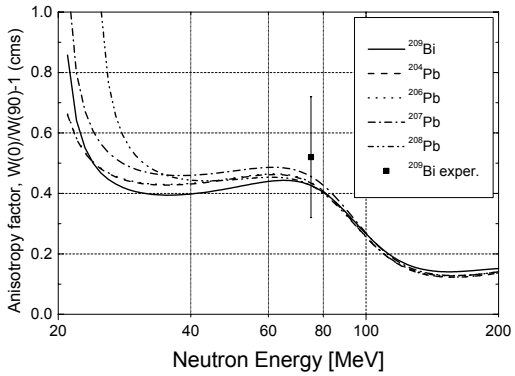

FIGURE 2. Energy dependence of the anisotropy factor for neutron-induced fission.

Comparison of Figs. 1 and 2 indicates somewhat higher values of the anisotropy coefficient for neutrons, C_n, than for protons, C_p, especially on the left side of the maximum, which is connected with the higher value of $\langle I^2 \rangle$. However, the energy dependences of C_n and C_p are essentially the same. Only one experimental result is published for C_n at E_n =75 MeV [12], shown in Fig. 2. It has large errors, but does not contradict the calculated data. Measurements of the anisotropy of neutron–induced fission are of most interest for ^{208}Pb and ^{209}Bi, having a closed neutron shell (N=128), where, according to the code TALYS, the fission branch of the composite nuclei ^{209}Pb and ^{210}Bi remains at more than 75% up to neutron energies of 50 MeV, as well as measurements for the ^{207}Pb nucleus, where the composite nucleus ^{208}Pb, with closed neutron (N=128) and proton (Z=82) shells, forms.

For determining the influence of the shells, differential calculations are necessary, i.e., taking into account a consecutive contribution to the anisotropy of all intermediate compound nuclei with their inherent $\langle I^2 \rangle$, K_o^2 and formation probability. The problem can be facilitated by the fact that at comparatively low proton and neutron energies, below 50 MeV, where the influence of shell effects may be significant, the contribution to fission and, correspondingly, to the anisotropy, is introduced by no more than 4–5 composite nuclei. Probably, with such a differential approach, conclusions can be made about the presence or absence of non-statistical pre-saddle neutrons, caused by a dynamic delay of the fission process.

CONCLUSION

It is shown that the magnitude of the angular anisotropy, and its dependence on energy, can be described in the framework of the standard statistical model, taking into account the characteristics of intermediate compound nuclei formed in the process of interaction of intermediate energy protons and neutrons with bismuth and lead nuclei. For studying the influence of shell effects, differential calculations are necessary.

REFERENCES

1. V. P. Eismont, I. V. Ryzhov, G. A. Tutin, *et al., J. Nucl. Sci. Technol.*, *Suppl.* **2**, 299 (2002).
2. H. Halpern V. M. Strutinskiy, *Proc. of the Second United Nations Int. Conf. on Peaceful Uses of Atomic Energy*, Geneva, Switzerland, 1958, (United Nations, Geneva, Switzerland, 1958) p.408.
3. R. Vandenbosch and R. Huizenga. *Nuclear Fission* (Academic Press, New York, 1973).
4. A. J. Koning, S. Hilaire, and M. C. Duijvestijn, "TALYS: Comprehensive Nuclear Reaction Modeling," in *International Conference on Nuclear Data for Science and Technology 2004*, AIP Conference Proceedings (Melville, New York, 2005).
5. V.P. Eismont (Project Manager), Final Project Technical Report of ISTC 1309-99, V.G. Khlopin Radium Institute, St.-Petersburg, 2002.
6. A. Michalowicz. Cinématique des réactions nucléaires, Paris, 1964.
7. A. I. Obukhov. "Nuclear fission induced by intermediate energy proton and neutron," *Phys. Part. Nuclei* **32**, 162 (2001).
8. A. V. Ignatyuk, M. G. Itkis, I. A. Kamenev *et al.*, *Sov. J. Nucl. Phys*. **40**, 25 (1984).
9. A. V. Ignatyuk, G. N. Smirenkin, M. G. Itkis *et al., J. Part. Nuclei* **16**(4), 162 (1985).
10. A.J. Sierk, *Phys. Rev.* **C33**, 2039 (1986).
11. P. Möller, J. R. Nix, K. H. Kratz. *At. Data Nucl. Data Table* **66**, 131 (1997).
12. V.P. Eismont, A.V. Kireev, I.V. Ryzhov, *et al.*, *Proc. Intern Conf. on Nuclear Data for Science and Technology*, May 19-24, 1997, Trieste, Italy, p. 658.

Correlation of Intermediate Energy Proton- and Neutron-Induced Fission Cross Sections in the Lead-Bismuth Region

Andrey N. Smirnov[1], Vilen P. Eismont[1], Nikolay P. Filatov[1], Sergey N. Kirillov, Jan Blomgren[2], Henri Condé[2], Nils Olsson[2,3] , Marieke Duijvestijn[4], and Arjan Koning[4]

[1]*V.G. Khlopin Radium Institute, 2oi Murinskiy Prospect 28, Saint-Petersburg 194021, Russia*
[2]*Department of Neutron Research, Uppsala University, Box 525, S-751 20 Uppsala, Sweden*
[3] *Swedish Defence Research Agency (FOI), S-172 90 Stockholm, Sweden*
[4] *Nuclear Research and Consultancy Group, Westerduinweg 3, NL – 1755 ZG Petten, Netherlands*

Abstract. Neutron- and proton-induced fission cross-sections of the lead isotopes $^{204,206\text{-}208}$Pb and ^{205}Tl in the intermediate energy region have been measured at the Svedberg Laboratory in Uppsala, Sweden. Average fissilities of the composite nuclei and the dependence on the nucleon energy and the parameter Z^2/A were determined. On this basis, the correlation between the proton- and neutron-induced fission cross sections has been established in the atomic mass region A ~ 200 and for nucleon energies above 50 MeV, where shell effects do not play a very significant role. The correlation is discussed in the frame of results from calculations by the code TALYS.

INTRODUCTION

A first comparison of the (p,f) and (n,f) reaction cross sections (as well as the (γ,f) reaction cross section) in the intermediate energy region has been undertaken in this work [1]. In this and succeeding works (see, e.g., [2] and references therein) it was found that at incident nucleon energies of 150-200 MeV the value of the (p,f)/(n,f) reaction cross-section ratio for nuclei from ^{243}Am to ^{181}Ta is higher than 1, increases with the decrease of the parameter Z^2/A of the target nucleus, and reaches a value of about 5 and higher. From the beginning, the effect was ascribed to the increase of the charge (Z), and therefore of the parameter Z^2/A of the fissioning nucleus by the incident proton [1,3]. However, some works published recently both confirm this explanation [4] and attribute the effect to a possible influence of the isovector term of the nucleon-nucleus optical potential [5].

The present work is devoted to a further experimental and theoretical study of the correlation between proton and neutron cross sections in the lead-bismuth region, which is of great importance for applied and fundamental research.

FISSION CROSS-SECTION MEASUREMENTS AND RESULTS

The neutron- and proton-induced fission cross-sections of ^{204,206,207,208}Pb and ^{205}Tl have been measured at the accelerator of The Svedberg Laboratory, Uppsala, Sweden, at nucleon energies up to 180 MeV [6], with the use of the thin-film breakdown counter (TFBC) technique. The experimental technique and data processing were described in detail in [2,6], and part of the results were presented in [2]. In the present paper all results and the analysis performed using calculations by the code TALYS [7] are under consideration. The results for protons and neutrons are shown in Fig. 1. The experimental errors of our measurements are about 10%. The curves are the best fits calculated using the following expression:

$$\sigma_f(E_n) = P_1 \cdot exp(-(P_2 / E_n)^{P_3}),$$

where E_n is the incident nucleon energy and P_1, P_2, and P_3 are fitting parameters depending on the target nuclide. The presented results for neutrons systematically disagree with some results obtained with the use of other techniques [8].

CP769, *International Conference on Nuclear Data for Science and Technology,*
edited by R. C. Haight, M. B. Chadwick, T. Kawano, and P. Talou
© 2005 American Institute of Physics 0-7354-0254-X/05/$22.50

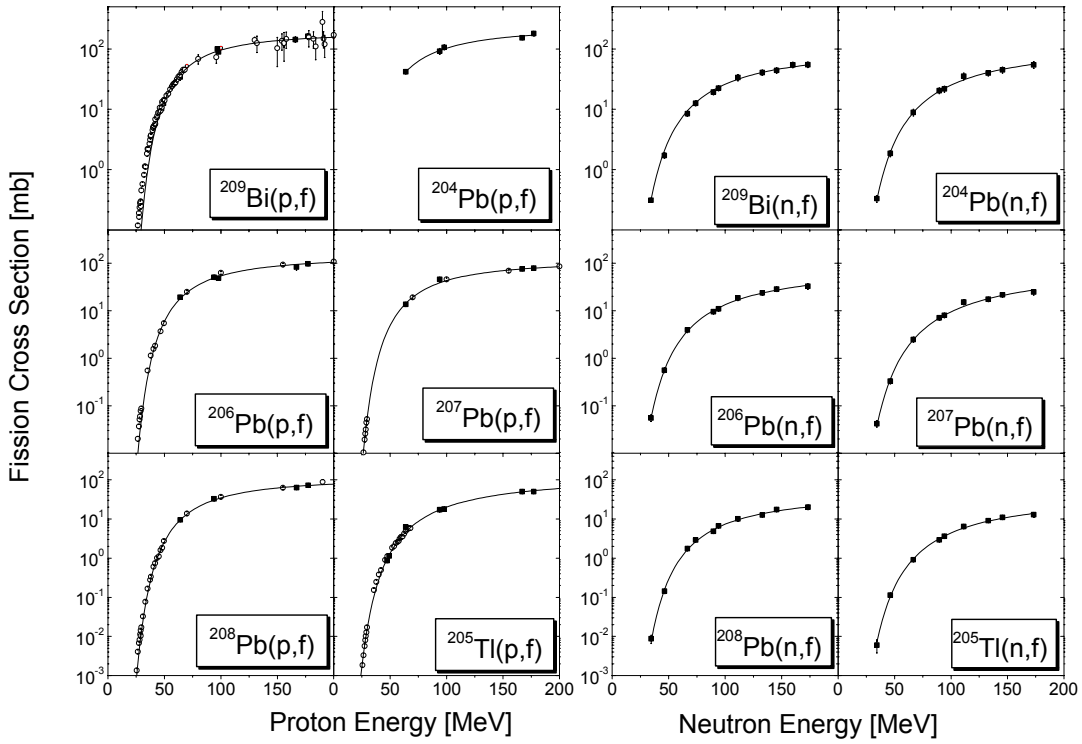

FIGURE 1. Proton- (left panel) and neutron-induced (right panel) fission cross-sections of nuclei in the lead region. Filled symbols are results of the present work, open symbols are results of other authors. Curves are the best fits.

The possible reason for the disagreement (about 20%) is that systematical errors declared by the authors are too optimistic. Thus, a value of 20% seems to be a more realistic estimation of the uncertainty of the up-to-date experimental results.

FISSILITY AND ITS DEPENDENCE ON NUCLEON ENERGY AND NUCLEON COMPOSITION OF COMPOSITE NUCLEI

To take into account the difference between reaction cross sections for protons and neutrons, the fission cross sections were divided by the corresponding reaction cross sections, and the obtained ratios were considered as the average fissilities, $P_f=\sigma_f/\sigma_r$, of the nuclei. The reaction cross sections, parameterized in accordance to Barashenkov [8], are shown in Fig. 2.

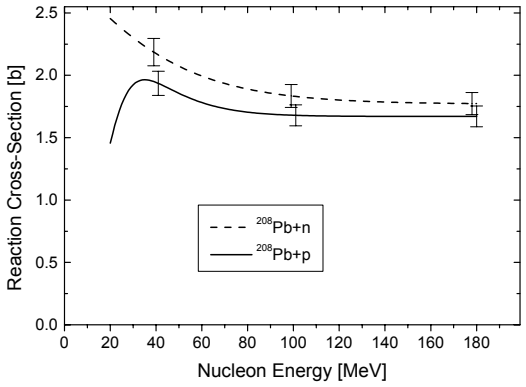

FIGURE 2. Reaction cross-sections for ^{208}Pb induced by neutrons and protons in the intermediate energy region.

It is seen that in the energy region 50-200 MeV (the region of lower energies is not considered because of the influence of shell effects) the reaction cross sections for neutrons and protons are close,

though the proton cross section is systematically lower than the neutron one by about 10%. This value does not exceed the experimental errors of the fission cross sections, but from the physics point of view the consideration in terms of fissility looks preferable. In Fig. 3 the dependences of the values P_f on the parameter Z^2/A of composite nuclei for reactions with protons and neutrons are presented for different projectile energies. It is seen from the figure that the dependences are of the same character – the lines in semi-logarithmic scale – the slope of which decreases with the increase of the projectile energy. It means that the (n,f) and (p,f) cross sections (with the accuracy of the factor σ_{rp}/σ_{rn}) for the reactions passing through the same composite nuclei have to be of the same magnitude.

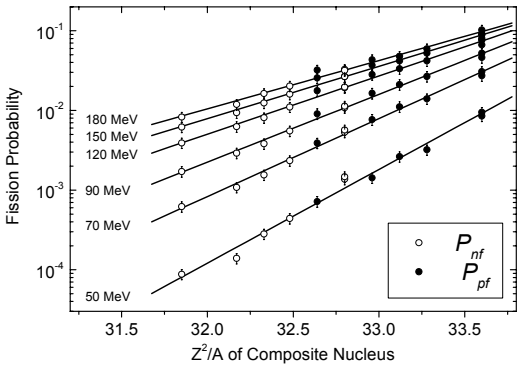

FIGURE 3. Average fissilities vs. the parameter Z^2/A of the composite nucleus. The lines are parameterizations.

In Fig. 4 parameterizations of the fission cross sections are presented for the reactions ^{209}Bi+n and ^{208}Pb+p, and ^{204}Pb+n, ^{206}Pb+n, and ^{205}Tl+p. It is seen from the figure that the fission cross section of the ^{209}Bi+n and ^{208}Pb+p reactions, passing through similar composite nuclei (with Z=83, A=210, and Z=83, A=209, respectively), are close, moreover in the case of ^{209}Bi+n, corresponding to a value of A which is larger by 1, the fission cross section is somewhat lower. The value, by which the cross section becomes lower, corresponds within the experimental uncertainties to the data shown in Fig. 3. It is seen also that in accordance with the conclusion on fissility the value of the cross section for ^{205}Tl+p (Z=82, A=206) lies between the ones for ^{204}Pb+n (Z=82, A=205) and ^{206}Pb+n (Z=82, A=207). Moreover, one can observe that at low energies the fission cross section of ^{205}Tl+p resembles the result for ^{206}Pb+n, while at high energies the ^{205}Tl+p curve approaches the ^{204}Pb+n result. This can be explained by the impact of direct and pre-equilibrium processes on the population of the evaporation chain, and hence on the population of the fissioning systems.

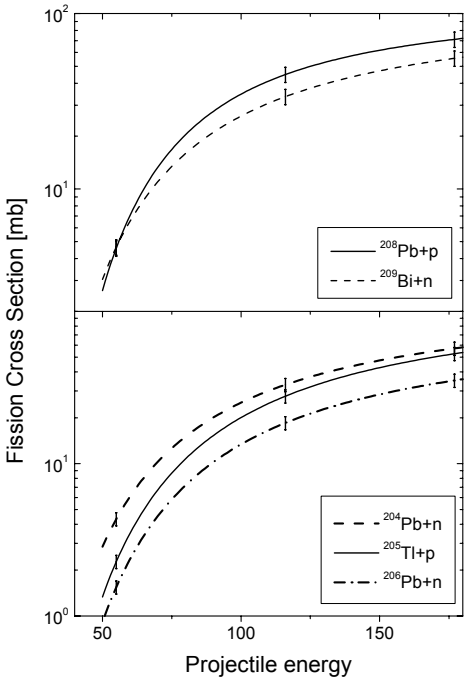

FIGURE 4. The ^{208}Pb(p,f), ^{209}Bi(n,f), ^{204}Pb(n,f), ^{205}Tl(p,f), and ^{206}Pb(n,f) cross sections.

ANALYSIS OF CALCULATIONS PERFORMED WITH THE CODE TALYS

Experimental results, pointing to an equality of the fissilities in reactions induced by protons and neutrons in the intermediate energy region, similar to the situation at low energies (below 20 MeV) where a compound nucleus is formed with high probability, seem to be unexpected. At incident nucleon energies around 20 MeV, direct processes (intranuclear cascade and preequilibrium emission) start to come into play, preceding a slower fission process. The sharing of nucleons and excitation energy of the target nucleus are taken away during the direct processes. As a result, a wide set of intermediate nuclei with different charges, masses, and excitation energies appears, which, reaching thermal balance, undergo fission, contributing to the fission cross section measured experimentally. The capacity of TALYS allows one to calculate the composition of intermediate equilibrium (compound) nuclei and their individual contributions into the observed fission cross section.

In Fig. 5 dependences of average charge, mass, fissility parameter, Z^2/A, and excitation energy of the

fissioning nucleus vs. incident nucleon energy are shown for two of the considered reactions: ^{209}Bi+n and ^{208}Pb+p. It is seen that changes with the energy are significant. It is also seen that the changes for both reactions are similar (differences in nucleon composition occur only at the end of the energy region, at E_{proj} above 150 MeV). This is what leads to the closeness of the cross sections observed experimentally.

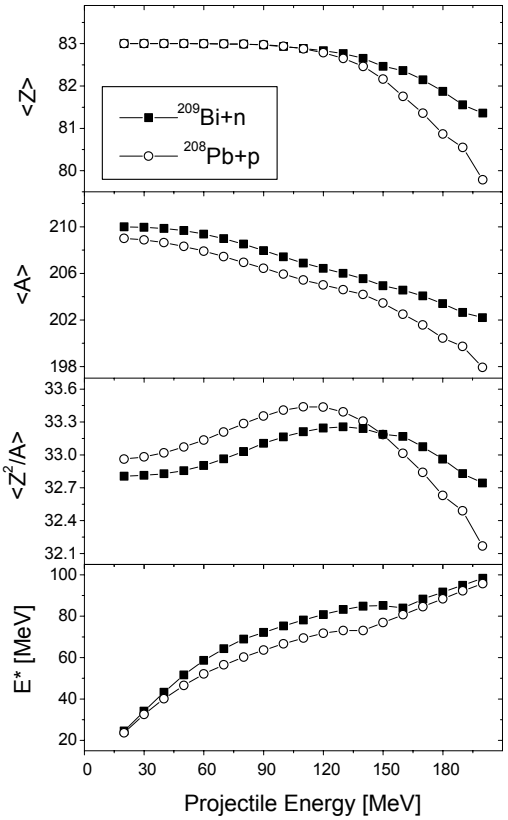

FIGURE 5. Average charge, mass, the parameter Z^2/A of the intermediate nuclei vs. projectile energy for the reactions ^{209}Bi+n and ^{208}Pb+p calculated by the code TALYS.

CONCLUSION

Equality of neutron- and proton-induced fission cross sections for composite nuclei, characterized by the same parameter Z^2/A, is found within experimental errors. With regard to the calculations performed with TALYS, this fact may be explained by similar changes in the nucleon composition and excitation energy in these two types of reactions, which take place in direct processes preceding fission. It seems to be interesting to compare also other characteristics of fissioning nuclei, for example charge and mass distributions of fission fragments.

REFERENCES

1. V.P. Eismont, A.V. Prokofiev and A.N. Smirnov, in *Proc. Int. Conf. on Nuclear Data for Science and Technology*, Gatlinburg, Tennessee, USA, May 9-13, 1994, ed. J.K. Dickens, ANS, USA, 1994, v. 1, p. 397.
2. V.P. Eismont, A.V. Prokofiev, I.V. Ryzhov, A.N. Smirnov, Condé, N. Olsson and P.-U. Renberg, *J. Nucl. Sci. Technol., Suppl.* **2**, 238 (2002).
3. V.P. Eismont, A.V. Prokofiev, A.N. Smirnov, K. Elmgren, J. Blomgren, H. Condé, J. Nilsson, N. Olsson, T. Rönnqvist, and E. Tranéus, *Phys. Rev. C* **53**, 2911 (1996).
4. V. E. Bunakov, L. V. Krasnov and A. V, Fomichev, *Eur. Phys. J. A* **8**, 447-450 (2000).
5. V. M. Maslov, Yu. V. Porodzinskij and A. Hasegava, in *Proc. VIII International seminar on Interactions of Neutrons with Nuclei*, Dubna, May 17-20, 2000, p. 277-287.
6. V.P. Eismont (Project Manager), "Measurements and Comparison of Proton- and Neutron-Induced Fission Cross-sections of Lead and Neighboring Nuclei in the 20-200 MeV Energy Region," Final Project Technical Report of ISTC 1309-99, V.G. Khlopin Radium Institute, St.-Petersburg, 2002.
7. A.J. Koning, S. Hilaire, M.C. Duijvestijn, "TALYS: Comprehensive Nuclear Reaction Modeling," in *International Conference on Nuclear Data for Science and Technology 2004*, AIP Conference Proceedings (Melville, New York, 2005).
8. O. Shcherbakov, A. Donets, A. Evdokimov, A. Fomichev, T. Fukahori, A. Hasegawa, A. Laptev, V. Maslov, G. Petrov, S. Soloviev, Y. Tuboltsev and A. Vorobyev, *J. Nucl. Sci. Technol., Suppl.* **2**, 230 (2002)
9. V.S. Barashenkov and V.D. Toneev, "Interaction of high energy particle and nuclei with atomic nuclei," Atomizdat, Moscow (1972) [in Russian].

Investigation of Three-Body Force Effects in Neutron-Deuteron Scattering at 95 MeV

P. Mermod[*], J. Blomgren[*], B. Bergenwall[*], A. Hildebrand[*], C. Johansson[*], J. Klug[*], L. Nilsson[†*], N. Olsson[***], M. Österlund[*], S. Pomp[*], U. Tippawan[‡*], O. Jonsson[†], A. Prokofiev[†], P.-U. Renberg[†], P. Nadel-Turonski[§¶], Y. Maeda[‖], H. Sakai[‖] and A. Tamii[‖]

[*]*Department of Neutron Research, Uppsala University, Box 525, S-75120 Uppsala, Sweden*
[†]*The Svedberg Laboratory, Uppsala University, Sweden*
[**]*Swedish Defence Research Agency (FOI), Stockholm, Sweden*
[‡]*Department of Physics, Chiang Mai University, Thailand*
[§]*Department of Radiation Sciences, Uppsala University, Sweden*
[¶]*George Washington University, Washington, D.C., USA*
[‖]*Department of Physics, University of Tokyo, Japan*

Abstract. We have measured the neutron-deuteron (*nd*) elastic-scattering differential cross section at 95 MeV incident neutron energy, using both the Medley and the SCANDAL setups at TSL in Uppsala. The full angular distribution was covered by detecting recoil deuterons from thin CD_2 targets, and the result was normalized to the neutron-proton (*np*) cross section. Recent theories predict that three-nucleon (3*N*) force effects, if present, would affect the cross section in the minimum region by about 30%. The results are compared with theoretical calculations and are well described if 3*N* forces are included.

A fundamental way to understand nuclei is to describe the forces between nucleons. In this microscopic approach, nuclei and nuclear interactions are modelled by summing all individual nucleon-nucleon (*NN*) interactions. Still, *NN* interactions alone seem to be insufficient, e.g., they are unable to reproduce the triton binding energy. Additional forces that may arise in the three-body system are called three-nucleon (3*N*) forces.

By solving the Faddeev equations for *nd* scattering using refined *NN* potentials [1, 2, 3, 4], the effects of introducing 3*N* forces have been investigated [5]. For instance, 3*N* forces are expected to affect the minimum region of the *nd* angular distribution at intermediate energies, filling the minimum by about 30%. Recent calculations based on chiral perturbation theory (CHPT) at next-to-next-to-leading order [6] include 3*N* forces in a natural way and predict a similar effect. The *nd* scattering data needed to study this effect are few [7, 8, 9, 10]. Proton-deuteron (*pd*) scattering data [11, 12, 13, 14, 15, 16, 17, 18, 19, 20] are easier to provide but more difficult to interpret because it is not known to that extent Coulomb force interactions affect the cross section in the minimum region.

Three *nd* scattering experiments at 95 MeV incident neutron energy have been performed at The Svedberg Laboratory (TSL) between August 2002 and February 2003. In the three cases, neutron-proton (*np*) scattering was also measured for the absolute normalization. In the first experiment, most of the angular range was covered using the Medley setup [21], by detecting recoil protons/deuterons from thin CH_2/CD_2 target foils. In the second experiment, recoil protons/deuterons from thin CH_2/CD_2 target foils disposed inside a multi-target box were detected with the SCANDAL setup [22], covering large neutron c.m. angles, i.e., the region of the *nd* cross-section minimum, where 3*N* forces are expected to be strongest. The third experiment consisted of a measurement of the *np* and *nd* angular distributions at small neutron c.m. angles by detecting scattered neutrons from water/heavy water with the SCANDAL setup. The results from the first experiment have been recently published [8]. The second and third experiments were performed with a different setup and are completely independent cross-check measurements. In the present article, the results from the first experiment (Medley) are briefly reported and compared with Faddeev calculations with and without 3*N* forces, and with preliminary data from the second experiment (SCANDAL).

The Medley setup is described in [21] and the TSL neutron beam facility as well as the SCANDAL setup

CP769, *International Conference on Nuclear Data for Science and Technology,*
edited by R. C. Haight, M. B. Chadwick, T. Kawano, and P. Talou
© 2005 American Institute of Physics 0-7354-0254-X/05/$22.50

are described in detail in [22]. The neutrons were produced by the ^{7}Li(p,n)^{7}Be reaction. In the present experiments, the neutron spectrum consisted of a peak at 94.8 ± 0.5 MeV with an energy spread of 2.7 MeV (FWHM), and a low-energy tail that was suppressed by time-of-flight (TOF) techniques. Two independent fission detectors for absolute monitoring of the neutron fluence were mounted near the experimental setup, about 10 m after the ^{7}Li target. The Medley setup contained eight telescopes, each of them equipped with one or two silicon detectors and one CsI detector, disposed at various angles in the forward hemisphere. The Medley targets, i.e., CD_2, CH_2, and graphite targets of about 0.2 mm thickness, were switched between the runs. The SCANDAL setup consisted of two identical detector arms, used one at a time either on the right side or on the left side of the beam, covering the angular region 10-45° for the deuteron detection. Each arm consisted of one ΔE plastic scintillator for triggering, two drift chambers for tracking, another ΔE plastic scintillator that was part of the trigger, and an array of 12 CsI detectors. The SCANDAL targets, i.e., CD_2, CH_2, and graphite targets of about 1 mm thickness, were disposed inside a multi-target box, interspaced with multi-wire proportional counters for identifying in which target the reaction took place.

The experimental procedure was almost the same for the Medley experiment as for the SCANDAL experiment. Angular bins were defined in Medley by the disposition of the detector telescopes and in SCANDAL by a position gate in the CsI crystals after tracking the protons/deuterons through the drift chambers. Protons and deuterons were identified by a selection in a $\Delta E/E$ two-dimensional plot. Events due to low-energy neutrons were partly rejected by TOF techniques, the non-rejected part being corrected for, knowing the neutron spectrum and the time/energy resolution of the detection system. The accepted events were projected as energy spectra. The carbon background (from a spectrum obtained with a graphite target) was subtracted and the remaining peak was integrated to obtain the number of elastic events. The data were corrected for effects such as the detection efficiency or the particle loss through the setup.

As both the *np* and *nd* angular distributions were obtained in the same experimental conditions, we have the opportunity to compare directly the two-body system to the three-body system. In fact, the ratio of the *nd* differential cross section to the *np* differential cross section, plotted as a function of the proton/deuteron angle in the laboratory frame, provides an excellent test for the investigation of three-nucleon force effects, and at the same time it is entirely free from normalization uncertainties. This ratio is shown in Fig. 1 where the Medley data [8] and the preliminary SCANDAL data are compared with each other and to a theoretical curve using the CD-Bonn potential [3], the *nd* cross section being obtained from

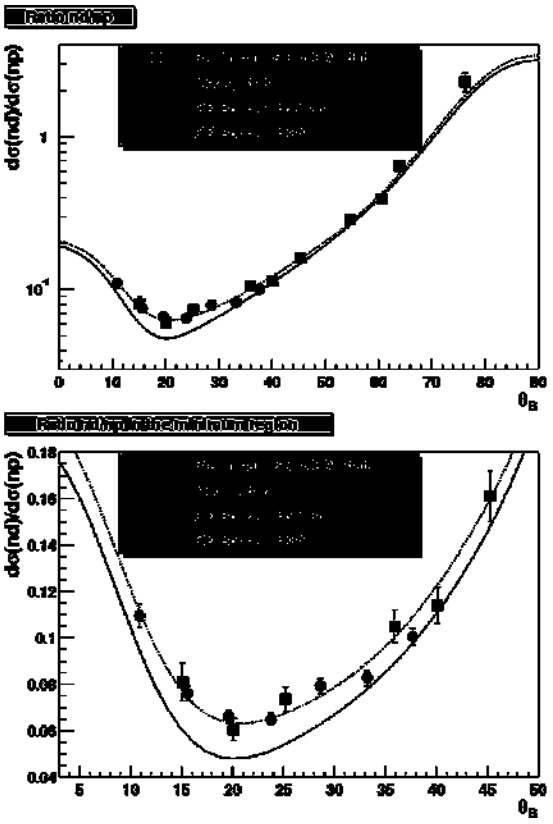

FIGURE 1. Ratio of the *nd* cross section to the *np* cross section at 95 MeV, as a function of the detected particle lab angle θ_B. The dots are preliminary SCANDAL data and the squares are the Medley data [8]. The uncertainty in θ_B is $\pm 0.25°$. The CD-Bonn potential [3] was used for the theoretical curve, the *nd* cross section being obtained from Faddeev calculations with and without 3*N* forces [5]. The same is plotted in the lower panel in the region of the minimum and with a linear vertical scale.

Faddeev calculations [5]. The Medley and SCANDAL data agree with each other. They are very well described by the calculations including 3*N* forces, whereas the calculations without 3*N* forces are unable to reproduce the data in the minimum region.

The *np* and *nd* differential cross sections are shown in Fig. 2. Since the neutron monitors have uncertainties of about 10% in the absolute neutron flux, the data need to be renormalized. The Medley and SCANDAL *np* data from the present experiments are normalized to the *np* LISA data [23] and are shown as filled and open dots, respectively. In the upper panel, the *np* data are compared with recent data at the same energy that were also taken with the SCANDAL setup [25, 26]. All sets of data are in agreement with each other. Thus, having the *np* data under good control, we can feel comfortable about the *nd* results, whose absolute normalization is set using the same normalization factors as for the *np* data. The *nd*

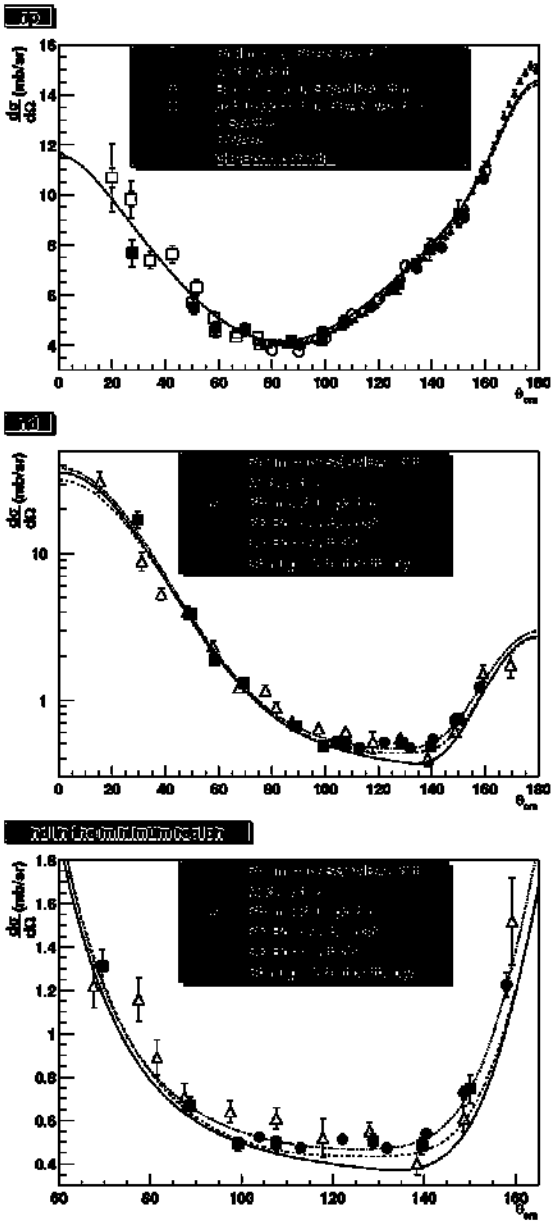

FIGURE 2. The *np* and *nd* differential cross sections at 95 MeV neutron energy versus neutron c.m. angle. The filled dots are preliminary SCANDAL data and the filled squares are the Medley data [8], both sets of data being normalized to the LISA *np* data [23]. In the upper panel the *np* results are compared to the LISA data, recent SCANDAL data [25, 26], the prediction of the CD-Bonn potential [3], and the Nijmegen partial-wave analysis PWA93 [24]. The middle panel shows the *nd* results together with *pd* data at the same energy [12]. The theoretical curves are calculations using the CD-Bonn potential with and without 3*N* forces [5], and CHPT calculations [6]. The same is plotted in the lower panel in the region of the cross-section minimum and with a linear vertical scale.

data are shown in the middle and bottom panels. Again, the data are in agreement with each other and strongly support the Faddeev calculations including 3*N* forces.

At the same energy in the c.m. system, *pd* data measured in inverse kinematics [12] are shown together with the present *nd* data in Fig. 2. The reduced χ^2 between *nd* and *pd* is about 2.5. The *pd* data are quite old (1954) and, although probably very good for their time, have larger uncertainties than the present *nd* data. This motivates a new *pd* experiment at this energy to study Coulomb effects in detail. Indeed, such an experiment has recently been performed at RCNP in Osaka, and the data are under analysis [27].

Furthermore, the data taken with SCANDAL in neutron detection mode, or the third experiment, will complete the lower part of the angular distribution (at small neutron c.m. angles). The new *nd* data will provide an additional cross-check of the Medley data, and will also allow interesting comparisons with *pd* data since Coulomb force effects are expected to be strongest in this angular range.

In conclusion, a combination of *pd* and *nd* elastic scattering data around 100 MeV permits understanding of the role of Coulomb interactions and performing a deep investigation of 3*N* force effects. We have measured the *nd* differential cross section at 95 MeV incident neutron energy and normalized the result to the *np* cross section. An inclusion of 3*N* forces is needed in order to describe the data in the minimum region, either by solving the Faddeev equations with an additional 3*N* force from a 2π-exchange model, or by performing CHPT calculations at next-to-next-to-leading order.

ACKNOWLEDGMENTS

We wish to thank the technical staff of The Svedberg Laboratory for enthusiastic and skillful assistance. We are very thankful to E. Epelbaum, W. Glöckle, H. Kamada and H. Witała for contributions concerning the theoretical part. We have appreciated the precious collaboration of K. Hatanaka and N. Kalantar-Nayestanaki. This work was supported by the Swedish Nuclear Fuel and Waste Management Company, the Swedish Nuclear Power Inspectorate, Ringhals AB, the Swedish Defence Research Agency, and the Swedish Research Council.

REFERENCES

1. V.G.J. Stoks, R.A.M. Klomp, C.P.F. Terheggen, and J.J. de Swart, Phys. Rev. C **49**, 2950 (1994).
2. R.B. Wiringa, V.G.J. Stoks, and R. Schiavilla, Phys. Rev. C **51**, 38 (1995).

3. R. Machleidt, F. Sammarruca, and Y. Song, Phys. Rev. C **53**, R1483 (1996).
4. R. Machleidt, Phys. Rev. C **63**, 024001 (2001).
5. H. Witała, W. Glöckle, D. Hüber, J. Golak, and H. Kamada, Phys. Rev. Lett. **81**, 1183 (1998).
6. E. Epelbaum, A. Nogga, W. Glöckle, H. Kamada, Ulf-G. Meissner, H. Witała, Phys. Rev. C **66**, 064001 (2002).
7. H. Rühl *et al.*, Nucl. Phys. A **524**, 377 (1991).
8. P. Mermod *et al.*, Phys. Lett. B **597**, 243 (2004).
9. J.N. Palmieri, Nucl. Phys. A **188**, 72 (1972).
10. Y. Maeda, Ph.D. thesis, University of Tokyo (2004).
11. H. Shimizu *et al.*, Nucl. Phys. A **382**, 242 (1982).
12. O. Chamberlain and M.O. Stern, Phys. Rev. **94**, 666 (1954).
13. H. Sakai *et al.*, Phys. Rev. Lett. **84**, 5288 (2000).
14. G. Igo *et al.*, Nucl. Phys. A **195**, 33 (1972).
15. H. Postma and R. Wilson, Phys. Rev. **121**, 1229 (1961).
16. K. Kuroda, A. Michalowicz, and M. Poulet, Nucl. Phys. **88**, 33 (1966).
17. K. Sekiguchi *et al.*, Phys. Rev. C **65**, 034003 (2002).
18. K. Ermisch *et al.*, Phys. Rev. C **68**, 051001(R) (2003).
19. R.E. Adelberger and C.N. Brown, Phys. Rev. D **5**, 2139 (1972).
20. K. Hatanaka *et al.*, Phys. Rev. C **66**, 044002 (2002).
21. S. Dangtip *et al.*, Nucl. Instrum. Methods A **452**, 484 (2000).
22. J. Klug *et al.*, Nucl. Instrum. Methods A **489**, 282 (2002).
23. J. Rahm *et al.*, Phys. Rev. C **63**, 044001 (2001).
24. V.G.J. Stoks, R.A.M. Klomp, M.C.M. Rentmeester, and J.J. de Swart, Phys. Rev. C **48**, 792 (1993).
25. V. Blideanu *et al.*, Phys. Rev. C **70**, 014607 (2004).
26. C. Johansson *et al.*, submitted to Phys. Rev. C (2004).
27. K. Hatanaka, private communication.

Neutrons for Science and Industry - Uppsala Neutron Beam Activities

J. Blomgren

Department of Neutron Research, Uppsala University, Sweden

Abstract. A wide programme on neutron-induced data for various applications is running at the 20–180 MeV neutron beam facility at the The Svedberg Laboratory, Uppsala. The main research areas are nuclear data for accelerator-driven transmutation of nuclear waste, single-event effects, and dose effects in fast-neutron cancer therapy and aviation environments. In addition, experiments on fundamental nuclear physics are undertaken. Moreover, commercial device testing motivated by single-event effects is a growing activity.

INTRODUCTION

Recently, a large number of applications involving high-energy (> 20 MeV) neutrons have become important. Accelerator-driven systems (ADS) for transmutation of spent nuclear fuel and nuclear weapons materials, fast-neutron cancer therapy, dose effects to the crew onboard aircraft due to cosmic-ray neutrons, as well as electronics failures induced by atmospheric neutrons, have all gotten increasing attention.

This paper outlines experimental activities motivated by the issues above. Brie y, these can be divided into two main categories: measurements of nuclear data, and direct testing, the latter being rapidly growing.

THE NEUTRON BEAM FACILITY

The results presented here were all obtained at the old neutron beam facility at the The Svedberg Laboratory (TSL), Uppsala, Sweden [1, 2], originally designed for high-quality nuclear physics experiments. Recently, a new facility has been commissioned for joint use in nuclear-data measurements and electronics testing, and it is described in a separate contribution to this conference [3].

Neutron Production

At the old neutron facility (see Fig. 1), quasi-monoenergetic neutrons are produced by the reaction ^{7}Li(p,n)^{7}Be in a target of 99.98% ^{7}Li. After the target, the proton beam is bent by two dipole magnets into an 8-m concrete tunnel, where it is focused and stopped in a well-shielded carbon beam dump. A narrow neutron beam is formed in the forward direction by a system of three collimators, with a total thickness of more than four metres.

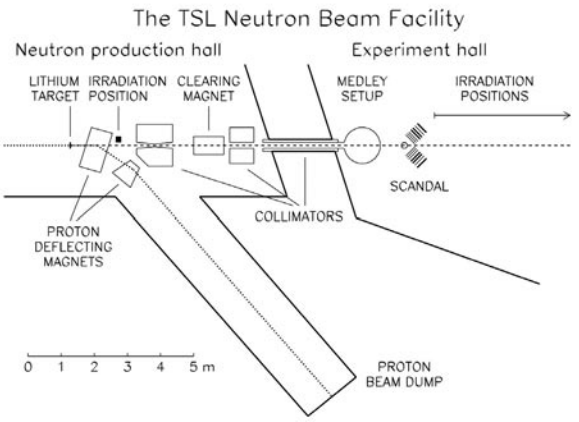

FIGURE 1. The TSL neutron beam facility, from [2].

The energy spectrum of the neutron beam is shown in Fig. 2. About half of all neutrons appear in the high-energy peak, while the rest are roughly equally distributed in energy, from the maximum energy and down to zero. The thermal contribution is small. The low-energy tail of the neutron beam can be reduced by time-of- ight measurements (see Fig. 2). With a proton beam of 5 μA onto a 4-mm lithium target, the total neutron yield in the full-energy peak at the experimental position, 8 m from the production target, is about $5 \cdot 10^4$ cm^{-2}s^{-1}. The energy resolution of the full-energy peak ($1-2$ MeV FWHM) depends on the choice of lithium target thickness.

CP769, *International Conference on Nuclear Data for Science and Technology,*
edited by R. C. Haight, M. B. Chadwick, T. Kawano, and P. Talou
© 2005 American Institute of Physics 0-7354-0254-X/05/$22.50

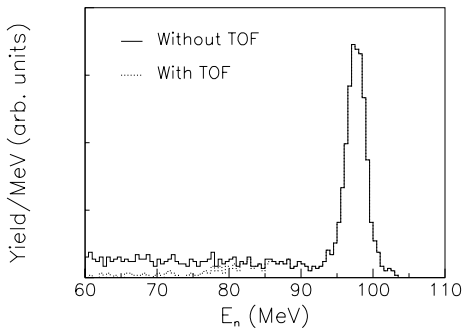

FIGURE 2. The neutron-energy spectrum with and without time-of-flight rejection of low-energy neutrons, from [2].

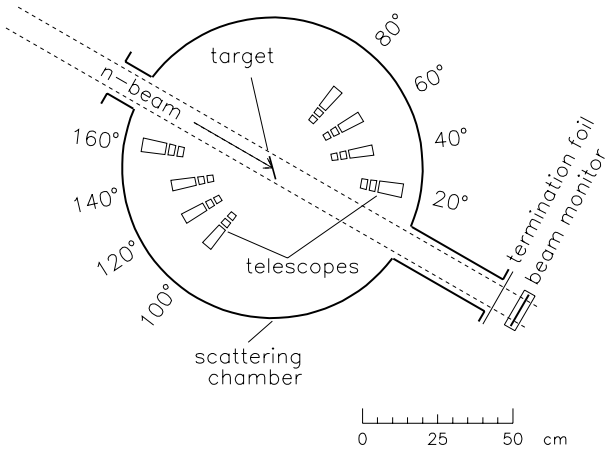

FIGURE 3. The MEDLEY facility, showing the scattering chamber and the eight telescopes [4].

Beam intensity monitoring is provided by three techniques. The proton beam intensity is monitored at the beam dump after the neutron production area, providing a relative monitor. Two fission-based neutron monitors are used, a thin film breakdown counter system and an ionization chamber.

Base Equipment

Two major experimental setups are semi-permanently installed. One of these is the MEDLEY detector telescope array [4], housed in a scattering chamber and operated in vacuum (see Fig. 3). At the exit of this chamber, a 0.1-mm stainless steel foil terminates the vacuum system, and from here on the neutrons travel in air. Immediately after MEDLEY follows SCANDAL (SCAttered Nucleon Detection AssembLy), a setup designed for large-acceptance neutron and proton detection (see Fig. 4).

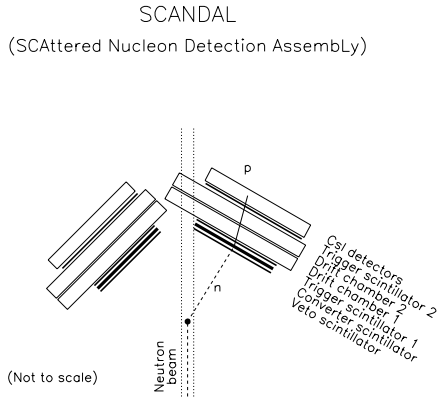

FIGURE 4. Schematic figure of the SCANDAL setup.

The MEDLEY detector array consists of eight particle telescopes, placed at 20-160 degrees with 20 degrees separation. Each telescope is a $\Delta E - \Delta E - E$ detector combination, with sufficient dynamic range to distinguish all light ions from a few MeV up to maximum energy, i.e., about 100 MeV. The ΔE detection is accomplished by fully depleted silicon surface barrier detectors, and CsI(Tl) crystals are used as E detectors. For some experiments, active collimators are used. These are plastic scintillators with a hole defining the solid angle. All the equipment is housed in a 100-cm-diameter scattering chamber, so that the charged particles can be transported in a vacuum.

Recently, the facility has been used also for fission studies. In that case, the silicon detectors are used for fission-fragment detection.

The SCANDAL (SCAttered Nucleon Detection AssembLy) setup [2] (see Fig. 4) has been designed for elastic neutron-scattering studies. It consists of two identical systems, placed to cover 10–50° and 30–70°, respectively. The energy of the scattered neutron is determined by measuring the energy of proton recoils from a plastic scintillator, and the angle is determined by tracking the recoil proton. In a typical neutron-scattering experiment, each arm consists of a 2-mm-thick veto scintillator for fast charged-particle rejection, a 10-mm-thick neutron-to-proton converter scintillator, a 2-mm-thick plastic scintillator for triggering, two drift chambers for proton tracking, a 2-mm-thick ΔE plastic scintillator that is also part of the trigger, and an array of CsI detectors for energy determination of recoil protons produced in the converter by np scattering. The trigger is provided by a coincidence of the two trigger scintillators, vetoed by the front scintillator. SCANDAL can also be used as a proton or deuteron detector. In those cases, the veto and converter scintillators are removed.

RESEARCH PROGRAMME

Fundamental Physics

Recently, the np scattering cross section at intermediate energies has been under intense debate (for a review, see [5]). The np scattering cross section is of utmost importance for applications because it is used for normalization of nuclear data measurements. It is also of great fundamental importance, because np scattering data are being used for determination of the pion-nucleon coupling constant, i.e., the absolute strength of the strong interaction in the nuclear sector. This coupling constant is of great relevance not only to basic nuclear physics, but also on a cosmological scale.

Previously, a series of backward-angle np scattering experiments have been undertaken [6, 7, 8, 9]. Recently, these measurements have been complemented by a measurement at forward angles at 96 MeV [10, 11]. In addition, a novel method to study backward-angle np scattering by tagging techniques has recently been developed at IUCF, and it is described in another contribution to this conference [12].

A number of experimental observations seem to indicate that three-body forces exist in atomic nuclei. Recent calculations [14] have indicated that measurements of the differential cross section for elastic nd scattering in the 60–200 MeV range should be useful in searches for three-nucleon ($3N$) force effects. The neutron-deuteron (nd) elastic scattering differential cross section has been measured at 95 MeV incident neutron energy. Models based on inclusion of $3N$ forces describe nd data in the angular region of the cross-section minimum very well, while models without $3N$ forces cannot account for the data [15, 16] (see Fig. 6).

Elastic Neutron Scattering

Elastic neutron scattering is of utmost importance for a vast number of applications. Besides its fundamental importance as a laboratory for tests of isospin dependence in the nucleon-nucleon, and nucleon-nucleus, interaction, knowledge of the optical potentials derived from elastic scattering come into play in virtually every application where a detailed understanding of nuclear processes is important. Elastic-neutron scattering is important also for fast-neutron cancer therapy, because the nuclear recoils account for 10%-15% of the dose. Up to now, data on ^{12}C and ^{208}Pb at 96 MeV have been published [17, 18] (see Fig. 7), and five other nuclei are under analysis. For a detailed description of the elastic-neutron scattering project, we refer to the contribution to this conference by Hildebrand *et al.* [19].

A facility for studies of inelastic-neutron scattering has recently been commissioned, and first data taking will soon commence [22].

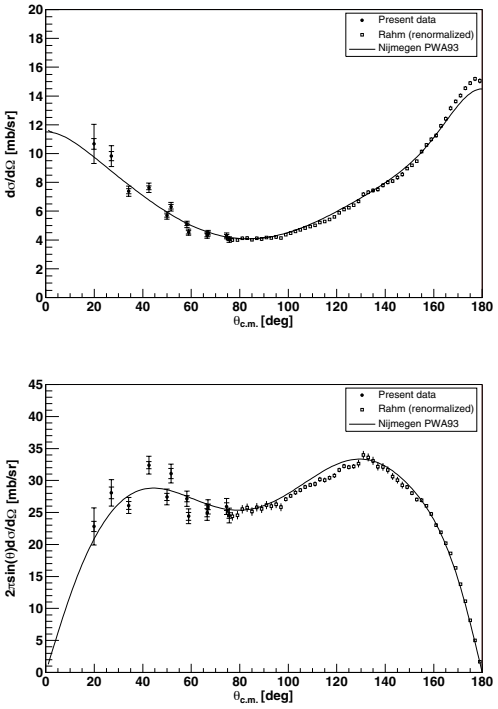

FIGURE 5. Angular distributions of np scattering cross sections at 96 MeV. Filled (open) circles represent data obtained by neutron (proton) detection. In the upper panel, experimental differential cross sections are shown together with the Nijmegen partial wave analysis PWA93 [13]. In the lower panel, data and PWA93 have been multiplied with the solid-angle element $2\pi sin\theta$ to illustrate the relative weight in the normalisation to the total cross section. In both panels, the present data are shown with double error bars; the inner bars representing the statistical error, and the outer the statistical and systematic errors, excluding normalisation errors, added in quadrature.

Light-Ion Production

Light-ion production is of major importance for assessment of the biological effects due to intermediate-energy neutrons (for a review, see, e.g., [23]). About half the dose in fast-neutron cancer therapy comes from np scattering, 10%-15% from elastic-neutron scattering, and the remaining 35%-40% from neutron-induced emission of charged particles, such as protons, deuterons, tritons, ^{3}He, and α-particles. Double-differential cross sections for all these reactions in tissue-relevant nuclei are presently being studied with the MEDLEY setup [24].

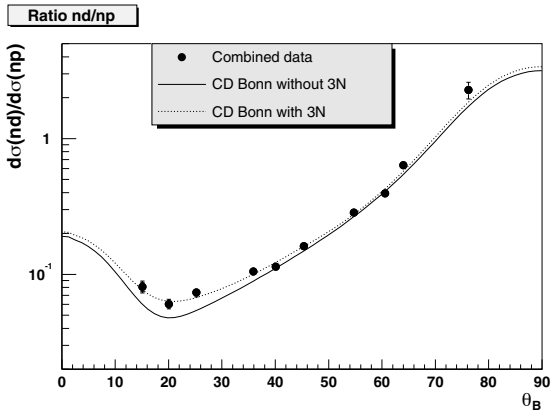

FIGURE 6. Ratio of the *nd* and the *np* cross sections at 95 MeV, as a function of the laboratory angle of the recoiling proton or deuteron [16]. The solid (dotted) line is a cross-section calculation, based on the CD-Bonn nucleon-nucleon potential, without (with) three-nucleon effects included.

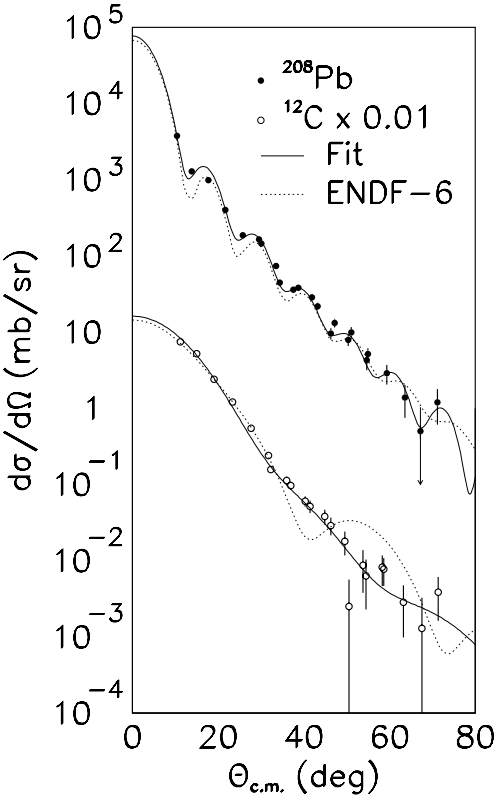

FIGURE 7. Angular distributions of elastic-neutron scattering from ^{12}C (open circles) and ^{208}Pb (solid circles) at 96 MeV incident energy [18]. The ^{12}C data and calculations have been multiplied by 0.01. The solid lines represent best fits to the present data, using a parameterization by Koning and Delaroche [20], while the dotted lines are cross sections given by the evaluated nuclear data file ENDF-6 [21].

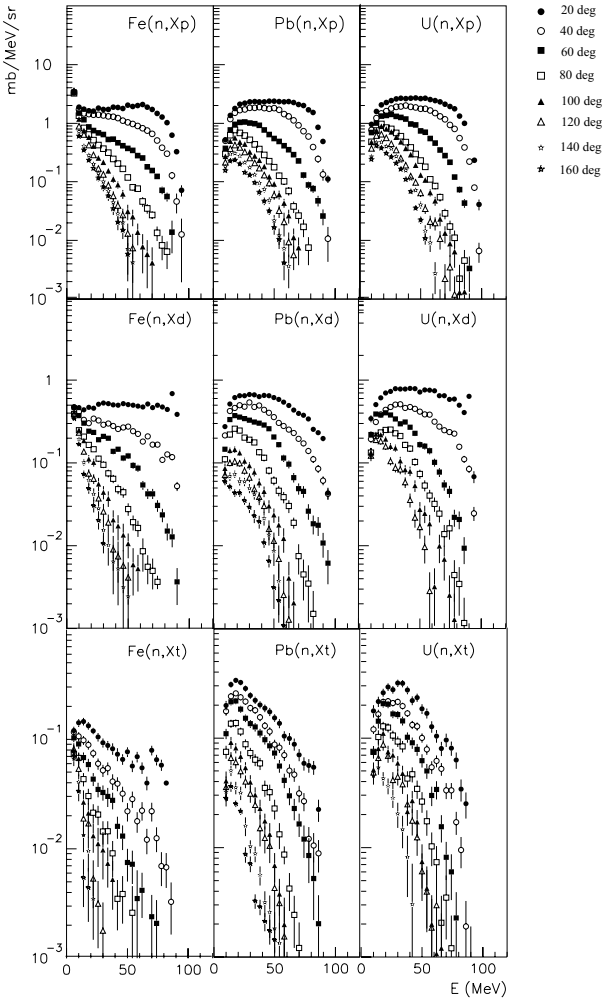

FIGURE 8. Double-differential cross sections for neutron-induced proton, deuteron, and triton production in iron, lead, and uranium at 96 MeV [25].

Although intended for medical purposes, the requirements from these led to a multipurpose detector design, which has turned out to be useful for many different applications. One of these is hydrogen and helium production in an ADS, exemplified with measurements on iron, lead, and uranium [25] (see Fig. 8). For electronics upsets, silicon has been studied [26] (see Fig. 9), which is described elsewhere at this conference [27].

Fast-Neutron Fission

Although the main fission effects in an ADS arise from neutrons at lower energies, the high-energy neutron fission gives significant contributions to the power released. Very little data exist on high-energy fission, but the situation is undergoing rapid improvement. This can be exemplified by the ongoing work at the TSL neutron beam,

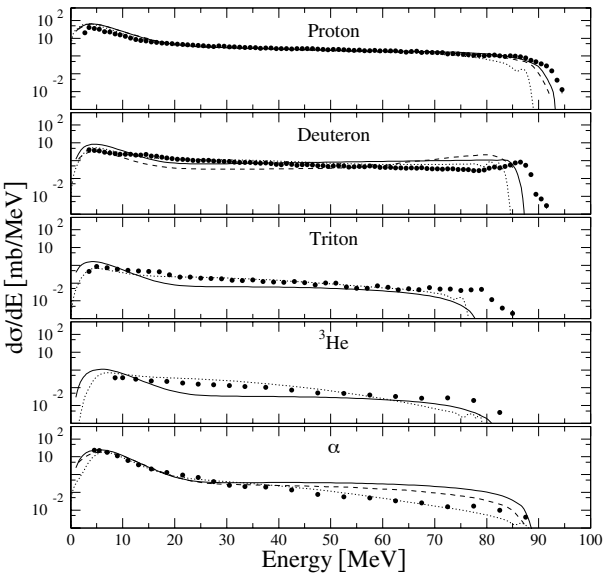

FIGURE 9. Energy-differential production cross sections for neutron-induced proton, deuteron, triton, ^{3}He, and alpha production in silicon at 96 MeV [26].

manifested in a number of contributions to this conference [28, 29, 30, 31, 32]. A new facility for studies also of angular distributions is under commissioning [33].

Neutron-Induced Electronics Failures

Recently, the importance of cosmic-radiation effects in aircraft electronics has been highlighted. (For reviews on this issue, see, e.g., [34] and references therein. Nuclear data aspects are outlined in [35].) When an electronic memory circuit is exposed to particle radiation, the latter can cause a flip of the memory content in a bit, which is called a single-event upset (SEU). This induces no hardware damage to the circuit, but evidently, unwanted re-programming of aircraft computer software can have fatal consequences.

At flight altitudes, as well as at sea level, the cosmic-ray flux is dominated by neutrons and muons. The latter do not interact strongly with nuclei, and therefore neutrons are most important for SEU.

Since neutrons have no charge, they can only interact via violent nuclear reactions, in which charged particles are created that occasionally induce an SEU. Thus, knowledge of the nuclear interaction of neutrons with silicon is needed to obtain a full understanding of the SEU problem. Firm experimental information about neutron-induced cross sections is very scarce. Thus, one has had to rely heavily on calculations based on nuclear models that have a poor and essentially unknown precision. Measurements of neutron-induced charged particle-production cross sections are therefore of utmost importance for a full understanding of the SEU problem in aviation electronics.

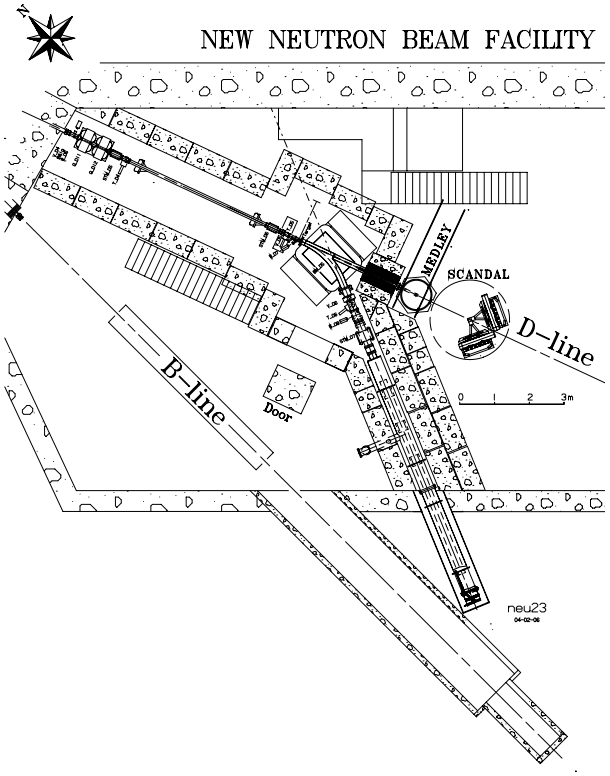

FIGURE 10. Overview of the new TSL neutron beam facility.

If the neutron-induced charged-particle production cross sections were known, and thus the energy deposition on a microscopic level, it might be possible to calculate the SEU rate with reasonable precision also for any future components. Up to now, direct in-beam component testing has been carried out to characterize the effect, especially its neutron-energy dependence [36, 37].

These studies have been further developed by measurements of cross sections for light-ion production (see above), and experiments at the CELSIUS storage ring on production of heavier ions [38].

OUTLOOK

The rapid growth in demand for neutrons has motivated the construction of a new 20 – 180 MeV neutron beam facility at TSL (see Fig. 10). The most important features of the new facility are increased intensity by reduction of the distance from neutron production to experiments, availability of much larger beam diameters, increased versatility concerning various beam parameters such as the shape, and reserved space for a future pulse-sweeping

system.

For nuclear data research, the increased intensity will facilitate a large experimental program at 180 MeV, hitherto excluded by count-rate limitations. For testing of electronics, the increased intensity in combination with a larger beam diameter, which facilitates testing of a large number of components simultaneously, will provide a total failure rate of about a factor 300 larger than for the present facility. This means that the new TSL neutron-beam facility can outperform any existing facility in the world.

ACKNOWLEDGMENTS

This work was financially supported by Vattenfall AB, the Swedish Nuclear Fuel and Waste Management Company, the Swedish Nuclear Power Inspectorate, Ringhals AB, Barsebäck Power AB, the Swedish Defense Research Agency, the Swedish Natural Science Research Council, the Swedish Nuclear Safety and Training Centre, and the European Union.

REFERENCES

1. H. Condé, *et al.*, Nucl. Instrum. Methods **A292**, 121 (1990).
2. J. Klug, *et al.*, Nucl. Instrum. Methods **A489**, 282 (2002).
3. S. Pomp, *et al.*, "The New Uppsala Neutron Beam Facility," in *International Conference on Nuclear Data for Science and Technology 2004*, AIP Conference Proceedings (Melville, New York, 2005).
4. S. Dangtip, *et al.*, Nucl. Instrum. Methods **A452**, 484 (2000).
5. Proceedings of Workshop on "Critical Points in the Determination of the Pion-Nucleon Coupling Constant," Uppsala, June 7-8, 1999, ed. J. Blomgren. Phys. Scr. **T87** (2000).
6. T. Rönnqvist, *et al.*, Phys. Rev. C **45**, R496 (1992).
7. T.E.O. Ericson, *et al.*, Phys. Rev. Lett. **75**, 1046 (1995).
8. J. Rahm, *et al.*, Phys. Rev. C **57**, 1077 (1998).
9. J. Rahm, *et al.*, Phys. Rev. C **63**, 044001 (2001).
10. C. Johansson, *et al.*, "Forward-Angle Neutron-Proton Scattering at 96 MeV," ND2004, *op. cit.*
11. C. Johansson, *et al.*, submitted to Phys. Rev. C.
12. S. Vigdor, "Measurement of Absolute np Scattering Differential Cross Sections with a Tagged Intermediate-Energy Neutron Beam," ND2004, *op. cit.*
13. V.G.J. Stoks, R.A.M. Klomp, M.C.M. Rentmeester, and J.J. de Swart, Phys. Rev. C **48**, 792 (1993).
14. H. Witała, *et al.*, Phys. Rev. Lett. **81**, 1183 (1998).
15. P. Mermod, *et al.*, "Investigation of Three-Body Force Effects in Neutron-Deuteron Scattering at 95 MeV," ND2004, *op. cit*.
16. P. Mermod, *et al.*, Phys. Lett. **B 597, 243 (2004)**.
17. J. Klug, *et al.*, Phys. Rev. C **67**, 031601(R) (2003).
18. J. Klug, *et al.*, Phys. Rev. C **68**, 064605 (2003).
19. A. Hildebrand, *et al.*, "Elastic Neutron Scattering at 96 MeV," ND2004, *op. cit.*
20. A.J. Koning and J.P. Delaroche, Nucl. Phys. **A713**, 231 (2003).
21. P.F. Rose and C.L. Dunford, ENDF-102: Data Formats and Procedures for the Evaluated Nuclear Data File ENDF-6, Technical Report BNL-NCS-44945 (Brookhaven National Laboratory, National Nuclear Data Center, Upton, NY, 1991), and V. McLane, ENDF201: ENDF/B-VI Summary Documentation, Technical Report BNL-NCS-17541, Ed. 4, **Suppl. 1** (Brookhaven National Laboratory, National Nuclear Data Center, Upton, NY, 1996). For Internet access, see www.nndc.bnl.gov.
22. F.-R. Lecolley, private communication (2004).
23. J. Blomgren and N. Olsson, Radiat. Prot. Dosim. **103(4)**, 293 (2003).
24. U. Tippawan, *et al.*, to be published.
25. V. Blideanu, *et al.*, Phys. Rev. C **70** (2004) 014607.
26. U. Tippawan, *et al.*, Phys. Rev. C **69**, 064609 (2004).
27. U. Tippawan, *et al.*, "Light-Ion Production in the Interaction of 96 MeV Neutrons with Silicon," ND2004, *op. cit.*
28. A.N. Smirnov, *et al.*, "Correlation of Intermediate Energy Proton- and Neutron-Induced Fission Cross Sections in the Lead-Bismuth Region," ND2004, *op. cit.*
29. O.I. Batenkov, *et al.*, "Comparison of Measured and Calculated Mass Distributions of Fission Fragments in Proton-Induced Fission of ^{232}Th, ^{235}U, ^{238}U, and ^{237}Np at Intermediate Energies," ND2004, *op. cit.*
30. V.P. Eismont, N.P. Filatov, A.N. Smirnov, *et al.*, "On Nuclear Structure Effects in the Nucleon-Induced Fission Cross Sections of Nuclei near ^{208}Pb at Intermediate Energies," ND2004, *op. cit.*
31. V.P. Eismont, N.P. Filatov, S.N. Kirillov, *et al.*, "Angular Anisotropy of Intermediate Energy Nucleon-Induced Fission of Pb Isotopes and Bi," ND2004, *op. cit.*
32. G.A. Tutin, *et al.*, "Measurements of Neutron-Induced Fission Cross Sections of ^{205}Tl, ^{204,206,207,208}Pb, and ^{209}Bi using Quasi-Monoenergetic Neutrons in the Energy Range 35 - 174 MeV," ND2004, *op. cit.*
33. A. Prokofiev, *et al.*, "A New Facility for High-Energy Neutron-Induced Fission Studies," ND2004, *op. cit.*
34. Single-Event Upsets in Microelectronics, topical issue, eds. H.H.K. Tang and N. Olsson, Mat. Res. Soc. Bull. **28** (2003).
35. J. Blomgren, Nuclear Data for Single-Event Effects, EU enlargement workshop on Neutron Measurements and Evaluations for Applications, Budapest, Hungary, November 5-8, 2003 (invited). EUR Report 21100 EN, Luxembourg: Office for Official Publications of the European Communities, ISBN 92-894-6041-5, European Communities, 2004.
36. K. Johansson, *et al.*, IEEE transactions on Nuclear Science **45**, 2519 (1998).
37. K. Johansson, *et al.*, IEEE transactions on Nuclear Science **46**, 1427 (1999).
38. J. Aichelin, *et al.*, Inverse kinematics for study of intermediate energy reactions relevant to SEE and medical problems, EU enlargement workshop on Neutron Measurements and Evaluations for Applications, Budapest, Hungary, November 5-8, 2003. EUR Report 21100 EN, Luxembourg: Office for Official Publications of the European Communities, ISBN 92-894-6041-5, European Communities, 2004.

The New Uppsala Neutron Beam Facility

S. Pomp[1], A. V. Prokofiev[2], J. Blomgren[1], O. Byström[2], C. Ekström[2], N. Haag[2], A. Hildebrand[1], C. Johansson[1], O. Jonsson[2], P. Mermod[1], L. Nilsson[1,2], D. Reistad[2], N. Olsson[1,3], P.-U. Renberg[2], M. Österlund[1], U. Tippawan[1,4], D. Wessman[2], and V. Ziemann[2]

[1]*Department of Neutron Research, Uppsala University, Sweden*
[2]*The Svedberg Laboratory, Uppsala University, Sweden*
[3]*Swedish Defence Research Agency (FOI), Stockholm, Sweden*
[4]*Fast Neutron Research Facility, Chiang Mai University, Thailand*

Abstract. A new quasi-monoenergetic neutron beam facility has been constructed at the The Svedberg Laboratory (TSL) in Uppsala, Sweden. Key features include an energy range of 20 to 175 MeV, high fluxes, and the possibility of large-area fields. Besides cross-section measurements, the new facility has been designed specifically to provide optimal conditions for testing of single-event effects in electronics and for dosimetry development. First results of the beam characterization measurements performed in early 2004 are reported.

INTRODUCTION

Over the past years, a growing interest in nuclear applications, such as accelerator-driven transmutation of nuclear waste [1], fast-neutron cancer therapy [2-5], measurement of dose delivery to personnel in aviation [2,6], as well as electronic failures due to neutrons produced by cosmic rays [7,8] has put new emphasis on the need for a detailed understanding of nuclear interactions involving neutrons at intermediate energies (20-200 MeV). To satisfy these needs, a new quasi-monoenergetic neutron-beam facility has been constructed at the The Svedberg Laboratory (TSL), Uppsala. Emphasis has been put on a high neutron beam intensity in combination with a high flexibility in energy and shape.

TECHNICAL SPECIFICATION

The facility uses the ^{7}Li(p,n)^{7}Be reaction (Q= 1.64 MeV) to produce a quasi-monoenergetic neutron beam. The proton beam is provided by the Gustaf Werner cyclotron with an energy variable in the 20-180 MeV range. A drawing of the neutron-beam facility is shown in Fig. 1. The proton beam is incident

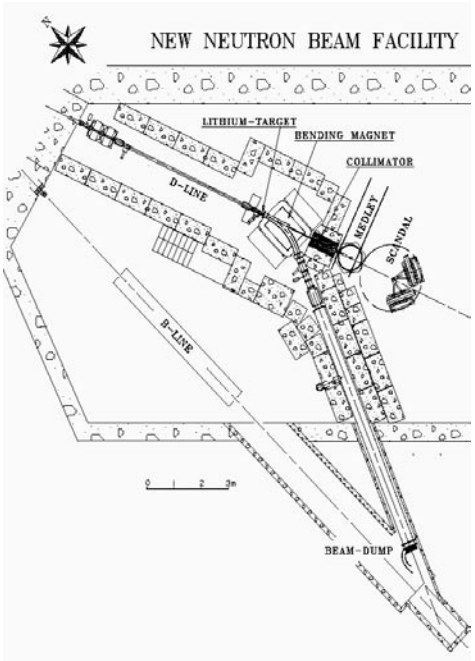

FIGURE 1. Drawing of the new neutron beam facility. The neutron beam is produced in the lithium target and continues along the D-line. The lithium target, the deflecting magnet, and the collimator are indicated. The drawing shows also the position for two permanent but movable experimental setups, Medley and SCANDAL.

CP769, *International Conference on Nuclear Data for Science and Technology,*
edited by R. C. Haight, M. B. Chadwick, T. Kawano, and P. Talou
© 2005 American Institute of Physics 0-7354-0254-X/05/$22.50

on a target of lithium, enriched to 99.99% in ^{7}Li. The available targets are 2, 4, 8, 16, and 24 mm thick. The targets are rectangular in shape, 20x32 mm^2, and are mounted in a remotely controlled water-cooled copper ring. An additional target position contains a fluorescent screen viewed by a TV camera, which is used for beam alignment and focusing. Downstream from the target, the proton beam is deflected by a magnet into a 10-m-long dumping line, where it is guided onto a heavily shielded water-cooled graphite beam dump.

The neutron beam is formed geometrically by a cylindrically shaped iron collimator block, 50 cm in diameter and 100 cm long, with a cylindrical hole of variable diameter. The collimator is surrounded by concrete to form the end wall of the production line towards the experimental area. Thereby, efficient shielding from the production target region is achieved. A modular construction of the collimator allows the user to adjust the diameter of the neutron beam to the needs of a specific experiment. The available collimator openings are 2, 3, 5.4, 10, 15, 20, and 30 cm. Other collimator diameters in the 0-30 cm range, as well as other shapes than circular can be provided upon request. Beam diameters of up to 1 m are obtainable at a larger distance from the production target, which may be used for testing a larger number of devices simultaneously, or larger devices like entire electronic boards. The facility is capable to deliver neutrons in the 20-175 MeV range. This makes TSL the only laboratory in the world offering full monoenergetic neutron testing according to the JEDEC standard [8].

Neutrons reach the experimental area at a distance of about 3 m from the production target. Reduction of this distance has led to an increase of the neutron flux by about one order of magnitude in comparison with the old TSL neutron facility [9,10], using the same target thickness, proton energy, and current. Beam currents of up to 10 μA can be achieved for energies below 100 MeV. Above 100 MeV, when the cyclotron operates in FM mode, the achievable beam current is about a factor of 12 lower. The resulting lower neutron fluence can be partly compensated for by the use of thicker lithium targets.

Two additional irradiation positions, which can be used parasitically with other experiments, are provided (see Table 1). The increase of the neutron flux at these positions is reached at the expense of limited accessibility, limited size of irradiated objects, and more intense γ-ray background.

TABLE 1. Parasitic irradiation positions.

Position	Distance from the Li Target (m)	Angle to the n-Beam Direction (°)	Gain in the Neutron Peak Flux
PARTY	1.9	1.6	2.5
TUNIS	1.1	7.5	1.7 – 2.2[1)]

[1)] dependent on the peak neutron energy.

CHARACTERIZATION OF THE FACILITY

The first neutron beam at the new facility was delivered in January 2004. Since then, extensive commissioning runs of the facility have been performed, including optimization of beam transport, diagnostics, vacuum and background conditions, as well as measurements of neutron flux, spectra, and profile. First results are reported below.

The measured contamination of the neutron beam at the experimental area due to interactions of the primary protons with beam transport elements such as the target frame did not exceed 0.2%. Such interactions only lead to a minor surplus of neutrons in the experimental area because charged particles produced near the Lithium target and upstream are removed by the deflection magnet. The relative contamination of protons with energies above 15 MeV in the neutron beam is about 10^{-5}. These measurements have been performed for a proton beam energy of 98 MeV.

The energy and angular distribution of neutrons delivered to the experimental area is mainly defined by the double-differential cross section of the ^{7}Li(p,n) reaction at forward angles. The reaction energy spectrum is dominated by a peak situated a few MeV below the energy of the primary protons and comprising about 40% of the total number of neutrons. Neutron spectra have been obtained by measuring elastic *np*-scattering with the Medley setup [11]. The scattered protons are registered at an angle of 20° relative to the neutron beam. Besides the energy of the scattered proton, the time-of-flight (TOF) relative to the RF signal from the cyclotron for each event is recorded. As an example, the measured proton energy vs. neutron TOF is shown in Fig. 2. All proton events for a peak neutron energy of 74.8 MeV are contained. The horizontal and vertical straight lines indicate the position of the proton peak in time and energy for elastic scattering events caused by peak neutrons. The bent line shows the calculated position of elastic scattering events for different neutron energies. The neutron spectrum is deduced by application of a cut

around this bent line, proper background subtraction, and calculation of the corresponding incoming neutron energy on an event-by-event basis. The measured neutron spectra for five incident proton energies between 24.7 and 147.4 MeV are shown in Fig. 3. The measurements are compared with the systematics by Prokofiev *et al.* [12] for the four higher energies (Fig. 3 b-e). The systematics is not applicable at the lowest beam energy (Fig. 3 a). Instead, an evaluation of Mashnik *et al.* [13] was employed for the description of the neutron spectrum. The differential cross section for high-energy peak neutron production at 0° was obtained by multiplication of the total cross section of the ^{7}Li(p,n)^{7}Be reaction [13] to the "index of forwardness" from the systematics of Uwamino *et al.* [14]. The narrow peaks in the upper continuum region correspond to excitation of higher states in residual ^{7}Be nuclei. This process was included in the model calculation of Mashnik *et al.* [13]. However, the energy resolution in the experiment does not allow us to observe these peaks.

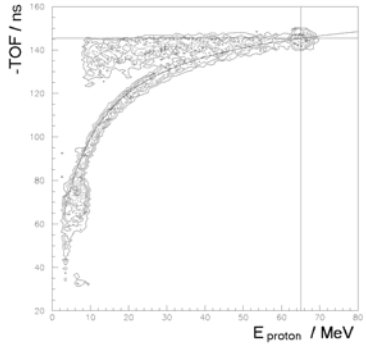

FIGURE 2. Measured proton energy vs. time-of-flight (TOF) for a peak neutron energy of 74.8 MeV registered at a scattering angle of 20° (see text).

The experimental data agree with the calculations except for the region below 10 MeV in the 24.7-MeV spectrum where the model overpredicts the experimental results by up to a factor of 2, and the region just below the peak in the 77.4-MeV spectrum. The later is due to the fact that no carbon background subtraction could be applied to these data. This would reduce the difference between the experiment and the calculation in the 30- to 70-MeV region where elastic events caused by tail neutrons and protons from ^{12}C(n,xp) reactions caused by peak neutrons overlap (cp. Fig. 2). Table 2 summarizes the main features of the measured spectra and the achieved neutron fluence. The later has been measured with the thin-film breakdown counter (TFBC) [15]. Another monitoring option is provided by an ionization-chamber monitor (ICM). Both monitors, usually installed after the Medley chamber, utilize neutron-induced fission of ^{238}U. Finally, a Faraday cup, installed in the proton beam dump, integrates the beam current and offers relative monitoring of the beam intensity.

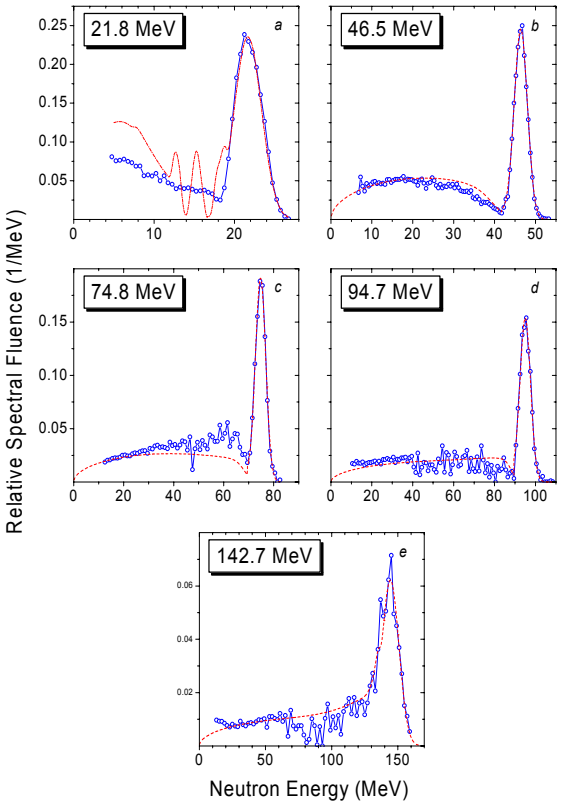

FIGURE 3. The neutron spectra at 0° for different peak neutron energies (see Table 2 for incident proton energies and ^{7}Li target thicknesses). Symbols connected by a solid line represent experimental data obtained in the present work. Predictions are shown as dashed lines (see text). Note that no carbon background subtraction could be applied to the 77 MeV data (c) (see text).

Figure 4 shows a horizontal beam profile for 143-MeV neutrons, measured at a distance of 4.77 m from the production target. The measurement was performed by counting neutron-induced single-event upsets in a set of electronic chips positioned across the beam [16]. Another measurement of the beam profile performed at 94.7 MeV is currently under analysis.

SUMMARY AND OUTLOOK

A new neutron beam facility has been constructed at TSL and is now available for regular operation. It is capable to deliver neutrons in the 20-175 MeV range, which makes TSL the only laboratory in the world

TABLE 2. First results for the neutron spectra and beam intensities. The fluences have been measured with the TFBC and refer to the entrance of the experimental hall. Higher fluences can be achieved by using thicker Li targets.

Proton Beam Energy (MeV)	Li Target Thickness (mm)	Beam Current (μA)	Resulting Average Energy of Peak Neutrons (MeV)	Fraction of Neutrons in the Mono-Energetic Peak (%)		Peak Neutron Fluence (10^5 neutrons/(cm^2 s))
				Measured	Calculated	
24.68 ± 0.04	2	10	21.8	~50	--	1.3
49.5 ± 0.2	4	9.5	46.5	39	36	2.8
77.4 ± 0.2	4	9.9	74.8	34 [1)]	40	2.4
97.9 ± 0.3	8	3.4	94.7	41	39	3.1
147.4 ± 0.6	24	0.26	142.7	55 [2)]	40	0.9

[1)] lower limit since no carbon background runs are available for this energy; [2)] upper limit due to poor energy resolution.

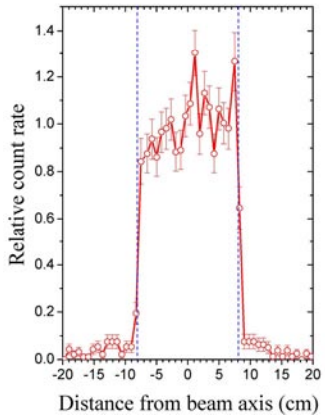

FIGURE 4. The horizontal beam profile for 142.7-MeV neutrons, measured at the distance of 4.77 m from the production target. Vertical dashed lines represent boundaries of the beam expected from the geometry of the collimator.

offering full monoenergetic neutron testing according to the JEDEC standard [8]. First beams for commercial electronics testing, as well as for nuclear physics research, have been delivered.

For spring 2005, it is planned to measure the flux of thermal neutrons in the experimental hall. As a response to the needs of SEE users, the possibility of delivering peak neutrons with lower energies (<20 MeV) is being considered.

ACKNOWLEDGMENTS

We would like to thank all the staff at the The Svedberg Laboratory for the excellent work in building this new facility. We are thankful to M. Olmos for providing us with the beam profile data.

REFERENCES

1. Koning, A., *et al*., High and Intermediate energy Nuclear Data for Accelerator-driven Systems (HINDAS), *J. Nucl. Sci. Technol.* **2**, 1161 (2002).
2. Blomgren, J., and Olsson, N., *Radiat. Prot. Dosim.,* **103**, 293 (2003).
3. Orecchia, R., *et al*., *Eur. J. Cancer* **34**, 459 (1998).
4. Schwartz, D. L., *et al.*, *Int. J. Radiat. Oncol. Biol. Phys.* **50**, 449 (2001).
5. Laramore, G. E., and Griffin, T. W., *Int. J. Radiat. Oncol. Biol. Phys.* **32**, 879 (1995).
6. ICRP, *1990 Recommendations of the International Commission on Radiological Protection: Publication 60, Annals of the ICRP, Vol. 21, No. 1-3*, Oxford: Pergamon Press, 1991.
7. Single-Event Upsets in Microelectronics, topical issue, edited by H. H. K. Tang and N. Olsson [*Mater. Res. Soc. Bull.* **28** (2003)].
8. JEDEC Standard. *Measurements and Reporting of Alpha Particles and Terrestrial Cosmic Ray-Induced Soft Errors in Semiconductor Devices. JESD89*, August 2001.
9. Condé, H., *et al.*, *Nucl. Instrum. Methods Phys. Res. A* **292**, 121 (1990).
10. Klug, J., *et al.*, *Nucl. Instrum. Methods Phys. Res. A* **489**, 282 (2002).
11. Dangtip, S., *et al.*, *Nucl. Instrum. Methods Phys. Res. A* **452**, 484 (2000).
12. Prokofiev, A. V., *et al.*, *J. Nucl. Sci. Techn.*, Suppl. 2, 112 (2002).
13. Mashnik, S. G., *et al.*, LANL Report LA-UR-00-1067 (2000).
14. Uwamino, Y., *et al.*, *Nucl. Instrum. Methods Phys. Res. A* **389**, 463 (1997).
15. Smirnov, A. N., *et al*., *Radiat. Meas.* **25**, 151 (1995).
16. M. Olmos, private communication.

A New Facility for High-Energy Neutron-Induced Fission Studies

A. Prokofiev[1], S. Pomp[2], U. Tippawan[2, 3], B. Bergenwall[2], J. Blomgren[2], M. Carlsson[1], S. Dangtip[3], L. Einarsson[1], N. Haag[1], A. Hildebrand[2], C. Johansson[2], P. Mermod[2], and M. Österlund[2]

[1]*The Svedberg Laboratory, Uppsala University, Sweden*
[2]*Department of Neutron Research, Uppsala University, Sweden*
[3]*Fast Neutron Research Facility, Chiang Mai University, Thailand*

Abstract. A new facility is constructed for measurements of neutron-induced fission cross sections in the 20-180 MeV energy region versus the *np* scattering cross section, which is adopted as the primary neutron standard. The advantage of the experiment compared to earlier studies is that the fission-fragment detection and the neutron-flux measurement via *np* scattering are performed simultaneously and at the same position in the beam, and, therefore, many sources of systematic errors cancel out. Further reduction of systematic errors is achieved due to "embedded" determination of effective solid angle of particle detectors using α-particles from the radioactive decay of the target nuclei. The performance of the facility is illustrated by first data obtained for angular distributions of fission fragments in the ^{238}U(n,f) reaction.

INTRODUCTION

Fission is one of the important processes that occurs in the spallation target and in the reactor core of an accelerator-driven system (ADS). The fission channel contributes to the neutron production, to the radioactivity produced in the target, as well as to the chemical and radiological toxicity of the reaction products.

Furthermore, neutron-induced fission reactions of ^{235}U, ^{238}U, and ^{209}Bi are internationally recommended as standards for monitoring of high-energy neutron beams [1]. The ^{238}U(n,f) reaction is most widely used due to the compromise between the magnitude of the cross section, the insensitivity to low-energy neutrons, and the availability of the target material. Monitors based on the ^{238}U(n,f) reaction are employed at many high-energy neutron facilities [2-6]. Schuhmacher *et al.* [3] have reported the use of the ^{238}U(n,f) reaction for neutron-spectrum measurements as well.

High-energy *(n,f)* data are important as well for a number of theoretical developments, *e.g.,* the understanding of dynamic effects in the fission process [7] and the theory of nuclear moments of inertia [8].

Despite the importance of the high-energy *(n,f)* cross-section data for theory and applications, there have been few attempts [4,9-12] to measure them in absolute scale, i.e., versus the *np* scattering cross section, which is adopted as the primary neutron standard [1]. Only two studies [9,11] have resulted in journal papers, one of which [9] is in apparent disagreement with newer data above 20 MeV. The current standard ^{235}U(n,f) and ^{238}U(n,f) cross sections recommended by IAEA [1] are based on the data sets of Lisowski *et al*. [10]. The latter data have undergone a few revisions, while a publication with the final results and a thorough description of the experimental technique is still awaited. The data of Newhauser *et al*. [12] have been superseded by newer results of the same group [4], which are not finally published either. Even fewer data sets are available for neutron-induced fission fragment angular distributions (FFAD) above 20 MeV [13-15].

CP769, *International Conference on Nuclear Data for Science and Technology,*
edited by R. C. Haight, M. B. Chadwick, T. Kawano, and P. Talou
© 2005 American Institute of Physics 0-7354-0254-X/05/$22.50

In the framework of the **FIRANDET** project (**Fi**ssion **R**esearch with **A**dva**n**ced **Det**ectors), a new facility is constructed for measurements of neutron-induced fission cross sections in absolute scale. As a first step towards the cross-section measurements, we have obtained data on angular distributions of fission fragments from the ^{238}U(n,f) reaction.

EXPERIMENTAL SETUP

The facility for neutron fission studies makes use of the Uppsala neutron beam produced via the ^{7}Li(p,n) reaction induced by protons in the 20-180 MeV energy range. The experiment described in the present work was performed in 2003, before the upgrade of the neutron beam. A thorough description of the neutron beam before the upgrade may be found in [6]. A description of the new neutron beam line, together with examples of neutron spectra, may be found in another contribution to this conference [16].

The present experimental program makes use of the Medley setup, which is extensively described in [17]. Only a brief description is given below, emphasizing features that are specific for studies of neutron-induced fission.

A schematic view of the Medley setup is shown in Fig. 1. The chamber was situated at a distance of about 9.2 m from the neutron production target. It has circular shape with a target assembly in the center and eight detector telescopes mounted at angles of 20 to 160° relative to the beam direction, in steps of 20°.

The target assembly consists of two layers of $^{238}UF_4$, each about 1 mg/cm^2 thick, deposited on polyethylene backings, about 90 μm thick, and mounted back-to-back. The angle between the normal to the target surface and the beam direction is 45°. The target assembly is 65 mm in diameter, and is fully covered by the central homogeneous area of the neutron beam.

Each detector telescope consists of two fully depleted surface barrier Si detectors, 50-60 and 400-500 μm thick, respectively, and a 5-cm long CsI(Tl) scintillator crystal. Both the α-particles from the radioactive decay of ^{238}U and the fission fragments are fully stopped and detected by the first Si detector. Recoil protons, coming from the H(n,p) reaction with the hydrogen nuclei in the target backing, pass through both Si detectors and are stopped in the CsI(Tl) scintillator. The protons are discriminated against other charged particles using ΔE-E techniques. Only information from the telescopes at 20° and 40° is useful for neutron beam monitoring, since the elastic peak becomes too wide at larger angles, and the relative contribution of background from the ^{12}C(n,p) reaction increases. Time-of-flight (TOF) techniques are employed to distinguish fission and recoil proton events due to the high-energy peak and the low-energy tail in the neutron spectrum.

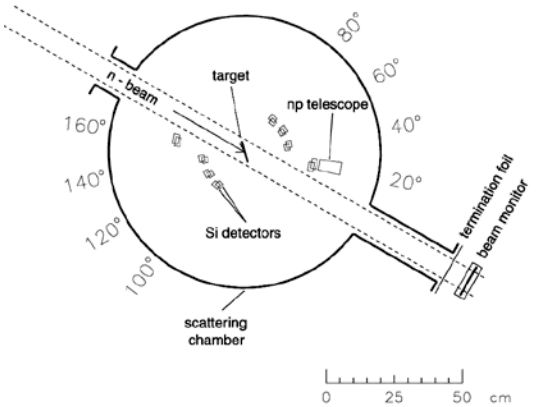

FIGURE 1. Schematic view of the Medley assembly. The neutron beam impinges on the target from the top left corner of the figure. A cross-section view below the main figure shows the arrangement of detectors in a fully equipped telescope.

DATA ANALYSIS

An advantage of the experiment compared to earlier studies is that the fission-fragment detection and the neutron-flux measurement via *np* scattering are performed simultaneously and at the same position in the beam, and, therefore, many sources of systematic errors cancel out, as it is shown below.

The count rate of fission events induced by high-energy peak neutrons and registered by *i*-th detector is:

$$n_f(\vartheta_i) = \frac{\Omega_i}{2\pi} m \frac{N_A}{A} j_n \frac{d\sigma_f}{d\Omega}(\vartheta_i), \qquad (1)$$

where Ω_i is the solid angle subtended by *i*-th detector, ϑ_i is its angular coordinate, *m* is the mass of the fission target, N_A is the Avogadro number, *A* is the atomic mass of the fissioning nuclide, j_n is the peak neutron flux on the target, and $\frac{d\sigma_f}{d\Omega}$ is the

differential fission cross section. The count rate of α-particles from radioactive decay of target nuclei is:

$$n_\alpha(\vartheta_i) = m a_{spec} \frac{\Omega_i}{4\pi}, \qquad (2)$$

where a_{spec} is the specific α-activity of the target nuclide. Combining Eqs. (1) and (2) gives:

$$\frac{d\sigma_f}{d\Omega}(\vartheta_i) = W(\vartheta) \frac{a_{spec} A}{2 N_A} \frac{1}{j_n}, \qquad (3)$$

where

$$W(\vartheta) = \frac{n_f(\vartheta_i)}{n_\alpha(\vartheta_i)} \qquad (4)$$

is the relative FFAD. Thus, the described procedure allows us to reduce the FFAD measurement to the simple counting of fragments and α-particles. The latter are counted either during the beamtime or in additional runs without the beam.

The second term in Eq. (3) includes only well-known physical constants, and the third one is the inverse neutron flux. Neither the amount of the target nuclide nor the solid angle subtended by the detector are present in Eq. (3). Thus, counting α-particles from radioactive decay of target nuclei provides an "embedded" determination of the effective solid angle of the detectors and allows us to reduce further the systematic errors. In particular, the described procedure is insensitive to a possible inhomogeneity of the target.

EXPERIMENTAL RESULTS

In order to illustrate the performance of the facility, we report FFAD in the ^{238}U(n,f) reaction at quasi-monoenergetic neutrons with a peak energy of 20.9 MeV.

Clear separation between fission fragments and products of non-fission reactions is observed in the energy spectra for all detectors, and, therefore, the uncertainty in the fission count rate is purely statistical. In Fig. 2, the FFAD, obtained according to Eq. (4), is shown. The line in Fig. 2 represents the least squares fit to the data according to the following equation:

$$W(\vartheta) \sim 1 + B \cos^2 \vartheta, \qquad (5)$$

where θ is the angle between the incident beam and the fragment direction in the frame of the fissioning nucleus, and B=0.443±0.052 is the angular anisotropy factor. Since the TOF information has not been used yet, the shown angular distribution is a superposition of contributions from reactions induced by neutrons of different energies in the incident spectrum.

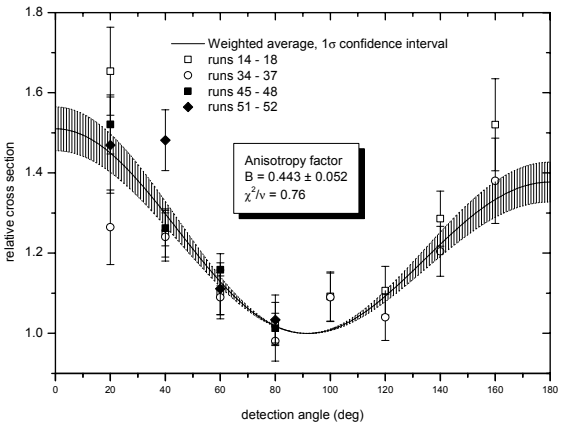

FIGURE 2. FFAD from the ^{238}U(n,f) reaction induced by quasi-monoenergetic neutrons with a peak energy of 20.9 MeV. Symbols represent the present measurement results. The curve represents a fit to the experimental data according to Eq. (5). All data are normalized to unity at 90°.

In order to deduce the angular anisotropy for the peak neutron energy, we have to correct for the contribution from reactions induced by low-energy tail neutrons, using either a TOF cut for the experimental data or a model calculation based on data on the incident neutron spectrum, the fission cross section, and the angular anisotropy in the low-energy region. In the present work, only the second option has been applied. The neutron spectrum from the ^{7}Li(p,n) reaction at 0° is taken from the evaluation of Mashnik *et al.* [18], included in the LA150 library. The ^{238}U(n,f) cross-section data come from the ENDF-VI library (below 20 MeV) and from the evaluation of Carlson *et al.* [1] (above 20 MeV). By folding the neutron spectrum and the fission cross section, we obtain the distribution of fission events on incident neutron energy. The resulted distribution is folded with fission anisotropy calculated using the STAPRE-H code [15,19] for the neutron energies below 20 MeV. The result is the contribution to the anisotropy due to the low-energy tail neutrons. Comparing it with the measured integral anisotropy factor given above, we arrive at the anisotropy factor related to fission induced by high-energy peak neutrons: B=0.48±0.09. The result is shown in Fig. 3 together with other

experimental data [20] and the model calculation [15,19]. The present result is in agreement with the data of Ryzhov *et al.* [14,15] and the STAPRE-H calculation [15,19].

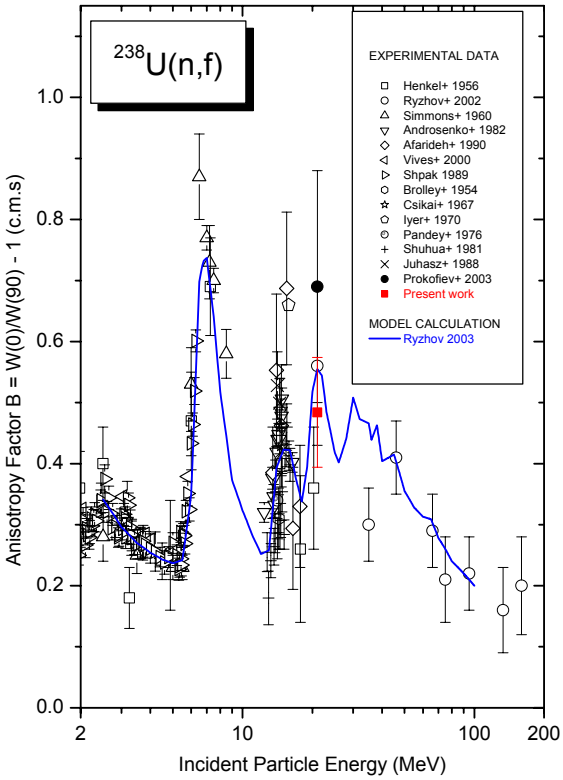

FIGURE 3. Anisotropy of neutron-induced fission of ^{238}U. The data from the present work have been corrected for the contribution from low-energy neutrons (see the text).

CONCLUSIONS AND OUTLOOK

A new facility has been used to obtain angular distributions of fragments from the ^{238}U(n,f) reaction. The results are in agreement with both earlier experiments and theoretical calculations. This ensures adequacy of the performance of the new setup and the used data analysis techniques. Measurements and processing of obtained experimental data will be continued.

ACKNOWLEDGMENTS

The authors are grateful to I.V. Ryzhov for valuable discussions. We are thankful to the staff of the The Svedberg Laboratory for providing us with the beam and for other various help.

REFERENCES

1. Carlson, A.D., *et al.*, *Proc. Int. Conf. on Nuclear Data for Science and Technology*, Trieste, Italy, May 19-24, 1997, Part II, 1223-1229.
2. Wender, S.A., *et al.*, *Nucl. Instrum. Methods Phys. Res. A* **336**, 226-231 (1993).
3. Schuhmacher, H., *et al.*, *Nucl. Instrum. Methods Phys. Res. A* **421**, 284-295 (1999).
4. Nolte, R., *et al.*, *J. Nucl. Sci. Technol., Suppl.* **2**, 311-314 (2002).
5. Baba, M., *et al.*, *Nucl. Instrum. Methods Phys. Res. A* **428**, 454-465 (1999).
6. Klug, J., *et al.*, *Nucl. Instrum. Methods Phys. Res. A* **489**, 282-303 (2002).
7. Grange, D. and Weidenmüller, H.A., *Phys. Lett. B* **96**, 26-30 (1980).
8. Halpern, I. and Strutinsky, V.M., *Proc. 2nd Conf. on the Peaceful Uses of Atomic Energy*, Geneva, 1958, v. 15, p. 408.
9. Pankratov, V.M., *Atomnaja Energiya* **14**, 177 (1963) (in Russian).
10. Lisowski, P.W., *et al.*, *Proc. of a Specialists' Meeting on Neutron Cross Section Standards for the Energy Region above 20 MeV,* Uppsala, Sweden, May 21-23, 1991, OECD/NEA Report NEANDC-305 'U,' pp. 177-186.
11. Eismont, V.P., et *al.*, *Phys. Rev. C* **53**, 2911-2918 (1996).
12. Newhauser, W.D., *et al.*, *Proc. Intern Conf. on Nuclear Data for Science and Technology,* May 19-24, 1997, Trieste, Italy, Part II, pp. 1236-1238.
13. Tutin, G. A., *et al.*, *Nucl. Instrum. Methods Phys. Res. A* **457**, 646-652 (2001).
14. Ryzhov, I.V., *et al.*, *J. Nucl. Sci. Technol.*, *Suppl.* **2**, 295-298 (2002).
15. Ryzhov, I.V., Ph.D. thesis, V.G. Khlopin Radium Institute, St. Petersburg (2003) (in Russian).
16. Pomp, S., *et al.*, "The New Uppsala Neutron Beam Facility," in International Conference on Nuclear Data for Science and Technology 2004, AIP Conference Proceedings (Melville, New York, 2005).
17. Dangtip, S., *et al.*, *Nucl. Instrum. Methods Phys. Res. A* **452**, 484-504 (2000).
18. Mashnik, S.G., *et al.*, Los Alamos National Laboratory document LA-UR-00-1067 (2000).
19. Avrigeanu, M., Ivascu, M., and Avrigeanu, V., Report NP-63 (1987).
20. The CSISRS data base, http://www.nndc.bnl.gov/nndc/exfor.html.

Forward-Angle Neutron-Proton Scattering at 96 MeV

C. Johansson[*], J. Blomgren[*], A. Ataç[*], B. Bergenwall[*], A. Hildebrand[*], J. Klug[*], P. Mermod[*], L. Nilsson[†*], N. Olsson[***], M. Österlund[*], S. Pomp[*], U. Tippawan[‡*], O. Jonsson[†], A. Prokofiev[†], P.-U. Renberg[†], K. Elmgren[**], S. Dangtip[‡] and P. Nadel-Turonski[§¶]

[*]*Department of Neutron Research, Uppsala University, Box 525, S-75120 Uppsala, Sweden*
[†]*The Svedberg Laboratory, Uppsala University, Sweden*
[**]*Swedish Defence Research Agency (FOI), Stockholm, Sweden*
[‡]*Department of Physics, Chiang Mai University, Thailand*
[§]*Department of Radiation Sciences, Uppsala University, Sweden*
[¶]*George Washington University, Washington, D.C., USA*

Abstract. The differential *np* scattering cross section has been measured at 96 MeV in the angular range $\theta_{\text{c.m.}} = 20° - 76°$. A full angular distribution coverage was obtained by combination with an earlier backward-angle data set at the same energy. An accurate normalization has been obtained by normalizing this extended data set to the experimental total *np* cross section. A novel normalization technique has been investigated. The results on forward *np* scattering are in reasonable agreement with theory models and partial wave analyses and have been compared with data from the literature.

Neutron cross sections are generally measured relative to the *np* cross section, and therefore the accuracy of most neutron data depend on how well the *np* cross section is known for various angles and energies. Besides its importance for fundamental physics, the interest in high-energy neutron data is rapidly growing since a number of potential large-scale applications involving fast neutrons are under development, or have been identified. These applications primarily fall into three sectors; nuclear energy and waste management, nuclear medicine, and radiation effects on electronics.

The neutron-proton scattering cross section plays an important role in fundamental physics, since it can be used to derive a value of the absolute strength of the strong interaction between nucleons, i.e., the pion-nucleon coupling constant, $g^2_{\pi NN}$. The actual value of the πNN coupling constant is indirectly available from experimental data at 180° *np* scattering. In such determinations, both the absolute normalization and the shape of the angular distribution at backward angles are of crucial importance.

Unfortunately, there are severe discrepancies in the differential *np* scattering cross section data base in the energy region $100 - 1000$ MeV [1]. It is dominated by two large data sets, data from Los Alamos National Laboratory (LANL) (Bonner *et al.* [2], Evans *et al.* [3, 4], Jain *et al.* [5] and Northcliffe *et al.* [6]) and from Paul Scherrer Institute (PSI) (Hürster *et al.* [7], recently replaced by Franz *et al.* [8]). The two data sets are incompatible when only statistical uncertainties are considered. Above about 500 MeV, the angular distribution shapes of these two sets agree reasonably well, while at 200 MeV, the 150°/180° cross-section ratios differ by as much as 10%-15%. It cannot be excluded that at least part of the discrepancies are related to systematic effects not taken into account [9].

Besides shape differences, there also seem to be inconsistencies in the normalization of *np* data, which is not surprising, because absolute measurements of neutron beam intensities are notoriously difficult [10]. This is because the only way to determine the number of neutrons in a beam is to detect charged particles produced in neutron-induced nuclear reactions, but to measure the cross section for those reactions, the beam intensity has to be known.

One successful normalization method is to combine a relative measurement of the *np* angular distribution with information about the total *np* cross section. The total cross section can be determined without knowledge of the absolute beam intensity; a measurement of the relative beam attenuation in a target is sufficient, and therefore total cross sections are often known to about 1%. Below the pion-production threshold, the inelastic channels in *np* interactions, i.e., capture and bremsstrahlung, are very weak and contribute far less than 1% to the total cross section. Thus, the total and differential *np* cross

CP769, *International Conference on Nuclear Data for Science and Technology,*
edited by R. C. Haight, M. B. Chadwick, T. Kawano, and P. Talou
© 2005 American Institute of Physics 0-7354-0254-X/05/$22.50

sections are directly linked via the relation

$$\sigma_T = \int \frac{d\sigma}{d\Omega} d\Omega = \int_{0^\circ}^{180^\circ} 2\pi \sin(\theta) \frac{d\sigma(\theta)}{d\Omega} d\theta. \quad (1)$$

Previously, our group has studied *np* scattering in the backward angular range. At 96 MeV, data in the $74-180^\circ$ angular range have been published [11]. Since part of the total angular range was missing, the normalization was obtained in a procedure where the undetected fraction of the angular distribution was obtained from partial-wave analyses and *NN* interaction models. This has motivated the present experiment on forward-angle *np* scattering. Extending the angular distribution to cover $20-180^\circ$ allows a purely experimental normalization. The missing part (0-20°) gives very small contributions to the uncertainty in the normalization, because the solid angle vanishes at zero degrees.

Recently, a novel technique for normalization of neutron-induced cross sections has been presented [12]. In elastic neutron scattering from nuclei, the absolute scale can be provided with a method similar to the one of Eq. 1, with the difference that a relative angular distribution of elastic scattering is normalized to the total elastic cross section. The latter, in turn, can be derived from the difference between the total cross section and the reaction cross section. In a recent experiment on elastic neutron scattering from ^{12}C and ^{208}Pb, this technique was found to have an uncertainty of 3%. Thereby, a measurement of the ^{12}C/^{1}H elastic neutron scattering cross section ratio could provide a new, independent normalization of *np* scattering.

The neutron beam facility at the The Svedberg Laboratory, Uppsala, Sweden, has recently been described in detail [13], and therefore only a brief outline will be given here. Neutrons were produced by the ^{7}Li(p,n)^{7}Be reaction. The resulting neutron spectrum consisted of a peak at 95.6 ± 0.5 MeV with an energy spread of 1.6 MeV (FWHM), and a low-energy tail that was suppressed by time-of-flight techniques. A fission detector for absolute monitoring of the neutron fluence was mounted near the experimental setup, about 10 m after the ^{7}Li target.

A full description of the present experiment has been made recently [14]. The SCANDAL (SCAttered Nucleon Detection AssembLy) setup was used. This detector setup, which has previously been described in [13], consists of two identical arms positioned on each side of the neutron beam, covering the angular ranges 10-50° and 30-70°. In the present experiment, each arm consisted of a 2-mm-thick veto scintillator for charged-particle rejection, two converter scintillators of 20 mm and 10 mm thickness for neutron-proton conversion, a 2-mm-thick ΔE plastic scintillator for triggering, two drift chambers (DCH) for proton tracking, another 2-mm-thick ΔE plastic scintillator that was part of the trigger, and an array of CsI detectors (12 on each arm) for energy determination of recoil protons produced in the converter by *np* scattering. The total neutron energy resolution is different for individual CsI crystals, but is on average 3.7 MeV (FWHM).

Calibration runs were performed by placing a thin CH_2 target in the beam and detecting recoil protons from *np* scattering. For the real measurement (in neutron detection mode), cylinders (16 cm high and 8 cm diameter) of graphite and CH_2 were used as scattering targets, where carbon was treated as a background to H(n,n) events in CH_2. Background data (no target) were also recorded.

In the first pre-sorting procedure, it was required that at least one CsI detector in the event had a pulse height above a certain threshold value. Another requirement was that each event had both vertical and horizontal drift-chamber information in two points along the path. At this point, the conversion point in one of the two converters was calculated. The depth of the conversion was determined from pulse-height information, and the conversion angle was calculated from DCH trajectory information. At the same time, the elastic neutron-scattering angle in the target was calculated from the knowledge of the conversion point, presuming neutron scattering in the target centre.

The calibration of the CsIs and plastic scintillators was made detector-by-detector with (n,p) data from the calibration runs. In each detector it was possible to identify two calibration points; the pedestal channel and the *np* proton peak. Energy losses inside the detector setup were taken into account.

Particle identification was achieved by a $\Delta E - E$ technique, where the sum of the detected energy losses in the two trigger scintillators was plotted against the energies in the CsI detectors. Each CsI crystal defined an angular bin, and it was considered important to associate every elastically scattered event with one specific CsI. Consequently, a position gate was applied on every crystal, ensuring that an accepted proton was stopped in a single CsI detector. Events from the low-energy tail of the neutron spectrum were rejected using a cut on the neutron time of flight (TOF). The TOF was defined as the time difference between the first trigger detector and a signal from the cyclotron RF.

The conversion of neutrons to protons in the converter scintillators can occur through the ^{12}C(n,p) reaction, instead of the H(n,p) reaction, since the scintillators contain carbon as well as hydrogen. On the other hand, the Q-value for ^{12}C(n,p) is -12.6 MeV, meaning that at forward angles, an energy cut is sufficient to separate the two reactions. However, at a conversion angle of about 20°, the proton energies from the two processes overlap, and it cannot be determined whether *np* scattering or the ^{12}C(n,p) reaction is responsible for the conversion. To

resolve this ambiguity, a maximum conversion angle criterion was applied, demanding that the conversion angle be less than 10°.

Energy spectra were obtained for the instrumental background (no target), the graphite target, and the CH_2 target. Background and signal spectra were normalized to the same neutron fluence (given by the fission monitor) and corrected for dead time before being subtracted from both graphite and CH_2. Then the carbon content was subtracted from CH_2.

Effects of multiple scattering in both the graphite and CH_2 targets were investigated with a Monte Carlo code [15]. The effect was found to be of importance only at the two most forward CsI detectors (at angles 10° and 14° in the laboratory system). At 10° the correction for multiple scattering was around 5% in CH_2 and 7% in graphite.

When determining the angular distribution of the elastic neutron-scattering cross section, the number of scattering events in every CsI was obtained from the hydrogen histograms. The solid angles for protons detected in the CsI crystals have been calculated from a computer code that has recently been described [12]. The data were corrected for detection efficiency effects and for the contribution from low-energy neutrons. The absolute scale was given by the TFBC neutron monitor that in itself has an uncertainty of more than 10%, making further normalization necessary.

The data were normalized to the total *np* cross section in the following way. The present data were to be combined with the earlier data by Rahm *et al.*, obtained with the LISA magnetic spectrometer [11], to form one data set covering the angular interval 20-180° in the c.m. system. To obtain a single relative distribution, the subsets were internally normalized using the Nijmegen partial wave analysis PWA93 [16]. A final normalization of the combined data set to the total *np* cross section measured with high precision by Lisowski *et al.* [17] was then made, using Eq. 1. The total renormalization for the present data is within the 10% uncertainty of the neutron monitor. The renormalization of the Rahm data is 0.7%, which is well within the normalization uncertainty of 1.9% stated in [11].

In the present experiment, the relative differential cross section was measured and then normalized using independent information. Uncertainties that affect all angles equally (e.g., drift-chamber inefficiencies, neutron monitoring, and computer dead time) are therefore taken care of by the normalization procedure. In the systematic uncertainties are included uncertainties that may affect the shape of the angular distribution, as the uncertainties due to the geometry, the event selection, the corrections, and the detector-to-detector relative efficiencies. The summed systematic uncertainty dominates compared to the statistical uncertainty and is typically

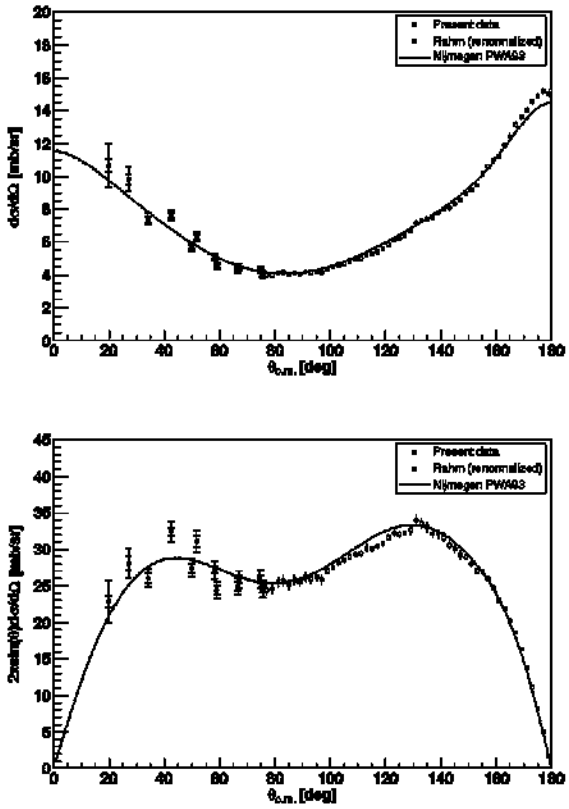

FIGURE 1. Angular distributions of *np* scattering cross sections at 96 MeV. Filled circles represent the present data and open squares are the renormalized Rahm *et al.* data [11]. In the upper panel, experimental differential cross sections are shown together with the Nijmegen partial wave analysis PWA93 [16]. In the lower panel, data and PWA93 have been multiplied with the solid-angle element $2\pi sin\theta$ to illustrate the relative weight in the normalization to the total cross section. In both panels, the present data are shown with double error bars, the inner bars representing the statistical error, and the outer the statistical and systematic errors, excluding normalization errors, added in quadrature.

4% except for the two most forward data points, which have an uncertainty of up to 12%.

The results of the present work consist of two parts; firstly the forward-angle *np* data measured in the present experiment, and secondly the backward-angle *np* data previously reported in [11] and now renormalized. Together, these two data sets cover an angular range of 160° in the c.m. system, i.e., the angles 20-180°. The results are shown in Fig. 1, where the upper panel presents the angular distribution of the two data sets together with Nijmegen PWA93 [16], and the lower panel shows the same information multiplied by the solid-angle element to illustrate the importance of each data point in the normalization to the total hydrogen cross section.

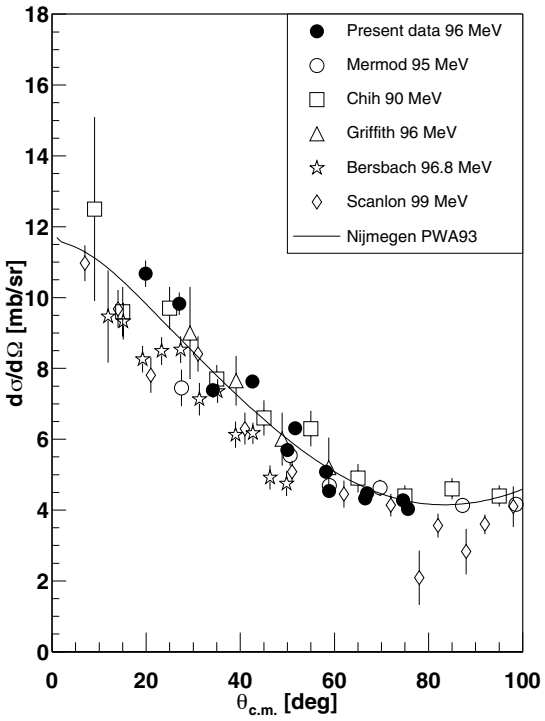

FIGURE 2. Differential scattering cross sections of the present work (filled circles). The data are shown together with the Nijmegen PWA93 [16] and with experimental data from the literature in the energy region 90-100 MeV [18, 19, 20, 21, 22]. Only statistical errors are shown.

Figure 2 shows data from the present experiment together with other forward *np* scattering data at 90-100 MeV from the literature, i.e., data from Mermod *et al.* [18], Chih and Powell [19], Griffith *et al.* [20], Bersbach *et al.* [21], and Scanlon *et al.* [22]. The partial wave analysis Nijmegen PWA93 [16] is also shown.

A novel technique for absolute scale normalization has been tested. We tried to obtain the absolute value of *np* scattering using elastic scattering from carbon (normalized to the total elastic ^{12}C(n,n) cross section) as a reference, for which an uncertainty of 3% has been estimated [12]. This method gave, however, an uncertainty of about 10% in the normalization. This comes from the fact that elastic scattering from carbon has a much steeper slope than *np* scattering; thus, the normalization of one versus the other becomes very sensitive to experimental uncertainties in the absolute angle.

It should be pointed out that the *np* data presented are not the only important results, but also the investigations of measurement techniques and normalization methods. The present experiment has reached a very high level of accuracy, given the fact that it deals with neutrons both in the incident and exit channel. With the present data in the 20-75° range, the normalization of the previous data by Rahm *et al.* [11] in the 74-180° range could be cross-checked. This resulted in a renormalization of these data of 0.7%, i.e., within the reported uncertainty of 1.9%.

ACKNOWLEDGMENTS

We wish to thank the technical staff of the The Svedberg Laboratory for enthusiastic and skillful assistance. This work was supported by Vattenfall AB, the Swedish Nuclear Fuel and Waste Management Company, the Swedish Nuclear Power Inspectorate, Barsebäck Power AB, Ringhals AB, the Swedish Defence Research Agency, and the Swedish Research Council.

REFERENCES

1. J. Blomgren, N. Olsson, and J. Rahm, Phys. Scr. T **87**, 33 (2000).
2. B.E. Bonner *et al.*, Phys. Rev. Lett. **41**, 1200 (1978).
3. M.L. Evans *et al.*, Phys. Rev. Lett. **36**, 497 (1976).
4. M.L. Evans *et al.*, Phys. Rev. C **26**, 2525 (1982).
5. Mahavir Jain *et al.*, Phys. Rev. C **30**, 566 (1984).
6. L.C. Northcliffe *et al.*, Phys. Rev. C **47**, 36 (1993).
7. W. Hürster *et al.*, Phys. Lett. B **90**, 367 (1980).
8. J. Franz, E. Rössle, H. Schmitt, and L. Schmitt, Phys. Scr. T **87**, 14 (2000).
9. B. Bonner, private communication (1999).
10. J. Blomgren, in Proceedings of Workshop on Nuclear Data for Science & Technology, Trieste, Italy (2001), eds. M. Herman, N. Paver, and A. Stanculescu, ICTP lecture notes **12**, 327 (2002).
11. J. Rahm *et al.*, Phys. Rev. C **63**, 044001 (2001).
12. J. Klug *et al.*, Phys. Rev. C **68**, 064605 (2003).
13. J. Klug *et al.*, Nucl. Instrum. Methods Phys. Res. A **489**, 282 (2002).
14. C. Johansson *et al.*, submitted to Phys. Rev. C (2004).
15. B. Holmqvist, B. Gustavsson, and T. Wiedling, Ark. Fys. **34**, 481 (1967). Modified version by N. Olsson (unpublished).
16. V.G.J. Stoks, R.A.M. Klomp, M.C.M. Rentmeester, and J.J. de Swart, Phys. Rev. C **48**, 792 (1993).
17. P.W. Lisowski, R.E. Shamu, G.F. Auchampaugh, N.S.P. King, M.S. Moore, G.L. Morgan, and T.S. Singleton, Phys. Rev. Lett. **49**, 255 (1982).
18. P. Mermod *et al.*, Phys. Lett. B **597**, 243 (2004).
19. C.Y. Chih and W.M. Powell, Phys. Rev. **106**, 539 (1957).
20. T.C. Griffith, A.P. Banford, M.Y. Uppal, and W.S.C. Williams, Proc. Phys. Soc. **71**, 305 (1958).
21. A.J. Bersbach, R.E. Mischke, and T.J. Devlin, Phys. Rev. D **13**, 535 (1976).
22. J.P. Scanlon, G.H. Stafford, J.J. Thresher, P.H. Bowen, and A. Langsford, Nucl. Phys. **41**, 401 (1963).

Elastic Neutron Scattering at 96 MeV

A. Hildebrand[*], J. Blomgren[*], A. Ataç[*], B. Bergenwall[*], C. Johansson[*], J. Klug[*], P. Mermod[*], L. Nilsson[*], S. Pomp[*], M. Ĕsterlund[*], S. Dangtip[*†], U. Tippawan[*†], P. Phansuke[†], O. Jonsson[**], P.-U. Renberg[**], A. Prokofiev[**], P. Nadel-Turonski[‡§], K. Elmgren[¶], N. Olsson[¶], V. Blideanu[‖], C. Le Brun[‖], J.-F. Lecolley[‖], F.-R. Lecolley[‖], M. Louvel[‖], N. Marie-Noury[‖], C. Schweitzer[‖], Ph. Eudes[††], F. Haddad[††], C. Lebrun[††] and A.J. Koning[‡‡]

[*]*Department of Neutron Research, Uppsala University, Box 525, S-75120 Uppsala, Sweden*
[†]*Fast Neutron Research Facility, Chiang Mai University, Thailand*
[**]*The Svedberg Laboratory, Uppsala University, Sweden*
[‡]*Department of radiation sciences, Uppsala university, Sweden*
[§]*George Washington University, Washington, D.C., USA*
[¶]*Swedish Defence Research Agency, Stockholm, Sweden*
[‖]*LPC, ISMRA and Université de Caen, France*
[††]*SUBATECH, Université de Nantes, France*
[‡‡]*Nuclear Research and Consultancy Group, Petten, The Netherlands*

Abstract. A facility for detection of scattered neutrons in the energy interval 50-130 MeV, SCANDAL (SCAttered Nucleon Detection AssembLy), has recently been installed at the $20-180$-MeV neutron beam line of The Svedberg Laboratory, Uppsala. Elastic neutron scattering from ^{12}C, ^{16}O, ^{56}Fe, ^{89}Y, and ^{208}Pb has been studied at 96 MeV in the $10-70^{\circ}$ interval. The results from ^{12}C and ^{208}Pb have recently been published, while the data from ^{16}O, ^{56}Fe, and ^{89}Y are under analysis. The achieved energy resolution, 3.7 MeV, is about an order of magnitude better than for any previous experiment above 65 MeV incident energy. The present experiment represents the highest neutron energy where the ground state has been resolved from the first excited state in neutron scattering. A novel method for normalization of the absolute scale of the cross section has been used. The estimated normalization uncertainty, 3%, is unprecedented for a neutron-induced differential cross section measurement on a nuclear target. The results are compared with modern optical model predictions, based on phenomenology or microscopic theory. Applications for these measurements are nuclear-waste incineration, single-event upsets in electronics, and fast-neutron therapy.

INTRODUCTION

The interest in high-energy neutron data is rapidly growing, since a number of potential large-scale applications involving fast neutrons are under development, or at least have been identified. These applications primarily fall into three sectors; nuclear energy and waste, nuclear medicine, and effects on electronics.

For all these applications, an improved understanding of neutron interactions is needed for calculations of neutron transport and radiation effects. The nuclear data needed for this purpose come almost entirely from nuclear scattering and reaction-model calculations, which all depend heavily on the optical model, which in turn is determined by elastic scattering and total cross-section data.

The present work is part of the EU project HINDAS (High and Intermediate energy Nuclear data for Accelerator-driven Systems) [1], which has been designed to meet the demand for new nuclear data for feasibility assessments of accelerator-based transmutation techniques. It is, however, also relevant for various biomedical applications.

Neutron-scattering data are also important for a fundamental understanding of the nucleon-nucleus interaction, in particular for determining the the isovector term [2]. Coulomb repulsion of protons creates a neutron excess in all stable nuclei with $A > 40$. Incident protons and neutrons interact differently with this neutron excess. The crucial part in these investigations has been neutron-nucleus elastic scattering data to complement the already-existing proton-nucleus data.

Above 50 MeV neutron energy, there has been only

CP769, *International Conference on Nuclear Data for Science and Technology,*
edited by R. C. Haight, M. B. Chadwick, T. Kawano, and P. Talou
© 2005 American Institute of Physics 0-7354-0254-X/05/$22.50

one measurement on neutron-elastic scattering with an energy resolution adequate for resolving individual nuclear states, an experiment at UC Davis at 65 MeV on a few nuclei [3]. In addition, a few measurements in the 0–20° range are available, all with energy resolution of 20 MeV or more. This is, however, not crucial at such small angles because elastic scattering dominates heavily, but at larger angles such a resolution would make data very difficult to interpret.

EXPERIMENTAL SETUP

The neutron beam facility at The Svedberg Laboratory, Uppsala, Sweden, has recently been described in detail [4], and therefore only a brief description is given here. The 96 ± 0.5 MeV (1.2 MeV FWHM) neutrons were produced by the ^{7}Li(p,n) reaction by bombarding a 427 mg/cm^2 disc of isotopically enriched (99.98%) ^{7}Li with protons from the cyclotron. The low-energy tail of the source-neutron spectrum was suppressed by time-of-flight techniques. After the target, the proton beam was bent into a well-shielded beam dump. A system of three collimators defined a 9-cm diameter neutron beam at the scattering target.

Scattered neutrons were detected by the SCANDAL (SCAttered Nucleon Detection AssembLy) setup [4]. It consists of two identical systems, placed to cover 10–50° and 30–70°, respectively. The energy of the scattered neutrons is determined by measuring the energy of proton recoils from a plastic scintillator, and the angle is determined by tracking the recoil proton. In the present experiment, each arm consisted of a 2-mm-thick veto scintillator for fast charged-particle rejection, a 10-mm-thick neutron-to-proton converter scintillator, a 2-mm-thick plastic scintillator for triggering, two drift chambers for proton tracking, a 2-mm-thick ΔE plastic scintillator that was also part of the trigger, and an array of CsI detectors for energy determination of recoil protons produced in the converter by np scattering. The trigger was provided by a coincidence of the two trigger scintillators, vetoed by the front scintillator. The total excitation energy resolution varies with CsI crystal, but is on average 3.7 MeV (FWHM). The angular resolution is in the $1.0 - 1.3°$ (rms) range.

RESULTS AND DISCUSSION

Data on ^{12}C and ^{208}Pb

Excitation energy spectra are presented in Fig 1. In these spectra, Gaussians representing known states are indicated. For ^{12}C, the ground state (0^+) and the two collective states at 4.4 MeV (2^+) and 9.6 MeV (3^-) are shown. In the case of ^{208}Pb, the ground state (0^+) and the two collective states at 2.6 MeV (3^-) and 4.1 MeV (2^+) are shown, as well as a Gaussian at 8.3 MeV representing a cluster of weak states. For both nuclei, a Gaussian at 12.6 MeV represents the opening of conversions due to ^{12}C(n,p) reactions in the converter scintillator, i.e., an instrument background. As can be seen, in no case does the population of excited states seriously affect the determination of the ground-state cross section.

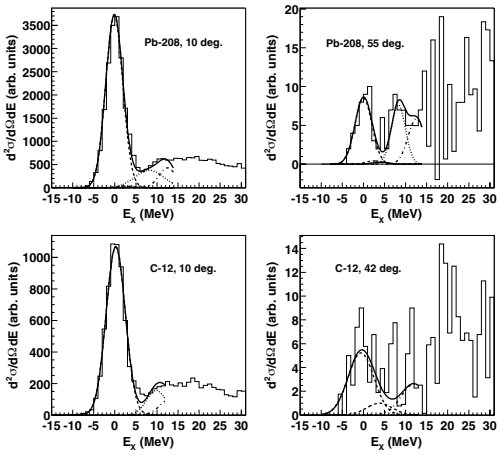

FIGURE 1. Excitation energy spectra for elastic-neutron scattering from ^{12}C and ^{208}Pb at 96 MeV incident neutron energy, together with Gaussians representing known excited states. See the text for details.

Angular distributions of elastic-neutron scattering from ^{12}C and ^{208}Pb at 96 MeV incident neutron energy are presented in Fig. 2. The data are compared with phenomenological and microscopic optical-model predictions in the upper and lower panels, respectively. The theoretical curves have all been folded with the experimental angular resolution to facilitate comparisons with data. The data by Salmon at 96 MeV [5] are also shown.

The angular distributions presented have been corrected for reaction losses and multiple scattering in the target. The contribution from other isotopes than ^{208}Pb in the lead data has been corrected for, using cross-section ratios calculated with the global potential by Koning and Delaroche [6]. The absolute normalization of the data has been obtained from knowledge of the total elastic cross section, which has been determined from the difference between the total cross section (σ_T) [7] and the reaction cross section (σ_R) [8, 9]. This σ_T - σ_R method, which is expected to have an uncertainty of about 3%, has been used to normalize the ^{12}C data. The present ^{208}Pb(n,n) data have been normalized relative to the present ^{12}C(n,n) data, knowing the relative neutron fluences, target masses, etc. The total elastic cross sec-

tion of ^{208}Pb has previously been determined with the σ_T - σ_R method. The accuracy of the present normalization has been tested by comparing the total elastic cross-section ratio (^{208}Pb/^{12}C) obtained with the σ_T - σ_R method above, and with the ratio determination of the present experiment, the latter being insensitive to the absolute scale. These two values differ by about 3%, i.e., they are in agreement within the expected uncertainty. A novel technique for normalization, which is based on relative measurements versus the *np* scattering cross section [10], has also been tested and was found to have an uncertainty of about 10% .

The data are compared with model predictions in Fig. 2, where the upper and lower panels show phenomenological (I–III, VII) and microscopic (IV–VI) models, respectively. The models are described in detail in [11] and [12].

When comparing these predictions with data, a few striking features are evident. First, all models are in reasonably good agreement with the ^{208}Pb data. It should be pointed out that none of the predictions contain parameters adjusted to the present experiment. In fact, they were all made before data were available. Even the absolute scale seems to be under good control, which is remarkable, given that neutron beam intensities are notoriously difficult to establish. Second, all models fail to describe the ^{12}C data in the 30–50° range. The models predict a saddle structure, which is not evident from the data. The reason for this mismatch might be that there are target correlations other than Pauli principle that are not included in the theoretical models.

It can be noted that proton-scattering data on ^{12}C at 95 MeV [13], which should agree with our data if isospin were a good symmetry, are closer to our data than the theory models are. The disagreement between models and ^{12}C data should not be overemphasized though. Models that presume mean-field properties of nuclei to be dominant can have problems describing ^{12}C data, because surface effects are very important in ^{12}C.

The models above are all valid for spherical nuclei. It is known, however, that ^{12}C to a significant degree displays properties of a three-alpha cluster. Coexistence of such a structure with a spherical shape might result in a matter distribution with a more diffuse edge than anticipated by the spherical models, and thus the predicted structure could be washed out.

We have developed a toy model to investigate this hypothesis. The increased effective radius of the ^{12}C ground state due to three-alpha cluster effects has been studied theoretically for proton-elastic scattering, however, at higher energies [14]. We have modified Model I, using the parameters of [14], to calculate the elastic neutron-scattering cross section (Model VII). As can be seen in Fig. 2, this modification moves the prediction closer to the data in the 30–50° range, but at the expense

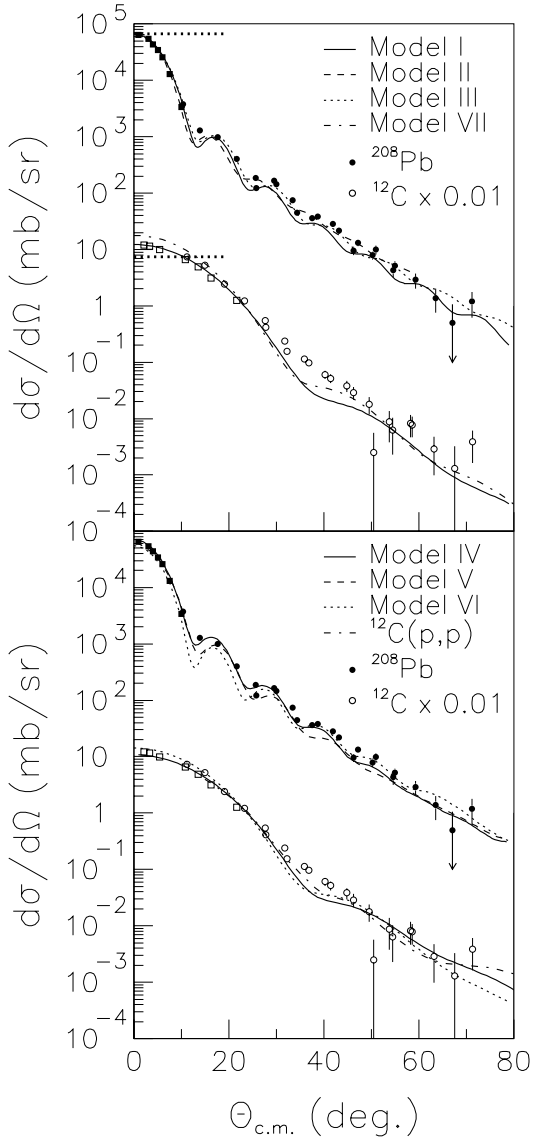

FIGURE 2. Angular distributions of elastic neutron scattering from ^{12}C (open circles) and ^{208}Pb (solid) at 96 MeV incident neutron energy. The ^{12}C data and calculations have been multiplied by 0.01. The data by Salmon at 96 MeV [5] are shown as squares. Upper panel: predictions by phenomenological models (I–III, VII). The thick dotted horizontal lines show Wick's limit for the two nuclei. Lower panel: predictions by microscopic models (IV–VI), and data on elastic-proton scattering from ^{12}C [13]. See the text for details.

that the description gets worse at small angles. It should be pointed out, however, that this should only be seen as an indication of a possible cause of the effect, since the model is too simplified to allow quantitative conclusions.

A basic feature of the optical model is that it establishes a lower limit on the differential elastic-scattering cross section at 0° if the total cross section is known, often referred to as Wick's limit. It has been observed in previous experiments at lower energies that for most nuclei, the 0° cross section falls very close to Wick's limit, although there is no *a priori* reason why the cross section cannot exceed the limit significantly. An interesting observation is that the present ^{208}Pb data are in good agreement with Wick's limit, while the ^{12}C 0° cross section lies about 70% above the limit. A similar behaviour has previously been observed in neutron-elastic scattering at 65 MeV [3], where the ^{12}C data overshoot Wick's limit by about 30%, whilst the ^{208}Pb data agree with the limit.

Other Nuclei

Preliminary data on ^{89}Y [15] are presented in Fig. 3, together with Model I [6]. The data have been normalized to the model and it can be seen that it describes the shape of the data points reasonably well.

The measurements on ^{16}O [16] and ^{56}Fe [17] have been completed and the data are under analysis. Measurements on ^{14}N, ^{28}Si, and ^{40}Ca are planned for 2005.

SUMMARY, CONCLUSION, AND OUTLOOK

In short, first results on elastic-neutron scattering from ^{12}C and ^{208}Pb at 96 MeV incident neutron energy are presented, and compared with theory predictions. This experiment represents the highest neutron energy where the ground state has been resolved from the first excited state in neutron scattering. The measured cross sections span more than four orders of magnitude. Thereby, the experiment has met - and surpassed - the design specifications. The overall agreement with theory model predictions, both phenomenological and microscopic, is good. In particular, the agreement in the absolute cross-section scale is impressive.

ACKNOWLEDGMENTS

This work was supported by the HINDAS project of the 5th EU framework programme, as well as by Vattenfall AB, Swedish Nuclear Fuel and Waste Management Company, Swedish Nuclear Power Inspectorate, Barsebäck Power AB, Ringhals AB, Swedish Defence Research Agency, and the Swedish Research Council.

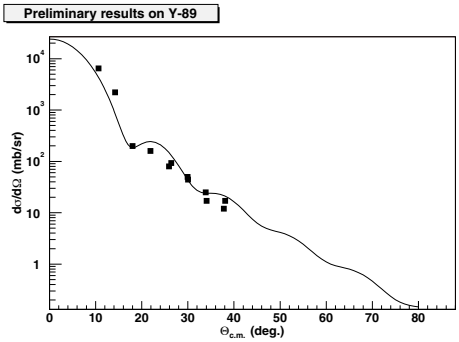

FIGURE 3. Preliminary angular distribution of elastic-neutron scattering from ^{89}Y at 96 MeV incident neutron energy together with a prediction by a phenomenological model [6].

REFERENCES

1. A. Koning, *et al.*, J. Nucl. Sci. Tech., Suppl. **2** 1161, (2002).
2. See, e.g., Neutron-Nucleus Collisions: A probe of Nuclear Structure, AIP Conference Proceedings **124** (AIP, New York, 1985).
3. E.L. Hjort, *et al.*, Phys. Rev. C **50**, 275 (1994).
4. J. Klug, *et al.*, Nucl. Instrum. Methods **A 489**, 282 (2002).
5. G.L. Salmon, Nucl. Phys. **21**, 15 (1960).
6. A.J. Koning, J.P. Delaroche, Nucl. Phys. **A713**,231 (2003)
7. R.W. Finlay, *et al.*, Phys. Rev. C **47**, 237 (1993).
8. J. DeJuren, N. Knable, Phys. Rev. **77**, 606 (1950).
9. R.G.P. Voss, R. Wilson, Proc. Roy. Soc. **A 236**, 41 (1956).
10. C. Johansson, *et al.*, this conference.
11. J. Klug, *et al.*, Phys. Rev. C**68**, 064605 (2003)
12. J. Klug, *et al.*, Phys. Rev. C **67**, 031601(R) (2003)
13. G. Gerstein, J. Niederer, K. Strauch, Phys. Rev. **108**, 427 (1957).
14. J. Matero, Z. Phys. **A351**, 29 (1995).
15. A. Hildebrand, *et al.*, to be published.
16. P. Mermod, *et al.*, to be published.
17. M. Österlund, *et al.*, to be published.

Measurements of Neutron-Induced Fission Cross Sections of ^{205}Tl, $^{204, 206, 207, 208}$Pb, and ^{209}Bi using Quasi-Monoenergetic Neutrons in the Energy Range 35 - 174 MeV

Gennady A. Tutin[*], Igor V. Ryzhov[*], Vilen P. Eismont[*], Andrey G. Mitryukhin[*], Valery S. Oplavin[*], Sergey M. Soloviev[*], Jan Blomgren[†], Henri Condè[†], Nils Olsson[†,‡], and Per-Ulf Renberg[§]

[*]*V.G. Khlopin Radium Institute, 194021 Saint-Petersburg, Russia*
[†]*Department of Neutron Research, Uppsala University, Box 525, SE-751 20 Uppsala, Sweden*
[‡]*Swedish Defence Research Agency (FOI), S-172 90 Stockholm, Sweden*
[§]*The Svedberg Laboratory, Uppsala University, Box 533, SE-751 21 Uppsala, Sweden*

Abstract. Cross sections for neutron-induced fission of ^{205}Tl, $^{204, 206, 207, 208}$Pb, and ^{209}Bi were measured in the energy range from 35 MeV to 174 MeV. The experiments were done at the neutron beam facility of The Svedberg Laboratory, using a multi-section Frisch-gridded ionization chamber for detection of the fission fragments. The neutron-induced fission cross section of ^{238}U was employed as a reference. The results of the measurements are compared with existing experimental data.

INTRODUCTION

Studies of intermediate energy neutron-induced fission of nuclei in the lead-bismuth region have both fundamental and applied aspects. In terms of applications, the data on sub-actinide neutron-induced fission at incident energies up to 200 MeV are required for development of accelerator-driven systems (ADS) for nuclear energy production and transmutation of nuclear waste [1]. Up-to-date ADS concepts consider lead or lead-bismuth eutectics as prospective materials for the neutron production target. Since the spallation neutrons will result in production and accumulation of long-lived fission products in the target material, a proper analysis of these unwanted processes is impossible without accurate data on neutron-induced fission cross sections for the target nuclides.

Significant experimental activity is being focused on the ^{209}Bi(n, f) cross section, which was recommended as a secondary neutron cross-section standard [2]. Insensitivity of bismuth-based neutron fluence monitors to low-energy (< 20 MeV) neutrons allows the use of such monitors under complex background conditions [3].

From the fundamental physics point of view, the (n, f) cross section of the sub-actinides is important for better understanding of the nucleon-nucleus interaction. In addition, one can expect a manifestation of nuclear shell effects in fission of nuclei in the vicinity of the double magic nucleus ^{208}Pb.

EXPERIMENT

The measurements were performed at the neutron beam facility at The Svedberg Laboratory (TSL) in Uppsala, Sweden [4]. The quasi-monoenergetic neutrons, with peak energies from 35 MeV to 174 MeV, were produced by the reaction ^{7}Li(p, n)^{7}Be in a target of 99.98% ^{7}Li. The neutron flux over the fissile targets was within 10^{5}-10^{6} sec^{-1}, depending on the incident proton energy and the lithium target thickness.

CP769, *International Conference on Nuclear Data for Science and Technology,*
edited by R. C. Haight, M. B. Chadwick, T. Kawano, and P. Talou
© 2005 American Institute of Physics 0-7354-0254-X/05/$22.50

The fission fragment detector, a multi-section Frisch-gridded ionization chamber, was mounted at a distance of about 10 m from the Li-target.

As can be seen in Fig. 1, the chamber consists of seven units. Each unit constitutes a twin Frisch-gridded ionization chamber with a common cathode. Anodes of two adjacent chambers are common. The electrode assembly is housed in a thin-walled cylindrical detector shell 200 mm in diameter and 520 mm in length. The anodes and cathodes are 50 μm thick duralumin foils, sandwiched between two rings with inner and outer diameters of 140 and 170 mm, respectively.

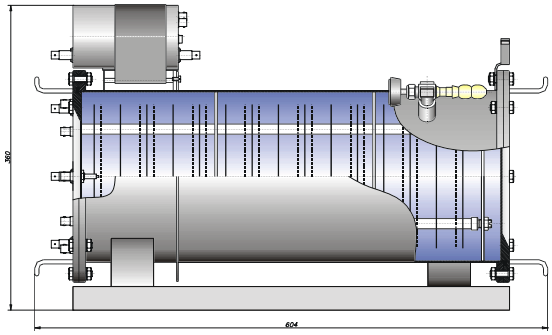

FIGURE 1. Multi-section Frisch-gridded ionization chamber.

The gas mixture was composed of 90% argon and 10% methane (P-10). The chamber operates at atmospheric pressure without a continuous gas flow.

The fissile samples have been prepared from the following materials: ^{205}Tl, $^{204,206\text{-}208}$Pb (enriched in the basic isotopes), ^{209}Bi, and ^{nat}U. The materials were deposited on each side of the cathode foils by thermal vacuum evaporation. The diameter of each target deposit was 80 mm. For metallic targets, the mass of fissile material was obtained by weighing before and after deposition. The mass of the uranium deposit was obtained by alpha counting using a Si-detector of 20 cm^2. For all targets, the uncertainty in the mass was no more than 2 %. The characteristics of the targets are given in Table 1.

TABLE 1. Fissile nuclide, compound, abundance of main isotope, and areal mass of forward and backward facing targets.

Target	Compound	Abundance (%)	Areal mass (mg/cm^2)
^{205}Tl	Metal	99.8	1.38/1.40
^{204}Pb	Metal	66.5	0.52/0.55
^{206}Pb	Metal	90.4	0.98/1.10
^{207}Pb	Metal	93.2	0.96/0.98
^{208}Pb	Metal	99.0	0.88/1.08
^{209}Bi	Metal	100.0	1.14/0.87
^{238}U	UF_4	99.3	0.21/0.20

DATA ANALYSIS AND CORRECTIONS

Time-of-flight techniques (TOF) were applied to discriminate fission events caused by "peak" neutrons from those induced by low-energy "tail" neutrons. The obtained TOF distributions of fission events were analyzed with a decomposition procedure described in [5]. Following this procedure the number of fission events induced by "peak" neutrons were obtained for both the forward- and backward-facing targets. These data were then corrected for the losses due to the pulse height threshold (K_{th}) and the self-absorption in the fissile deposits (K_{abs}). The latter was calculated as

$$K_{abs} = 1-(t/2R)(1+B/3)^{-1} \quad , \qquad (1)$$

where B is the anisotropy coefficient, t is the thickness of the deposit, and R is the average range of the fission fragments in the deposited material. Due to the linear momentum transferred (LMT) to the fissioning nuclei, the average range of the forward-emitted fragments is larger than that of the backward-emitted ones. For the same reason, the forward and backward anisotropy coefficients differ from each other. To take the LMT effect into account, we have calculated the fragment ranges for both emission directions using our experimental data on fragment energy distributions and the SRIM code [6]. The anisotropy coefficients were obtained by fitting the fission fragment angular distributions measured in the present experiment.

The determination of K_{th} is complicated by the presence of the low-energy background from light charged particles. As shown in [7], an ionization chamber with Frisch grids (apart from a simple parallel-plate ionization chamber) makes it possible to eliminate the background particles. The discrimination principle is based on the fact that fission fragments and light charged particles give different ratios of anode to cathode signals, and thus may be separated from each other by off-line processing. To find K_{th} values, we have used the "cleared" energy spectra of fission fragments with linear extrapolation from about 27 MeV down to zero fragment energy.

The fission cross-section ratios of ^{205}Tl, $^{204,206\text{-}208}$Pb to ^{238}U were calculated for both the forward- and the backward-facing targets as follows:

$$\left(\frac{\sigma_i}{\sigma_U}\right)^{F(B)} = \frac{N_{f,i}^{F(B)}}{N_{f,U}^{F(B)}} \cdot \frac{m_U^{F(B)}}{m_i^{F(B)}} \cdot \qquad (2)$$

In this formula the superscript *F(B)* denotes the forward (backward) direction. N_f is the number of

"peak" fission events, corrected for K_{abs} and K_{th}, while *m* is the number of target nuclei. The uncertainties in K_{abs} and K_{th} we estimate to be 2% and 3%, respectively. The resulting ratios were obtained as a linear average of "forward" and "backward" ratios:

$$\frac{\sigma_i}{\sigma_U} = \frac{1}{2}\left(\left(\frac{\sigma_i}{\sigma_U}\right)^F + \left(\frac{\sigma_i}{\sigma_U}\right)^B\right). \qquad (3)$$

Fission cross-section ratios for the lead isotopes ^{204}Pb, ^{206}Pb, and ^{207}Pb to ^{238}U were obtained taking into account the isotope composition of the targets. The absolute values of neutron-induced fission cross sections were obtained relative to the ^{238}U(n, f) cross-section standard [2].

RESULTS AND DISCUSSION

The absolute neutron-induced fission cross sections of ^{205}Tl, $^{204, 206-208, nat}$Pb, and ^{209}Bi obtained in the present work are given in Table 2 and Fig. 2. The first column in Table 2 contains the mean energy of the neutrons in the main peak and its half-width. The data for ^{nat}Pb have been derived from the cross sections of the separate lead isotopes. The cross section uncertainties include the uncertainty of the measured cross section ratios, as well as the uncertainty of the cross-section standard.

Our data for ^{209}Bi and ^{nat}Pb are compared with those of other authors in Fig. 3. The solid line on the left-hand side of Fig. 3 represents the ^{209}Bi(n, f) cross-section standard [2]. The cross sections are given in logarithmic scale to cover the variation of the cross section over more than 6 orders of magnitude in the neutron energy interval between 18 and 200 MeV.

As can be seen in Fig. 4, our data for both ^{209}Bi and ^{nat}Pb agree well with the data of Shcherbakov et al. [9] over practically all neutron energies. Unfortunately, only statistical errors in the cross section ratios are given in [9]. Taking into account that the ^{238}U(n, f) cross section obtained in [9] is 6-8% smaller than the cross-section standard [2], one can expect an accidental agreement between our results and the data from [9].

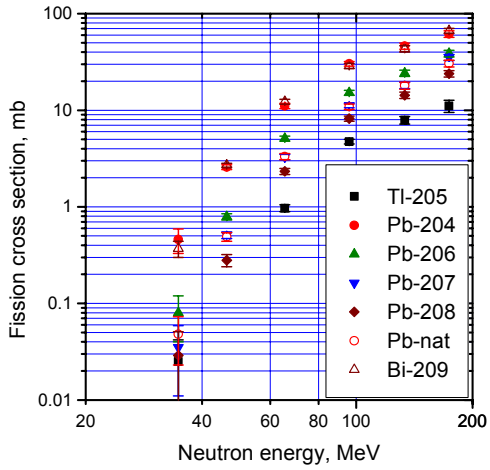

FIGURE 2. Fission cross sections of ^{205}Tl, $^{204, 206-208, nat}$Pb, and ^{209}Bi.

The database for ^{209}Bi and ^{nat}Pb in the neutron energy range 30-200 MeV contains results obtained with "white" source neutron beams: at the LANSCE/WNR facility by Staples et al. [8] and at the GNEIS facility by Shcherbakov et al. [9]. There are also data for ^{209}Bi and upper limits of the fission cross section of ^{nat}Pb obtained at monoenergetic neutron sources at energies of 18-23.3 MeV by Vorotnikov and Larionov [10], and the recent data for ^{209}Bi and ^{nat}Pb, obtained at quasi-monoenergetic neutron beams of 46, 61, 97, and 145 MeV by Nolte et al. [11]. Our earlier data for ^{209}Bi and ^{nat}Pb at 96 and 133 MeV [7,12] are not shown, as an equipment operation fault during that experiment was detected recently.

TABLE 2. Neutron-induced fission cross sections of ^{205}Tl, $^{204, 206-208, nat}$Pb, and ^{209}Bi.

Neutron Energy (MeV)	Fission Cross Section (mb)						
	^{205}Tl	^{204}Pb	^{206}Pb	^{207}Pb	^{208}Pb	^{nat}Pb	^{209}Bi
34.7±1.4	0.025±0.017	0.46±0.13	0.08±0.04	0.035±0.024	0.029±0.022	0.048±0.025	0.37±0.07
46.3±1.1	–	2.58±0.15	0.79±0.06	0.51±0.04	0.28±0.04	0.49±0.05	2.70±0.12
65.4±0.9	0.97±0.08	11.1±0.7	5.1±0.3	3.28±0.22	2.33±0.17	3.32±0.24	12.3±0.7
96.0±1.4	4.73±0.26	30.3±1.7	15.2±0.9	11.2±0.6	8.2±0.5	10.9±0.7	28.8±1.7
133.6±1.9	7.9±0.7	46.2±3.4	24.2±1.8	18.2±1.4	14.3±1.1	18.0±1.5	43.3±3.3
173.9±1.9	11.1±1.6	61.7±4.8	38.7±3.1	35.3±2.5	23.9±1.8	30.5±2.4	66.6±3.8

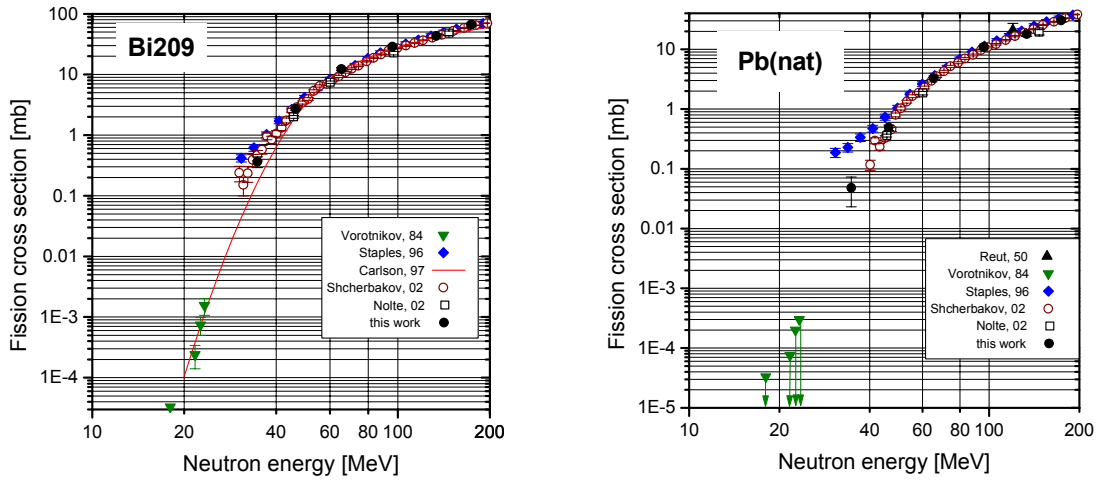

FIGURE 3. Comparison of the neutron-induced fission cross section of ^{209}Bi and ^{nat}Pb with available data [8-11] and recommended standard [2].

The data of Staples et al. [8] at neutron energies above 50 MeV are consistent (both for ^{209}Bi and ^{nat}Pb) with the present data, as well as with the data by Shcherbakov et al. [9]. At neutron energies below 50 MeV, there is a large discrepancy between our data and the data of Staples et al. [8]. The latter exceed our data at 35 MeV by a factor of two for ^{209}Bi and by a factor of four for ^{nat}Pb.

The data of Nolte et al. [11] lie somewhat below the present data but are consistent with the latter within the stated uncertainties.

The data of Vorotnikov and Larionov [10] are unique at neutron energies below 25 MeV. They are not in contradiction with a smooth extrapolation of our data to low neutron energies for both ^{209}Bi and ^{nat}Pb.

ACKNOWLEDGMENTS

We wish to thank the operating crew of the Gustaf Werner Cyclotron, The Svedberg Laboratory in Uppsala, for the excellent beams they provided for these experiments.

This work was supported by the ISTC projects #1309 and #2213.

REFERENCES

1. Koning A.J., Delaroche J.-P., and Bersillon O., *Nucl. Instrum. Methods Phys. Res.* **A414**, 49-67 (1998).
2. Carlson A.D. et al., *IAEA Report INDC (NDS)-368,* Vienna, 1997; *Conference Proceedings* Vol. **59**, edited by G. Reffo et al., Bologna: SIF, 1997, pp. 1223-1229.
3. Glasser W. et al., *Journal of Nuclear Science and Technology*, Supplement 2, August 2002, pp. 373-376.
4. Condè H. et al., *Nucl. Instrum. Methods Phys. Res.* **A292**, 121-128 (1990).
5. Eismont V.P. et al., *Proceedings of the 2nd International Conference on Accelerator Driven Transmutation Technologies and Applications, Kalmar, Sweden, 3-7 June 1996,* ed. by H. Condè, Uppsala: Uppsala University, 1997, vol. 2, pp. 618-623.
6. Ziegler J.F., Biersack J.P., Littmark U, *The Stopping Power and Range of Ions in Solids,* Pergamon Press, New York, 1985.
7. Eismont V.P. et al., *Proc. 3rd Int. Conf. on Accelerator-Driven Transmutation Technologies and Applications, Praha, Czech Republic, June 7-11, 1999, http://www.fjfi.cvut.cz/con_adtt99/a_confer/a_info/list_pap.htm*, Mo-O-C7.
8. Staples P., Lisowski P.W., and Hill N.W., *Bull. Am. Phys. Soc.* **40**, 962 (1995); Updated data, Private communication by P. Staples (1996).
9. Shcherbakov O. et al., *Journal of Nuclear Science and Technology*, Supplement 2, August 2002, pp.230-233.
10. Vorotnikov P.E. and Larionov L.S., *Yad. Fiz.,* **40**, 867 (1984)(in Russian); *Sov. J. Nucl. Phys.,* **40**, 552 (1984).
11. Nolte R. et al, *Journal of Nuclear Science and Technology*, Supplement 2, August 2002, pp.311-314.
12. Ryzhov I.V. et al, *Journal of Nuclear Science and Technology*, Supplement 2, August 2002, pp.1410-1413.

Light-Ion Production in the Interaction of 96 MeV Neutrons with Silicon

U. Tippawan[a,b], S. Pomp[a], A. Atac[a], B. Bergenwall[a], J. Blomgren[a], S. Dangtip[a,b], A. Hildebrand[a], C. Johansson[a], J. Klug[a], P. Mermod[a], L. Nilsson[a,d], M. Österlund[a], K. Elmgren[c], N. Olsson[a,c], O. Jonsson[d], A.V. Prokofiev[d], P.-U. Renberg[d], P. Nadel-Turonski[e,i], V. Corcalciuc[f], Y. Watanabe[g], and A.J. Koning[h].

[a]*Department of Neutron Research, Uppsala University, Sweden*
[b]*Fast Neutron Research Facility, Chiang Mai University, Thailand*
[c]*Swedish Defence Research Agency (FOI), Stockholm, Sweden*
[d]*The Svedberg Laboratory, Uppsala University, Sweden*
[e]*Department of Radiation Sciences, Uppsala University, Sweden*
[f]*Institute of Atomic Physics, Heavy Ion Department, Bucharest, Romania*
[g]*Department of Advanced Energy Engineering Science, Kyushu University, Japan*
[h]*Nuclear Research and Consultancy Group NRG, Petten, The Netherlands*
[i]*George Washington University, Washington, D.C.,USA*

Abstract. Radiation effects induced by terrestrial cosmic rays in microelectronics, on board aircrafts as well as at sea level, have recently attracted much attention. The most important particle radiation is due to spallation neutrons, created in the atmosphere by cosmic-ray protons. When, e.g., an electronic memory circuit is exposed to neutron radiation, charged particles can be produced in a nuclear reaction. The charge released by ionization can cause a flip of the memory content in a bit, which is called a single-event upset (SEU). This induces no hardware damage to the circuit, but unwanted re-programming of memories, CPUs, etc., can have consequences for the reliability, and ultimately also for the safety of the system.

Data on energy and angular distributions of the secondary particles produced by neutrons in silicon nuclei are essential input for analyses and calculation of SEU rate. In this work, double-differential cross sections of inclusive light-ion (p, d, t, ^{3}He and α) production in silicon, induced by 96 MeV neutrons, are presented. Energy distributions are measured at eight laboratory angles from 20° to 160° in steps of 20°. Deduced energy-differential and production cross sections are reported as well. Experimental cross sections are compared to theoretical reaction model calculations and existing experimental data in the literature.

INTRODUCTION

Radiation effects induced by terrestrial cosmic rays in microelectronics, on board aircrafts as well as at sea level, have recently attracted much attention. The most important particle radiation is due to spallation neutrons, created in the atmosphere by cosmic-ray protons. When a neutron collides with a silicon nucleus, charged particles can be produced in a nuclear reaction. If the charge released by ionization exceeds a critical threshold, the memory content in a bit flips. This is called a single-event upset (SEU) [1]. In some cases, two or more bits in a single memory word may flip, which is called single-word multi-bit upset (SMU) [2].

Light charged particles (p, d, t, ^{3}He and α) are normally not considered in SEU calculations since the energy deposited by these particles within the sensitive volume is very small. The memory residing in highly integrated microchip devices are today formed by very small charges. With the expected advances in technology, the development towards higher scale integration includes reducing the operation voltage, which means that the critical threshold is decreased.

CP769, *International Conference on Nuclear Data for Science and Technology,*
edited by R. C. Haight, M. B. Chadwick, T. Kawano, and P. Talou
© 2005 American Institute of Physics 0-7354-0254-X/05/$22.50

For this reason, also the contribution from light ions, such as alpha particles, is expected to become significant for SEU, and it might also affect the SMU rate [2].

In this work, experimental double-differential cross sections (inclusive yields) for protons, deuterons, tritons, ^{3}He and alpha particles produced by 96 MeV neutrons incident on silicon [3] are presented. Measurements have been performed at the cyclotron of The Svedberg Laboratory (TSL), Uppsala, using the dedicated MEDLEY experimental set-up [4]. Spectra have been measured at 8 laboratory angles, ranging from 20° to 160° in 20° steps. Extrapolation procedures are used to obtain coverage of the full angular distribution and consequently energy-differential and production cross sections are deduced. The experimental data are compared to results of calculations with nuclear reaction codes and to existing experimental data in the literature.

EXPERIMENTAL METHODS

The neutron beam facility at TSL uses the ^{7}Li(p,n)^{7}Be reaction to produce a quasi-monoenergetic neutron beam [5]. The lithium target was 26 mm in diameter and 8 mm thick in the present experiment and enriched to 99.98% in ^{7}Li. The 98.5 ± 0.3 MeV protons from the cyclotron impinge on the lithium target, producing a full energy peak of neutrons at 95.6 ± 0.5 MeV with a width of 1.6 MeV FWHM. The neutron beam is directly monitored by a thin-film breakdown counter (TFBC). Relative monitoring can be obtained by charge integration of the proton beam from a Faraday cup located in the proton beam dump. The agreement between the two beam monitors was very good during the measurements.

The charged particles are detected by the MEDLEY setup [4]. It consists of eight three-element telescopes mounted inside a 90 cm diameter evacuated reaction chamber. Each telescope has two fully depleted ΔE silicon surface barrier detectors and one E CsI(Tl) detector.

The time-of-flight (TOF) obtained from the radio frequency of the cyclotron and the timing signal from each telescope, is measured for each charged-particle event.

The silicon target used has a 32x32 mm^2 quadratic shape and a thickness of 303 μm. For absolute cross section normalization, a 25 mm diameter and 1.0 mm thick polyethylene $(CH_2)_n$ target is used. The n-p cross section at 20° laboratory angle provides the reference cross section [6]. Background is measured by removing the target from the neutron beam.

DATA REDUCTION PROCEDURES

The ΔE-E technique is used to identify light charged particles ranging from protons to lithium ions. Good separation of all particles is obtained over their entire energy range and the particle identification procedure is straightforward.

Energy calibration of all detectors is obtained from the data itself. Events in the ΔE–E bands are fitted with respect to the energy deposited in the two silicon detectors. This energy is determined from the detector thicknesses and calculations of energy loss in silicon. The energy of each particle type is obtained by adding the energy deposited in each element of the telescope.

Knowing the energy calibration and the flight distances, the TOF for each charged particle from target to detector can be calculated and subtracted from the registered total TOF. The resulting neutron TOF is used for selection of charged-particle events induced by neutrons in the main peak of the incident neutron spectrum. Background events, measured in target-out runs and analyzed in the same way as target-in events, are subtracted from the corresponding target-in runs after normalization to the same neutron fluence.

Absolute double-differential cross sections are obtained by normalizing the silicon data to the number of recoil protons emerging from the CH_2 target. After selection of events in the main neutron peak and proper subtraction of the target-out and ^{12}C(n,px) background contributions, the latter taken from a previous experiment, the cross section can be determined from the recoil proton peak, using n-p scattering data [6]. All data have been normalized using the n-p scattering peak in the 20° telescope.

Due to the target thickness, a correction for energy-loss and particle-loss is applied. Details about this and other corrections can be found in [3].

RESULTS AND DISCUSSION

Double-differential cross sections at laboratory angles of 20°, 40°, 100° and 140° for protons and alpha particles, compared to the calculations based on standard GNASH [3,7], a GNASH-based model with a modified parameter set [3,8] and TALYS [3,9] models are shown in Figs. 1 and 2. The recent TALYS calculations include a transformation from the c.m. to the lab system. The error bars represent statistical uncertainties only.

The overall relative statistical uncertainties of individual points in the double-differential energy spectra at 20° are typically 3% for protons and 15% for alpha particles. As the angular distributions are

forward-peaked, these values are increasing with angle. The systematic uncertainty contributions are due to thick target correction (1-20%), collimated solid angle (1-5%), the absolute cross section (5%), beam monitoring (2-3%), the number of silicon nuclei (1%), CsI(Tl) intrinsic efficiency (1%), particle identification (1%) and dead time (<0.1%).

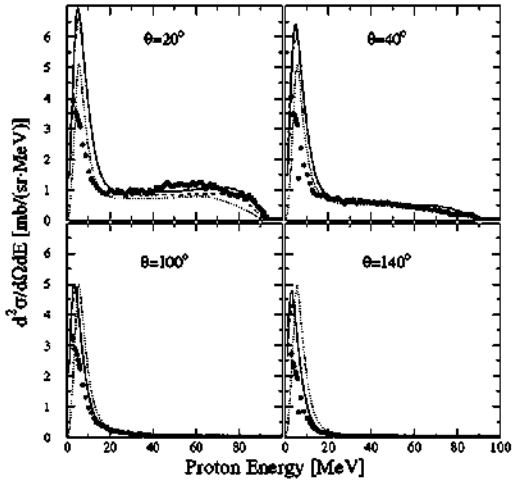

FIGURE 1. Experimental double-differential cross sections (filled circles) of the Si(n,px) reaction at 96 MeV at four laboratory angles. The curves indicate theoretical calculations based on standard GNASH [3,7] (dashed), GNASH-based model with a modified parameter set [3,8] (solid) and TALYS [3,9] (dotted).

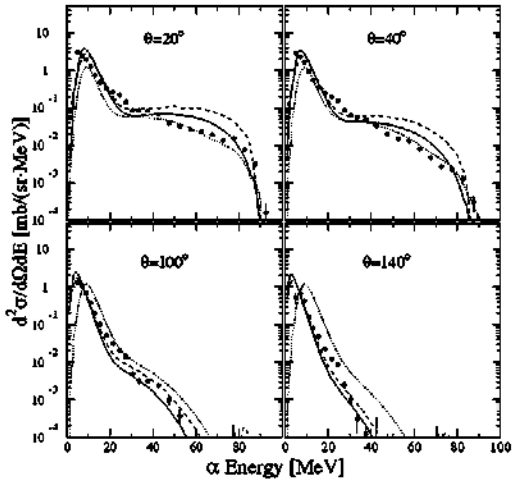

FIGURE 2. Experimental double-differential cross sections (filled circles) of the Si(n,αx) reaction at 96 MeV at four laboratory angles. The curves indicate theoretical calculations based on standard GNASH [3,7] (dashed), GNASH-based model with a modified parameter set [3,8] (solid) and TALYS [3,9] (dotted).

For protons above 25 MeV, all calculations give a good description of the spectra. Below this energy, some differences can be observed, e.g., at forward angles. TALYS gives a better description of the statistical peak than the GNASH calculations. For alpha particles, TALYS underpredicts the evaporation peak at forward angles.

By integration of the angular distribution, energy-differential cross sections (dσ/dE) are obtained for each ejectile. These are shown in Fig. 3 together with the theoretical calculations. All calculations are in good agreement with the experimental proton data over the whole energy range. In the cases of deuterons and alpha particles, the models overpredict the high-energy parts of the spectra.

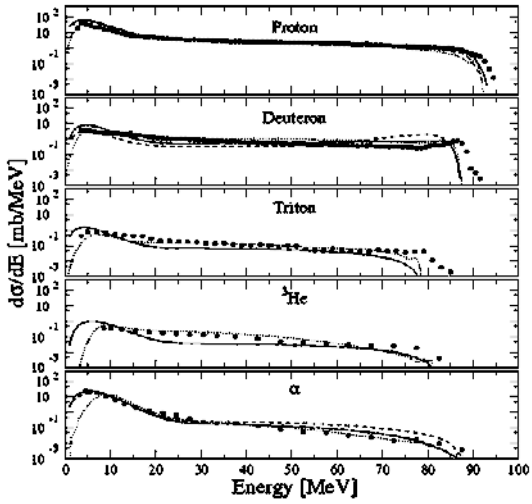

FIGURE 3. Experimental energy-differential cross sections (filled circles) for neutron-induced p, d, t, ^{3}He and α production at 96 MeV. The curves indicate theoretical calculations based on standard GNASH [3,7] (dashed), GNASH-based model with a modified parameter set [3,8] (solid) and TALYS [3,9] (dotted).

The production cross sections are deduced by integration of the energy-differential spectra (see Table 1). The experimental values in Table 1 have to be corrected for the undetected particles below the low-energy cutoff by using the GNASH-based model with a modified parameter set [3,8] and the TALYS [3,9] calculations. The low-energy cutoff corrected values, Using TALYS, the resulting cutoff corrected values are significantly lower than those obtained by the GNASH-based model. As mentioned above TALYS clearly underestimates the evaporation peak for alpha particles. Thus the cutoff correction for alpha particles obtained with TALYS is too low. For the other types of particles, the experimental data cannot discriminate between the model calculations.

TABLE 1. Experimental production cross sections for protons, deuterons, tritons, ^{3}He and alpha particles from the present work. Theoretical values resulting from GNASH and TALYS calculations are given as well. The experimental data in the second column have been obtained with cutoff energies of 2.5, 3.0, 3.5, 8.0 and 4.0 MeV for p, d, t, ^{3}He and alpha particles, respectively. The third and forth columns show data corrected for these cutoffs, using the GNASH-based model with a modified parameter set [3,8] and the TALYS [3,9] calculations, respectively.

σ_{prod}	Experiment (mb)	Energy Cutoff Corrected Experiment [GNASH]	[TALYS]	GNASH [3,7]	GNASH [3,8]	TALYS [3,9]
(n,px)	436 ± 22	507	452	670.3	701.9	554.4
(n,dx)	81 ± 4	90	82	77.0	109.6	106.9
(n,tx)	15.2± 0.8	17.9	15.3	–	15.0	10.3
(n, ^{3}Hex)	7.8 ± 0.5	13.0	8.6	–	10.6	11.2
(n,αx)	144 ± 7	183	145	175.8	202.4	107.4

The proton and deuteron production cross sections are compared with previous data measurements at lower energies [10] in Fig. 4a and b, respectively. There seems to be general agreement between the trend of the previous data and the present data. The curves in these figures are based on standard GNASH calculation [3,7].

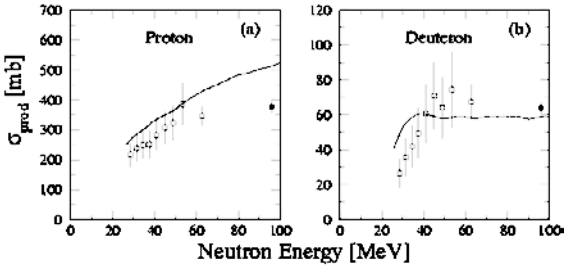

FIGURE 4. Neutron-induced proton (a) and deuteron (b) production cross section as a function of neutron energy. The full circle is from the present work, whereas the open squares are from a previous work [10]. The curve is based on standard GNASH calculation [3,7]. The data as well as the calculations correspond to cutoff energies of 4 MeV for proton and 8 MeV for deuteron cases. Note that the cutoff energies are different from those in Table 1.

CONCLUSIONS

In the present paper, we report an experimental data set for light-ion production induced by 96 MeV neutrons on silicon. Experimental double-differential cross sections ($d^2\sigma/d\Omega dE$) are measured at eight angles between 20° and 160°. Energy-differential ($d\sigma/dE$) and production cross sections are obtained for the five types of outgoing particles. Theoretical calculations based on nuclear reaction codes including direct, pre-equilibrium and statistical calculations give generally a good account of the magnitude of the experimental cross sections. For proton emission, the shape of the spectra for the double-differential and energy-differential cross sections are well described. The calculated and the experimental alpha-particle spectra are also in fair agreement with the exception of the high-energy part, where the theory predicts higher yields than experimentally observed.

ACKNOWLEDGMENTS

This work was supported by the Swedish Natural Science Research Council, the Swedish Nuclear Fuel and Waste Management Company, the Swedish Nuclear Power Inspectorate, Ringhals AB, and the Swedish Defence Research Agency. The authors wish to thank the The Svedberg Laboratory for excellent support.

REFERENCES

1. Single-Event Upsets in Microelectronics, topical issue, eds. H.H.K. Tang and N. Olsson, *Mat. Res. Soc. Bull.* **28** (2003).
2. K. Johansson, *et al*., *IEEE Trans. Nucl. Sci.* **46**, 1427 (1999)
3. U. Tippawan, *et al*., Phys. Rev. C **69**, 064609 (2004).
4. S. Dangtip, *et al*., *Nucl. Instrum. Methods Phys. Res. A* **452**, 484 (2000).
5. J. Klug, *et al*., *Nucl. Instrum. Methods Phys. Res. A* **489**, 282 (2002).
6. J. Rahm, *et al*., *Phys. Rev. C* **63**, 044001 (2001).
7. ICRU Report 63, International Commission on Radiation Units and Measurements Bethesda, MD, March 2000.
8. Y. Watanabe, Internal note (unpublished).
9. A. J. Koning, S. Hilaire , M.C. Duijvestijn, TALYS-0.64: A nuclear reaction program, User manual, December 5, 2004, NRG Report 21297/04.62741/p FAI/AK/AK.
10. S. Benck, I. Slypen, J. P. Meulders, V. Corcalciuc, *Nucl. Sci. Eng.* **141**, 55 (2002).

Inverse Kinematics Studies of Intermediate-Energy Reactions Relevant for SEE and Medical Problems

J. Aichelin[5)], Ch. Bargholtz[7)], J. Blomgren[2)], A. Budzanowski[9)], M. Chubarov[1)], B. Czech[9)], C. Ekström[3)], L. Gerén[7)], B. Jakobsson[4)], A. Kolozhvari[3)], O. Lozhkin[1)], Yu. Murin[1)], P. Nomokonov[8)], N. Olsson[2)], H. Persson[3)], V. Pljuschev[1)], I. Skwirczynska[9)], H.H.K. Tang[6)], P.-E. Tegnér[7)], L. Westerberg[3)], I. Zartova[7)], M. Zubkov[1)], and Y. Watanabe[10)]

1) V.G.Khlopin Radium Institute, 2-nd Murinsky 28, 194021, St.Petersburg, RU
2) Department of Neutron Research, Angström Laboratory, Uppsala University Box 525, S-751 20, Uppsala, SE
3) The Svedberg Laboratory, Box 553, S-751 21, Uppsala, SE
4) Department of Physics, University of Lund, Box 118, S-221 00, Lund, SE
5) SUBATEX, University of Nantes, F-44307, Nantes, FR
6) IBM T.J.Watson Research Center, NY 105 98, Yorktown Heights, USA
7) Department of Physics, Stockholm University, S-106 91, Stockholm, SE
8) High Energy Laboratory, JINR, 141980, Moscow Region, Dubna, RU
9) Institute of Nuclear Physics, 31-342 Krakow, PL
10) Kyushu University, Kasuga 86-8580, JP

Abstract. The lack of systematic experimental checks on the intermediate-energy nuclear model simulations of heavily ionizing recoils from nucleon-nucleus collisions – critical inputs for the Single Event Effect analysis of microelectronics and dosimetry calculations including high-LET components in the cancer tumor radiation therapy – has been a primary motivation for a new experiment planned at the CELSIUS nuclear storage ring of The Svedberg Laboratory, Uppsala, Sweden. Details of the experiment and the first results from a feasibility study are presented here.

INTRODUCTION

The importance of cosmic radiation induced Single Event Effects (SEEs) in space electronics has been known for a long time. In the last two decades, the impact of SEEs has also been recognized by the microelectronics industry that focuses on terrestrial applications [1,2]. Though the fundamental nuclear physics related to SEEs is generally understood [3], the quantitative predictions of the SEE impacts need to be worked out in detail for each new technology. The microscopic origin of SEEs is always traced down to the energy deposition from ionizing particles in a small, sensitive volume. The charge released along an ionizing particle track is collected by a sensitive node, and the resulting transient current, depending on the specific structure of the underlying device, may cause a change of state in the circuit. Experimental measurements and theoretical simulations of the heavy recoils from nucleon-nucleus reactions are particularly important since the energy deposited by heavy recoils is a major source of secondary radiation. Another technologically important motivation for recoil studies is the microdosimetry applications in proton-beam cancer therapy and radiobiology. Recoil energy deposition in micro-volumes is a key problem common to all these apparently different fields [4].

High-quality nuclear reaction data are essential: SEE simulations and radiobiological microdosimetry calculations require certain nuclear data as inputs. While in the past much effort has been devoted to the study of light particle emission (e.g., H and He isotopes) in intermediate-energy inelastic proton-

CP769, *International Conference on Nuclear Data for Science and Technology,*
edited by R. C. Haight, M. B. Chadwick, T. Kawano, and P. Talou
© 2005 American Institute of Physics 0-7354-0254-X/05/$22.50

nucleus collisions, very few experiments [5] have been done to study the characteristics of slow recoils and especially to the yields and energy spectra of stable heavy recoils (e.g., Al, Mg, etc.) – which are most effective in causing single-event upsets (SEUs) in silicon chips. Notable exceptions are found in [5] and [6], in which some early recoil measurements are reported. In radiobiology, up until now, there are few detailed studies of secondary radiation effects from heavy recoils. A major experimental difficulty in recoil work is that of identification of the heavy fragments – which have short ranges (of the order of 10 um or less) – among other lighter reaction products in a standard setup in which the Si target is at rest in the laboratory system. The lack of direct measurements of recoil spectra (in the form of double differential cross sections) renders it difficult to make systematic checks on the standard nuclear reaction codes [3,7-9]. Presently these reactions codes are indispensable research tools in the studies of SEE and radiobiological problems.

EXPERIMENTAL SETUP AT CELSIUS

An experimental setup has been developed at The Svedberg Laboratory (TSL), Uppsala, Sweden, to measure the production of recoil ions, using an inverse kinematics scheme. The setup is built at the CELSIUS nuclear accelerator and storage facility of TSL (see Fig. 1). It consists of four detector systems designed for the registration of reaction products emitted in collisions of 100-470A MeV Si ions with atoms of the internal hydrogen cryogenic cluster-jet target of CELSIUS. Secondary particles are registered simultaneously by the Small Angle Detector (SAD), Forward Wall Detector (FWD), Zero Angle Detector (ZAD), and the Spectator Tagging Detector (STD). SAD plays a key role in the present research project since it detects the nuclear fragments – recoils of Si and the secondary particles – all of which are capable of causing SEUs in microelectronic devices.

The Small Angle Detector (SAD) detects fragments of the Si ions emitted at angles 0.6^{o}-1.1^{o} from the intersection point of the stored ion beam with the cluster-jet target of CELSIUS. Here the unique features of the CELSIUS cooled beam are fully exploited. During the injection-acceleration cycle, the beam occupies the whole volume of the CELSIUS vacuum chamber; only after the beam has been cooled that it shrinks to 2 mm. To prevent the SAD detectors from radiation damage they are moved out during the beam injection and are moved back to the working position only when the beam has finally formed.

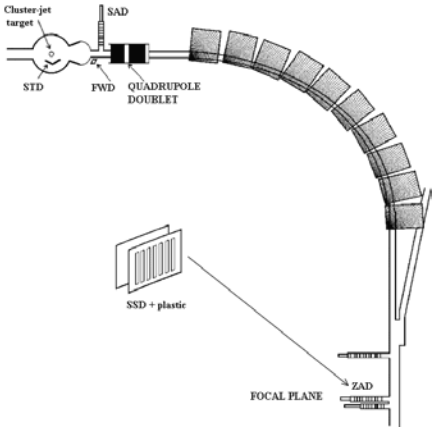

FIGURE 1. Layout of the experiment on the Si +H reaction at TSL.

SAD consists of a telescope with two 300-um custom-made silicon strip detectors (SSD) and a 5-mm-thick plastic scintillator (see Fig. 2). The first SDD has circular and the second radial strips, with a total 16 of each type. Plastic scintillators are used as triggers of the readout cycle and for timing. The position of the particle registered simultaneously by both detectors is derived from the circular and radial strip numbers that identify one of the 512 pixels of SAD; the charge of the recoil is identified from SAD SSD pulse amplitude analysis.

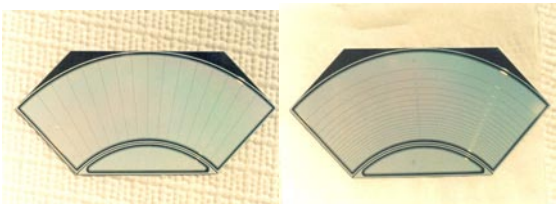

FIGURE 2. Silicon strip detectors for SAD manufactured by SENSOR, city of Zelenograd, Russia, prior to mounting on boards.

The Zero Angle Detector (ZAD) is also a telescope made up of silicon strip detectors and plastic scintillator. Here we take the advantage of the technique developed at TSL [10] and use the quadrant after the cluster-jet target of CELSIUS as a magnetic spectrometer. ZAD is positioned at 22757 mm from the target, at the focal plane of the spectrometer [11]. As distinct from SAD, strips of ZAD make up the 32x32 rectangular net. Vertical strips of one of ZAD SSDs are used to register projectile fragments, identify the charge (Z), and determine the position (X) of the hit point with respect to the nominal beam centerline. Electronic schemes of SAD and ZAD are identical. The Forward Wall Detector (FWD) [12] is used for the

detection of light secondaries (A<5) emitted within the polar angle of 3.9°-11.7° in coincidence with the recoil registered by SAD.

We plan to use the Spectator Tagging Detector (STD) [13] or the CHICSi detector [14] tagging the spectator-protons emitted within 60°-120°.

EXPERIMENTAL RESULTS

Figure 3 shows the results of a feasibility study. A good-quality 200A MeV Si beam was accelerated and stored by CELSIUS, with the fragment detectors located very close to the cooled beam. The experiment was conducted in October 2003 with an 8x10-mm^2 8mm-thick plastic scintillator placed at the planned position of SAD. Positions of the peak amplitudes are proportional to the charge of the products from the 200A MeV Si+p reaction measured with an average Si ion beam current of 50 μA and hydrogen target thickness of around $2 \cdot 10^{14}$ atoms/cm^2. It was shown that it was practical to make the projectile fragment identification as close to the nominal beam position as 10-12 mm.

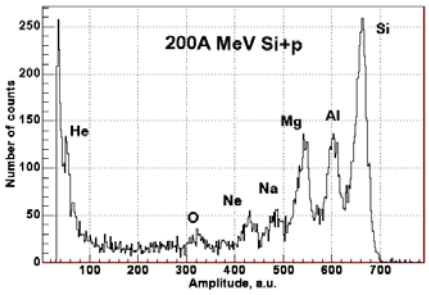

FIGURE 3. Pulse height distribution from the scintillation detector in position of SAD.

Recently, the combined SAD-FWD setup has been commissioned in the experiment with 100A MeV and 300A MeV Ne beam bombarding cluster-jet target of hydrogen atoms. Figure 4 demonstrates the typical charge resolution in radial (l.h.s.) and circular (r.h.s.) SSDs obtained within a single pixel of SAD. Charge identification of recoils is performed within 10^{-3} msrad solid angle. Production yields of recoils have been measured in coincidence with hydrogen and helium secondary nuclei registered by the FWD. The first production experiment run on the Si+p reaction is scheduled for November 2004. All detectors described in this paper will be used in this experiment.

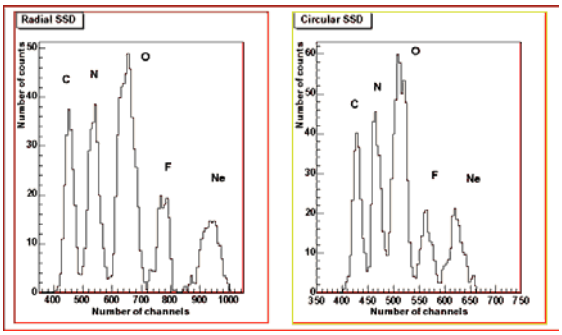

FIGURE 4. Energy spectra of Ne+p reaction fragments from SAD radial (l.h.s.) and circular (r.h.s.) silicon strip detectors in the SAD commission experiment.

ACKNOWLEDGMENTS

This work is supported by the International Scientific Technological Center (Project #1956), Moscow, Russian Federation. We also acknowledge the active participation in this work of Drs. M. Merkin and A. Voronin, SINP (Moscow State University) as well as the excellent support team of the CELSIUS nuclear storage ring.

REFERENCES

1. IBM J. Res. Dev. 40, No.1, 1996. (Special issue on terrestrial soft errors in microelectronic systems).
2. MRS Bulletin vol. 28, Feb. 2003. (Special issue on Single Event Upsets in Microelectronics).
3. Tang, H. H. K., IBM J. Res. Dev. 40, 91-107 (1996).
4. Tang H. H. K. and Romero J.L., Hadron-Induced Reactions: From Basic Research to New Technological Applications, AIP Conference Proceedings No. 392, 325-327 (1997).
5. Romero J.L., Tang H.H.K., et al., Nucleon-Induced Secondaries: A Review and Future Experimental Developments, AIP Conference Proceedings No. 392, 655-658 (1997).
6. Kwiatkowski K. et al., Phys. Rev. Lett. 50, 1648-1651 (1983).
7. Tang H.H.K. et al., Phys. Rev C42, 1598-1622 (1990).
8. Mashnik G., Gudima K.K., Sierk A.J., Prael R.E., ``Improved Intranuclear Cascade Models for the Codes CEM2k and LAQGSM, LANL Report LA-UR-04-0039, Los Alamos (2004).
9. Niita, K., Chiba, S. et al., Phys. Rev. C52, 2620-2635(1995).
10. Chr. Bargholtz, K. Lindh et al., Nucl. Instrum. Methods A390, 160-166 (1997).
11. Ringbom A., Tibell G. et al., Nucl. Instrum. Methods A373, 57-64 (1996).
12. Budzanowski A. et al., Nucl. Instrum. Methods A482, 528-535 (2002).
13. Bilger, R. Bodowski, W., Calen H. et al., Nucl. Instrum. Methods A457, 64-74 (2001).
14. Jakobsson B., Nucl. Phys. News, 9, 22-27 (1999).

Proceedings of EPAC 2004, Lucerne, Switzerland

A NEW MONO-ENERGETIC NEUTRON BEAM FACILITY IN THE 20-180 MeV RANGE

L.-O. Andersson, A. Bäcklund, T. Bergmark, O. Byström, H. Calen, L. Einarsson, C. Ekström, J. Fransson, K. Gajewski, N. Haag, T. Hartman, E. Hellbeck, T. Johansen, O. Jonsson, B. Lundström, R. Peterson, L. Pettersson, A. Prokofiev, D. Reistad, P.-U. Renberg, D. van Rooyen, R. Wedberg, D. Wessman, L. Westerberg, V. Ziemann
The Svedberg Laboratory, Uppsala University, Uppsala, Sweden
J. Blomgren, S. Pomp, U. Tippawan, M. Österlund
Department of Neutron Research, Uppsala University, Uppsala, Sweden

Abstract

Recent interest in nuclear applications involving neutrons, like transmutation of nuclear waste, fast-neutron cancer therapy, dose to personnel in aviation and electronics failures due to cosmic-ray neutrons, motivates the development of a facility producing intense mono-energetic neutron beams. At The Svedberg Laboratory (TSL), Uppsala, Sweden, we have developed such a facility by utilizing the existing cyclotron and inserting a flexible Lithium target in a rebuilt beam line. The new facility can operate at unsurpassed quasi-monoenergetic neutron intensities and provides large flexibility of the neutron beam properties, like energy and shape.

INTRODUCTION

The need for a detailed understanding of nuclear interaction of neutrons is driven by a large number of different applications. Transmutation of nuclear waste [1] is one application that may provide a solution to the problem of long-lived nuclear waste storage. The materials used in, for example, the containment of the transmutation reactor are exposed to extreme neutron fluxes that will affect the material properties. Understanding the involved mechanism is essential to guarantee the reliability of the transmutation plant.

The second field of applications is based on the interaction of neutrons with biological matter that needs to be understood thoroughly in order to design treatment plans for fast neutron therapy. The increased radiation dose due to the effect of neutrons generated in cosmic ray cascades that air-plane personnel is exposed to [2] needs to be investigated in order to draw proper radiation protection guidelines for them.

The third field of applications is motivated by the quest for smaller structures in the semiconductor industry which causes the logical states in memory chips to be represented by only a relatively small number of electrons. Thus, the indirect ionization caused by nuclear reactions of neutrons that originate from cosmic ray cascades can alter the logical state of the semiconductor memory cells or cause a burnout in high-voltage power diodes [3] which poses a significant threat for their reliability. In particular, mission-critical applications such as computers in airplanes are reasons for concern.

Careful testing of these neutron-induced single-event effects (SEE) in semiconductor materials [4] using the natural flux of cosmic neutrons is very time-consuming. To speed up the measurements, one needs to use neutron beams produced with particle accelerators. This has led the standardizing body of the electronics industry (JEDEC) to establish a standard for the procedures for accelerated testing of memory devices. The standard is summarized in Ref. [5] and states that one of the ways to perform the accelerated testing is to irradiate a device under study by monoenergetic neutrons with nominal energies of 20, 50, 100, and 150 MeV. Such an approach is a viable alternative to the testing with a *white* neutron spectrum, if the intensity of mono-energetic neutrons is enough to cause reasonably high SEE rates.

To satisfy these needs, an upgrade of the old neutron facility [6, 7] at The Svedberg Laboratory (TSL) has been undertaken with the primary goal to increase the neutron beam intensity and, thereby, to make the facility competitive for SEE testing and for studies of SEE mechanisms. In addition, the new facility offers an unsurpassed flexibility of the neutron beam properties, like energy and shape.

THE NEW FACILITY

A drawing of the new neutron beam facility is presented in Fig. 1. The facility makes use of the proton beam from the Gustaf Werner cyclotron [8] with the energy variable in the range 20 to 180 MeV. The proton beam impinges on a target of Lithium, enriched to 99.99 % in ^{7}Li with a thickness of 2, 4, 8, 16, and 24 mm. The targets are rectangular in shape, 20×32 mm, and are mounted in a remotely controlled water-cooled copper rig. An additional target position contains a fluorescent screen viewed by a TV camera, which is used for beam alignment and focusing. Downstream the target, the proton beam is deflected by a magnet into a 10-m long dumping line, where it is guided onto a heavily shielded water-cooled graphite beam dump. In order not to preclude the later installation of a kicker that can be used to alter the time structure of the proton beam by kicking one out of two proton bunches such that they miss the Lithium target, we have avoided quadrupoles in the dump line, because they would have to have very large apertures. We chose to use a wide beam pipe with a diameter of 40 cm to prevent excessive proton beam losses to

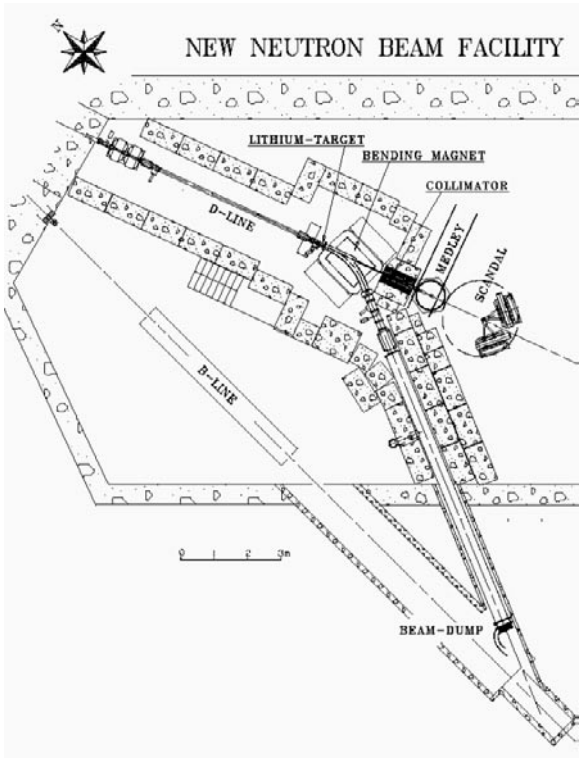

Figure 1: *Drawing of the new neutron beam facility.*

cause background for the experiments.

The neutron beam is geometrically formed by a cylindrically shaped iron collimator block, 50 cm in diameter and 100 cm long, with a cylindrical or conical hole of variable diameter. The collimator is surrounded by concrete to form the end wall of the production line towards the experimental area. Thereby efficient shielding from the production target region is achieved. A modular construction of the collimator allows the user to adjust the diameter of the neutron beam to the needs of a specific experiment. At present, the available collimator openings are 2, 3, 5.5, 10, 15, 20, and 30 cm. Other collimator diameters in the 0-30 cm range, as well as other shapes than circular can be provided upon request. Even beam diameters of up to 1 m are obtainable at a larger distance from the production target. The increased diameter of the beam may be used for testing a larger number of devices simultaneously, or a larger device like the whole electronic wafer.

After passing the collimator, neutrons reach the experimental area at a distance of about 3 m from the production target. Reduction of this distance to the minimum has led to an increase of the neutron flux by about one order of magnitude in comparison with the old TSL neutron facility.

The first neutron beam at the new facility was delivered in January 2004. At present, commissioning of the facility is being performed, including optimization of beam transport, diagnostics, vacuum and background conditions, as well as measurements of neutron flux, spectra, and profile.

The typical neutron flux during the test run amounted to about 5×10^5 /(cm^2 s) at the entrance to the experimental area. This value is about one order of magnitude larger than at the old neutron facility at TSL [6, 7] with the same target thickness, proton energy and current.

The dumping efficiency, i.e. the share of primary protons that reach the beam dump after passing the Lithium target, was typically 90-95%. Taking into account the uncertainty in the current measurement of about 10% and loss of protons due to nuclear reactions in the target (up to 2% depending on proton energy and target thickness), this is acceptable.

The measured contamination of the neutron beam at the experimental area due to interactions of the primary protons with elements in the beam line such as the target frame did not exceed 0.2%. Such interactions only lead to a weak surplus of neutrons in the experimental area, because charged particles produced near the Lithium target and upstream are removed by the deflection magnet. The relative contamination with protons in the neutron beam that have energies above 15 MeV is about 10^{-5}.

EXPERIMENTS

The energy and angular distribution of neutrons at the experimental area is mainly defined by the double-differential cross-section of the ^{7}Li(p,n) reaction at forward angles. The reaction energy spectrum is dominated by a peak situated a few MeV below the energy of the primary protons. Thus, the facility is capable to deliver neutrons in the 20 to 175 MeV range. This makes TSL the only laboratory offering fully monoenergetic neutron testing according to the JEDEC standard [5].

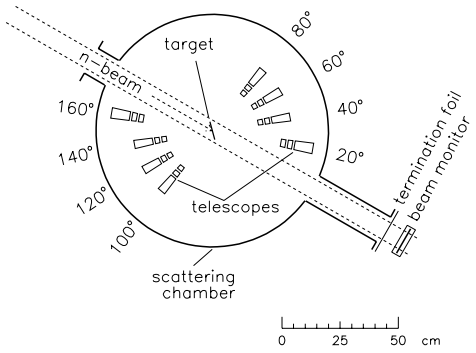

Figure 2: *The Medley detector*

Apart from experimental stations for direct irradiation two detectors, Medley and SCANDAL, are available to detect the reaction products of neutron induced reactions. The Medley setup [9] has been constructed for detection of light ions, ranging from protons to alpha particles, with an almost complete coverage both in energy and emission angle. Figure 2 shows a schematic view. The spectrometer

consists of eight detector telescopes, housed in a scattering chamber with 80 cm inner diameter. The telescopes are mounted on rails, allowing the distance to the target to be varied. In the standard configuration, the telescopes are located at 20 degree intervals, ranging from 20 to 160 degrees emission angle. This can be changed by mounting the rails differently. The entire setup is mounted onto a plate which can be rotated from outside.

Each telescope consists of three detectors; a thin silicon detector (50 to 60 μm), a thicker silicon detector (400 to 500 μm) and a CsI(Tl) crystal, about 3 cm thick. Using different combinations of detectors for different energy ranges, the charged particles can be identified by ΔE-E techniques, and their energies can be determined down to about 2 to 3 MeV. The upper energy limit is about 130 MeV for protons.

The SCANDAL detector [7], see Fig. 3, detects neutrons and light ions in the 20 to 130 MeV energy interval but is primarily intended for neutron detection. The setup consists of two identical telescopes, located on each side of the neutron beam, and movable around a pivot point. For proton measurements, each telescope contains two plastic scintillators for triggering, two drift chambers for tracking, and a CsI(Na) detector array for energy determination. In neutron mode, a plastic scintillator converter is added for active conversion of neutrons to protons, and a veto detector is placed in front of the converter to reject charged particles from the target.

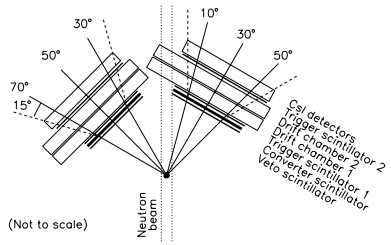

Figure 3: *The Scandal detector*

FIRST RESULTS

The high-energy peak in the neutron spectrum comprises about half of the total number of neutrons. Further details on the neutron spectra from the ^{7}Li(p,n) reaction may be found in Ref. [10]. Dedicated measurements of the facility neutron spectrum and the neutron beam profile at the experimental area are under way. A first preliminary result of a neutron spectrum from the new facility is shown in Fig. 4.

CONCLUSIONS

A new neutron facility, optimized for SEE testing, has been constructed and put into operation at TSL, Uppsala, Sweden. The SEE rate at the new facility exceeds that of other facilities by a factor of ten. TSL is the only laboratory offering full monoenergetic neutron testing according to the JEDEC standard. In addition, TSL offers testing with protons in the 20 to 180 MeV energy range, and with a wide range of heavy ions. Thus, TSL has the unique feature to provide neutron, proton, and heavy ion testing in the same laboratory.

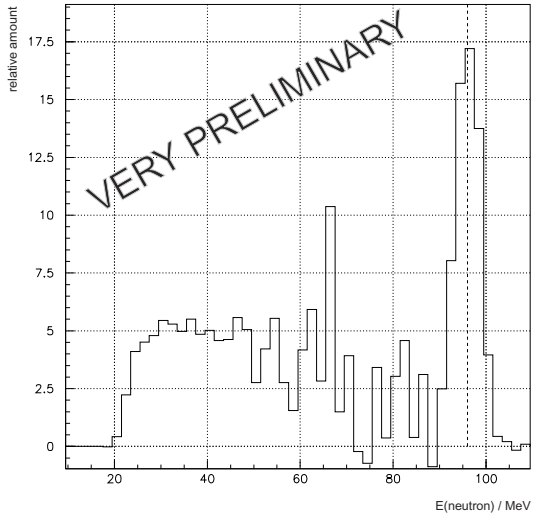

Figure 4: *Preliminary neutron spectrum from the new facility.*

REFERENCES

[1] H. Condé (ed.) Proceedings of the 2nd International Conference on Accelerator-Driven Transmutation Technologies and Applications, 3 - 7 June, 1996, Kalmar, Uppsala University, Sweden (1997).

[2] ICRP, 1990 Recommendations of the International Commission on Radiological Protection: Publication 60, Annals of the ICRP, Vol. 21, No. 1-3, Pergamon Press, Oxford, 1991.

[3] G. Sölkner, et.al., IEEE Trans. Nucl. Sci. 47, 2365 (2000).

[4] Single-Event Upsets in Microelectronics, topical issue, eds. H.H.K. Tang and N. Olsson, Mat. Res. Soc. Bull. vol. 28, 2003.

[5] JEDEC Standard. Measurements and Reporting of Alpha Particles and Terrestrial Comic Ray-Induced Soft Errors in Semiconductor Devices. JESD89, August 2001.

[6] H. Condé, et.al., Nucl. Instr. Meth. A, vol. 292, pp. 121-128 (1990).

[7] J. Klug, et. al. Nucl. Instr. Meth. A, vol. 489, pp. 282-303 (2002).

[8] S. Holm, A. Johansson, S. Kullander, D. Reistad, "New Accelerators in Uppsala," Physica Scripta, **34,** 513, 1986.

[9] S. Dangtip, et al., Nucl. Instr. Meth. A 452, pp. 484-504, 2000.

[10] A.V. Prokofiev, M.B. Chadwick, S.G. Mashnik, N. Olsson, and L.S. Waters, J. Nucl. Sci. Techn., Suppl. 2, pp. 112-115 (2002).

NIMB 51524
27 July 2005 Disk Used
ARTICLE IN PRESS
No. of Pages 4, DTD = 5.0.1

Available online at www.sciencedirect.com
SCIENCE DIRECT®

ELSEVIER
Nuclear Instruments and Methods in Physics Research B xxx (2005) xxx–xxx

NIM B
Beam Interactions with Materials & Atoms

www.elsevier.com/locate/nimb

The uppsala neutron beam facility for electronics testing

M. Österlund [a,*], J. Blomgren [a], S. Pomp [a], A.V. Prokofiev [b], U. Tippawan [a,c], L.-O. Andersson [b], T. Bergmark [b], O. Byström [b], H. Calén [b], L. Einarsson [b], C. Ekström [b], J. Fransson [b], K. Gajewski [b], N. Haag [b], T. Hartman [b], E. Hellbeck [b], T. Johansen [b], O. Jonsson [b], B. Lundström [b], L. Pettersson [b], D Reistad [b], P.-U. Renberg [b], D. Wessman [b], V. Ziemann [b]

[a] *Department of Neutron Research, Uppsala University, Box 525, S-751 20 Uppsala, Sweden*
[b] *The Svedberg Laboratory, Uppsala University, Box 533, S-751 21 Uppsala, Sweden*
[c] *Fast Neutron Research Facility, Chiang Mai University, P.O. Box 217, Chiang Mai 50202, Thailand*

Available online

Abstract

A new facility producing intense mono-energetic neutron beams has been developed at The Svedberg Laboratory (TSL), Uppsala, Sweden. The facility utilizes the existing cyclotron and a flexible lithium target in a rebuilt beam line. The new facility can operate at unsurpassed mono-energetic neutron intensities and provides flexibility of the neutron beam properties, like energy and geometrical shape.
© 2005 Elsevier B.V. All rights reserved.

PACS: 28.20.−v; 28.20.Cz; 29.25.Dz

Keywords: Neutron beam

1. Introduction

Careful testing of neutron-induced single-event effects (SEE) in semiconductor materials [1] using the natural flux of cosmic neutrons is very time-consuming. To speed up the measurements, one needs to use neutron beams produced with particle accelerators.

The procedures for the accelerated testing of memory devices are summarized in the recent JEDEC test specification [2]. According to the standard, one of the ways to perform the accelerated testing is to irradiate a device under study by mono-energetic neutrons with nominal energies

* Corresponding author. Tel.: +46 184715840; fax: +46 184713853.
E-mail address: michael.osterlund@tsl.uu.se (M. Österlund).

0168-583X/$ - see front matter © 2005 Elsevier B.V. All rights reserved.
doi:10.1016/j.nimb.2005.07.052

UNCORRECTED PROOF

of 20, 50, 100, and 150 MeV. Such an approach is a viable alternative to the testing with a "white" neutron spectrum, if the intensity of mono-energetic neutrons is enough to cause reasonably high SEE rates.

To satisfy these needs, an upgrade of the old neutron facility [3,4] at The Svedberg Laboratory (TSL) has been undertaken with a primary goal to increase the neutron beam intensity and, thereby, to make the facility competitive for SEE testing and for studies of SEE mechanisms. In addition, the new facility offers an unsurpassed flexibility of the neutron beam properties, like energy and geometrical shape.

2. Technical specification

An overview of the neutron beam facility is presented in Fig. 1. The facility makes use of the proton beam from the Gustaf Werner cyclotron with the energy variable in the 20–180 MeV range. The proton beam is incident on a target of lithium, enriched to 99.99% in ^{7}Li. The available targets are 2, 4, 8, 16, and 24 mm thick. The targets are rectangular in shape, 20×32 mm^2, and are mounted in a remotely controlled water-cooled copper rig. An additional target position contains a fluorescent screen viewed by a TV camera, which is used for beam alignment and focusing. Downstream of the target, the proton beam is deflected by a magnet into a 10-m long dumping line, where it is guided onto a heavily shielded water-cooled graphite beam dump.

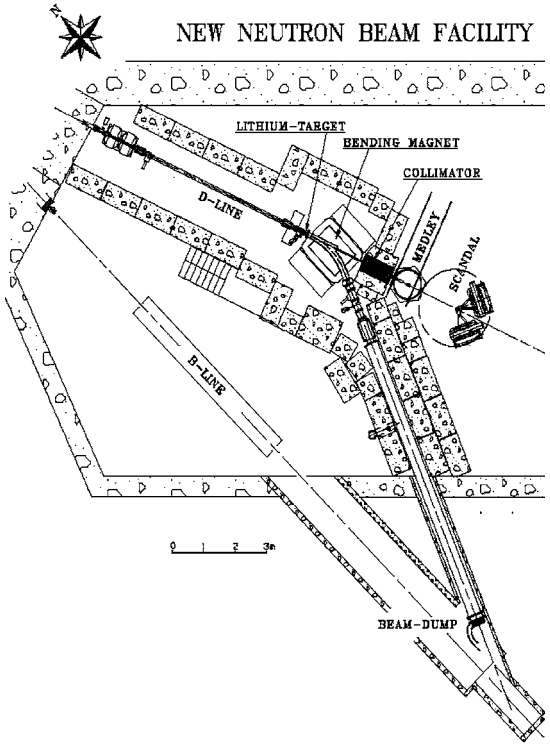

Fig. 1. An overview of the neutron beam facility.

The neutron beam is formed geometrically by a cylindrically shaped iron collimator block, 50 cm in diameter and 100 cm long, with a cylindrical or conical hole of variable diameter. The collimator is surrounded by concrete to form the end wall of the production line towards the experimental area. Thereby, efficient shielding from the production target region is achieved. A modular construction of the collimator allows the user to adjust the diameter of the neutron beam to the needs of a specific experiment. At present, the available collimator openings are 2, 3, 5.5, 10, 15, 20, and 30 cm. Other collimator diameters in the 0–30 cm range, as well as other shapes than circular can be provided upon request. Even beam diameters of up to 1 m are obtainable at a larger distance from the production target. The increased diameter of the beam may be used for testing a larger number of devices simultaneously, or a larger device like a whole electronic card.

After passing the collimator, neutrons reach the experimental area at a distance of about 3 m from the production target. Reduction of this distance to the minimum has led to an increase of the neutron flux by about one order of magnitude in comparison with the old TSL neutron facility [3,4].

3. Commissioning, tests and characterization of the facility

The first neutron beam at the new facility was delivered in January 2004. An extensive characterization of the facility has been performed, includ-

UNCORRECTED PROOF

ing measurements of neutron flux, spectra, and profile. Below, first results are reported. They were acquired with a proton beam of about 100 MeV energy and about 5 μA intensity, incident on an 8-mm thick lithium target.

3.1. Dumping efficiency

The dumping efficiency, i.e. the share of primary protons that reach the beam dump after passing the lithium target, was typically 90%–95%. Taking into account the uncertainty in the measurement of about 10% and loss of protons due to nuclear reactions in the target (up to 2% depending on proton energy and target thickness), one can conclude that few protons are lost on their way from the target to the dump.

3.2. Neutron flux

The typical neutron flux during the test runs amounted to about $5 \times 10^5\ \mathrm{cm}^{-2}\,\mathrm{s}^{-1}$ at the entrance to the experimental area. This value is about one order of magnitude larger than at the old neutron facility at TSL [3,4] with the same target thickness, proton energy and current.

3.3. Neutron spectrum

First results for the neutron spectrum at the experimental area are shown in Fig. 2. The spectrum is mainly defined by the double-differential cross-section of the ^{7}Li(p,n) reaction at forward angles. The reaction energy spectrum is dominated by a peak situated a few MeV below the energy of the primary protons. The high-energy peak in the neutron spectrum comprises about half of the total number of neutrons. The measured spectra (shown by symbols connected by a solid line) are compared with predictions of the systematics for the ^{7}Li(p,n) reaction developed by Prokofiev et al. [5] (shown by a dashed line in panels b, c, d). For the lowest of the studied incident energies (24.7 MeV), the systematics [5] is not applicable. Instead, an evaluation of Mashnik et al. [6] was employed for the description of the neutron spectrum. The differential cross-section for high-energy peak neutron production at 0° was obtained my

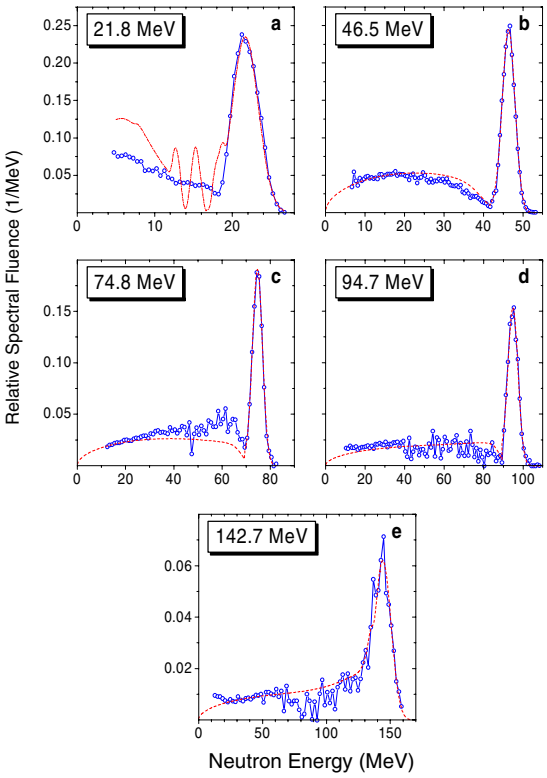

Fig. 2. The neutron spectra at 0° for different peak neutron energies and ^{7}Li target thicknesses. Symbols connected by a solid line represent experimental data obtained in the present work. A dashed line in panels b, c, d and e represents the predictions of the systematics developed by Prokofiev et al. [5]. A dash-dotted line in panel a represents the LA150 evaluation [6] combined with systematics of Uwamino et al. [7]. In all cases, the width of the predicted high-energy peak component is adjusted to the experimental data. Both experimental and calculated data are normalized so that the area under the high-energy peak is unity.

multiplication of the total cross-section of the ^{7}Li(p,n)^{7}Be reaction [6] to the "index of forwardness" from the systematics of Uwamino et al. [7]. The narrow peaks in the upper continuum region correspond to excitation of higher states in residual ^{7}Be nuclei. This process was included in the model calculation of Mashnik et al. [6]. However, the energy resolution in the experiment does not allow us to observe these peaks.

The overall agreement between the presented experimental data and the calculations [5,6] is not worse than to a factor of 2.

UNCORRECTED

3.4. Contamination of the neutron beam

Measured contamination of the neutron beam at the experimental area due to interactions of the primary protons with beam transport elements (mainly the target frame) did not exceed 0.2%. Such interactions can only lead to a weak surplus of neutrons at the experimental area, because any charged particles produced near the lithium target and upstream are bent away by the deflection magnet.

The contamination of protons (above 15 MeV) in the neutron beam amounts to about 10^{-5}, which can hardly be a problem for any application.

3.5. Residual radioactivity

No significant excess of radioactivity over natural background has been detected in the experimental area. This, together with the fully functional laboratory radiation protection system, ensures safety for beam users and personnel.

3.6. Availability for users

The facility is now available for regular operation. First beams for commercial electronics testing, as well as applied nuclear physics research, have already been delivered.

4. Summary and outlook

A new neutron facility, optimized for SEE testing, has been constructed and put into operation at TSL, Uppsala, Sweden. The facility is capable to deliver neutrons in the 20–175 MeV range. This makes TSL the only laboratory in the world offering full mono-energetic neutron testing according to the JEDEC test specification [2]. In addition, TSL offers testing with protons in the 20–180 MeV energy range, and with a wide range of heavy ions. Thus, TSL has the unique feature to provide neutron, proton, and heavy ion testing at the same laboratory.

Further information on the neutron facility and characterization measurements is presented elsewhere [8].

References

[1] H.H.K. Tang, IBM J. Res. Develop. 40 (1996) 91.
[2] JEDEC Standard, Measurements and Reporting of Alpha Particles and Terrestrial Comic Ray-Induced Soft Errors in Semiconductor Devices. JESD89, August 2001.
[3] H. Condé, S. Hultqvist, N. Olsson, T. Rönnqvist, R. Zorro, J. Blomgren, G. Tibell, A. Håkansson, O. Jonsson, A. Lindholm, L. Nilsson, P.-U. Renberg, A. Brockstedt, P. Ekström, M. Österlund, F.P. Brady, Z. Szeflinski, Nucl. Instr. and Meth. A 292 (1990) 121.
[4] J. Klug, J. Blomgren, A. Ataç, B. Bergenwall, S. Dangtip, K. Elmgren, C. Johansson, N. Olsson, S. Pomp, A.V. Prokofiev, J. Rahm, U. Tippawan, O. Jonsson, L. Nilsson, P.-U. Renberg, P. Nadel-Turonski, A. Ringbom, A. Oberstedt, F. Tovesson, V. Blideanu, C. Le Brun, J.F. Lecolley, F.R. Lecolley, M. Louvel, N. Marie, C. Schweitzer, C. Varignon, Ph. Eudes, F. Haddad, M. Kerveno, T. Kirchner, C. Lebrun, L. Stuttgé, I. Slypen, A.N. Smirnov, R. Michel, S. Neumann, U. Herpers, Nucl. Instr. and Meth. A 489 (2002) 282.
[5] A.V. Prokofiev, M.B. Chadwick, S.G. Mashnik, N. Olsson, L.S. Waters, J. Nucl. Sci. Technol. 1 (Suppl. 2) (2002) 112.
[6] S.G. Mashnik, M.B. Chadwick, P.G. Young, R.E. MacFarlane, L.S. Waters, LANL Report LA-UR-00-1067, 2000.
[7] Y. Uwamino et al., Nucl. Instr. and Meth. A 389 (1997) 463.
[8] S. Pomp et al., in: International Conference on Nuclear Data for Science and Technology, Santa Fé, NM, September 26–October 1, 2004, in press.

UNCORRECTED PROOF

Appendix XXI

Neutron data for accelerator-driven systems - Experiments above 20 MeV

J. Blomgren[1)]

1) Department of Neutron Research, Uppsala University, Box 525, S – 751 20 Uppsala, Sweden. Jan.Blomgren@tsl.uu.se

Abstract: The available commercial reactors as well as fusion research has motivated extensive programs on nuclear data up to 20 MeV. Accelerator-driven transmutation will make use of neutrons up to GeV energies. Although only a minor fraction of the neutrons will be at these high energies, they nevertheless need to be well characterized.

Measuring all relevant data is impossible; even if all existing laboratories on earth would be dedicated to this, it would take centuries. Therefore, the work has to be focused on measuring key data for theory development.

HINDAS – High- and Intermediate-Energy Nuclear Data for Accelerator-Driven Systems – is a European coordinated effort for accomplishing this goal for energies above 20 MeV. The collaboration consists of 16 universities or institutes, whereof 6 laboratories, from seven EU countries. The work is divided into two energy ranges, 20-200 MeV and 200-2000 MeV. In each of these ranges, there are three experimental work packages, on light charged-particle production, neutron production and production of residual nuclei, resp. In addition, there are work packages on data libraries and theory development, making a total of 8 work packages.

Introduction

One of the outstanding new developments in the field of Partitioning and Transmutation (P&T) concerns Accelerator-Driven Systems (ADS), which consist of a combination of a high-power, high-energy accelerator, a spallation target for neutron production, and a sub-critical reactor core.

The development of the commercial critical reactors of today motivated a large effort on nuclear data up to about 20 MeV, and presently several million data points can be found in various data libraries. At higher energies, data are scarce or even non-existent. With the development of nuclear techniques based on neutrons at higher energies, there is nowadays a need also for higher-energy nuclear data.

The nuclear data needed for transmutation in an ADS can roughly be divided into two main areas. First, the initial proton beam produces neutrons via spallation reactions. This means that data on proton-induced neutron production is needed. In addition, data on other reactions are needed to assess the residual radioactivity of the target. Second, the produced neutrons can induce a wide range of nuclear reactions, and knowledge of these are useful in the design of an ADS. Among these reactions, some cross sections can be used directly. Examples are elastic scattering for neutron transport, proton and alpha production for assessment of the hydrogen and helium gas production in the target window or core, and fission for obvious reasons.

In most cases, however, direct data determination is not the ultimate goal. The global capacity for such measurements is insufficient to obtain complete coverage of important data. It is even impossible in theory to supply all relevant data. In a reactor core, large quantities of short-lived nuclides affect the performance of the core during operation, but measuring cross sections for these nuclides is impossible because experiment targets cannot be made. A good example from critical reactors is ^{135}Xe, the well-known villain of the Chernobyl disaster, with its half-life of 9 h that makes nuclear data measurements almost impossible. In this respect, accelerator-driven systems are not fundamentally different than critical reactors.

This means that the experimental work must be focused on providing benchmark data for theory development, making it possible to use theoretical models for unmeasured parameters in a core environment.

An often overlooked aspect is *why* nuclear data should be measured in the first place. Nuclear data are not needed for a demonstration of the principle of driving a sub-critical assembly with an external neutron source. The need for nuclear data becomes imminent

when a realistic large-scale facility is the goal. With large uncertainties in the nuclear data, large safety margins have to be used, which results in excessive costs. Thus, the role of nuclear data is to reduce the cost for reaching a certain level of safety.

Another important aspect is the trade-off between general and particular information. Below 20 MeV, a single cross section can be of paramount importance to the entire application. An example is the neutron capture resonance in ^{238}U that provides the Doppler effect of utmost significance to the stability of critical reactors. Moreover, some cross sections are fundamentally inaccessible to theory, in particular in the resonance region. As a result, at low energies more or less complete data coverage for major elements is required. Above 20 MeV, the situation is fundamentally different. The cross sections are smooth, and the behaviour of the total technical system is always dictated by the sum of a large number of reactions, neither of which strongly dominates the performance. Therefore, getting a grip on the overall picture is more important than precision data on a single reaction.

The HINDAS project

HINDAS was a joint European effort, which gathered essentially all European competence on nuclear data for transmutation in the 20-2000 MeV range [1]. The program was designed to obtain a maximal improvement in high-energy nuclear data knowledge for transmutation. It was conceived that this goal could only be achieved with a well-balanced combination of basic cross section measurements, nuclear model simulations and data evaluations. The work was focused on three elements, iron, lead and uranium, selected to give a representative coverage of typical materials for construction, target and core, respectively, especially relevant to ADS, as well as a wide coverage of the periodic table of elements.

In total, 16 universities or laboratories participated, whereof 6 had experimental facilities. This means that HINDAS involved essentially all relevant European laboratories in its energy range. This distribution and coordination of experiments at many laboratories made the work very efficient. What is noteworthy is that HINDAS involved many partners and even laboratories that had previously not been involved at all in activities on nuclear data for applications. Thus, HINDAS has contributed to a widening of the field of applied nuclear physics.

HINDAS was coordinated by UCL, Louvain-la-Neuve, Belgium, and ran during 2000-2003. The total EU funding was 2.1 MEUR. To this should be added matching funding, equipment and infrastructure from the participating countries.

Organization of the research work

The project was carried out in eight work packages (WP). WP 1-3 concerned experiments in the 20-200 MeV range, WP 4-6 dealt with 200-2000 MeV experiments, and WP 7 and 8 were devoted to theory for the 20-200 and 200-2000 MeV regions, resp.

The division into two energy ranges is natural, since there appears to be a transition region around 200 MeV for the theoretical models. Below this energy the theoretical calculations have to include direct interactions, as well as pre-equilibrium, fission and statistical models, whereas at higher energies the intra-nuclear cascade model, together with fission and evaporation models, has to be considered. As a coincidence, the experimental facilities and the measurement techniques are also different below and above about 200 MeV.

The experimental WPs are structured according to type of particles produced. This means that for each energy range, there are WPs on production of light ions, neutrons and residues, resp. Below, the WPs are described in some more detail:

1. Light charged-particle production induced by neutrons or protons between 20 and 200 MeV (Lead contractor: Université Nantes, France).

The double-differential cross sections for proton- and neutron-induced production of hydrogen and helium ions on iron, lead and uranium isotopes were measured at UCL-Louvain, TSL-Uppsala and KVI-Groningen. These measurements provided essentially complete data in both emission angle and ejectile energy. Such double differential cross sections constitute a very stringent test for theoretical models in this energy domain. In addition, charged-particle multiplicities in proton-induced reactions have been measured at KVI.

2. Neutron production induced by neutrons or protons between 20 and 200 MeV (Lead contractor: Uppsala University, Sweden).

Neutron elastic scattering measurements (p,xn) and (n,xn) measurements on iron, lead and uranium have been performed at UCL-Louvain and TSL-Uppsala. Elastic scattering measurements are useful not only for optical model development, but can also be used directly for neutron transport calculations.

3. Residual nuclide production induced by neutrons and protons between 20 and 200 MeV and production of long-lived radionuclides (Lead contractor: Hannover University, Germany)
Measurements of proton-induced production of residual nuclei were carried out at PSI, and neutron-induced production at UCL-Louvain and TSL-Uppsala, where also neutron-induced fission was measured. For the short-lived residual radionuclides, cross sections were determined using activation techniques. The production of long-lived radionuclides was studied by Accelerator-Mass Spectroscopy (AMS) after chemical separation at ETH.

4. Light charged-particle production above 200 MeV (Lead contractor: FZ Jülich, Germany)
Proton- and deuteron-induced production cross sections of protons and alpha particles were measured with a 4π silicon ball detector at the COSY accelerator in Jülich. Experiments on thin targets aimed for tests of the intra-nuclear cascade model, while thick-target studies were focused on benchmarking transport codes. These measurements have also been used to evaluate gas production in the window and structure materials of an ADS, which will give implications for the lifetime of such components.

5. Neutron production induced by protons above 200 MeV in thin and thick targets (Lead contractor: CEA-Saclay, France)
Double-differential neutron production cross sections, for both thin and thick targets, have recently been measured at CEA-Saclay using time-of-flight or magnetic spectrometer techniques. At FZ Jülich, multiplicities of neutrons up to 150 MeV have been studied event-wise with a 4π liquid scintillator, using both thin and thick targets. The two experiments are complementary, both for technical and physics reasons. E.g., comparisons can be made between the directly measured multiplicities with those inferred from integration of the double-differential data.

6. Residual nuclide production above 200 MeV in inverse kinematics (Lead contractor: GSI, Germany)
Proton- and deuteron-induced nuclide production was measured in inverse kinematics, i.e., a lead or uranium beam hits a liquid hydrogen or deuterium target, and the spallation products are identified in flight using a high-resolution magnetic spectrometer. In this way all spallation products, irrespective of half-life, can be measured. These new data are useful when calculating the radioactive inventory, the radiotoxicity and the breeded impurities in a realistic spallation target of an ADS.

7. Nuclear data libraries and related theory (Lead contractor: NRG, Netherlands)
This work package concerned nuclear model calculations for analysis of the experimental data provided by WP 1-3, i.e., between 20 and 200 MeV. Special emphasis has been put on providing as complete information as possible on cross sections for all possible outgoing channels of iron, lead and uranium, and to construct improved nuclear data libraries, extending to 200 MeV.

8. High energy models and codes (Lead contractor: Université de Liège, Belgium)
This work package was devoted to theory for WP 4-6, i.e., above 200 MeV, and regarded mainly intra-nuclear cascade models and evaporation and fission models. The main objective was the development of powerful and accurate tools to calculate nucleon-nucleus spallation reactions.

Neutron data above 20 MeV

Examples of experimental work with charged-particle beams above 200 MeV are presented in the contribution by Kelic to these proceedings. Therefore, the presentation in this contribution is focused on neutron-induced reactions.

Two neutron-beam facilites, at UCL Louvain-la-Neuve, Belgium [2] and the old facility at TSL Uppsala, Sweden [3] were used in the HINDAS project. Recently, a new facility has been commissioned at TSL. All these facilities employ the ^{7}Li(p,n) reaction for neutron production. UCL was used for all measurements up to 70 MeV, and TSL at higher energies. Below, examples of results from TSL Uppsala are presented.

Base equipment

Two major experimental setups are semi-permanently installed. These are the MEDLEY detector telescope array [4], housed in a scattering chamber and operated in vacuum, and SCANDAL (SCAttered Nucleon Detection AssembLy) [3], a setup designed for large-acceptance neutron and proton detection.

The MEDLEY detector array consists of eight particle telescopes, placed at 20-160 degrees with 20 degrees separation. Each telescope is a ΔE- ΔE-E detector combination, with sufficient dynamic range to distinguish all light ions from a few MeV up to maximum energy, i.e., about 100 MeV. Recently, the facility has been used also for fission studies.

The SCANDAL (SCAttered Nucleon Detection AssembLy) setup has been designed for elastic neutron scattering studies. The energy of the scattered neutron is determined by measuring the energy of proton recoils from a plastic scintillator, and the angle is determined by tracking the recoil proton. SCANDAL can also be used as proton or deuteron detector. In those cases, the veto and converter scintillators are removed.

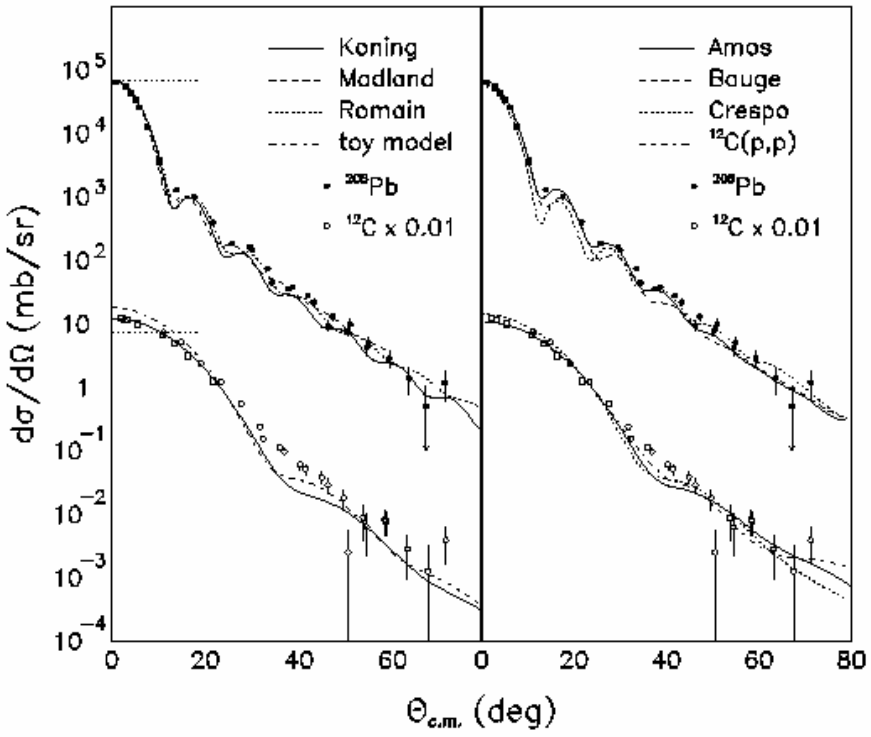

Figure : Elastic neutron scattering at 96 MeV [5].

Neutron scattering

Elastic neutron scattering is of utmost importance for a vast number of applications. Besides its fundamental importance as a laboratory for tests of isospin dependence in the nucleon-nucleon, and nucleon-nucleus, interaction, knowledge of the optical potentials derived from elastic scattering come into play in virtually every application where a detailed understanding of nuclear processes are important. Elastic neutron scattering is important also for fast-neutron cancer therapy, because the nuclear recoils account for 10-15 % of the dose. Up to now, data on ^{12}C and ^{208}Pb at 96 MeV have been published [5], and eight other nuclei are underway. A facility for studies of inelastic neutron scattering has recently been commissioned, and first data taking, ^{nat}Fe and ^{nat}Pb at 96 MeV, has been completed.

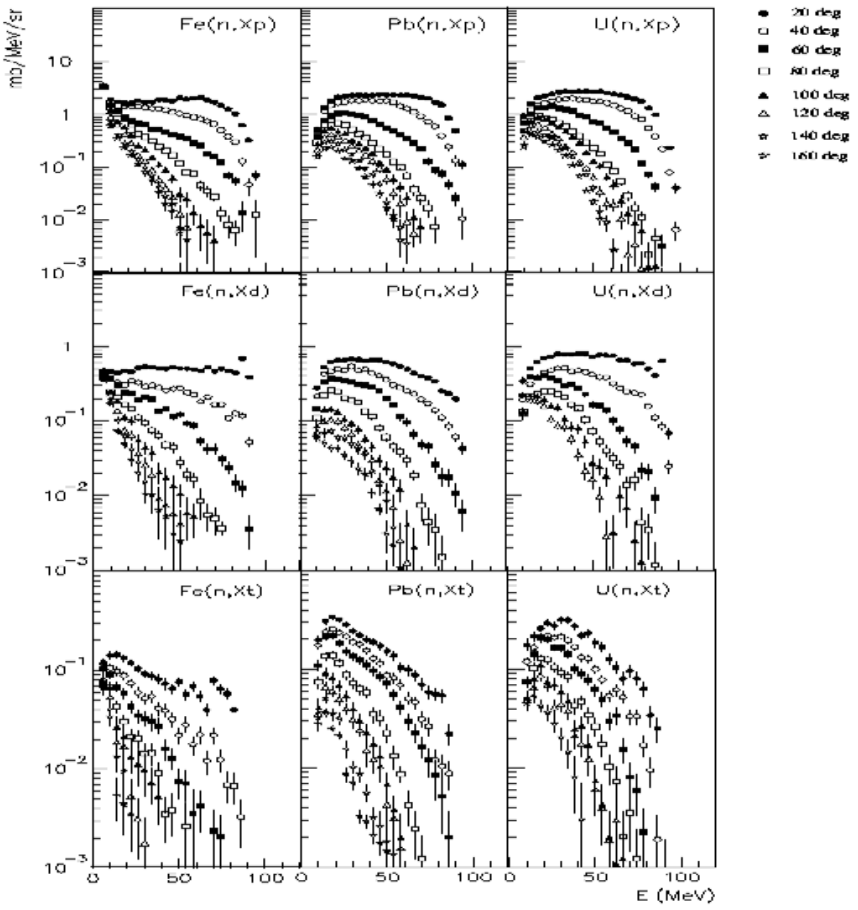

Figure : Neutron-induced production of protons, deuterons and tritons on lead at 96 MeV [6].

Light-ion production
Nuclear reactions with nucleons in both the incident and exit channel are of great use in development of nuclear models. Therefore, neutron-induced light-ion emission has been thoroughly studied. Moreover, hydrogen and helium production constitutes a safety and materials degradation problem in an ADS. This has motivated measurements on iron, lead and uranium at 96 MeV [6].

Fast-neutron fission
Although the main fission effects in an ADS arise from neutrons at lower energies, the high-energy neutron fission gives significant contributions to the power released. Very little data exist on high-energy fission, but the situation is under rapid improvement. This can be exemplified by the ongoing work at the TSL neutron beam [7]. A new facility for studies also of angular distributions is under commissioning. Fission was not studied in HINDAS, but is instead carried out under the auspices of ISTC.

Residue production
A series of studies of residue production has been carried out in parallel with the other experiments mentioned here, at an irradiation facility located just outside the primary neutron beam.

Outlook

The rapid growth in demand for neutrons has motivated the construction of a new 20-180 MeV neutron beam facility at TSL [8]. The most important features of the new facility are

increased intensity by reduction of the distance from neutron production to experiments, availability of much larger beam diameters, increased versatility concerning various beam parameters, like the shape, and reserved space for a future pulse sweeping system.

For nuclear data research, the increased intensity will facilitate a large experimental program at 180 MeV, hitherto excluded by count rate limitations. The main use of the facility, however, will be commercial testing of electronics [9]. For this, the increased intensity in combination with a larger beam diameter, which facilitates testing of a large number of components simultaneously, will provide a figure-of-merit about a factor 300 larger than for the present facility. This means that the new TSL neutron beam facility can outperform any existing mono-energy facility in the world.

Acknowledgements
This work was supported by the European Union Council, the Swedish Natural Science Research Council, the Swedish Nuclear Fuel and Waste Management Company, the Swedish Nuclear Power Inspectorate, Ringhals AB, the Swedish Defence Research Agency, the Swedish International Development Authority, the Thai Ministry of University Affairs and the International Program in the Physical Sciences at Uppsala University.

References

[1] A. Koning, H. Beijers, J. Benlliure, O. Bersillon, J. Blomgren, J. Cugnon, M. Duijvestijn, Ph. Eudes, D. Filges, F. Haddad, S. Hilaire, C. Lebrun, F.-R. Lecolley, S. Leray, J.-P. Meulders, R. Michel, R.-D. Neef, R. Nolte, N. Olsson, E. Ostendorf, E. Ramström, K.-H. Schmidt, H. Schuhmacher, I. Slypen, H.-A. Synal, R. Weinreich, J. Nucl. Sci. Tech., Suppl. **2** (2002) 1161.

[2] H. Schuhmacher, H.J. Brede, V. Dangendorf, M. Kuhfuss, J.P. Meulders, W.D. Newhauser, R. Nolte, Nucl. Instr. Meth. **A421** (1999) 284.

[3] J. Klug, J. Blomgren, A. Atac, B. Bergenwall, S. Dangtip, K. Elmgren, C. Johansson, N. Olsson, S. Pomp, A.V. Prokofiev, J. Rahm, U. Tippawan, O. Jonsson, L. Nilsson, P.-U. Renberg, P. Nadel-Turonski, A. Ringbom, A. Oberstedt, F. Tovesson, V. Blideanu, C. Le Brun, J.F. Lecolley, F.R. Lecolley, M. Louvel, N. Marie, C. Schweitzer, C. Varignon, Ph. Eudes, F. Haddad, M. Kerveno, T. Kirchner, C. Lebrun, L. Stuttgé, I. Slypen, A. Smirnov, R. Michel, S. Neumann, U. Herpers, Nucl. Instr. Meth. **A 489** (2002) 282.

[4] S. Dangtip, A. Atac, B. Bergenwall, J. Blomgren, K. Elmgren, C. Johansson, J. Klug, N. Olsson, G. Alm Carlsson, J. Söderberg, O. Jonsson, L. Nilsson, P.-U. Renberg, P. Nadel-Turonski, C. Le Brun, F.-R. Lecolley, J.-F. Lecolley, C. Varignon, Ph. Eudes, F. Haddad, M. Kerveno, T. Kirchner, C. Lebrun, Nucl. Instr. Meth. **A452** (2000) 484.

[5] J. Klug, J. Blomgren, A. Atac, B. Bergenwall, A. Hildebrand, C. Johansson, P. Mermod, L. Nilsson, S. Pomp, U. Tippawan, K. Elmgren, N. Olsson, O. Jonsson, A.V. Prokofiev, P.-U. Renberg, P. Nadel-Turonski, S. Dangtip, P. Phansuke, M. Österlund, C. Le Brun, J.F. Lecolley, F.R. Lecolley, M. Louvel, N. Marie-Noury, C. Schweitzer, Ph. Eudes, F. Haddad, C. Lebrun, A.J. Koning, X. Ledoux, Phys. Rev. C **68** (2003) 064605.

[6] V. Blideanu, F.R. Lecolley, J.F. Lecolley, T. Lefort, N. Marie, A. Atac, G. Ban, B. Bergenwall, J. Blomgren, S. Dangtip, K. Elmgren, Ph. Eudes, Y. Foucher, A. Guertin, F. Haddad, A. Hildebrand, C. Johansson, O. Jonsson, M. Kerveno, T. Kirchner, J. Klug, Ch. Le Brun, C. Lebrun, M. Louvel, P. Nadel-Turonski, L. Nilsson, N. Olsson, S. Pomp, A.V. Prokofiev, P.-U. Renberg, G. Rivière, I. Slypen, L. Stuttgé, U. Tippawan, M. Österlund, Phys. Rev. C. **70** (2004) 014607.

[7] A.N. Smirnov, N.P. Filatov, V.P. Eismont, H. Condé, J. Blomgren, A.V. Prokofiev, P.-U. Renberg, N. Olsson, Measurement of neutron-induced fission cross-sections for ^{nat}Pb, ^{208}Pb, ^{197}Au, ^{nat}W, and ^{181}Ta in the intermediate energy region, accepted for publication in Phys. Rev. C.

[8] S. Pomp, A.V. Prokofiev, J. Blomgren, C. Ekström, O. Jonsson, D. Reistad, V. Ziemann, N. Haag, A. Hildebrand, L. Nilsson, B. Bergenwall, C. Johansson, P. Mermod, N. Olsson, M. Österlund, U. Tippawan, The new Uppsala neutron beam facility, International Conference on Nuclear Data for Science and Technology, Santa Fé, New Mexico, USA, September 26 - October 1, 2004 (accepted).

[9] J. Blomgren, Nuclear Data for Single-Event Effects, EU enlargement workshop on Neutron Measurements and Evaluations for Applications, Budapest, Hungary, November 5-8, 2003. EUR Report 21100 EN, Luxembourg: Office for Official Publications of the European Communities, ISBN 92-894-6041-5, European Communities, 2004.

Appendix XXII

The Nuclear Physics Reason That Your Laptop Crashes During Flight

J. Blomgren
Department of Neutron Research, Uppsala university,
Box 525, 751 20 Uppsala, SE
Jan.Blomgren@tsl.uu.se

Keywords: Single event effects, electronics, computer memory, bit flip, neutron-induced nuclear reactions.

Abstract. The importance of cosmic radiation effects in electronics, on board aircrafts as well as at sea level, has been highlighted during the last decade. When, e.g., an electronic memory circuit is exposed to particle radiation, the latter can cause a flip of the memory content in a bit, which is called a single-event upset (SEU). This induces no hardware damage to the circuit, but unwanted re-programming of memories, CPUs, etc., can have consequences for the reliability, and ultimately also for the safety of the system. Since neutrons have no charge, they can only interact via violent, nuclear reactions, in which charged particles are created. In this paper, the SEU problem is presented from a nuclear physicist's perspective. Experimental efforts to improve the nuclear reaction database for silicon are described, as well as the conclusions about the nuclear physics origin of the effect that can be drawn from device testing activities.

Introduction

The importance of cosmic radiation effects in electronics, on board aircrafts as well as at sea level, has been highlighted recently. When, e.g., an electronic memory circuit is exposed to particle radiation, the latter can cause a flip of the memory content in a bit, which is called a single-event upset (SEU). This induces no hardware damage to the circuit, but unwanted re-programming of memories, CPUs, etc., can have consequences for the reliability, and ultimately also for the safety of the system. Such software errors were in fact discovered by accident in a portable PC used at an airplane a few years ago, and later the effect has been verified under controlled conditions, both in flight measurements [1,2], as well as in the laboratory [3-5].

The reason that these errors are referred to as single-event upsets is that they are induced by a single particle hitting the device (see Figure 1). This is in contrast to radiation damage of electronics, a phenomenon caused by the integrated dose, which is normally delivered by a large quantity of particles.

The cosmic ray particles in space are mainly protons and alpha-particles. When passing the atmosphere, most of these particles are absorbed, and some of them create cascades of secondary particles. At flight altitudes, as well as at sea level, the cosmic ray flux is dominated by neutrons and muons. The latter do not interact strongly with nuclei, and therefore neutrons are most important for SEU [6-8].

Since neutrons have no charge, they can only interact via violent, nuclear reactions, in which charged particles are created. If this happens in the silicon

substrate of an electronic device, the free charge created by the ionization of these secondary particles can be large enough to induce an SEU. Thus, to obtain a full understanding of the SEU problem, knowledge is needed about both the nuclear interaction of neutrons with silicon and the electrical and dynamical properties of pn junctions.

The research on these effects essentially follow two main lines, direct testing of devices in neutron beams and measurements of probabilities (cross sections) of the relevant nuclear reactions ultimately causing these effects. In this paper, the SEU problem will be discussed from a nuclear physicist's perspective. An extended discussion can be found in reference [9]. Some experimental efforts to improve the nuclear reaction database for silicon, as well as device testing activities, will be described, followed by an outlook.

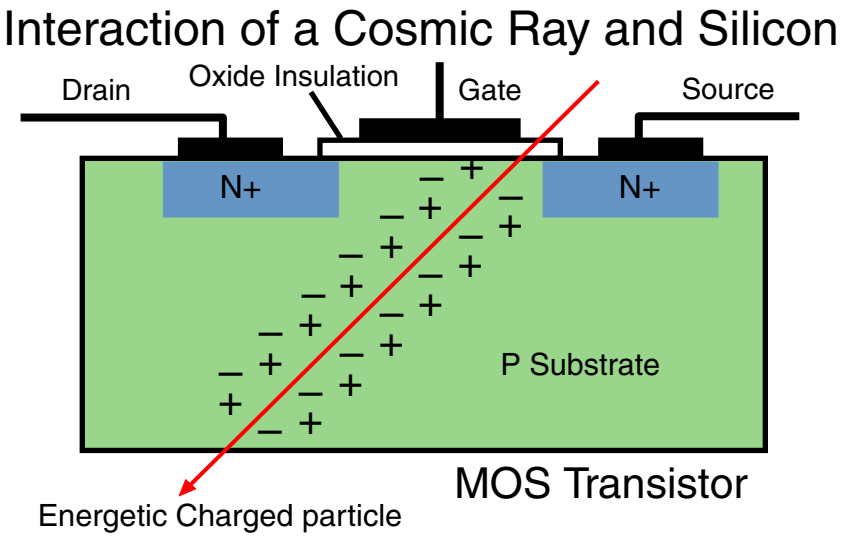

Figure 1. Illustration of a single event in a memory device.

Neutron beams for testing

It is very time-consuming to use the natural flux of cosmic neutrons for testing of SEU effects in devices. Thus, it is of interest to perform accelerated testing, i.e., using a neutron flux far larger than the natural one. This can be provided by neutron production using particle accelerators. An example of such a facility is the original neutron beam [10,11] at The Svedberg Laboratory, Uppsala, Sweden, at which the examples presented in this article were obtained.

Industry research teams, as well as groups from universities, have performed device testing of several different devices at various neutron sources over the years. Most of the testing has been performed by device manufacturers and companies within the airplane business. Up to now, extensive series of SRAMs and DRAMs have been tested in-beam, as well as FIFOs and a few processors. These tests have shown that memory devices, computer caches included, are especially susceptible to neutron radiation.

Results of the first neutron-energy resolved measurements [12], carried out at TSL, are shown in Figure 2. As can be seen, the data for different devices show similar energy dependencies, although the absolute magnitude differs. Furthermore,

the cross section curves seem to saturate, or even decrease slightly, at energies beyond 100 MeV. This indicates that the dominant nuclear physics origin of these effects is production of heavy ions, a conclusion corroborated by basic device parameters.

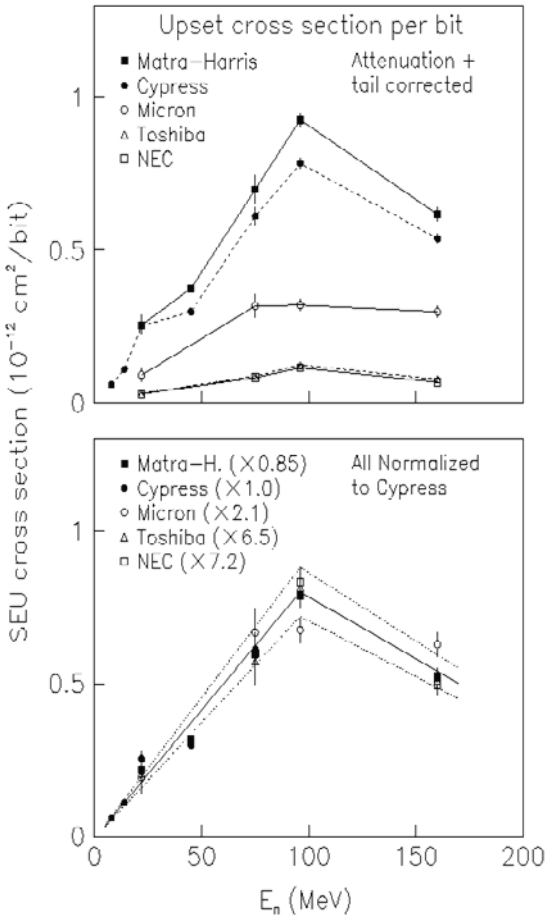

Figure 2. The SEU sensitivity versus incident neutron energy for some memory devices [12]. The upper panel shows the absolute SEU cross sections. In the lower panel, all devices are normalized to Cypress, showing that the energy dependence is similar for all devices, but the absolute magnitude differs. The solid line is an eye-guide showing an average, and the dotted lines indicate 10 % deviation from the average. See reference [12] for details.

Measurements of neutron-induced cross sections in silicon

Relying completely on experimental information for assessment of the SEE problem is difficult for a number of reasons. First, the energy range to be covered is very large. Therefore, theory modelling is needed for interpolation in between energies where data are available. Second, many of the reactions causing the effect are not accessible to experimental determination. Especially, experimental data can be obtained for production of one particle type at the time (singles), but coincidence data are unavailable, and will probably remain so for a foreseeable future. Thus, the role of experimental data is to guide theory, which in turn will be used as input to device

simulation codes. A collaboration Uppsala University – Chiang Mai University has been formed to address these issues.

This in turn means that the data to measure should provide important information for theory development. With these constraints, roughly three types of data are important; elastic neutron scattering, light-ion production and heavy recoil production.

Elastic scattering plays a major role in the determination of the effective interaction between a neutron and a nucleus, which is used in virtually every cross section calculation with a neutron in the incident or exit channel. Until recently, the maximum energy where high-quality neutron elastic scattering data have been produced has been 65 MeV. Recently, data at 96 MeV on carbon and lead have been published [13], and a series of nuclei, including silicon, are under study.

Light-ion production is at present motivated by theory development only, but it might be possible that such data can be of direct importance in a not so distant future, i.e., alpha-production reactions might cause SEEs in future technologies with lower critical charge needed for a bit flip. The data situation for light-ion production resembles the elastic scattering data situation, in that up to now high-quality data up to about 70 MeV have been available. The MEDLEY detector set-up [14] at TSL has been designed for production of p, d, t, ^{3}He, and α data (and possibly also ^{6}Li and ^{7}Li) in the 50-130 MeV range. Recently, silicon data at 96 MeV have been obtained that will be provided for improvement of the data bases, and finally for use within the SEU community [15]. Additional experiments at 180 MeV are planned, which requires a moderate upgrade of MEDLEY.

As has been discussed above, the most important nuclear reactions ultimately causing the SEE effects in present technologies are probably neutron-induced production of heavy, low-energy recoils. Direct measurement of such cross sections with a neutron beam on a silicon target is in reality impossible with present technology, because these recoils have such low energies that an extremely thin target is needed if they should escape it to be able to hit a detector, but then the count rate is so small that reasonable statistics cannot be obtained in a reasonable time. This problem can be circumvented if using inverse kinematics. Such an experiment is under development at TSL [16].

Outlook

The single-event effect is now an established phenomenon in the electronics industry, and its importance is growing. The continuing trend of gradually smaller dimensions of the active volumes in computer devices is expected to make the problem even worse. In fact, it is a common prediction that the single-event effect can terminate further development of the presently dominant silicon technology in a near future. The problem is no longer confined to space and aviation applications, but is progressively becoming significant also at ground level. For instance, present commercial off-the-shelf work stations at sea level experience system crashes with average intervals of typically two weeks due to these effects.

The fact that the SEE phenomenon seems to be here to stay has motivated a new neutron beam facility to be built at TSL, with dramatically improved intensity [17]. The facility is operational since early 2004, and it has already been successfully used both for physics experiments and commercial testing.

References

1. J. Olsen, et al., IEEE Trans. Nucl. Sci. **40** (1993) 74.

2. A. Taber and E. Normand, IEEE Trans. Nucl. Sci. **40** (1993) 120.

3. E. Normand, et al., IEEE Trans. Nucl. Sci. **41** (1994) 2203.

4. C.A. Gossett, et al., IEEE Trans. Nucl. Sci. **40** (1993) 1845.

5. E. Normand, et al., IEEE Trans. Nucl. Sci. **42** (1995) 1815.

6. A.J. Sims, et al., IEEE Trans. Nucl. Sci. **41** (1994) 2361.

7. J.F. Ziegler, IBM J. Res. Develop. **40** (1996) 19.

8. E. Normand and T.J. Baker, IEEE Trans. Nucl. Sci. **40** (1993) 1484.

9. J. Blomgren, Nuclear Data for Single-Event Effects, EU enlargement workshop on Neutron Measurements and Evaluations for Applications, Budapest, Hungary, November 5-8, 2003 (invited). EUR Report 21100 EN, Luxembourg: Office for Official Publications of the European Communities, ISBN 92-894-6041-5, European Communities, 2004.

10. H. Condé, et al., Nucl. Instr. Meth. **A292** (1990) 121.

11. J. Klug, et al., Nucl. Instr. Meth. **A489** (2002) 282.

12. K. Johansson, et al., IEEE Trans. Nucl. Sci. **45** (1998) 2519.

13. J. Klug, et al., Phys. Rev. C **68** (2003) 064605..

14. S. Dangtip, et al., Nucl. Instr. Meth. **A452** (2000) 484.

15. U. Tippawan, et al., Phys. Rev. C **69** (2004) 064609.

16. J. Aichelin, Y. Murin, et al., Inverse kinematics for study of intermediate energy reactions relevant to SEE and medical problems, International Conference on Nuclear Data for Science and Technology, Santa Fé, New Mexico, USA, September 26 - October 1, 2004 (accepted).

17. S. Pomp, et al., The new Uppsala neutron beam facility, International Conference on Nuclear Data for Science and Technology, Santa Fé, New Mexico, USA, September 26 - October 1, 2004 (accepted).

Paper received March 2005

A NEW HIGH-ENERGY NEUTRON BEAM FACILITY IN UPPSALA

A. V. Prokofiev[1], S. Pomp[2], J. Blomgren[2], O. Byström[1], C. Ekström[1], O. Jonsson[1], D. Reistad[1], U. Tippawan[2, 3], D. Wessman[1], V. Ziemann[1], and M. Österlund[2]

[1]*The Svedberg Lab, Uppsala University, Box 533, S-751 21 Uppsala, Sweden*

tel. +46-70-326-3866; fax: +46-18-471-3833; e-mail: Alexander.Prokofiev@tsl.uu.se

[2]*Department of Neutron Research, Uppsala University, Sweden*

[3]*Fast Neutron Research Facility, Chiang Mai University, Thailand*

Abstract

A new quasi-monoenergetic neutron beam facility has been constructed at The Svedberg Laboratory (TSL) in Uppsala, Sweden. Key features include an energy range of 20 to 175 MeV, high fluxes and the possibility of large-area neutron fields. The new facility has been designed specifically to provide optimal conditions for testing of single-event effects in electronics. First results of the beam characterization measurements are reported.

Scientific and technical background

The interest in high-energy neutrons is rapidly growing, since a number of potential large-scale applications involving fast neutrons are under development, or have been identified. These applications primarily fall into three sectors: nuclear energy and waste, medicine and effects on electronics.

The recent development of high-intensity proton accelerators has resulted in ideas to use subcritical reactors, fed by external spallation-produced neutrons, for transmutation of waste from nuclear power reactors or nuclear weapons material. This might result in less problematic waste material and/or energy production; see, e.g., Ref. [1].

Conventional radiation treatment of tumors, i.e., by photons or electrons, is a cornerstone in modern cancer therapy. Some rather common types of tumors, however, cannot be treated successfully. For some of these, very good treatment results have been reached with neutron therapy, which is the largest used non-conventional therapy worldwide [2, 3].

It has been established during recent years that air flight personnel receives among the largest radiation doses in civil work, due to cosmic-ray neutrons. This poses a relatively new dosimetry problem, which is currently under investigation [4].

During the last few years, it has become evident that electronics in aircraft suffer effects from cosmic-ray neutrons, so-called single-event effects (SEE) [5, 6]. The presently most well known effect is that a neutron can induce a nuclear reaction in the silicon substrate of a memory device, releasing a free charge, which in turn flips the memory content. This random re-programming is obviously not wanted. Similar effects causing hardware damage have recently been identified also on ground level. Testing of SEE using the natural flux of cosmic neutrons is time-consuming. To speed up the measurements, one needs to use neutron beams produced with particle accelerators. The procedures for the accelerated testing of memory devices are summarized in the recent JEDEC standard [6]. According to this standard, one of the ways to perform the accelerated testing is to irradiate a device under study by monoenergetic neutrons with nominal energies of 20, 50, 100, and 150 MeV. Such an approach is a viable alternative to the testing with a "white" neutron spectrum, if the intensity of monoenergetic neutrons is enough to cause reasonably high SEE rates.

Finally, fundamental nuclear physics with intermediate-energy neutrons has recently got widespread attention due to the experimental studies of the absolute strength of the strong interaction in the nuclear sector, derived from neutron–proton scattering data; see, e.g., Ref. [7].

All the applications mentioned above involve neutrons at much higher energies than for the traditional applied areas, e.g., nuclear power. Extensive evaluated data libraries have been established for the development of nuclear fission and fusion for energy production, which have a 20 MeV upper limit. Very little high-quality neutron-induced data exist above this energy.

To satisfy these needs, a new quasi-monoenergetic neutron-beam facility has been constructed at the The Svedberg Laboratory (TSL), Uppsala. Emphasis has been put on high neutron beam intensity in combination with flexibility in energy and neutron field shape.

Technical specification

The facility uses the ^{7}Li(p,n)^{7}Be reaction (Q=-1.64 MeV) to produce a quasi-monoenergetic neutron beam. The proton beam is provided by the Gustaf Werner cyclotron with an energy variable in the 20-180 MeV range. A drawing of the neutron-beam facility is shown in Fig. 1. The proton beam is incident on a target of lithium, enriched to 99.99% in ^{7}Li. The available targets are 1, 2, 4, 8, and 24 mm thick. The targets are rectangular in shape, 20x32 mm^2, and are mounted in a remotely controlled

water-cooled copper rig. An additional target position contains a fluorescent screen viewed by a TV camera, which is used for beam alignment and focusing. Downstream the target, the proton beam is deflected by a magnet into a 10-m long dumping line, where it is guided onto a heavily shielded water-cooled graphite beam dump.

The neutron beam is formed geometrically by a cylindrically shaped iron collimator block, 50 cm in diameter and 100 cm long, with a cylindrical, conical or rectangular hole of variable size. The collimator is surrounded by concrete to form the end wall of the production line towards the experimental area. Thereby, efficient shielding from the production target region is achieved. A modular construction of the collimator allows the user to adjust the diameter of the neutron beam to the needs of a specific experiment. The available collimator openings are 1, 2, 3, 5.4, 10, 15, 20, and 30 cm. Other collimator diameters in the 0-30 cm range, as well as other shapes than circular can be provided upon request. Beam diameters of up to 1 m are obtainable at a larger distance from the production target, which may be used for testing a larger number of devices simultaneously, or larger devices like entire electronic boards. The facility is capable to deliver neutrons in the 20-175 MeV range. This makes TSL the only laboratory in the world offering full monoenergetic neutron testing according to the JEDEC standard [6].

Neutrons reach the experimental area at a distance of about 3 m from the production target. Reduction of this distance has led to an increase of the neutron flux by about one order of magnitude in comparison with the old TSL neutron facility [8, 9], using the same target thickness, proton energy and current. Beam currents of up to 10 μA can be achieved for energies below 100 MeV. Above 100 MeV, the achievable beam current is about a factor of 10 lower. The resulting lower neutron fluence can be partly compensated by the use of thicker lithium targets.

Two additional irradiation positions, which can be used parasitically with other experiments, are provided (see Table I). The increase of the neutron flux at these positions is reached at the expense of limited accessibility, limited size of irradiated objects, and more intense γ-ray background.

Characterization of the facility

The first neutron beam at the new facility was delivered in 2004. Since then, commissioning runs have been performed, including measurements of neutron flux, spectra, and profile. First results are reported below.

The measured contamination of the neutron beam at the experimental area due to interactions of the primary protons with beam transport elements such as the target frame did not exceed 0.2%. Such interactions only leads to a minor surplus of neutrons in the experimental area because charged particles produced near the lithium target and upstream are removed by the deflection magnet. The relative contamination of protons with energies above 15 MeV in the neutron beam is about 10^{75}. These measurements have been performed for a proton beam energy of 98 MeV.

The energy and angular distribution of neutrons delivered to the experimental area is mainly defined by the double-differential cross-section of the ^{7}Li(p,n) reaction at forward angles. The reaction energy spectrum is dominated by a peak situated a few MeV below the energy of the primary protons and comprising about 40% of the total number of neutrons. Neutron spectra have been obtained by measuring elastic *np*-scattering with the Medley setup [10]. The scattered protons are registered at an angle of 20° relative to the neutron beam. Besides the energy of the scattered proton, the time-of-flight (TOF) relative to the RF signal from the cyclotron for each event is recorded. As an example, the measured proton energy vs. neutron TOF is shown in Fig. 2. All proton events for a peak neutron energy of 74.8 MeV are contained. The horizontal and vertical straight lines indicate the position of the proton peak in time and energy for elastic scattering events caused by peak neutrons. The bent line shows the calculated position of elastic scattering events for different neutron energies. The neutron spectrum is deduced by application of a cut around this bent line, proper background subtraction and calculation of the corresponding incoming neutron energy on an event-by-event basis. The measured neutron spectra for four peak energies between 21.8 and 142.7 MeV are shown in Fig. 3. The peak energies are chosen in compliance with recommendations of the JEDEC standard [6]. The measurements are compared with the systematics by Prokofiev *et al.* [11] for the three higher energies (Fig. 3 b-d). The systematics is not applicable at the lowest beam energy (Fig. 3 a). Instead, an evaluation of Mashnik *et al*. [12] was employed for the description of the neutron spectrum. The differential cross-section for high-energy peak neutron production at 0° was obtained by multiplication of the total cross-section of the ^{7}Li(p,n)^{7}Be reaction [12] to the "index of forwardness" from the systematics of Uwamino *et al*. [13]. The narrow peaks in the upper continuum region correspond to excitation of higher states in residual ^{7}Be nuclei. This process was included in the model calculation of Mashnik *et al*. [12]. However, the energy resolution in the experiment does not allow us to observe these peaks. The experimental data agree with the calculations except for the region below 10 MeV in the 21.8 MeV spectrum where the model overpredicts the experimental results by up to a factor of 2.

Table II summarizes the main features of the measured

spectra and the achieved neutron flux. The later has been measured with the thin-film breakdown counter (TFBC) [14]. Another monitoring option is provided by an ionization-chamber monitor (ICM). Both monitors, usually installed after the Medley chamber, utilize neutron-induced fission of ^{238}U. Finally, a Faraday cup, installed in the proton beam dump, integrates the beam current and offers relative monitoring of the beam intensity.
Figure 4 shows a horizontal beam profile for 143 MeV neutrons, measured at a distance of 4.77 m from the production target. The measurement was performed by counting neutron-induced SEE in a set of electronic chips positioned across the beam [15].

Summary and outlook

A new neutron beam facility has been constructed at TSL and is now available for regular operation. It is capable to deliver neutrons in the 20-175 MeV range. First beams have been delivered for nuclear physics research, as well as for commercial electronics testing.

Acknowledgements

We would like to thank all the staff at The Svedberg Laboratory for the excellent work in building this new facility. We are thankful to M. Olmos for providing us with the beam profile data.

References

1. A. Koning, *et al.*, High and Intermediate energy Nuclear Data for Accelerator-driven Systems (HINDAS), J. Nucl. Sci. Technol. **2**, 1161 (2002).
2. R. Orecchia, *et al.*, Eur. J. Cancer **34**, 459 (1998).
3. D. L. Schwartz, *et al.*, Int. J. Radiat. Oncol. Biol. Phys. **50**, 449 (2001).
4. D. T. Bartlett, *et al.*, Radiat. Res. Congress Proceedings **2**, 719–723 (2000).
5. Single-Event Upsets in Microelectronics, topical issue, edited by H. H. K. Tang and N. Olsson [Mater. Res. Soc. Bull. **28** (2003)].
6. JEDEC Standard. Measurements and Reporting of Alpha Particles and Terrestrial Cosmic Ray-Induced Soft Errors in Semiconductor Devices. JESD89, August 2001.
7. J. Blomgren (Ed.), Proceedings of Workshop on Critical Issues in the Determination of the Pion-Nucleon Coupling Constant, Physica Scripta, T87, 2000.
8. H. Condé, *et al.*, Nucl. Instrum. Methods Phys. Res. A **292**, 121 (1990).
9. J. Klug, *et al.*, Nucl. Instrum. Methods Phys. Res. A **489**, 282 (2002).
10. S. Dangtip, *et al.*, Nucl. Instrum. Methods Phys. Res. A **452**, 484 (2000).
11. A. V. Prokofiev, *et al.*, J. Nucl. Sci. Techn., Suppl. 2, 112 (2002).
12. S. G. Mashnik, *et al.*, LANL Report LA-UR-00-1067 (2000).
13. Y. Uwamino, *et al.*, Nucl. Instrum. Methods Phys. Res. A **389**, 463 (1997).
14. A. N. Smirnov, *et al.*, Radiat. Meas. **25**, 151 (1995).
15. M. Olmos, priv. comm.

Position	Distance from the Li target (m)	Angle to the proton beam direction (°)	Gain in the peak neutron flux
PARTY	1.9	1.6	2.5
TUNIS	1.1	7.5	1.7 – 2.2[1)]

[1)] dependent on the peak neutron energy.

Table I. Parasitic irradiation positions.

Proton beam energy (MeV)	Li target thicknes s (mm)	Proton beam current (μA)	Resulting average energy of peak neutrons (MeV)	Fraction of neutrons in the mono-energetic peak (%)		Peak neutron flux (10^5 neutrons/(cm^2 s))
				measured	calculated	
24.68 ± 0.04	2	10	21.8	~50	--	1.3
49.5 ± 0.2	4	10	46.5	39	36	2.9
97.9 ± 0.3	8	5	94.7	41	39	4.6
147.4 ± 0.6	24	0.6	142.7	55 [1)]	40	2.1

[1)] upper limit due to poor energy resolution.

Table II. Neutron beam parameters. The fluxes refer to the entrance of the beam line to the experimental hall.

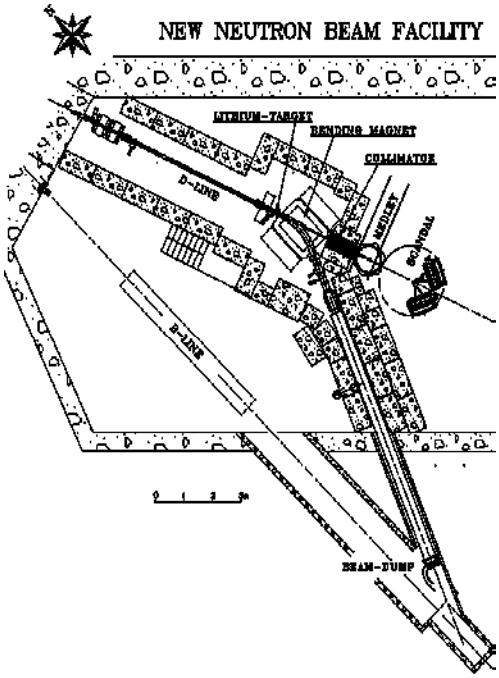

Figure 1. Drawing of the new neutron beam facility. The neutron beam is produced in the lithium target and continues along the D-line. The lithium target, the deflecting magnet, and the collimator are indicated. The drawing shows also the position for two permanent but movable experimental setups, Medley and SCANDAL.

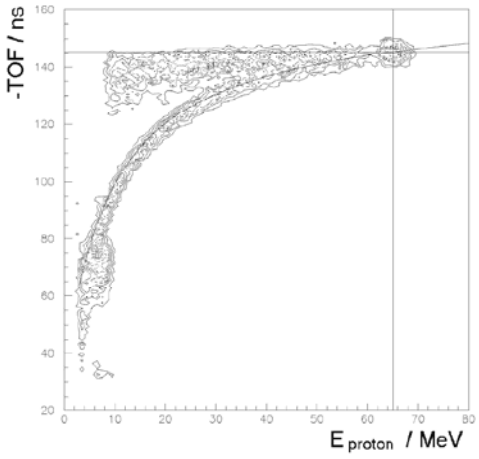

Figure 2. Measured proton energy vs. time-of-flight (TOF) for a peak neutron energy of 74.8 MeV registered at a scattering angle of 20 degrees (see text).

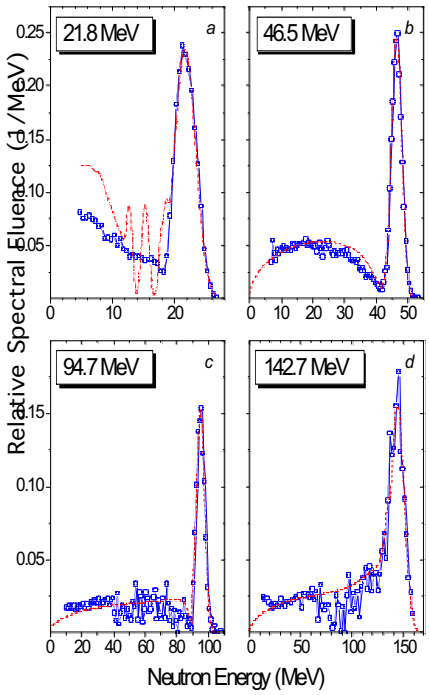

Figure 3. The neutron spectra at 0° for different peak neutron energies (see Table II for incident proton energies and ^{7}Li target thicknesses). Symbols connected by a solid line represent experimental data obtained in the present work. Predictions are shown as dashed lines (see text).

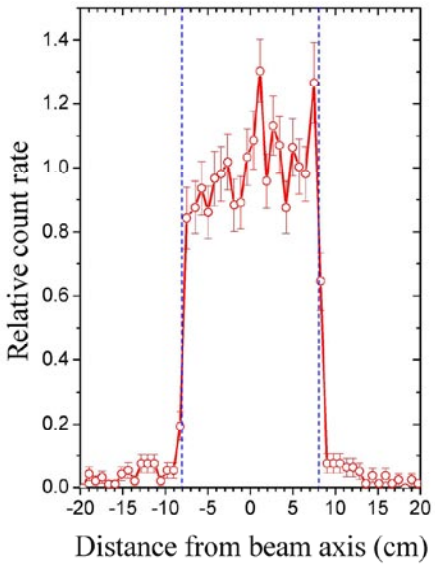

Figure 4. The horizontal beam profile for 142.7-MeV neutrons, measured at the distance of 4.77 m from the production target. Vertical dashed lines represent boundaries of the beam expected from the geometry of the collimator.

Appendix XXIV

Accepted for presentation at IEEE International Reliability Physics Symposium (IRPS'2005),
San Jose, California, April 17-21, 2005,
Paper SE02

A NEW NEUTRON FACILITY FOR SINGLE-EVENT EFFECT TESTING

A. V. Prokofiev[1], S. Pomp[2], J. Blomgren[2], O. Byström[1], C. Ekström[1], O. Jonsson[1], D. Reistad[1], U. Tippawan[2,3], D. Wessman[1], V. Ziemann[1], and M. Österlund[2]
[1]The Svedberg Laboratory, Uppsala University, Box 533, S-751 21 Uppsala, Sweden
+46-70-326-3866; fax: +46-18-471-3833; e-mail: Alexander.Prokofiev@tsl.uu.se
[2]Department of Neutron Research, Uppsala University, Sweden
[3]Fast Neutron Research Facility, Chiang Mai University, Thailand

ABSTRACT

A new quasi-monoenergetic neutron beam facility has been constructed at The Svedberg Laboratory (TSL) in Uppsala, Sweden. Key features include an energy range of 20 to 175 MeV, high fluxes and the possibility of large-area fields. The new facility has been designed specifically to provide optimal conditions for testing of single-event effects in electronics. First results of the beam characterization measurements are reported. [*Keywords:* neutron; neutron beam; cyclotron; neutron-induced SEE; SEE testing]

INTRODUCTION

Testing of neutron-induced single-event effects (SEE) in semiconductor materials using the natural flux of cosmic neutrons is time-consuming. To speed up the measurements, one needs to use neutron beams produced with particle accelerators.

The procedures for the accelerated testing of memory devices are summarized in the recent JEDEC standard [1]. According to the standard, one of the ways to perform the accelerated testing is to irradiate a device under study by monoenergetic neutrons with nominal energies of 20, 50, 100, and 150 MeV. Such an approach is a viable alternative to the testing with a "white" neutron spectrum, if the intensity of monoenergetic neutrons is enough to cause reasonably high SEE rates.

To satisfy these needs, an upgrade of the old neutron facility [2] at The Svedberg Laboratory (TSL) has been undertaken with a primary goal to increase the neutron beam intensity and, thereby, to make the facility competitive for SEE testing and for studies of SEE mechanisms. In addition, the new facility offers an unsurpassed flexibility of the neutron beam properties, like energy and geometrical shape.

TECHNICAL SPECIFICATION

An overview of the neutron beam facility is presented in Fig. 1. The facility makes use of the proton beam from the Gustaf Werner cyclotron with the energy variable in the 20-180 MeV range. The quasi-monoenergetic neutron beam is produced via the ^{7}Li(p,n)^{7}Be reaction. The proton beam is incident on a target of lithium, enriched to 99.99% in ^{7}Li. The available lithium targets are 2, 4, 8, 16, and 24 mm thick. The targets are rectangular in shape, 20x32 mm, and are mounted in a remotely controlled water-cooled copper rig. Typically, proton energy loss in the target amounts to 2-6 MeV depending on the incident proton energy. An additional target position contains a fluorescent screen viewed by a TV camera, which is used for beam alignment and focusing. Downstream the target, the proton beam is deflected by a magnet into a 10-m long dumping line, where it is guided onto a heavily shielded water-cooled graphite beam dump.

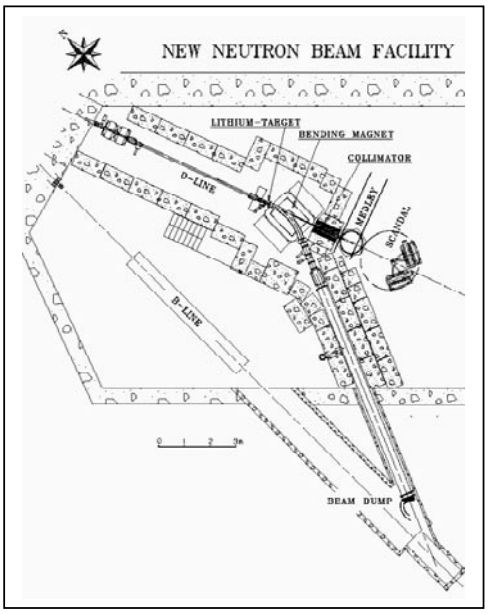

FIGURE 1. AN OVERVIEW OF THE NEUTRON BEAM FACILITY

The neutron beam is formed geometrically by a cylindrically shaped iron collimator block, 50 cm in diameter and 100 cm long, with a cylindrical or conical hole of variable diameter. The collimator is surrounded by concrete to form the end wall of the production line towards the experimental area. Thereby, efficient shielding from the production target region is achieved. A modular construction of the collimator allows the user to adjust the diameter of the neutron beam to the needs of a specific experiment. At present, the available collimator openings are 2, 3, 5.5, 10, 15, 20, and 30 cm. The collimators are swiftly changeable. Other collimator diameters in the 0-30 cm range, as well as other shapes than circular can be provided upon request. After passing the collimator, neutrons reach the experimental area at a distance of about 3 m from the production target. Beam diameters of up to 1 m are obtainable at a larger distance from the production target. The increased diameter of the beam may be used for testing a larger number of devices simultaneously, or larger devices like entire electronic boards.

CHARACTERIZATION OF THE FACILITY

The measured contamination of the neutron beam at the experimental area due to interactions of the primary protons with beam transport elements such as the target frame did not exceed 0.2%. Such interactions only leads to a minor surplus of neutrons in the experimental area because charged particles produced near the lithium target and upstream are removed by the deflection magnet. The relative contamination of protons with energies above 15 MeV

in the neutron beam is about 10^{-5}. These measurements have been performed for a proton beam energy of 98 MeV.

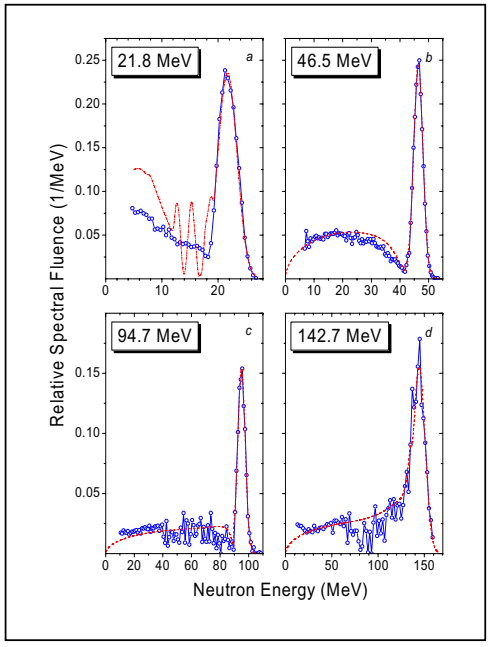

FIGURE 2. THE NEUTRON SPECTRA AT 0° FOR DIFFERENT PEAK NEUTRON ENERGIES (SEE TABLE 1 FOR INCIDENT PROTON ENERGIES AND ^{7}LI TARGET THICKNESSES). SYMBOLS CONNECTED BY A SOLID LINE REPRESENT EXPERIMENTAL DATA OBTAINED IN THE PRESENT WORK. PREDICTIONS ARE SHOWN AS DASHED LINES (SEE TEXT).

Neutron spectra have been obtained by measuring elastic *np*-scattering with the Medley setup [3]. The measured neutron spectra for four peak energies between 24.7 and 147.4 MeV are shown in Fig. 2. The peak energies are chosen in compliance with recommendations of the JEDEC standard [1]. The measurements are compared with the systematics by Prokofiev *et al.* [4] for the three higher energies (Fig. 2b-d). The systematics is not applicable at the lowest beam energy (Fig. 2a). Instead, an evaluation of Mashnik *et al*. [5] was employed for the description of the neutron spectrum. The differential cross-section for high-energy peak neutron production at 0° was obtained by multiplication of the total cross-section of the ^{7}Li(p,n)^{7}Be reaction [5] to the "index of forwardness" from the systematics of Uwamino *et al*. [6]. The narrow peaks in the upper continuum region correspond to excitation of higher states in residual ^{7}Be nuclei. This process was included in the model calculation of Mashnik *et al*. [5]. However, the energy resolution in the experiment does not allow us to observe these peaks. The experimental data agree with the calculations except for the region below 10 MeV in the 24.7 MeV spectrum where the model overpredicts the experimental results by up to a factor of 2. Table 1 summarizes the main features of the measured spectra and the achieved neutron fluxes. The later has been measured with the thin-film breakdown counter (TFBC) [7]. Another monitoring option is provided by an ionization-chamber monitor (ICM). Both monitors utilize neutron-induced fission of ^{238}U. This reaction possesses well-known cross-section recommended as standard [8]. Finally, a Faraday cup, installed in the proton beam dump, integrates the beam current and offers relative monitoring of the beam intensity.

As seen in Fig. 2, the neutron spectrum is dominated by a peak situated a few MeV below the energy of the primary protons and comprising about 40% of the total number of neutrons. The fact that the spectrum has a low-energy tail requires that a proper correction is applied to measured SEE rates. The correction can be obtained using an iterative unfolding procedure, as it is discussed in another contribution to this Symposium [9].

SUMMARY AND OUTLOOK

A new neutron beam facility has been constructed at TSL and is available for regular operation. It is capable to deliver neutrons in the 20-175 MeV range, which makes TSL the only laboratory in the world offering full monoenergetic neutron testing according to the JEDEC standard. First beams for commercial electronics testing have been delivered.

REFERENCES

[1] JEDEC Standard. *Measurements and Reporting of Alpha Particles and Terrestrial Comic Ray-Induced Soft Errors in Semiconductor Devices*. JESD89, August 2001.
[2] J. Klug, *et al.*, *Nucl. Instrum. Methods Phys. Res. A* **489**, 282 (2002).
[3] S. Dangtip, *et al.*, *Nucl. Instrum. Methods Phys. Res. A* **452**, 484 (2000).
[4] A. V. Prokofiev, *et al.*, *J. Nucl. Sci. Techn.*, Suppl. 2, 112 (2002).
[5] S. G. Mashnik, *et al.*, LANL Report LA-UR-00-1067 (2000).
[6] Y. Uwamino, *et al.*, *Nucl. Instrum. Methods Phys. Res. A* **389**, 463 (1997).
[7] A. N. Smirnov, *et al.*, *Radiat. Meas.* **25**, 151 (1995).
[8] A. D. Carlson, *et al.,* in *Proc. Int. Conf. on Nuclear Data for Science and Technology*, Trieste, Italy, May 19-24, 1997, p. 1223-1229 (1997).
[9] M. Olmos, *et al.*, "Unfolding Procedure for SER Measurements Using Quasi-Monoenergetic Neutrons", submitted to this Symposium.

TABLE 1. NEUTRON BEAM PARAMETERS. THE FLUXES REFER TO THE ENTRANCE OF THE EXPERIMENTAL HALL.

Proton beam energy (MeV)	Li target thickness (mm)	Proton beam current (μA)	Resulting average energy of peak neutrons (MeV)	Fraction of neutrons in the mono-energetic peak (%)		Peak neutron flux (10^5 neutrons/(cm^2 s))
				measured	calculated	
24.68 ± 0.04	2	10	21.8	~50	--	1.3
49.5 ± 0.2	4	10	46.5	39	36	2.9
97.9 ± 0.3	8	5	94.7	41	39	4.6
147.4 ± 0.6	24	0.6	142.7	55 [1)]	40	2.1

[1)] upper limit due to poor energy resolution.

Appendix XXV

For Official Use **NEA/SEN/NSC(2005)3**

Organisation de Coopération et de Développement Economiques
Organisation for Economic Co-operation and Development **12-Jul-2005**

English text only

NUCLEAR ENERGY AGENCY
NUCLEAR SCIENCE COMMITTEE

NEA/SEN/NSC(2005)3
For Official Use

SUMMARY RECORD

Sixteenth Meeting of the Nuclear Science Committee

8-10 June 2005
NEA Headquarters Issy-les-Moulineaux

English text only

JT00187638

Document complet disponible sur OLIS dans son format d'origine
Complete document available on OLIS in its original format

TABLE OF CONTENT

SUMMARY RECORD OF THE SIXTEENTH MEETING OF THE NUCLEAR SCIENCE COMMITTEE

8-10 June 2005

The Chair, **T. Lefvert**, opened the meeting and welcomed the delegates. The following two new members of the committee were announced: **Walter Tromm**, Germany (replacing **D. Cacuci**) and **Desmond MacMahon**, UK (replacing **D. Simister**). **C. Ganguly**, head of the IAEA Fuel Cycle and Materials section, participated for the first time.

B. Briggs, chairman of the Working Party on Nuclear Criticality Safety (WPNCS) was invited to present the status of the Working Party. **C. Dean**, UK and **M. Kellett**, IAEA were invited for the in-depth discussion on "Performance of the JEFF-3 data library" and **F. D'Auria**, Italy, **E. Royer**, France and J**-M. Martinez**, France were invited for the in-depth discussion on "Uncertainty analysis in modelling".

Apologies for absence had been received from **E. Nonbøl**, Denmark, **Y.-J. Kim**, Korea, **W. Wiesenack**, Norway, **N. Olsson**, Sweden and **J. Herczeg**, US. **F. Goldne**r, US replaced **J. Herczeg**. A list of participants is given in Annex 1.

Adoption of the Agenda **[NEA/SEN/NSC(2005)1]**

The proposed agenda was adopted without modifications. The in-depth discussions were scheduled for the morning of the second day (9 June 2005).

Introduction by the Director General

In the absence of the NEA Director General, **T. Dujardin,** Deputy Director, informed the committee of recent events in the nuclear field, with special focus on the OECD and the NEA. He highlighted the fact that the World Energy Council had, at their congress in Sidney in 2004 and for the first time since many years, discussed nuclear energy at the same level as all other energy sources, concluding that "all energy options must be kept open and no technology should be idolised or demonised". He also mentioned that the OECD and NEA had cooperated in the organisation of the IAEA International Ministerial Conference on Nuclear Power in the 21st Century, and that the OECD Secretary General had addressed the 2004 ANS meeting on the role of nuclear energy for limiting green-house gas emission.

T. Dujardin described the OECD outreach policy and noted that the NEA was encouraged to increase the cooperation with Russia and China, based on criteria of mutual benefit. He also mentioned that the Generation-IV International Forum (GIF) framework agreement had been signed at the French embassy in Washington DC, US on 28 February 2005, that the OECD Secretary General is the depositary of the international treaty and that the NEA acts as the technical secretariat of GIF.

At its meeting in April 2005, the NEA Steering Committee had approved the new mandates of all standing technical committees, including the NSC and its Executive Group. From the Steering Committee meeting it was also noted that the French authorities asked the NEA to organise peer-reviews of the scientific reports prepared according to the 1991 law on nuclear waste, and that **W. Magwood** stepped down as chairman of the Steering Committee. Moreover, **T. Dujardin** informed the committee that any feedback on the IAEA report on Multilateral Approaches to the Nuclear Fuel Cycle (MNA) could be communicated to him.

The annual coordination meeting between the NEA and the IAEA had mainly been devoted to nuclear safety issues. The cooperation with the IEA had for example resulted in a joint publication on the cost of electricity generation, and in participation in a workshop on "security of supply", an issue which will be the subject of the next policy debate in the NEA Steering Committee.

Finally, **T. Dujardin** informed the committee that **Stan Gordelier** had replaced **Peter Wilmer** as head of the NEA Nuclear Development Division and that **Julia Schwartz** had replaced **Patrick Reyners** as head of the NEA Legal Section. **Yolanda Rugama** and **Hans Henriksson** had recently joined the Data Bank to work mainly on nuclear data related activities.

Self-evaluation of Committee Meetings

The OECD Council has decided to encourage all OECD committees to evaluate the general usefulness and the impact in member countries of their programme of work, as well as the committee meetings themselves, as part of the need to prioritise work and to assess the added value of each committee. The NSC Secretariat had, in line with this decision, developed a questionnaire, which was distributed to all delegates. The NSC members were asked to return the questionnaire to the Secretariat by the end of June 2005.

The chair asked if the Secretariat could provide a list of NSC activities during the last five years, indicating, for each activity, the planned and actual duration, as well as the expected and real output. Such a list was considered useful as background information when filling in the questionnaire. The Secretariat agreed to provide the requested list.

Approval of the Summary Record of the 15th Meeting [NEA/SEN/NSC(2004)3]

The summary record of the fifteenth meeting of the NSC was approved without modifications.

Status of Committee Projects [NEA/SEN/NSC(2005)2]

Review of progress of the NSC Working Parties

Working Party on Scientific Issues of Reactor Systems (WPRS)

K. Hesketh, chair of WPPR, informed the committee that the Working Party had met for the first time in September 2004 and planned to hold its second meeting in the second half of June 2005 in conjunction with the WPFC. The WPRS had so far mainly maintained continuity with the former WPPR, and continued to hold their meetings in conjunction with the Expert Group on Reactor-based Plutonium Disposition (TFRPD), but the scope was being re-directed and expanded in line with new WPRS mandate, agreed by the NSC in June 2004. A number of activities related to High Temperature Reactors (HTR) were undertaken, such as a PBMR core physics benchmark, and a workshop on PBMR coupled neutronics/thermal-hydraulics. The PWR related activities comprised benchmark on a rod ejection in a MOX fuelled PWR core and a benchmark on discharge isotope inventories as a function of burn-up. Among the new proposals were mentioned Generation-IV associated activities related to lead fast reactors, to Uranium nitride cores, and to super critical water reactors.

R. Chawla asked if the proposed new activities were decoupled from the Generation-IV International Forum (GIF) project. **K. Hesketh** answered that there were no formal links between WPRS and GIF, and that the WPRS activities were complementary to the more technology focused GIF activities. **T. Lefvert** asked about the availability of experts and **K. Hesketh** replied that he was not aware of the resources allocated to GIF, but expected that some experts would be working in both GIF and WPRS activities.

C. Ganguly notified the NSC that the IAEA conducted projects related to nitride fuel and asked if the WPRS would be devoted to mixed nitride or only to uranium nitride fuels. **K. Hesketh** answered that this would be decided at a future WPRS meeting.

Working Party on Scientific Issues of the Fuel Cycle (WPFC)

B-C. Na presented the status of work in the WPFC. The work of the three subgroups covers accelerator utilisation, fuels and materials, and chemical partitioning. After having issued, under the former WPPT, a status report on accelerator and spallation target technologies for ADS applications, the subgroup on accelerators is preparing the 5th workshop on "Utilisation and reliability of high power proton accelerators (HPPA)" to be held in Europe in spring 2006. In the field of fuel and materials the WPFC is working on a handbook on Lead-Bismuth Eutectic (LBE) technology. The group will hold its 3rd meeting at SCK-CEN, Mol, Belgium on 30 June-1 July 2005 to review the draft chapters of the handbook. The first version of the handbook would be published in early 2006. The chemical partitioning activity comprised the publication of a state-of-the-art report on national programmes in partitioning, comprising both aqueous and pyro processes. The final report will be published by the end of 2005.

In addition to the subgroups mentioned above, there are also three working groups undertaking studies on detailed flowsheets, on separations criteria and on fuel cycle transition scenarios. After having assisted the NDC Expert Group on the Impact of Advanced Fuel Cycle Options on Waste Management Policies, the group of flowsheet studies is now working on a draft report describing the details and underlying assumptions of individual fuel cycle process flowsheets. A report will be published in early 2006. The WPFC group on separations criteria was established to develop a scientific basis for optimisation of the use of future nuclear waste repositories and to establish a methodology for evaluating impacts of various fuel cycle scenarios on potential repositories and storage. The group had met twice and a third meeting will be held in September 2005. The group devoted to fuel cycle transition scenarios is well advanced. The definition of key issues had been completed, the assessment of technologies was underway and the review of different scenarios had started. A benchmark of system codes for different fuel cycle transition scenarios had been started.

Following questions from **S. Qaim**, **B-C. Na** confirmed that the state-of-the-art report on national programmes in partitioning covered both aqueous and dry processes and that the handbook on LBE technology was limited to lead-bismuth and lead systems only. It was noted that activities related to ADS had been reduced and split between WPFC and WPRS. **A. Hasegawa** stressed the importance of ADS related activities and suggested that they be addressed in a well-structured way in the NSC programme of work.

Working Party on Nuclear Criticality Safety (WPNCS)

B. Briggs, chair of WPNCS, presented a summary of the Working Party activities and the efforts to obtain new experiments to support MOX fabrication. The group on burn-up credit had recently finalised a benchmark on sensitivity to burn-up profile asymmetry and a benchmark on control rod effects on spent fuel composition was underway. The group on source convergence had finalised a report on the analysis of four test problems and considered a proposal for writing guidelines on source convergence issues. The group on criticality excursions was about to publish the results of two transient analysis benchmarks. The group on minimal critical values had recently completed a final report for publication in early autumn 2005. The 2004 edition of the International Criticality Safety Benchmark Evaluation Project (ICSBEP) handbook contained 3331 critical and sub-critical benchmark configurations and it is expected that the 2005 edition will contain about another 300 new configurations.

The efforts to stimulate new experiments to support MOX fabrication had, in 2004, resulted in the recommendations to obtain the release of unpublished experimental data especially the French ERASME/S and the Russian BFS-49 experiments and to define a framework for the selection of new experimental program(s) of interest, specifically for damp MOX. The effort to release the unpublished ERASM/S and BFS-49 experiments had succeeded and the data would be incorporated in future releases of the ICSBEP handbook. Concerning the proposed new experiments, it was concluded that the Russian proposal would be performed within the ISTC framework and that the financial resources for other proposals were presently not available.

T. Dujardin asked if China participated in the ICSBEP project. **B. Briggs** answered that although China had in principle agreed to participate, they had so far not contributed to the project.

Working Party on International Nuclear Data Evaluation Cooperation (WPEC)

A. Koning, chair of WPEC, informed the committee about the status of the WPEC activities. At its meeting in April 2005, the Working Party had reviewed the status of the participating nuclear data evaluation projects and of the associated experimental activities. The longer-term subgroup on nuclear model codes had been completed, whereas the subgroups on formats and on the high priority request list for nuclear data would continue. Five short-term subgroups had been completed and the results would be published later in 2005. The issues covered were: nuclear data standards, activation cross-sections, covariances in the resonance region, assessment of fission product cross-sections and data for improved LEU-LWR reactivity predictions. The following three new short-term subgroups had been established: covariance data in the fast energy region, decay heat calculations and nuclear data needs for advanced reactor systems.

S. Qaim asked how the experimental activities were handled within WPEC, following the merger a few years ago with the Working Party on Measurement Activities (WPMA). **A. Koning** answered that the WPEC provided a framework for information exchange among experimentalists and maintained the High Priority Request List (HPRL) for nuclear data. **P. Rullhusen** informed the committee that the JEFF project had established a specific group on measurement activities, but, as there were not many requests for experiments, they had decided to rely on the HPRL. **J.M. Aragones** asked about the availability of covariance information and **A. Koning** replied that the WPEC was mainly devoted to developing methods and that each evaluation project would then use these methods to evaluate covariances.

Internal organisation of Working Parties

The delegates discussed the differences in structures between the Working Parties. It was noted that WPRS was the only Working Party that hadn't established a sub-structure to handle its activities. It was also noted that the nomenclature of the sub-structures were different. The WPEC had subgroups, the WPNCS had expert groups and WPFC had both subgroups and working groups. It was recognised that it was difficult to establish a unified structure for all Working Parties, due to the differences in activities.

Follow-up to recent NSC organised workshops and meetings

Eighth Information Exchange Meeting on Actinide and Fission Product P&T

B-C. Na presented the outcome of the 8th information exchange meeting on Actinide and Fission Product Partitioning and Transmutation, held at Las Vegas, USA in November 2004. The meeting had been started with a general session covering national and international programmes in P&T, followed by five technical sessions. The theme of the meeting had been on the impact of P&T on waste management strategies. However, comments expressed after the meeting indicated that various aspects of P&T, such as accelerators and nuclear data, had not been properly covered during the meeting and that future meetings should better take into account all aspects of P&T, including waste management aspect.

The 9th meeting in the series will be held in Nîmes, France on 26-28 September 2006.

Third Workshop on Advanced Reactors with Innovative Fuels (ARWIF)

The ARWIF-2005 workshop was held in Oak Ridge, USA on 16-18 February 2005, hosted by the Oak Ridge National Laboratory. The workshop was attended by 50 participants from 11 countries representing 22 different organisations. **E. Sartori** informed the committee that the goal of the workshop was to identify research and development needs for advanced reactor systems and the roles which can be played by existing experimental facilities, as well as possible needs for new experimental facilities. The summary of the workshop and the proceedings will be published in autumn 2005.

Short review of NSC expert groups and task forces

Preservation of Reactor Physics Experiments (IRPhE)

J. Gado introduced the IRPhE project and **E. Sartori** provided more details about the status of evaluations. The integral data considered in IRPhE comprise fundamental mode lattice experiments, heterogeneous core configurations, power reactor start-up data, and specific application experiments. The first technical review meeting, held in December 2004 had been beneficial, especially in clarifying uncertainties in the methodology and interpretation of guidelines for evaluating experimental data. The voluntary contribution by the Japanese Government to support the project was gratefully acknowledged. It was envisaged that the first official IRPhE publication on CD-ROM will be issued in early 2006.

Reactor-based Plutonium Disposition

P. D'Hondt reported on the outcome of the 9th meeting of the group, where both Russia and USA had presented status reports. He also presented the progress in the different activities, covering three benchmarks in the area of MOX fuel behaviour (hollow and full MOX pellets, PRIMO experiment and DOE WG-MOX fuel irradiation) and four benchmarks related to the physics of MOX loaded cores (KRITZ-2, VENUS-2, VENUS-07, and VVER-1000 whole core). As many of these benchmarks were either recently completed or close to completion, it was agreed to review the future of the group at the next NSC, when the mandate of the group was up for renewal.

Basic Phenomena in Fuel Behaviour

E. Sartori reported on the fuel behaviour activities, especially the development of the database on International Fuel Performance Experiments (IFPE) and the fuel related activities in CSNI. The IFPE contains at present 842 cases, with a number of new experiments being released or requested. The IFPE data are also used in the IAEA coordinated Fuel Modelling Exercise, FUMEX-II. The nuclear industry is also making increased use of these data. The CSNI activities related to fuel behaviour comprised one new (PAKS) and three existing (Halden, CABRI and SCIP) separately funded projects.

A proposal to integrate the activity into WPRS was accepted by **K. Hesketh**. **R. Chawla** pointed out that the activity should preserve a clear identity within the new framework and that the connection with CSNI should be highlighted.

Reactor Stability and LWR Transient Benchmarks

J.M. Aragones presented the status of the on-going reactor stability and transient benchmarks. The specifications of the NUPEC BWR Full-Size Fine-Mesh Bundle Test (BFBT) benchmark will be finalised in a meeting at the end of June 2005. The benchmark will consists of two phases, one on void distribution and one on critical power. The committee expressed its gratitude to JNES for having released the BFBT data.

Two meetings, devoted respectively to phase I and phase II of the VVER-1000 benchmark for validation of coupled three-dimensional (3-D) neutron-kinetics/system thermal-hydraulics codes, were held in April 2005. The second volume of the BWR Turbine Trip benchmark has been sent to print and the third volume is expected to be published by the end of 2005. The NEA has also published three reports from the EC coordinated activity CRISSUE-S.

Following the expiration of the mandate of the group, **J.M. Aragones** proposed to integrate the activity into the WPRS framework. This proposal was supported by **R. Chawla**, who felt that such an integration would further strengthen the WPRS contacts with CSNI. The NSC adopted the proposal and asked the WPRS chair, **K. Hesketh**, to report back to the NSC in November 2005 on the integration of the new activities.

Radiation Shielding and Dosimetry

E. Sartori presented the status of activities and proposals for new activities in the areas of radiation shielding and dosimetry. Following the in-depth discussion on "shielding and dosimetry for accelerators" at the last NSC meeting, **P. Vaz** had contacted the Technical Group on Computational Medical Physics and the European Radiation Dosimetry Group (EURADOS) with a proposal to organise benchmark exercises on radiation shielding and dosimetry for non-energy applications. **E. Sartori** also informed the committee that the next SATIF meeting (SATIF-8) would be held in Korea in May 2006, and that the draft specifications for the Skyshine benchmark had been received from the Research and Development Institute of Power Engineering in Moscow, Russia.

I. Kodeli reported on the status of the database of radiation shielding experiments (SINBAD), which presently contained 72 experiments, covering radiation shielding and pressure vessel dosimetry, fusion blanket neutronics, and accelerator shielding. He also described the EU concerted action on Quality Assurance for Numerical Dosimetry (QUADOS), which is part of the CONRAD project.

N. Ramamoorthy informed the NSC that the IAEA had a large programme on medical applications and that the question of cooperation between the two agencies in this area could be discussed at a regular IAEA-NEA coordination meeting.

The delegates discussed whether non-energy related benchmarks should be undertaken by the NSC or not. **T. Dujardin** recalled that the issue had already been discussed by the Steering Committee during the revision of the NEA Strategic Plan. The Steering Committee agreed that the nuclear energy field includes applications of ionizing radiation. However, the Steering Committee stressed that the NEA should keep its focus on nuclear power to avoid dilution of resources and should not deal with non-power topics well covered elsewhere, e.g. within IAEA.

As it became clear that there was no general consensus within NSC to undertake non-energy related benchmarks, the chair concluded that any proposals for such activities would have to be reviewed on a case by case basis. **P. Vaz** was therefore asked to further specify the above-mentioned benchmark proposals and present them to the NSC for approval.

3-D Radiation Transport Benchmarks

B-C. Na described the status of the 3-D extension to the deterministic 3-D MOX fuel assembly transport calculation benchmark. Nineteen participation forms had been received, but some participants had withdrawn their solutions, providing an indication of the difficulty of the benchmark. The solutions provided were compiled and analysed, and a final report is in print. A medical physics computational benchmark was proposed as a follow-up activity.

Considering the conclusions from the discussion of the non-energy related activities above, the NSC did not approve the proposed extension to perform a medical physics computational benchmark, but asked the group to present a proposed new mandate for circulation to the NSC in time for the bureau meeting in December 2005.

High Burn-up Fuel

K. Hesketh informed the committee on the status of the report on Very High Burn-up Fuel Cycles in LWRs. At the last meeting of the group, in November 2004, it had been decided to issue an integrated draft report by February 2005. This report is available for group members to review. The last meeting of the group is scheduled to be held at the end of September 2005, with a target publication date for the final report of early 2006. **K. Hesketh** also presented some preliminary conclusions from the draft report.

R. Chawla expressed concern about some of the preliminary conclusions and asked for a more in-depth review of the report before publication. The NSC agreed to prolong the mandate of the group to provide each member a chance to thoroughly review the report. **K. Hesketh** was asked to circulate the final draft report to all committee members.

Irradiation Induced Property Change of Graphite at High Temperatures

M. Caron-Charles presented the status of the activity devoted to assessing the mechanistic understanding of the relationship between irradiation-induced micro-structural changes and bulk material property changes in graphite, SiC and carbon-carbon (C/C) composites at high temperatures. The first meeting of the expert group, organised to assign work responsibilities, had been held in January 2005 at Manchester, UK. The next meeting of the group would be held in France in September 2005.

Needs of R&D Facilities in Nuclear Science

P. D'Hondt presented the outcome of the first meeting of the expert group on reviewing the status of research and test facilities worldwide and to clarifying future requirements in field of nuclear science. The expected outcome is a report on the subject and a database containing information about research and test facilities in nuclear science. A preliminary table of content of the report has been agreed and the next meeting of the group is planned for the beginning of December 2005. A draft final report should be ready by late autumn 2006. The project is supported by a voluntary contribution from the Japanese Government.

A. Zaetta expressed concern about the large scope of the study. **P. D'Hondt** responded that the expert group was confident that it could cover the large scope thanks to good cooperation with other similar activities, especially the CSNI SFEAR project.

Proposals for new NSC Activities

Study of Pebble Bed and Prismatic Fuel Configurations in HTGRs

At the NSC bureau meeting in December 2004, **Won S. Park** had presented a proposal for a study of pebble bed and prismatic fuel configurations in High Temperature Gas-cooled Reactors (HTGR). The objectives of the study would be to identify the technical issues and to evaluate quantitatively the performance of each type of system for hydrogen and electricity production, considering factors such as technical maturity, in-core safety characteristics, achievable outlet temperature, fuel cycles and possibly economy. The proposal was felt to be too ambitious for a two-year programme, and it was therefore suggested that **W. S. Park**, in collaboration with the NEA Secretariat, would review the availability of input data for the study and return with a more focused proposal to the NSC meeting in June 2005.

M. Caron-Charles presented a proposal comprising three distinct areas of work, namely application of computer codes to reactor physics performance assessment, fuel cycle flow sheet and cost evaluation studies, and integration of HTGs with other nuclear energy systems with special emphasis on the fuel cycle. The global objective was to provide data for the analysis of in-core and out-of-core fuel cycles, using simplified concepts for the prismatic block and the pebble bed-type reactors. Such a performance evaluation was presented as being complementary to GIF projects and as an extension to existing NSC projects within WPRS and WPFC.

A. Hasegawa expressed an unfavourable view on the proposal, as he felt that such studies should be undertaken within the framework of GIF. In addition, he noted that many countries had already performed such studies and that it should be up to each country to select their preferred system. **F. Goldner** expressed concern about the availability of resources for such a study. **A Zaetta** recalled that most of the proposed work areas, including HTR concepts, were already covered by other NSC projects. **R. Chawla** felt that the proposal was still too ambitious and supported **F. Goldner's** proposal to organise a workshop on the subject in about 1-2 years time.

The committee decided that there was presently no support for starting the proposed project in its present form.

Prediction of Irradiation Damage Effects in Reactors

C. Nordborg informed the committee that the chair of ANS, **J. Tulenko**, had, during a recent visit to NEA, asked if the NSC would consider coordinating international activities related to the development of a first principles model and simulation of nuclear fuel and structural material performance. It was noted that there were on-going activities within the Advanced Fuel Cycle Initiative (AFCI) in the US, within the EC coordinated PERFECT project in Europe, and within similar activities in Japan, as presented by **A. Hasegawa**.

The delegates welcomed the proposal and asked the Secretariat to contact the different groups and to present a proposal to the next NSC meeting.

Future NSC organised workshops and meetings

Third Information Exchange Meeting on Nuclear Production of Hydrogen

I. Yamagishi informed the committee about the preparations for the third workshop on Nuclear Production of Hydrogen that would be held at the JAERI Oarai site in Japan on 5-7 October 2005. Thirty-seven persons had so far registered and 30 abstracts had been submitted, in addition to the foreseen seven invited papers.

Workshop on Perspectives on Nuclear Data for the Next Decade

P. Nagel reported on the workshop devoted to the future of theory- and experiment-based nuclear data evaluations. The workshop will be organised by CEA Bruyères-le-Châtel, France on 26-28 September 2005. The scope of the workshop is diverse, encompassing experimental, modelling, and theoretical works, relevant to all aspects of nuclear data evaluation, as envisioned for the next decade. Thirty-five invited presentations and a final round table session are scheduled.

Other Meetings and Sponsorship of Future Conferences

Following a proposal in December 2004 from Korea (KAERI) to organise a 9th conference on Reactor Noise (SMORN-9) under the auspices of the NEA, the NSC Bureau had concluded that this

activity had few links with the rest of the NSC work programme and that a more specific proposal, comprising new issues for SMORN-9, such as instrumentation of future reactors and noise from pumps and valves, should be made before any decision could be taken. After having received the feedback from the NSC Bureau, Korea withdrew its offer to host the SMORN-9 conference.

The IAEA, having a number of activities related to reactor noise, had recently contacted the NEA and expressed an interest to organise the next SMORN meeting. The NSC delegates discussed the request from IAEA and concluded that, as the interest within NSC was limited, the IAEA was welcome to take over the responsibility for the SMORN series of conferences.

A proposal to co-sponsor the Joint International Conference on Mathematics & Computations and Supercomputing in Nuclear Applications (M&C + SNA-2007) in Monterey, USA, on 1-5 April 2007 was endorsed by the committee.

In-depth discussions

Performance of the JEFF-3 Data Library

K. Hesketh introduced the three speakers **A. Koning**, **C. Dean** and **M. Kellett**. **A. Koning** started by outlining the organisation of the JEFF project, by describing the content of the recently released JEFF-3.1 library and by providing a few examples of results from calculations with the TALYS code. He also indicated the plans for the next release of the library (JEFF-3.2), comprising for example more emphasis on minor actinides and on covariance data. **C. Dean** presented the history of the JEFF project and provided a number of illustrations of the performance of the JEFF data for different applications. Finally, **M. Kellett** informed the committee about the compilation and testing of the JEFF-3.1 decay data and fission yield files.

A. Zaetta asked about the availability of experimental facilities and what impact it had on the JEFF project. **A. Koning** answered that the main contributor of experimental data to the JEFF project was IRMM, Geel. The n-TOF facility at CERN had so far not produced many results. **H. Leeb** informed the NSC that the analysis of the n_TOF data was underway and that the future of the facility would be decided in October 2005. It was also noted that most of the evaluated data above 20 MeV were based on model calculations.

J Gado and **R. Chawla** asked about the similarities between different evaluated nuclear data libraries and about the possibility to create a unique file. **A. Koning** replied that it is important to maintain at least two independent projects to be able to compare different methods and approaches to nuclear data evaluation, as is done within the framework of the WPEC. The idea of creating a unique evaluated data file is indirectly a long-term goal of the WPEC in trying to eliminate the most important discrepancies in the major evaluated libraries.

It was concluded that the presentations and the discussion had been useful in preparing for the renewal of the JEFF mandate in June 2006.

Uncertainty Analysis in Modelling

J.M. Aragones started with a general introduction and a presentation of the speakers. The main issue to be discussed was the uncertainty analysis in non-linearly coupled multi-physics methods. **E. Royer** and **J-M. Martinez** presented proposals to combine experiences in multi-physics and uncertainty analysis in international benchmarks. The uncertainty analysis methods for coupled neutronics / thermal-hydraulics transient studies were then presented by **F. D'Auria**.

J.M. Aragones informed the committee that the European NURESIM project would study the methods used in uncertainty analysis and suggested that the NSC could act as a forum for Europe, Japan and US to discuss the subject. **R. Chawla** and **J.M. Aragones** noted that the NSC and the Data Bank were already involved in the first two steps of a chain of uncertainty analysis shown by **F. D'Auria** (nuclear data and neutronics benchmarks) and that this part of the chain could be tested in a benchmark exercise.

The committee agreed to the last proposal above and asked **J.M. Aragones** and **R. Chawla** to prepare a more specific proposal that could be circulated to the NSC well before the NSC bureau meeting in December 2005.

Report from the 14th meeting of the NSC Executive Group

P. D'Hondt presented a summary of the Executive Group meeting held in the morning of 8 June 2005. The report is given in Annex 2.

J.M. Aragones suggested that the Data Bank should, within available resources, consider extending further the computer program activities to include recent "open source" code management methods in co-ordination with the code authors.

T. Dujardin explained the delay in the signing of the exchange agreement between the NEA Data Bank and the US DOE and **F. Goldner** agreed to investigate possibilities to speed up the procedure.

The committee endorsed the presented programme of work and budget for the NEA Data Bank for 2006.

Cooperation with CSNI

J. Reig introduced a document proposing methods for an enhanced cooperation between the NSC, including its Executive Group, and the CSNI, in line with the recently adopted Strategic Plan of the NEA. The document consists of a main part, describing the main responsibilities of each committee and ways to cooperate, and an appendix providing more details about the current activities of each committee. The appendix would be updated at regular intervals.

The committee agreed to a proposal by **T. Lefvert** to provide feedback and comments on the document to the NEA Secretariat before 1 October 2005. The comments from all concerned committees would then be incorporated and a new version that would be sent to the committees for final approval by the time of the NSC bureau meeting in December 2005.

Reports from other NEA Divisions and other International Organisations

The NEA Nuclear Safety and Nuclear Development divisions

Nuclear Safety

J. Reig informed the committee that the CSNI and CNRA had recently issued a joint strategic plan to face the main challenges in the area of nuclear safety. He also described the many joint research projects undertaken by the CSNI. More detailed information was given on the SFEAR activity, of interest to the NSC project on "Needs of R&D Facilities in Nuclear Science", and the SEGFSM activity, focusing on high burn-up fuel issues.

Nuclear Development

E. Bertel described four NDC activities of relevance to the NSC programme of work: "Impact of advanced fuel cycles on waste management policies", which had received support from the WPFC, "Innovation in nuclear energy technology" and "Management of recycled fissile materials", both presented also at the last NSC meeting, and the preparations for the "9th Information Exchange meeting on P&T", jointly organised with the NSC.

The EC

P. Rullhusen provided information on selected EC framework programmes and Joint Research Centre (JRC) activities. The EUROTRANS project within the 6th framework programme was described, as well as a Technology Platform on Partitioning and Transmutation and the NUDAME and EFNUDAT initiatives in relation to nuclear data activities at IRRM, Geel.

The IAEA

In his presentation, **N. Ramamoorthy** put special emphasis on the work programme of the IAEA Nuclear Data Section and its close cooperation with the NEA Data Bank. He also highlighted the IAEA participation in the WPEC and JEFF projects, and described the IAEA organised workshops at ISTC, Trieste.

C. Ganguly presented the IAEA programme and activities on the nuclear fuel cycle and materials, comprising mainly the areas of uranium production cycle and environment, water-cooled fuel performance and technology, management of spent fuel from power reactors, and topical nuclear fuel cycle issues and information systems.

Next NSC meeting

Date of next meeting

It was agreed to hold the next meeting of the committee on 31 May-2 June 2006, at the NEA Headquarters in Issy-les-Moulineaux, France.

After the present NSC meeting, it has been decided that the NSC bureau will meet on 13 December 2005.

Topics for in-depth discussion

The delegates were reminded of last year's proposal by **R. Chawla** to discuss the "progress of advanced reactor concepts". **T. Dujardin** proposed to organise a follow-up to the debate of the preliminary conclusions of the NSC expert group on Very High Burn-up Fuels.

The committee noted that each of the above proposals could easily fill a complete morning session, so the final decision on the in-depth discussion would also have to consider the limitations of the subject(s) chosen. Delegates were encouraged to communicate additional proposals in time for the final decision by the NSC bureau in December 2005.

Election of Committee Officers

The chair was handed over to **T. Dujardin**, who suggested re-electing the chair and vice-chair. As no other proposals were forwarded, the committee unanimously re-elected the bureau for one year.

Any other business

J.M. Aragones asked whether Working Parties could consider organising meetings in different member countries. **T. Dujardin** answered that, although it was not excluded, it could cause a problem for the Secretariat to participate due to limitations in the regulations and the available resources for official travel.

It was agreed that the Secretariat would circulate, within one week, a list of actions adopted at the meeting

Annex 1

List of Participants

AUSTRIA

LEEB, Helmut
Atominstitut der Österreichischen Universität
Technische Universität Wien
Wiedner Hauptstrasse 8-10
A-1040 WIEN

Tel: +43 (0)1 58801 14258
Fax: +43 (0)1 58801 14299
Eml: leeb@kph.tuwien.ac.at

BELGIUM

D'HONDT, Pierre Joseph
Director Reactor Safety
SCK-CEN
200 Boeretang
B-2400 MOL

Tel: +32 14 33 22 00
Fax: +32 14 32 15 29
Eml: pdhondt@sckcen.be

CZECH REPUBLIC

KROUZEK, Petr
Counsellor
Delegation of the Czech Republic to the OECD
40, rue Boulainvilliers
75016 PARIS

Tel: +33 (0)1 45 20 35 47
Fax: +33 (0)1 45 20 35 54
Eml: petr_krouzek@mzv.cz

MACH, Rostislav
Nuclear Physics Institute
Academy of Science
CZ-250 68 Rez

Tel: +420 (2) 66172136
Fax: +420 (2) 20941002
Eml: mach@ujf.cas.cz

FINLAND

ANTTILA, Markku
VTT Processes
P.O. Box 1604
FIN-02044 VTT

Tel: +358 20 722 5012
Fax: +358 20 722 5000
Eml: Markku.Anttila@vtt.fi

FRANCE

GUERIN, Yannick
CEA
Department of Fuel Studies
Cadarache, Bat. 151
F-13108 St. Paul-lez Durance Cedex

Tel: +33 4 42 25 79 14
Fax: +33 4 42 25 47 47
Eml: yannick.guerin@cea.fr

MADIC, Charles
CEA/Saclay
Direction de l'Energie Nucléaire
DEN/DDIN, Bat. 125
F-91191 Gif-sur-Yvette

Tel: +33 1 69 08 82 07 / (4) 66 79
Fax: +33 1 69 08 79 90 /(4) 66 79 6
Eml: charles.madic@cea.fr

ZAETTA, Alain
CEA-DEN/DER
Cadarache
Bat. 707 – B.P. 1
F-13108 St.-Paul-lez-Durance

Tel: +33 (0) 4 42 25 27 61
Fax: +33 (0) 4 42 25 76 27
Eml: alain.zaetta@cea.fr

GERMANY

QAIM, Syed M.
Institut fuer Nuklearchemie
Forschungszentrum Juelich
Postfach 1913
D-52425 JUELICH

Tel: +49 (2461) 613282 / 614141
Fax: +49 (2461) 612535
Eml: s.m.qaim@fz-juelich.de

SCHOLTEN, Christoph
Counsellor
Delegation of Germany to the OECD
9, rue Maspéro
F-75116 PARIS

Tel: +33 (0)1 55 74 57 08
Fax: +33 (0)1 55 74 57 40
Eml: christoph.scholten@germany-oecd.org

TROMM, Th. Walter
Programme Manager
Nuclear Safety Research Program
Forschungszentrum Karlsruhe GmbH
P.O Box 3640
D-76344 Eggenstein-Leopoldshafen

Tel: +49 7247 82 55 09
Fax: +49 7247 82 55 08
Eml: walter.tromm@nuklear.fzk.de

HUNGARY

GADO, Janos
Director
KFKI Atomic Energy Research Institute
1121 Budapest
Konkoly Thege Miklos u. 29-33
H-1525 Budapest, Pf. 49

Tel: +36 1 395 9159
Fax: +36 1 395 9293
Eml: gado@sunserv.kfki.hu

ITALY

MENAPACE, Enzo
E.N.E.A. C.R. E. Clementel
Division for Advanced Physics Technology
Via Don G. Fiammelli 2
I-40128 BOLOGNA

Tel: +39 051 60 98 239
Fax: +39 051 60 98 359
Eml: enzo.menapace@bologna.enea.it

JAPAN

HASEGAWA, Akira
Deputy Director
Department of Nuclear Energy System
Japan Atomic Energy Research Institute
2-4 Shirakata, Tokai-mura, Naka-gun
Ibaraki-ken 319-1195
Tel: +81 29 282 6929
Fax: +81 29 282 6122
Eml: hasegawa@ndc.tokai.jaeri.go.jp

MORI, Takamasa
Research Group for Reactor Physics
Department of Nuclear Energy System
Japan Atomic Energy Research Institute
Shirakta-shirane, Tokai-mura, Naka-gun
Ibaraki-ken, 319-1195
Tel: +81 29 282 5360
Fax: +81 29 282 6122
Eml: mori@mike.tokai.jaeri.go.jp

TAKEUCHI, Ei
First Secretary
Permanent Delegation of Japan to the OECD
11, Avenue Hoche
F-75008 PARIS
Tel: +33 (0)1 53 76 61 81
Fax: +33 (0)1 45 63 05 44
Eml: takeuchi@deljp-ocde.fr

NETHERLANDS

KONING, Arjan
NRG Nuclear Research and Consultancy Group
Building 34.213
Westerduinweg 3, P.O. Box 25
NL-1755 ZG PETTEN
Tel: +31 (224) 56 4051
Fax: +31 (224) 56 8490
Eml: koning@nrg-nl.com

PORTUGAL

VAZ, Pedro
Instituto Tecnologico e Nuclear/DPRSN
Estrada Nacional 10
P-2686-953 SACAVEM
Tel: +351 21 994 62 30
Fax: +351 21 994 19 95
Eml: pedrovaz@itn.mces.pt

SLOVAK REPUBLIC

BAHNA, Ján
VUJE
Dept. 0190
Okruzna 5
918 64 TRNAVA
Tel: +421 33 599 1197
Fax: +421 33 599 1157
Eml: bahna@vuje.sk

SPAIN

ARAGONES BELTRAN, Jose Maria
Dpto. Ingenieria Nuclear
ETSI-Industriales
Univ. Politecnica de Madrid
Jose Gutierrez Abascal 2
E-28006 MADRID
Tel: +34 91 336 3108
Fax: +34 91 336 3002
Eml: arago@din.upm.es

PENA GUTIERREZ, Jorge
Desarrollo de Aplicaciones
Computing Centre
Consejo de Seguridad Nuclear
C/ Justo Dorado, 11
E-28040 MADRID
Tel: +34 91 346 0123
Fax: +34 91 346 0275
Eml: jpg@csn.es

SWEDEN

LEFVERT, Tomas
Director, Swedish Center for Nuclear Tech
Dept. of Physics, Royal Institute of Tech
Stockholm Center for Astronomy,
Physics and Biotechnology
SE-106 91 Stockholm
Tel: +46 8 55 37 82 25
Fax: +46 8 20 80 76
Eml: tomas@physics.kth.se

SWITZERLAND

CHAWLA, Rakesh
Laboratory for Reactor Physics
and Systems Behaviour
Paul Scherrer Institute
CH-5232 VILLIGEN PSI
Tel: +41 56 310 23 26
Fax: +41 56 310 23 27
Eml: Rakesh.Chawla@psi.ch

UNITED KINGDOM

HESKETH, Kevin
British Nuclear Fuels plc
Nexia Solutions
B709 Springfields
Salwick Preston
Lancashire PR4 0XJ
Tel: +44 1772 76 23 47
Fax: +44 1772 76 24 70
Eml: Kevin.W.Hesketh@nexiasolutions.com

MACMAHON, T. Desmond
Quality of Life Division
National Physical Laboratory
Hampton Road
Teddington
Middlesex TW11 0LW
Tel: +44 20 8943 8573
Fax: +44 20 8943 8700
Eml: desmond.macmahon@npl.co.uk

UNITED STATES OF AMERICA

BRIGGS, J. Blair
Idaho National Laboratory
P.O. Box 1625, MS-3860
2525 North Fremont
IDAHO FALLS, ID 83415-3860
Tel: +1 (208) 526 7628
Fax: +1 (208) 526 2930
Eml: j.briggs@inl.gov

GOLDNER, Frank
Technical Director, USDOE AFCI Program
U.S. Department of Energy
1000 Independence Ave.
Washington, DC 20585
Tel: +1 301 903-3346
Fax: +1 301 903-0180
Eml: frank.goldner@nuclear.energy.gov

LISANN, Beth G.
Science Advisor for Energy Affairs
United States Delegation
to the OECD
12, avenue Raphael
F-75016 PARIS
Tel: +33 (0)1 45 24 74 59
Fax: +33 (0)1 45 24 74 68
Eml: lisanneg@usoecd.org

INTERNATIONAL ORGANISATIONS

GANGULY, C.
Head, Fuel Cycle & Materials Section
Dept. of Nuclear Energy
IAEA
P.O.Box 100
A-1400 WIEN
Tel: +43 1 2600 22766
Fax: +43 1 26007
Eml: c.ganguly@iaea.org

KELLETT, Mark A.
IAEA
Nuclear Data Section
P.O. Box 100
A-1400 Vienna
Tel: +43 1 2600 21708
Fax: +43 1 2600 721708
Eml: M.A.Kellett@iaea.org

RAMAMOORTHY, N.
Director
Division of Physical and Chemical Science
Dept. of Nuclear Sciences and Application
IAEA
P.O. BOX 100
A-1400 Vienna
Tel: +43 1 2600 21700
Fax: +43 1 26007
Eml: n.ramamoorthy@iaea.org

RULLHUSEN, Peter
EC – JRC - Institute for Reference
Materials and Measurements
Joint Research Center
Retieseweg 111
B-2440 GEEL
Tel: +32 (14) 57 14 76
Fax: +32 (14) 57 18 62
Eml: peter.rullhusen@cec.eu.int

Nuclear Energy Agency (NEA)

DUJARDIN, Thierry Deputy Director, Science and Development	Tel: +33 1 45 24 10 06 Eml: thierry.dujardin@oecd.org
REIG, Javier Head, Nuclear Safety Division	Tel: +33 1 45 24 10 50 Eml: javier.reig@oecd.org
BERTEL, Evelyne Deputy Head, Nuclear Development Division	Tel: +33 1 45 24 10 65 Eml: bertel@nea.fr
NORDBORG, Claes Head, Nuclear Science Section	Tel: +33 1 45 24 10 90 Eml: nordborg@nea.fr
SARTORI, Enrico Data Bank	Tel: +33 1 45 24 10 72 Eml: sartori@nea.fr
CARON-CHARLES, Marylise GIF technical secretariat	Tel: +33 1 45 24 10 70 Eml: marylise.caron-charles@oecd.org
GALAN, Juan Data Bank	Tel: +33 1 45 24 10 08 Eml: galan@nea.fr
HREHOR, Miroslav Nuclear Safety Division	Tel: +33 1 45 24 10 58 Eml: miroslav.hrehor@oecd.org
JERNG, Dong-Wook GIF technical secretariat	Tel: +33 1 45 24 10 75 Eml: dongwook.jerng@oecd.org
KODELI, Ivo IAEA representative at the NEA Data Bank	Tel: +33 1 45 24 10 74 Eml: kodeli@nea.fr
NA, Byung-Chan Data Bank	Tel: +33 1 45 24 10 91 Eml: na@nea.fr
NAGEL, Pierre Data Bank	Tel: +33 1 45 24 10 82 Eml: nagel@nea.fr
YAMAGISHI, Isao Nuclear Science Section	Tel: +33 1 45 24 11 52 Eml: yamagishi@nea.fr

Annex 2

Report to the Nuclear Science Committee from the 14th Meeting of the Executive Group

Pierre D'Hondt

Introduction

1. 17 delegates from 11 member countries attended the meeting, including one delegate from the EC and two from the IAEA. **Walter Tromm**, Germany and **Desmond MacMahon**, UK participated for the first time.

2. **Thierry Dujardin** started by introducing two new staff members, **Yolanda Rugama** and **Hans Henriksson**, who replaced **Ali Nouri** and **Mark Kellett** respectively. He informed the delegates that the new, more concise mandate for the Nuclear Science Committee and the Executive Group had been approved by the NEA Steering Committee in April 2005. He also expressed optimism about the prospects of having the new exchange arrangement between the Data Bank and the US DOE signed in the course of the next few months.

Progress report and programme of work

Nuclear data services

3. **Hans Henriksson** informed the Executive Group that the compilation of experimental nuclear data into the EXFOR database had proceeded as planned in 2004 with close to 200 new data sets entered. The effort to transform the bibliographic CINDA database to a new format, that would incorporate also gamma and charged-particle data, had started and the new database was expected to be available in late autumn 2005. The Data Bank had also assumed the task to revise and maintain the High Priority Request List for nuclear data coordinated by the NSC Working Party on International Nuclear Data Evaluation Co-operation (WPEC).

4. **Yolanda Rugama** presented the work on the JEFF project that led up to the release of the JEFF-3.1 library in May 2005. The new library is composed of a general purpose file, an activation file, a radioactive decay data file, a fission yield file, a proton file and a thermal scattering law file. All files have been systematically checked for format and physics errors and have undergone a first round of benchmark testing. It is envisaged to continue the testing of the library and to develop and distribute application libraries for MCNP and TRIPOLI, based on JEFF-3.1. It was also noted that a new version of the nuclear data-plotting software JANIS (JANIS-2.2) would be released in June 2005.

5. **Federico Mompean** gave an overview of the status of the separately funded Thermochemical database (TDB) project. The last reviews from the second phase of the project, comprising data for Zirconium, Selenium, Nickel and selected organic compounds, had now been published or sent to the publisher for printing. The third phase of the project covers evaluation of inorganic complexes and compounds of Thorium, Iron, Tin and a specific expert team focusing on Solid Solutions. It is planned to finish this phase of the project by the end of 2006.

Computer program services

6. **Enrico Sartori** presented the statistics about computer program services in 2004. The Data Bank had acquired 55 new or revised versions of computer codes and had dispatched close to 1 850 programs. The distribution of computer codes was somewhat less than in recent years, mainly due to the fact that the co-operative arrangement between US-DOE and NEA Data Bank was not in force during the last three years. The distribution of integral data sets was however higher than normal in 2004, with close to 3 500 data sets distributed. The Data Bank had also issued five electronic newsletters and two new editions of the program abstracts on CD-ROM. Three tutorial courses had been organised in conjunction with the International Conference on Radiation Shielding in May 2004 and one training course on PENELOPE-2003 (electron-photon transport code) had been held in Barcelona, Spain in October 2004.

7. **Ivo Kodeli** reported on the computer program and integral data services to non-OECD countries, which in 2004 amounted to a total of 1 060 dispatched packages, out of the 5 318 packages dispatched by the Data Bank in 2004. The number of distributed programs originating in a non-OECD member country was 256.

Computational methods

8. **Juan Galan** introduced a session where the progress in the project to develop a graphical user interface allowing the user to solve radiation transport problems (the GERALD project) and the project to update the SUSD3D code for sensitivity and uncertainty analysis were presented by **Cassiano de Oliveira** and **Ivo Kodeli** respectively.

In-house computer system

9. **Pierre Nagel** described the in-house software development activities and the improvements to the Data Bank's computer system. It was noted that the special efforts in 2004 to improve the overall security and performance of the computer installation comprised the installation of a new network monitoring system and of a more efficient e-mail spam filter.

Future perspectives and priorities for the Data Bank

10. **Thierry Dujardin** introduced the subject, added to the agenda following the request of the chair, by observing that a new strategic plan for 2005-2009 had recently been adopted following broad consultations with member countries. He noted that apart from the Data Bank core activities, i.e. knowledge preservation and services to member countries as well as to other parts of NEA, the available expertise and resources in the secretariat were limited and any additional activities would have to be clearly prioritised. He also posed questions related to a possible closer NEA cooperation with EC, to the format of the Executive Group meetings and to the amount of Data Bank provision of expertise to other parts of the NEA. **Enrico Sartori** noted that, in recent years, the Data Bank had received fewer European codes and asked the delegates to assist in trying to release more codes from, for example, EC coordinated activities.

11. The Executive Group discussed possible future perspectives and it was suggested that the Data Bank should try to obtain more feedback on the present activities by intensifying the collaboration with users. This feedback could then be used as a basis for a further development of the services and to better anticipate requests.

Proposed budget for 2006

12. **Claes Nordborg** presented the proposed Data Bank budget for 2005-2006, which the OECD Council had approved in December 2004 on the basis of an overall nominal increase of 1.9% in 2005 and 2.0% in 2006. Apart from the normal statutory adjustments, the 2005 budget contained a reduction of 23 700 Euros to permanently cover the 2004 salary increases. The 2005 budget also comprised increased costs for a post upgrade and for the rental of additional office space, both items offset by corresponding savings in other budget lines.

Conclusions and recommendations

13. The Executive Group approved the proposed Data Bank budget and programme of work for 2006 and recommends the Nuclear Science Committee to endorse the approval.

Annex 3

List of Actions
Adopted at the Sixteenth Meeting of the NEA Nuclear Science Committee
8–10 June 2005

1.	**NEA secretariat**	Produce a CD-ROM containing all oral presentations and room documents presented at the meeting and send to all NSC members in the week following the committee meeting.
2.	**NSC members**	Any comments on the IAEA report on Multilateral Approaches to the Nuclear Fuel Cycle should be sent to the NEA Secretariat (Thierry Dujardin) before 1 October 2005.

Self-evaluation of committee work and meetings

3.	**NEA secretariat**	Collect information about the timing and outcome of the different NSC projects during the last five years and send the information to NSC members as soon as possible
4.	**NSC members**	Fill in the self-evaluation questionnaire and send to the NEA secretariat (Isao Yamagishi) before 30 June 2005

Working Party on Scientific Issues of Reactor Systems (WPRS)

5.	**WPRS Chair** (K. Hesketh)	Report back to the NSC before 1 November 2005 on the organisation of work within WPRS, following the incorporation of three existing NSC expert groups (Reactor stability and LWR transients, Fuel behaviour and the IRPhE project).
6.	**WPRS Chair** (K. Hesketh)	In co-operation with the WPFC chair (D. Hill), discuss the prospective of LWRs to reduce minor actinide inventories, identify the underlying scientific issues and write a concise review report.

Reactor-based Plutonium disposition

7.	**TFRPD Chair** (P. D'Hondt)	Prepare a discussion of the future of the expert group at the next NSC meeting.

Radiation shielding and dosimetry

8.	**3D Radiation Transport Chair** (E. Lewis)	Prepare a proposal for the future of the Expert Group on 3D Radiation Transport Benchmarks and report back to the NSC before 1 November 2005.

High Burn-up Fuels

9.	**High Burn-up Fuel Chair** (K. Hesketh)	Send the final draft report on Very High Burn-up Fuels to NSC members for review before publication.

Prediction of Irradiation Damage Effects in Reactors

10.	**NEA secretariat**	Investigate the possibility to establish a cooperative project in the field of predicting irradiation damage effects in reactors and report back to the NSC before 1 November 2005.

Uncertainty analysis in modelling

11.	**J.M. Aragones**	Prepare, with the help of R. Chawla, a specific proposal in the area of uncertainty analysis for a possible follow-up action by the NSC and circulate the proposal before 1 November 2005.

Cooperation with CSNI

12.	**NSC members**	Review the draft paper describing an enhanced cooperation between NSC and CSNI and send any comments or suggested modifications to the NEA secretariat (C. Nordborg) before 1 October 2005.

Topics for In-depth Discussion

13.	**NSC members**	Send additional suggestions for topics for in-depth discussion to the NEA secretariat (C. Nordborg) before 1 November 2005.